

**Development and Optimization of Polyethylene glycol
methyl ether-Polycaprolactone based Glyburide and
Vanillic acid co-loaded Amphiphilic Polymeric Micelles
for the management of Type-2 Diabetes Mellitus**

A THESIS

SUBMITTED IN PARTIAL FULFILLMENT
OF THE REQUIREMENTS FOR THE DEGREE OF
DOCTOR OF PHILOSOPHY

In

Pharmacology

By

Jaskiran

(Registration Number: 41700206)

Under the guidance of

Supervised by

Dr. Sachin Kumar Singh

(Professor, Pharmaceutical Analysis)

Co-supervised by

Dr. Monica Gulati

(Professor/Sr. Dean, Pharmaceutics)



School of Pharmaceutical Sciences

Lovely Professional University

Punjab, India

2022

[4]

DECLARATION

I hereby declared that the presented work in the thesis entitled “**Development and optimization of polyethylene glycol methyl ether-polycaprolactone based Glyburide and Vanillic acid co-loaded amphiphilic polymeric micelles for the management of Type-2 Diabetes Mellitus**” in fulfillment of degree of **Doctor of Philosophy (Ph.D)** is outcome of reaserch work carried out by me under the supervision Dr. Sachin Kumar Singh , working as professor , in the school of pharmaceutical sciences of Lovely Professional University , Punjab, India. In keeping with general practice of reporting scientific observations, due acknowledgement has been made whenever work described here has been based on the findings of the investigators. The work has not been submitted in part or full to any other University or Institute for the award of any degree.

A handwritten signature in black ink, appearing to read 'Sachin Singh', enclosed within a circular scribble. The signature is written on a light-colored background.

(Signature of supervisor)

Name of Scholar: Jaskiran

Registration No.: 41700206

Department/School: School of Pharmaceutical Sciences

Lovely Professional University

Punjab, India

CERTIFICATE

This is to certify that the work reported in the Ph.D thesis entitled “**Development and optimization of polyethylene glycol methyl ether-polycaprolactone based Glyburide and Vanillic acid co-loaded amphiphilic polymeric micelles for the management of Type-2 Diabetes Mellitus**” submitted in fulfillment of the requirement for the reward of degree of **Doctor of Philosophy (Ph.D)**, in the School of Pharmaceutical Sciences, is a research work carried out by Jaskiran , 41700206, is bonafide record of his/her original research work carried out under my supervision and that no part of thesis has been submitted for any other degree, diploma, or equivalent course.



(Signature of supervisor)

Name of supervisor: Dr. Sachin Kumar Singh
Designation: Professor
Department/School: Pharmaceutical Sciences
Lovely Professional University
Punjab, India



(Signature of co-supervisor)

Name of co-supervisor: Dr. Monica Gulati
Designation: Professor
Department/School: Pharmaceutical Sciences
Lovely Professional University
Punjab, India

Dedicated to my parents

No words can ever be strong enough to express my gratitude to my parents for their unconditional love. Thank you for not only being a parent to me but also being a friend, teacher and a mentor. You are the reason for all the achievements in my life.

“You nurtured and protected me and taught me with great care. And every time I have needed you were always there”.

ACKNOWLEDGEMENT

We cannot reach the goal by mere words alone. Without training your mind to think nothing can be achieved and excelled.

*I would like to express my deepest appreciation to my parents **Mr. Nichhatter Singh Kang** and **Mrs. Gurmit Kang** who gave me the encouragement I needed throughout this process. They have been with me throughout my journey like my shadow. This does not solely belong to me more than that it belongs to my parents who have always prioritized me than themselves. I am greatfull to my parent's upbringing who have made me an ambitious, independent and a confident person. Thank you for teaching me the difference between dreams and goals in life to achieve success. Your unconditional believe in me and positivity has always motivated me to keep going and stay focused despite all odds. No words can express my heartfelt thanks for my parents.*

*No words can define the support given by my loved ones **Mr. Paras Famta**, Department of Pharmaceutics, National Institute of Pharmaceutical Education and Research, Hyderabad, India, throughout my PhD journey. Your immense support has guided me in completing my tasks. More than that, your emotional support and positivity has made me strong through this process. Thank you for always standing by my side and motivating me to do higher in my carrier.*

*The completion of this study could not be possible without the support of my friends **Mr. Leander Corrie**, **Mr. Ankit Awasthi**, and **Ms. Bhuman** Research Scholars of Lovely Professional University, Phagwara, Punjab, India, who helped and supported me throughout during my journey. Thank you for your unwavering support and for reminding me to take breaks and have fun when I have been stressed out.*

*I would like to extend my thanks to **Dr. Ankit Yadav**, Assistant Professor, School of Pharmaceutical Sciences, Lovely Professional University, Phagwara, Punjab, India, for helping in my thesis compilation.*

*It is a genuine pleasure to express me deep sense of thanks and gratitude to my supervisor **Dr. Sachin Kumar Singh**, Professor, School of Pharmaceutical Sciences, Lovely Professional University, Phagwara, who made this work possible. His guidance and advice*

carried me through all the stages of writing my project. His dedication and keen interest above all his overwhelming attitude to help his students had been solely and mainly responsible for completing my work. His timely advice, meticulous scrutiny, scholarly advice, and scientific approach have helped me to a very great extent to accomplish this task. His guidance motivated me to keep going and doing hard work to achieve the expected outcomes.

*I owe a deep sense of gratitude to my co-supervisor **Dr. Monica Gulati**, Professor, School of Pharmaceutical Sciences, Lovely Professional University, Phagwara, for her prompt inspirations, constant support, enthusiasm, and providing opportunities to present the work on various scientific platforms.*

*I would also like to express my utmost gratitude to **Dr. Bimlesh Kumar** and **Dr. Navneet Khurrana**, Associate Professor, School of Pharmaceutical Sciences, Lovely Professional University, Phagwara, for their sincere and selfless support, prompt, and useful advice during my research work. Thankyou sir for being the part of my journey in LPU and I will never forget your sincere inputs and learnings. I am greatly indebted to the opportunities that they have provided to enhance my skills on animal experimentations.*

*I would like to express my heartfelt thanks to **Dr. Gopal Lal Khatik**, NIPER, Raebareli, Uttar Pradesh, for creating a prototype, his initial exemplary foresight, thrust, constant motivation helped in creating a solid base for this project. Thankyou sir for being a lead forerunner of this project and all of above being an extremely genuine and motivating person I have ever met.*

*I would like to express my gratitude to **Dr. Gowthamarajan Kuppusamy**, Professor and head, Department of Pharmaceutics, JSS College of Pharmacy, Ooty, Karnataka, India for supporting the research work and providing facilities to accomplish my research tasks. I would also like to thanks his students **Mrs. Divya** and **Mr. Sanju**, for their positive attitude and help during my visit to carry out my research work in JSS College of Pharmacy, Ooty.*

*I would like to extend my gratitude to **Dr. Madhunapantula Subbarao** and his Ph.D. Scholar **Ms. Vidya**, Professor of Cellular and Molecular Biology, CEMR Laboratory, Department of Biochemistry, JSS Medical College, Mysore, Karnataka, India for their able guidance and support with all the facility that was required in completing my project.*

*I am thankful to **Central Instrumentation Facility**, Lovely Professional University, and **SAIF**, Punjab University, having excellent instrumentation facilities for their contribution in accomplishing my research tasks.*

*I extend my warm thanks to the faculty members **Dr. Sumant, Dr. Bhupinder Kapoor, Dr. Navneet Khurana, Dr. Vijay Mishra, Dr. Dileep Singh, Dr. Rakesh Kumar** and the master students of LPU **Mr. Sourabh Chatterjee, Mr. Mahesh Tidke, Ms. Anuradha**, for their suggestions, help and co-operation during my research work.*

*I would like to thanks **DP Traders**, Chandigarh, for providing me the high quality chemicals (TCI, Japan) for the conduct of my research work. Also, the technical and support staff members of the Lovely Professional University, **Mr. Gopal Lal Krishan, Mr. Madan, Mrs. Malti, Mr. Ramji, Mr. Raju, Mr. Sonu, Mr. Sandeep, Mr. Fedrick, and Mr. Manawar** for their practical assistance, vital support and help in conducting my research work.*

*Finally, extremely thankful indeed to the **Mr. Ashok Mittal**, Chancellor and **Mrs. Rashmi Mittal**, Pro-chancellor, LPU, Punjab for providing the laboratory based structural and functional facilities to successfully complete my research work in the their wonderful vibrant LPU campus.*

I express my deep sense of gratitude to the experimental animals used in my research work for sacrificing their life for a novel cause.

Table of contents

Sections	Chapters	Page no.
Chapter 1		
1.0	<i>Introduction</i>	20-22
Chapter 2		
2.0	<i>Review of literature</i>	23
2.1	<i>Type 2 diabetes mellitus</i>	24
2.2	<i>Pathogenesis of T2DM</i>	24
2.2.1	<i>Oxidative stress</i>	24-25
2.2.2	<i>Inflammation</i>	25-26
2.2.3	<i>Islet amyloidogenesis</i>	26
2.3	<i>Biological targets</i>	26
2.3.1	<i>Toll like receptors</i>	28-29
2.3.2	<i>Glucagon receptor</i>	29-30
2.3.3	<i>G-protein receptor-21</i>	30-31
2.3.4	<i>Free fatty acid receptor -1</i>	31
2.3.5	<i>Protein tyrosine phosphatase-1B</i>	31-32
2.3.6	<i>Prolyl hydroxylase domain enzyme</i>	32
2.3.7	<i>Nuclear response factor-2</i>	32-33
2.3.8	<i>Histone deacetylase-3</i>	33
2.4	<i>Major anti-diabetic drug families</i>	33
2.4.1	<i>Sulfonylureas</i>	34-36
2.4.2	<i>Glinides</i>	36-37
2.4.3	<i>Biguanides</i>	37-38
2.4.4	<i>Thiazolidinediones</i>	38-39
2.4.5	<i>GLP-1 receptor agonist</i>	39-41
2.4.6	<i>DPP-4 Inhibitors</i>	41-42
2.4.7	<i>α-glucosidase inhibitors</i>	42-43
2.4.8	<i>Sodium-glucose co-transporter-2 inhibitors</i>	43-47
2.5	<i>Oral/Nasal insulin</i>	48
2.6	<i>Pharmacological approaches of the American diabetes association (ADA)</i>	48-50

2.7	<i>Advanced treatment strategies for T2DM</i>	51
2.7.1	<i>Nanocarrier-based approaches</i>	51
2.7.1.1	<i>Lipid-based nanocarriers</i>	51
2.7.1.1.1	<i>Liposomes</i>	51-53
2.7.1.1.2	<i>Niosomes</i>	53-54
2.7.1.1.3	<i>SNEDDS</i>	54-56
2.7.1.1.4	<i>Solid-lipid nanoparticles (SLNs)</i>	56-57
2.7.1.2	<i>Micelles</i>	57-59
2.7.1.3	<i>Polymeric nanoparticles</i>	59-60
2.7.1.4	<i>Nanocrystals</i>	60-61
2.7.1.5	<i>Miscellaneous</i>	61-68
2.8	<i>Glyburide</i>	69-71
2.9	<i>Vanillic acid</i>	71-72
2.9.1	<i>Botanical sources of VA and their geographical distribution</i>	72
2.9.1.1	<i>Actinidia species</i>	72-73
2.9.1.2	<i>Angelica decursiva</i>	73
2.9.1.3	<i>Leonurus sibiricus</i>	73
2.9.1.4	<i>Berberis orthobotrys</i>	73
2.9.1.5	<i>Angelica sinensis</i>	73
2.9.1.6	<i>Cucurbita pepo</i>	74-76
2.9.2	<i>Pharmacological activity of VA in T2DM</i>	77-78
2.9.3	<i>Safety studies of VA</i>	78-79
2.9.4	<i>Future direction</i>	79-80
2.10	<i>Amphiphilic block copolymers</i>	80-82
2.10.1	<i>Amphiphilic polymeric micelles</i>	82-83
2.10.2	<i>Factors affecting physicochemical properties of APMs</i>	83-86
2.10.3	<i>Methods of preparation of APMs</i>	86
2.10.3.1	<i>Chemical conjugation methods</i>	86
2.10.3.2	<i>Physical methods</i>	86-87
2.10.3.2.1	<i>Direct dissolution method</i>	87

2.10.3.2.2	<i>Dialysis method</i>	87
2.10.3.2.3	<i>Thin film hydration method</i>	87
2.10.3.2.4	<i>o/w emulsion solvent evaporation method</i>	87
2.10.3.2.5	<i>Direct freeze-drying method</i>	88
2.10.3.2.6	<i>Fast heating method</i>	88-89
2.11	<i>Therapeutic applications of APMs in T2DM</i>	90
2.11.1	<i>Oral drug delivery</i>	90
2.11.2	<i>Stimuli-triggered insulin delivery</i>	91-92
2.11.3	<i>“On-off” insulin release</i>	92-93
Chapter 3		
3.0	<i>Rationale of study</i>	95
3.1	<i>Hypothesis</i>	96-97
3.2	<i>Aim</i>	98
3.3	<i>Objectives</i>	98
3.4	<i>Plan of work</i>	98-99
Chapter 4		
4.1	<i>Experimental</i>	101
4.1.1	<i>Equipment's</i>	101
4.1.2	<i>Chemicals</i>	102
4.2	<i>Preformulation studies</i>	103
4.2.1	<i>Identification of raw drugs and excipients</i>	103
4.2.1.1	<i>Physical examination</i>	103
4.2.1.2	<i>Melting point analysis</i>	103
4.2.1.3	<i>DSC</i>	103
4.2.1.4	<i>FTIR spectroscopy</i>	103
4.2.1.5	<i>XRD</i>	104
4.2.1.6	<i>Partition coefficient</i>	104
4.2.2	<i>Solubility study</i>	104
4.2.2.1	<i>Solubility in surfactants</i>	104-105
4.2.2.2	<i>Solubility in buffer systems and organic solvents</i>	105
4.3	<i>Development of RP-HPLC analytical method</i>	105
4.3.1	<i>Selection of chromatographic conditions</i>	106

4.3.2	<i>Preparation of stock and sample solution</i>	106
4.3.3	<i>Development of calibration curve</i>	106
4.3.4	<i>Validation</i>	106
4.3.5	<i>Linearity and range</i>	106
4.3.6	<i>Accuracy</i>	106-107
4.3.7	<i>Precision</i>	107
4.3.8	<i>Roboustness</i>	107
4.3.9	<i>System suitability and assessment of LOD and LOQ</i>	107
4.4	<i>Formulation development</i>	107
4.4.1	<i>Synthesis of mPEG-b-PCL copolymer</i>	107
4.4.2	<i>Liquid antisolvent precipitation method for APMs formation</i>	108
4.4.3	<i>Design of experiment (DoE)</i>	108-109
4.5	<i>Characterization of synthesized mPEG-b-PCL and APMs</i>	109
4.5.1	<i>Product yield</i>	109
4.5.2	<i>CMC determination</i>	110
4.5.3	<i>FTIR</i>	110
4.5.4	<i>¹HNMR</i>	110
4.5.5	<i>DSC</i>	110
4.5.6	<i>ESI-MS</i>	110-111
4.5.7	<i>SEM</i>	111
4.5.8	<i>Particle size and zeta potential</i>	111
4.5.9	<i>HR-TEM</i>	111
4.5.10	<i>Entrapment efficiency (EE%)</i>	111
4.5.11	<i>Drug loading (DL%)</i>	111
4.5.12	<i>In vitro release study</i>	112
4.6	<i>In vitro cell line study</i>	112
4.6.1	<i>Caco-2 cytotoxicity study</i>	112
4.6.2	<i>Passive glucose uptake study</i>	113
4.6.3	<i>Insulin-resistant HepG2 cell model</i>	113

4.6.4	<i>Selection of non-cytotoxic concentration</i>	113
4.6.5	<i>Glucose uptake in insulin-resistant cells</i>	113-114
4.7	<i>In vivo studies</i>	114
4.7.1	<i>Animals</i>	114
4.7.2	<i>Development of bioanalytical method</i>	114
4.7.2.1	<i>Chromatographic conditions</i>	114
4.7.2.2	<i>Extraction of plasma from rat's blood samples</i>	114
4.7.2.3	<i>Preparation of blank plasma</i>	115
4.7.2.4	<i>Preparation of standard stock solution</i>	115
4.7.2.5	<i>Preparation of internal standard (IS)</i>	115
4.7.2.6	<i>Method specificity</i>	115
4.7.2.7	<i>Development of calibration curve</i>	115
4.7.2.8	<i>Accuracy studies</i>	115-116
4.7.2.9	<i>Precision studies</i>	116
4.7.2.10	<i>Determination of LOD and LOQ</i>	116
4.7.2.11	<i>System suitability</i>	116
4.7.2.12	<i>Stability study</i>	116-117
4.7.3	<i>Pharmacokinetics study</i>	117-118
4.7.4	<i>In vitro/in vivo correlation (IVIVC) studies</i>	118
4.7.5	<i>Pharmacodynamics study</i>	118
4.7.5.1	<i>HFD plus low dose of STZ model</i>	118-119
4.7.5.2	<i>OGTT</i>	119
4.7.5.3	<i>Body weight and lipid markers</i>	119
4.7.5.4	<i>STZ injection</i>	120-121
4.7.6	<i>Parameters for evaluation</i>	122
4.7.6.1	<i>Body weight</i>	122
4.7.7	<i>Biochemical parameters</i>	122
4.7.7.1	<i>Blood glucose levels</i>	122
4.7.7.2	<i>Serum lipid markers</i>	122
4.7.7.2.1	<i>Serum cholesterol</i>	122
4.7.7.2.2	<i>Serum HDL</i>	122-123
4.7.7.2.3	<i>Serum triglycerides</i>	123

4.7.7.2.4	<i>Others</i>	123
4.7.8	<i>Serum inflammatory markers</i>	123-124
4.7.9	<i>Serum hepatic and renal markers</i>	124
4.7.10	<i>Euthanasia</i>	124
4.7.11	<i>Determination of pancreatic oxidative stress</i>	124-125
4.7.12	<i>Histology study</i>	125
4.7.13	<i>Statistical analysis</i>	125
Chapter 5		
5.0	<i>Results and discussion</i>	127
5.1	<i>Physical examination</i>	127
5.2	<i>Melting point analysis</i>	127
5.3	<i>DSC, XRD, FTIR analysis</i>	127
5.4	<i>Partition coefficient (Log P)</i>	127
5.5	<i>Solubility in surfactants</i>	130
5.6	<i>Solubility in solvents and buffer systems</i>	131-132
5.7	<i>Development of RP-HPLC analytical method</i>	132
5.7.1	<i>Selection of chromatographic conditions</i>	132
5.7.2	<i>Linearity and range</i>	132
5.7.3	<i>Accuracy</i>	133
5.7.4	<i>Precision</i>	133
5.7.5	<i>Robustness</i>	135
5.7.6	<i>System suitability</i>	135
5.8	<i>Formulation development</i>	141
5.8.1	<i>Synthesis and characterization of mPEG-b-PCL copolymer</i>	141
5.8.2	<i>CMC determination</i>	142
5.8.3	<i>FTIR</i>	143
5.8.4	<i>NMR</i>	143
5.8.5	<i>DSC</i>	143
5.8.6	<i>ESI-MS</i>	143
5.8.7	<i>Examination of process variables for optimization of formulation</i>	146-157

5.8.8	<i>Graphical optimization</i>	158
5.9	<i>Characterization of optimized GV-APMs</i>	159
5.9.1	<i>FTIR</i>	159
5.9.2	<i>DSC</i>	159-160
5.9.3	<i>SEM</i>	161
5.9.4	<i>Particle size and zeta potential</i>	162
5.9.5	<i>HR-TEM</i>	163
5.9.6	<i>EE and DL of GV-APMs</i>	163
5.9.7	<i>In vitro drug release kinetics modelling studies</i>	164-166
5.9.8	<i>In vitro Caco-2 toxicity study</i>	166-167
5.9.9	<i>Passive glucose uptake study</i>	167
5.9.10	<i>Insulin-resistant HepG2 cell model</i>	167
5.9.11	<i>Selection of non-cytotoxic concentration</i>	167-168
5.9.12	<i>Glucose uptake study in insulin-resistant HepG2 cells</i>	168-170
5.10	<i>Development of bioanalytical method</i>	171
5.10.1	<i>Chromatograms of mixture</i>	171
5.10.2	<i>Specificity studies</i>	171
5.10.3	<i>Calibration curve development</i>	171-172
5.10.4	<i>Accuracy studies</i>	173
5.10.5	<i>Precision estimation of the developed method</i>	173
5.10.6	<i>LOQ and LOD</i>	173-175
5.10.7	<i>System suitability</i>	175
5.10.8	<i>Stability study</i>	175-179
5.11	<i>In vivo studies</i>	180-185
5.11.1	<i>IVIVC</i>	186-188
5.12	<i>Pharmacodynamics study</i>	188
5.12.1	<i>OGTT</i>	188-190
5.12.2	<i>BGLs</i>	191-193
5.12.3	<i>Body weight</i>	194-196
5.12.4	<i>Lipid profile</i>	197-201
5.12.5	<i>Hepatic and renal markers</i>	202-203

<i>5.12.6</i>	<i>Serum inflammatory markers</i>	<i>204-205</i>
<i>5.12.7</i>	<i>Pancreatic oxidative stress</i>	<i>205-207</i>
5.13	<i>Histopathology study</i>	<i>208-209</i>
<i>Chapter 6</i>		
<i>6.0</i>	<i>Conclusion and future perspective</i>	<i>211-212</i>
7.0	<i>References</i>	<i>213</i>

Abstract

The foremost objective of this study was to develop a novel nano combination therapy of antidiabetic drug glyburide (Gly) with a natural product vanillic acid (VA) using an amphiphilic block copolymer-surfactant system i.e., polyethylene glycol methyl ether-block-polycaprolactone (mPEG-b-PCL) and cetyl trimethyl ammonium bromide (CTAB) for the effective management of type 2 diabetes mellitus (T2DM). The copolymer mPEG-b-PCL was selected due to its self-assembly property into micellar configuration upon addition in water above their critical micelle concentration (CMC) value. The mPEG block forms the corona and the PCL block forms the core that results in the formation of amphiphilic polymeric micelles (APMs). While the CTAB was used as a steric stabilizer in the formulation for good dispersity of the particles.

The aim of the research work conducted was to optimize the design of amphiphilic polymeric micelles (APMs) for the oral co-delivery of Gly and VA to improve their therapeutic benefits and to limit the common shortcomings related with present drug regimens i.e., their side effects, complexity or recurrent dosing.

The APMs co-loaded with Gly and VA (GV-APMs) was developed using the liquid antisolvent precipitation (LAP) method and the composition of the developed APMs was optimized using Box Behnken Design (BBD) in the design of expert (DoE 2.0) software by taking various process/formulation based variables to achieve the desired micellar traits. This includes drug to copolymer, drug to surfactant and solvent to antisolvent ratio. Total of 17 batches of APMs was developed from such variables and was characterized to determine the responses such as particle size, entrapment efficiency (EE), zeta potential and polydispersity index (PDI) respectively. The set of data obtained was statistically analysed using DoE tools such as the sequential model sum of squares, model summary statistics and Analysis of variance (ANOVA). Such tools were applied to compare the models, interaction among the variables, variation in each response, and significant differences between the runs. The final polynomial equations obtained for each response by DoE software revealed a quadratic design.

Furthermore, the Box behnken design (BBD) was used to optimize the developed formulation using design expert software (DoE) which provided particle size (R1) in the range of 31.8-57.4 nm, EE of VA (R2) in the range of 90.3-100.0, EE of Gly (R3) in the range of 98.8-100.0, zeta potential (R4) in the range of 15.3-30.5, and PDI (R5)

in the range of 0.256-0.405 respectively. The predicted values obtained through BBD were used to develop the optimized batch of the GV-APMs. The particle size, EE (VA), EE (Gly), zeta potential, and PDI of the optimized GV-APMs were found to be 46.82 ± 2.1 nm, $93.4 \pm 0.15\%$ (VA), $97.9 \pm 0.24\%$ (Gly), 12.5 ± 3.1 mV, and 0.281 ± 0.2 respectively. The TEM images revealed the spherical shape of the developed APMs with a smooth surface and an average particle size of 34.3 nm. TEM analysis revealed less particle size in comparison to the DLS particle size analysis. DLS measure the hydrodynamic particle size; however, the loss of water during TEM analysis can be credited for a decrease in the particle diameter.

The results of *in vitro* release study revealed a 1.5- and 1.9-folds, and 1.0-fold increase in the percentage dissolution of Gly from the GV-APMs than that of the physical mixture with VA, raw Gly and Gly-APMs. In addition to this, the GV-APMs sustained the release of VA by 2.9- and 2.4-folds in 2h, and 1.7-folds in 4h than that of the raw VA, physical mixture with Gly in 2 and 4h respectively. Furthermore, sustained the release by 1.2-folds than that of the VA-APMs respectively. Gly from the optimized GV-APMs were predominantly released by zero-order release kinetics and VA by Higuchi release kinetic model with AIC more than 90 respectively.

The *in vitro* cytotoxicity study of GV-APMs on Caco-2 cells revealed 70% cell viability in a concentration-dependent manner. The inhibitory concentration (IC_{50}) value of the raw drugs and their value upon loading in APMs was obtained using Graph pad prism 2.0 software. The IC_{50} value of the raw Gly was found to be $1.42 \mu\text{g/mL}$ while upon loading in APMs it was found to be $1.10 \mu\text{g/mL}$. In the case of VA, the IC_{50} value was found to be $1.17 \mu\text{g/mL}$ and $1.03 \mu\text{g/mL}$ upon its loading in APMs. However, in GV-APMs the IC_{50} value was found to be $0.96 \mu\text{g/mL}$. This indicated that both the drugs are effective at the lowest concentrations in APMs and will exhibit lower systemic toxicity upon oral administration.

The preventive effects of Gly and VA co-loaded in GV-APMs on glucose uptake was studied in insulin-responsive human HepG2 cells treated with high glucose. The co-loading of both the drugs in optimized GV-APMs exhibited synergistic glucose-lowering activity ($p < 0.001$) than raw drugs with low cytotoxicity on HepG2 cells within the test concentration. This could be attributed to an increase in the relative oral

bioavailability of both the drugs in GV-APMs i.e., 868% for Gly and 87% for VA respectively.

In agreement with this, the results of the pharmacokinetic study revealed an increase in the area under the curve ($AUC_{0-\infty}$) of Gly co-loaded in GV-APMs by 1362.8-, 840.7- and 3.5-folds than that of the raw Gly, physical mixture with VA, and Gly-APMs respectively. While the ($AUC_{0-\infty}$) of VA co-loaded in GV-APMs was increased by 10.7-, 2.8- and 1.3-folds than that of raw VA, physical mixture with Gly and VA-APMs respectively. In addition to this, the pharmacodynamics study carried out for 48 days using high fat diet (HFD) and low dose of streptozotocin (STZ) model indicated improved therapeutic efficacy ($p < 0.05$) of the developed formulation i.e., GV-APMs (G11 and G12) in a dose-dependent manner pertaining to blood glucose levels (BGLs), lipid profile, hepatic and renal markers, serum inflammatory markers, and pancreatic oxidative stress with respect to raw drugs and their physical mixture respectively.

The results of histopathological study achieved for GV-APMs (G11 and G12) were found to be in a positive co-relation with the biochemical changes obtained. The treatment with GV-APMs in diabetic rats for 28 days ameliorated the vacuolar degeneration and vascular congestion of pancreatic islets cells, and hepatic steatosis (fatty liver) as a measure of increased number of viable cells observed. In contrast the rats of experimental control group (G2) showed extreme fat deposition in hepatic cells (higher steatosis) in liver of diabetic rats, higher vascular congestion and vacuolar degeneration in pancreas as a measure of reduced number of viable cells. Thus, the designed formulation i.e., APMs containing a natural product VA and a synthetic drug Gly co-loaded in the micellar core have potential to improve T2DM in future.

Chapter 1

Introduction

Chapter 1

1.0 Introduction

Diabetes mellitus (DM) is a commonly occurring metabolic disease with a higher prevalence rate globally [1]. The increasing economic burden of DM is a major concern in healthcare worldwide. In recent years it has become a common cause of mortality in the past few years and the overall number of diabetics is expected to be increased by 700 million globally by 2045 [2,3]. There are four forms of DM i.e., type 1, type 2, pre-diabetes, and gestational diabetes. Amongst these, type 1 and type 2 account for more than 90-95% of the diagnosed forms worldwide with type 2 being the most protuberant one reaching 80-85% of total diabetes [4].

The existing treatment strategies including oral hypoglycemic drugs and life-long insulin therapy provides tight control of glycosylated haemoglobin ($HbA1c \leq 7.0\%$) levels in DM patients [5]. However, poor oral bioavailability, susceptibility for enzymatic degradation, and immediate release profile of potent anti-diabetic drugs increase the severity of side effects and poor patient compliance in long run [6–9]. Overall, these limitations make these therapies ineffective to maintain glucose homeostasis and urge the need for frequent dosing in DM patients.

Therefore, treatment of type 2 DM (T2DM) is not only limited by the drug's efficacy but also due to its adverse effect profile. These include hepatotoxicity and GIT disturbances (biguanide, α -glucosidase inhibitors, thiazolidinediones, glucagon-like-peptide-1), hypoglycemia, weight gain, and incidence of cancer (sulfonylurea and meglitinides), GIT disturbances (α -glucosidase inhibitors), congestive heart failure, bladder cancer (thiazolidinediones), acute pancreatitis (glucagon-like-peptide-1, DPP-IV inhibitors), nasopharyngitis and upper respiratory infections (DPP-IV inhibitors), and genitourinary tract infection (SGLT2 inhibitors) [10].

Amongst the various oral anti-hyperglycaemic agents, sulfonylureas are widely prescribed by physicians to manage increased blood glucose levels. These are the first oral antihyperglycemic drugs approved by FDA in 1958 to treat type II DM. These are insulin secretagogues whose effect is dependent on the functioning of β -cells in pancreatic islets via which these drugs control hyperglycaemia [11]. Glyburide (Gly) is a potential second-generation, longer-acting sulfonylurea that is widely prescribed due to its lower risk of cardiovascular complications than first-generation sulfonylureas [11]. Gly reduces glycated haemoglobin levels by 1.5-2% in T2DM patients [12].

Generally, the oral antihyperglycemic drugs that are rapidly absorbed by the gastrointestinal tract (GIT) are required to prevent a sudden increase in blood glucose levels after food ingestion in T2DM. However, the poor oral bioavailability of Gly due to its poor dissolution via GIT impedes its clinical performance. It is also associated with higher hypoglycemic episodes i.e., by 80% than other sulfonylureas with a maximum of 20 mg daily dose [12]. It is mostly used in combination with metformin to achieve a glycated haemoglobin target (<7%). However, their administration, in the long run, increases the risk of cardiovascular events more than the Gly monotherapy [13]. Therefore, there is a need to develop an effective and safe combination therapy of Gly for diabetics. Hence, co-administration of natural antioxidants with improved toxicity profiles could be a suitable alternative option in increasing the therapeutic efficacy of Gly.

Vanillic acid (VA) is a phenolic compound that is obtained from the roots of *Angelica sinensis* plant. It is the oxidized product of vanillin. It is popular as a flavouring agent in various food industries [14]. Its natural antioxidant property caught the attention of various scientists to treat several human diseases. Several studies claimed the potential of VA in treating cancer, depression, Alzheimer's, inflammatory diseases, cardiovascular diseases, obesity, insulin resistance etc [14–18]. However, its rapid elimination from the systemic circulation limits its oral bioavailability, which is a great challenge for oral formulation development [14].

The amphiphilic polymeric micelles (APMs) formed from amphiphilic block copolymers are excellent candidates for entrapping multiple lipophilic drugs in their hydrophobic core [19]. This contributes to the release of loaded drugs from the core in a controlled manner. Further, the hydrophilic corona confers aqueous solubility upon exposure to the aqueous environment of GIT. Polyethylene glycol monomethyl ether-block-polycaprolactone (mPEG-b-PCL) is a diblock amphiphilic block copolymer (ABC) that self-assembles into nanoparticles with core-corona supramolecular configuration: PCL forms the core and mPEG forms the corona [20]. Entrapment of Gly and VA in mPEG-b-PCL APMs will possibly improve the constancy, higher absorption from GIT, systemic distribution of drugs and release drugs at sustained time intervals [21]. This could overcome the rapid absorption and elimination related challenges of VA as well maintain the residence time of both the drugs in systemic circulations leading to sustained glycaemic control in the body [22]. In addition, this

combination therapy via APMs as a nanocarrier could reduce the dosing frequency of Gly owing to its sustained release from the APMs [23].

In the present study, a novel nano-combination therapy of Gly and VA is proposed composed of ABC and surfactant system i.e., mPEG-b-PCL/Cetyl trimethyl ammonium bromide (CTAB) system, which self-assembles in APMs. The pharmacology of Gly is well documented for the management of T2DM i.e., by acting on ATP-sensitive potassium ion channels on pancreatic β -cells and reported to be a broad-spectrum ATP-binding cassette transporter inhibitor. In addition to this, Gly exhibits protective effects against inflammation by inhibiting sulfonyleureas receptor 1 (Sur1)- transient receptor potential melastatin 4 channels by directly binding the Sur1 subunit [24].

On the other hand, several studies have demonstrated the role of VA in ameliorating obesity conditions by reducing lipid and inflammatory markers. Further studies also indicated the potential for its use in obesity-associated hepatic insulin resistance [17]. VA's treatment in high-fat diet (HFD) fed rats are reported to ameliorate the hepatic insulin resistance by increasing the expression of the insulin receptor, phosphoinositide 3-kinase (PI3K) and glucose transporter 2 (GLUT-2) protein [25]. Furthermore, it claimed to down-regulate the expression of cyclooxygenase 2 (COX-2) and monocyte chemoattractant protein-1 (MCP-1) in HFD fed rats [17]. It also increased the hepatic phosphorylated acetyl CoA carboxylase (ACC) protein expression with reduced hepatic non-esterified fatty acid (NEFA) levels [17]. In addition, VA is reported to exert anti-obesity effect by stimulating AMP-activated protein kinase- α (AMPK- α) and thermogenesis in obese rodents, anti-inflammatory effect by inhibiting nuclear factor kappa-light-chain-enhancer of activated B cells (NF κ B) p65 activation and antioxidant effect by induction of nuclear factor erythroid 2-related factor 2 (Nrf2) [18,26]. Despite such beneficial outcomes, the therapeutic potential of VA has been less explored. Till now its combination has been explored with thiazolidinedione's (TZD) in adipocyte cell line study, which indicated additive pharmacological interaction [27]. Further, *in vivo* studies are required to study the pharmacokinetics and pharmacological interaction between two drugs. With the aforementioned objectives, the present state of the art is being proposed to develop a novel combination containing Gly and VA co-loaded in APMs formed from mPEG-b-PCL/CTAB system for the effective management of T2DM.

Chapter 2
Review of literature

2.0 Diabetes Mellitus

DM is a chronic metabolic disease characterized by hyperglycemia owing to lack of insulin production or non-responsive insulin signal transduction. There are four forms of DM i.e., type 1, type 2, pre-diabetes, and gestational diabetes [3]. Amongst these, type 1 and type 2 account for more than 90-95% of the diagnosed forms worldwide with type 2 being the most protuberant one reaching 80-85% of total diabetes [2,28].

2.1 Type 2 diabetes mellitus

T2DM can be characterized by insulin resistance and variable insulin secretion that is associated with increased blood glucose levels and glucotoxicity. The number of diabetics globally is expected to reach 642 million by 2040 [2]. Increased body mass index (BMI) or obesity is found to be in strong association with many pathophysiological conditions, notably T2DM, as both share insulin resistance. Obese individuals can be up to 80 times more likely to develop T2DM in comparison to individuals with body mass index (BMI) < 22 [29,30]. Therapeutic targets include tight control of glycosylated hemoglobin (HbA1c \leq 7.0 %) levels, to prevent long-term complications and mortality [2]. In case of obesity (BMI \geq 27 for Asian countries, or BMI \geq 30 in the Western world), medications are recommended, and it is a prerequisite to review the weight gain or weight loss effect of antidiabetic medications before prescribing.

A minimum 5% weight loss in obese T2DM patients is desired, and if the goal is not attained, alternative medication with good efficacy and reduced risk of hypoglycemia should be considered [31]. Weight reduction in overweight and obese individuals could help in improving insulin sensitivity, as well as attenuating the risk of metabolic and cardiovascular complications [30].

2.2 Pathogenesis of T2DM

Various factors play a significant role in the development and progression of this chronic metabolic disease, the most prevalent being oxidative stress and the generation of inflammatory responses, especially through Interleukin-6 and tumor necrosis factor- α (TNF- α) [32].

2.2.1 Oxidative stress

Oxidative stress originates from an increase in the generation of reactive oxygen species (ROS) through an altered redox balance in the mitochondria. This condition leads, in the majority of cases, to the destruction of pancreatic β -cells alongside an increased

prevalence of other vascular complications [33]. Poorly controlled hyperglycaemia in DM patients increases the risk of oxidative stress because of the activation of certain pathways suppressing the defence mechanisms of antioxidant enzymes, including the polyol pathway, the activation of protein kinase C and the overactivity of the hexosamine pathway [34]. The activation of the polyol pathway results in an increase in enzymatic glucose conversion to polyalcohol sorbitol, which ultimately reduces intracellular NADPH and glutathione concentrations. The activation of protein kinase C inhibits the insulin-stimulated endothelial Nitric Oxide Synthase (eNOS) expression in endothelial cells, decreasing nitric oxide production in smooth muscle cells, as well as an increase in the activation of nuclear redox-sensitive transcription factor B (NF- κ B), stimulating the generation of pro-inflammatory cytokines. Additionally, hyperglycemia impairs the activation of the insulin receptor substrate (IRS)/phosphatidylinositol 3-kinase (PI3-K)/Akt pathway, resulting in the deregulation of eNOS activity [32,35]. Therefore, this oxidative stress is associated with the overproduction of pro-inflammatory cytokines and chemokines, which have a significant impact on the correct β -cell function.

2.2.2 Inflammation

Lifestyle choices were reported to have a strong impact on the development of insulin resistance where chronic inflammation due to obesity is a critical factor. Obesity causes an increase in lipid synthesis, activating the essential enzyme acetyl CoA carboxylase (ACC) by dephosphorylation, leading to the transformation of acetyl CoA to malonyl CoA via carboxylation [17]. An increase in the phosphorylation of ACC reduces non-esterified fatty acid (NEFA) deposition in the peripheral tissue, including the liver. The excessive formation of NEFA inhibits insulin signalling and causes hepatic inflammation potentially leading to the development of T2DM. A higher concentration of NEFA is reported to be associated with an increase in the expression of cyclooxygenase-2 (COX-2) and the monocyte chemoattractant protein-1 (MCP-1) in the hepatocytes [36].

In addition to this, the release of pro-inflammatory cytokines (TNF- α , and IL-6) in patients with adiposis not only affects the liver and adipose tissues but also acts on the pancreas and skeletal muscles. In obese people, the increased level of TNF- α is strongly linked with hyperinsulinemia, which is an indication of insulin resistance in peripheral tissues. Its mechanism involves the activation of stress-related protein kinesis, such as inhibitor kappa beta kinase beta (IKK β), Jun N-terminal kinase (JNK) and the NF- κ B

pathway. Moreover, the production of TNF- α causes apoptosis of pancreatic islets [32,37]. Similarly, IL-6 also induces insulin resistance in peripheral tissues, pancreatic apoptosis, and the expression of a suppressor of the cytokine signalling 3 (SOCS-3) pathway, which inhibits insulin signalling. IL-6 receptors are linked to the family of cytokine class I receptors, involving Janus kinases/signal transducers and activators of transcription (JAK/STAT) pathways. Activation of JAK induces STAT phosphorylation, dimerization and translocation to the nucleus, regulating the target gene transcription. Therefore, IL-6 impairs phosphorylation of the insulin receptor and the insulin receptor substrate-1 [32,38].

2.2.3 Islet amyloidogenesis

Amyloidosis is a localized condition that occurs in a specific organ associated with ageing or age-related diseases, such as Alzheimer's disease and T2DM. The islet amyloid in the pancreatic islets has been detected in 50–90% of patients with T2DM, with a significantly lower percentage in non-diabetic age-matched controls. Insulin amyloid polypeptide (IAPP) and insulin are co-secreted from the same β -cell granules and the production of these two β cell-specific hormones is co-regulated through β cell-specific regulatory elements in the promoter regions of the encoding genes [39]. To meet the increased demand for insulin under insulin resistance conditions, β -cells increase the production of both insulin and IAPP. The increased concentration of IAPP promotes aggregation and fibril formation, thus causing islet amyloidosis from IAPP. Islet amyloidosis (soluble oligomers) can then induce the apoptosis of pancreatic β -cells by membrane destabilization [40,41].

2.3 Biological targets

The biological targets, which are commonly involved in the pathogenesis of T2DM, include toll like receptors (TLRs) [42], glucagon receptor [43], orphan G protein-coupled receptor-21 (GPR21) [44], free fatty acid receptor 1 (FFAR1) [43], protein tyrosine phosphatase 1B (PTP1B) [43,45], prolyl hydroxylase domain enzyme (PHD), Kelch like ECH associated protein 1/ nuclear factor erythroid 2-related factor (Keap-1/Nrf2) [46] and histone deacetylase 3 (HDAC3) [47]. The drugs acting on these novel targets would be an efficient approach for the successful control of blood glucose levels. A brief overview on the novel targets and some of the studies pertaining to these are mentioned in *Table 2.1*.

Table 2.1: Table enlisting the potential role of stated targets for managing T2DM and its associated comorbidities

Receptors	Inference	References
TLR2	In <i>in vivo</i> study, anti-TLR2 monoclonal antibody (TLR2 mAb) 0.5 mg improved fasting blood glucose levels and inflammatory response	[48]
TLR4	In <i>in vivo</i> study, cyclohexene derivative (CLI-095) 1 mg/ml inhibited TLR4 signalling, reduced the CD4+ T lymphocyte activation, infiltrative insulinitis and onset of spontaneous diabetes	[49]
TLR4	In <i>in vitro</i> study, extracellular vesicles containing microRNA-26a-5p ameliorated the symptoms of diabetic neuropathy by inhibiting TLR4 and NF- κ B pathway	[50]
Glucagon receptor	A phase 2 clinical trial of glucagon receptor antagonist RVT-1502 15 mg in T2DM patients with good safety profile reduced glycosylated haemoglobin levels ($p < 0.001$) with respect to placebo	[51]
GPR21	<i>In silico</i> , screening studies revealed improved insulin signalling in HEK293 cells overexpressing the orphan receptor with higher binding affinity	[44]
FFAR1/GPR40	In diabetic rats, MR1704 (potent, highly selective and orally bioavailable agonist) at dose 10 mg/kg improved glucose homeostasis ($p < 0.01$) with respect to control without risk of hypoglycaemia and pancreatic toxicity	[52]
FFAR1/GPR40	In <i>in vivo</i> study, vincamine at dose 30 mg/kg enhanced glucose-stimulated insulin release and decreased serum sugar levels ($p < 0.001$) in comparison to control	[53]
PTP1B	In <i>in vitro</i> study on human HepG2 cells, honeydew extracts (IC_{50} 12 μ L/mL) inhibited PTP1B activity, increased the transcription of genes expressing for insulin receptor and glucose uptake	[54]
PTP1B	In <i>in vivo</i> study, uncharged bromophenol derivative (potent PTP1B inhibitor) 100 mg/kg enhanced insulin sensitivity and protected mice from obesity without any toxicity	[55]
PTP1B	In <i>in vitro</i> enzymatic assay, lobeglitazone (IC_{50} 42.8 μ M) moderately inhibited PTP1B activity and exhibited a reversible non-competitive type of inhibition	[56]
PHD enzyme	<i>In vivo</i> study of pan-PHD inhibitor compound at dose 3 mg/kg in C57BL6 mice exhibited good glucose control by increasing liver insulin sensitivity via hepatic HIF-2 α -dependent regulation	[57]
PHD enzyme	In <i>in vivo</i> study, enarodustat (PHD inhibitor) 0.05 mg/g reduced blood glucose levels, body weight (body wt.) and showed renoprotective effects	[58]
Keap1/Nrf2	In <i>in vivo</i> study, curcumin 50 mg/kg inhibited Keap1 expression and activated Nrf2 system in HFD-fed mice, improved insulin sensitivity, redox homeostasis and inhibited inflammatory signalling	[59]
Keap1/Nrf2	In <i>in vitro</i> study, polypodiside 10 μ M inhibited free radical generation and deposition of glomerular meangial cells under high-glucose conditions by acting as a Keap1-dependent Nrf2 activator Indicated potential to treat microvascular complications	[60]
HDAC3	In <i>in vivo</i> study, RGFP966 10 mg/kg reduced the transendothelial permeability and downregulated the junction proteins in mice by HDAC3 inhibition-mediated miR-200a/Keap1/Nrf2 signalling pathway	[61]

HDAC3 In *in vivo* study, RGFP966 10 mg/kg reduced the endothelial injury [47]
under T2DM condition by HDAC3 inhibition-mediated Keap1–
Nrf2–Nox4 signalling pathway

Abbreviations: TLR, Toll like receptor; GPR21, G-protein receptor 21; FFAR1, Free fatty acid receptor1; PTP1B, Protein tyrosine phosphatase 1B; PHD, Prolyl hydroxylase domain; Keap1/Nrf2, Kelch like ECH associated protein 1/ nuclear factor erythroid 2-related factor; HDAC3, Histone deacetylase 3

2.3.1 Toll like receptors

These receptors (TLRs) plays essential role in the generation of innate immune responses [62]. TLRs are composed of ectodomain with leucine-rich repeats, which mediates recognition of pathogen-associated molecular pattern, a transmembrane domain and a cytoplasmic Toll/IL-1 receptor domain, which stimulates downstream signalling cascades [62]. These receptors are of two types depending on to their locality i.e., cell-surface TLRs and intracellular TLRs. Cell-surface TLRs (i.e., TLR-2 and 4) are the important mediators of insulin resistance and its comorbidities [63]. Notably, TLR-2 and 4 are found on many insulin sensitive cells such as, liver, adipose tissue, skeletal muscles, brain, pancreatic β cells and vasculature [63,64]. Their activation induces inflammation associated insulin resistance in obese states [63]. Elevated levels of exogenous ligands (i.e., dietary fat) and endogenous ligands (i.e., free fat) in obesity, stimulates activation of these receptors [63].

The TLR-2 activation initiates MAPK and MyD88-dependent pathways [42]. The activation of MyD88 results in phosphorylation and induction of pro-inflammatory transcription factors such as IRF3, IRF7, AP-1 and NF κ B [42,64]. TLR-4 activation initiates two signalling pathways, i.e., MyD88/TIRAP, which stimulates IKK, p38, JNK, AP1 and NF κ B, which initiates the expression of pro-inflammatory cytokines. The second pathway is regulated via TRAM and TRIF, which needs TLR-4 uptake for cell-entry. This activates IKK, NF κ B and IRF-3, which activates type-1 interferon genes [63]. Such cascades dampen the insulin action directly by inducing inflammatory cascade and oxidative stress, and indirectly by activating cytokine signalling cascades with generation of inflammatory and insulin desensitizing factors. Largely, these pathways inhibit the components of insulin signalling via IRS1 serine phosphorylation [63].

Several reports have claimed that the elevated gene expression of these TLRs promotes high glucose-induced catabolic and inflammatory responses in patients with T2DM [65]. Reyna *et al.* (2008), reported elevated gene expression of TLR-4 and protein content in skeletal muscles of obese and T2DM patients.

This study reported increased TLR-4 driven (I κ B/NF κ B) signalling in muscles of insulin resistant patients. Therefore, blocking of TLR-4 signalling can be effective in enhancing insulin sensitivity in insulin resistant patients [66]. Dasu *et al.* (2010) reported elevated mRNA expression levels of TLR-2 and 4, and protein in monocytes of T2DM patients ($p < 0.05$) with respect to control patients. Ligands such as TLR-2 and 4 such as heat shock protein 60 and 70; endotoxin, hyaluronan levels, and TLR-MyD88-NF κ B signaling were found elevated in newly diagnosed T2DM patients [67]. Kuo *et al.* (2011) reported that the genetically modified obese mice without TLR-2 ameliorated glucose intolerance and IR despite the administration of fat rich diet. Such effect was observed because of reduced transcription of genes expressing for inflammatory cytokines and stimulation of extracellular signal-regulated kinase in liver. This study indicated that the obese mice without TLR-2 fed with fat rich diet could be resistant from obesity and adipocyte hypertrophy-induced IR [64].

2.3.2 Glucagon receptor

Glucagon receptor is a G-protein receptor found on plasma membrane and has binding affinity for glucagon. The activation of this receptor induces gluconeogenesis by increasing the transcription of glucose 6-phosphatase and phosphoenolpyruvate carboxykinase enzymes via protein kinase-A pathway. Protein kinase-A also elevates fructose 1, 6 bisphosphate levels by stimulating the activity of pyruvate kinase, which inhibits glycolysis. In addition to this, inhibits glycogen synthase, which induces the conversion of glycogen into glucose-1-phosphate. The overall effect results in increase hepatic glucose production [68]. With this context, various studies claimed the role of glucagon receptor in insulin resistance. Conarello *et al.* (2007), reported that the targeting of glucagon receptor gene deletion can provide improved plasma glucose levels and good metabolic control in T2DM patients. In one of the studies, glucagon knockout mice fed with normal diet exhibited reduced plasma glucose levels, ameliorated oral and intraperitoneal glucose intolerance in comparison with wild-type mice. In addition, augmented the GLP-1 (glucagon like peptide-1) levels and induced resistivity for STZ-induced degeneration of pancreatic β -cell resulting in T1DM [69]. Similarly, Christensen *et al.* (2011), using animal models revealed that the blockade of glucagon receptor reduces glucose and triglycerides (TGs) levels, and increases GLP-1 levels [51]. In contrary to this, Gelling *et al.* (2009) revealed that the overexpression of glucagon receptor on pancreatic β cells can provide protective effect against hyperglycemia and impaired glucose tolerance (Gelling 2009). In *in-vivo* study, mice

overexpressing glucagon receptor on pancreatic β -cells. This exhibited increased glucose levels (3.9-folds) and insulin levels (50%) in mice in comparison to control. Moreover, insulin resistance was successfully induced upon administration of high fat diet in mice overexpressing glucagon receptor and in control to similar extent. However, severity of fasting blood glucose levels and glucose intolerance was less in mice overexpressing glucagon receptor with respect to control [70].

2.3.3 G-protein receptor 21

GPR21 claimed to have a significant importance in the development of obesity associated T2DM. Its increased expression levels have been identified in C57BL/6J mice [44]. Its highest levels have been identified in hypothalamus, macrophages and spleen of the diabetic mice [44,71,72]. Overexpression studies on HEK293 cells revealed that the activation of this receptor increases phosphorylation of JNK, ERK, p38, and PKC δ , which inhibits insulin signaling. However, the influence of GPR21 on insulin signaling in the presence of serum was found less due to the presence of native inhibitory ligand in the serum [44]. Homology modelling and ligand docking studies identified the compound named GRA2 as an inverse agonist of GPR21 [44]. With this agreement, Gardner *et al.* (2011), in an *in vivo* study revealed that the GPR21 knockout mice were resistant to diet-induced obesity ($p < 0.001$) and displayed improved glucose tolerance ($p < 0.0001$) with reduced inflammatory markers ($p < 0.01$) in comparison to wild-type mice [72]. Similarly, Osborn *et al.* (2011), revealed that the deletion of GPR21 receptor in the HFD-fed mice remarkably reduced the pro-inflammatory gene expression in the adipocytes and liver ($p < 0.05$), which led to increased insulin sensitivity [71].

2.3.4 Free fatty acid receptor 1

This receptor (FFAR1) is a G-protein receptor encoded by FFAR1 gene and are highly expressed in pancreatic islet cells and enteroendocrine cells [73]. Activation of FFAR1 have been suggested to possess potential benefits to treat T2DM by facilitating glucose-induced insulin release and release of incretin hormones [74]. This receptor is also known as G-protein-coupled receptor 40 (GPR40). Various studies have claimed their role in reducing plasma glucose levels [75]. Steneberg *et al.* (2005), reported divergent role of FFAR1 on insulin release from β -cells. In agreement to this, GPR40 deficient β -cells released low levels of insulin towards its respective ligand (free fatty acid). However, deletion of this receptor ameliorated obesity-induced hyperglycaemia, hyperinsulinemia, glucose intolerance, and hypertriglyceridemia in mice. Therefore,

this receptor exerts both acute and severe effects on insulin release and its overexpression is associated with metabolic diseases [76].

Nagasumi *et al.* (2009), claimed that the transgenic mice with highly activated hGPR40 gene displayed higher production of insulin with respect to hyperglycaemia ($p < 0.01$) in comparison to nontransgenic mice. In addition, transgenic mice found resistant to HFD-induced glucose intolerance [77].

2.3.5 Protein tyrosine phosphatase 1B

This protein (PTP1B) is a 435 amino acid protein and is the first enzyme isolated from human placental tissue. It is mainly localized on the surface of endoplasmic reticulum [78]. It is the major insulin receptor phosphatase in liver and muscles [79]. It acts as a negative regulator of insulin action via dephosphorylating the insulin receptor [78]. In addition, it also acts as a negative regulator of leptin signalling [56]. Therefore, it could be an ideal target for the prophylaxis of T2DM and obesity [78]. Goldstein, 2001, reported that the in the genetically modified mice with reduced PTP1B expression exhibited improved insulin signalling and glucose tolerance. In addition, PTP1B inhibition helps in reducing storage of triglycerides in fat tissues under HFD treatment [80].

Similarly, Ramachandran *et al.* 2003, revealed that PTP1B deficient mice ameliorated IR with improve glucose levels with respect to wild-type control. In addition to this, PTP1B deficient mice showed resistivity to HFD-induced obesity, which could be due to lack of insulin sensitivity in adipocytes. Thus, this study indicated that the deficiency of PTP1B produces insulin-sensitizing phenotype that could be beneficial to treat hyperglycemia [78]. Recently, thiazolidinediones derivatives reported as promising PTP1B inhibitors [56].

2.3.6 Prolyl hydroxylase domain enzyme

Prolyl hydroxylase domain (PHD) have significant importance in the modulation of hypoxia-induced factor proteins (HIF α), which contributes in balancing glucose and lipid metabolism in healthy and diabetic patients [81]. However, under hypoxic environment, this enzyme is suppressed and the stability of HIF α and its protein expression increases. Several studies have claimed that the expression of HIF-1 α upregulates in adipocytes and liver during obese state that contributes to insulin resistance. Increased expression of HIF-2 α in liver and adipocytes reported to play protective role against HFD-induced glucose intolerance and inflammation by

increasing *Irs2* expression. Thus, the PHD enzyme can be an ideal therapeutic target to treat T2DM and diabetes [57]. The inhibition of PHD enzyme in obese mice improved glucose tolerance and insulin resistance. The underlying mechanism reported for glucose control is via HIF-2 α -dependent increase in *Irs2* and cAMP-specific PDE gene expression in liver [57].

2.3.7 Nuclear-response factor 2

The oxidative stress long back claimed to be a major perturbing factor in the development of IR [59]. The oxidative stress under IR conditions is known to be regulated by Kelch like ECH associated protein 1/ nuclear factor erythroid 2-related factor (Keap1/Nrf2). Keap1 is known to have significant importance in the modulation of oxidative stress/redox metabolism by interacting with Nrf2 [46,82]. Keap1 targets Nrf2 for polyubiquitination and degradation by the ubiquitin/proteasome system [59]. It consists of four protein domains and encoded by Keap1 gene [46,82]. Under oxidative stress conditions, Keap1 sense redox alterations and dissociates from Nrf2 for the induction of Nrf2 translocation to nucleus to activate the transcription of antioxidant enzymes [59]. In one of the studies, Nrf2 knockout mice showed reduced insulin release from β -cells. The upregulation of Nrf2 reported to improve insulin-releasing potential of pancreatic β -cells [83]. In the other study, Keap1 knockout in mice resulted in increased expression of Nrf2, which improved mitochondrial redox homeostasis, insulin sensitivity and obesity in mice [83].

2.3.8 Histone deacetylase 3

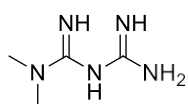
Recently, histone deacetylase 3 (HDAC3) have received tremendous attention as a potential target in T2DM [84]. Inhibition of HDAC3 has been suggested as a new therapeutic intervention in T2DM [84]. Sathiskumar *et al.* (2016), reported increased mRNA levels of HDAC3 in T2DM patients ($p < 0.05$) with respect to control. The increased activity of HDAC3 resulted in significantly higher levels of pro-inflammatory mediators in T2DM patients ($p < 0.05$) with respect to control. Thus indicated the association of HDAC3 with pro-inflammation and IR in diabetics [84]. Fu *et al.* (2020), revealed that the expression of HDAC3 in retinal ganglionic cells of *db/db* mice having increased body wt. and blood sugar levels was greater ($p < 0.01$) than control. Thus, this study indicated the role of HDAC3 inhibition to treat diabetic retinopathy [85]. Zhao *et al.* (2019), reported the increased mRNA/protein expression and activity of HDAC3 in the hippocampus and cortex region ($p < 0.05$) of *db/db* mice as compared to non-

hyperglycemic control, which contributes to neurovascular complications in T2DM [61]. Huang *et al.* (2021), revealed that the increased expression of HDAC3 in *db/db* mice elevates oxidative stress by interacting with Nrf2 signalling, which leads to endothelial impairments or T2DM-associated cardiovascular diseases. Thus, the inhibition of HDAC3 can be advantageous in the management of IR and its related comorbidities [47].

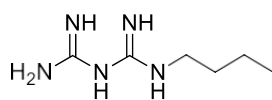
2.4 Major Antidiabetic drug families

Oral anti-hyperglycemic drugs are commonly employed for treating T2DM for many years given their worth and suitability. Metformin and sulfonylureas are the first line agents employed for more than 50 years and their main secondary complications are extensively known [86]. In addition to this, there are glinides, thiazolidinediones (TZD), α -glucosidase inhibitors, dipeptidyl peptidase-4 inhibitors (DPP-4I) and the recently introduced sodium-glucose cotransporter-2 inhibitors (SGCT-2I). The chemical structures of some of the commonly used oral anti-hyperglycemic drugs are presented in *Fig 2.1*.

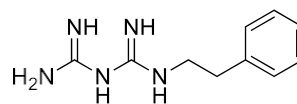
Biguanide



Metformin

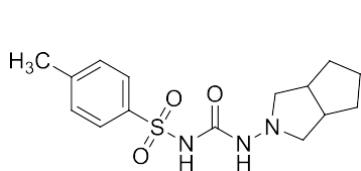


Buformin

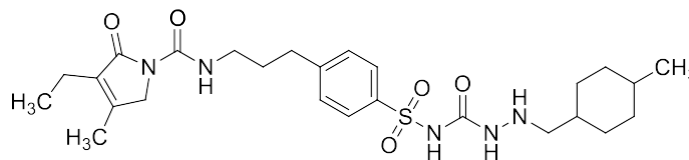


Phenformin

Sulfonylurea

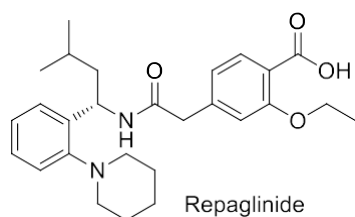


Gliclazide



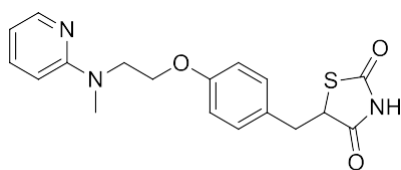
Glipizide

Glinide

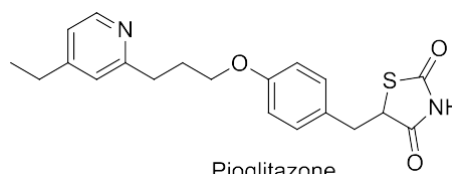


Repaglinide

Thiazolidinediones



Rosiglitazone



Pioglitazone

Fig 2.1: Currently available oral anti-hyperglycemic drugs

2.4.1 Sulfonylureas

Sulfonylureas (SUs) were the first oral antidiabetic agents approved by FDA, starting in 1958. Their origin is tracked to the observation in 1942, that some sulfonamide antibacterial products triggered critical hypoglycaemia in typhoid patients [2]. These are produced from substitution at a para position on benzene ring, and at one nitrogen residue of urea moiety [87]. First-generation SUs are rarely used, as they carry a great risk of hypoglycemia in contrast to modern SUs. In addition to this, they are not used in patients with cardiovascular diseases, liver, and renal dysfunction, as well as those exhibiting hypersensitivity to the drug.

2.4.1.1 Mechanism of action

SUs act as insulin secretagogues by modulating ATP sensitive potassium ion channels (K_{ATP} channel), via sulfonylurea receptor present on the pancreatic beta-cell membrane. SUs binds with K_{ATP} channel and causes its inhibition, that leads to an increase in the

concentration of K^+ ions in the cytoplasm of beta-cells, and depolarizes calcium ion channels. This leads to the increased influx of calcium ions into the beta-cell, that provoke exocytosis of insulin granules and stimulate insulin release. To some extent, SUs also binds and activates Epac2 (guanine nucleotide exchange factor), which further works together with Rap1 protein to increase the approachability of insulin vesicles, to meld with the plasma membrane of the beta cell [88].

2.4.1.2 Extra-pancreatic actions

Increased expression of glucose transporter GLUT-4 in the periphery, and reduced peripheral insulin resistance are recognized. Suppression of sarcolemma and mitochondrial ATP channels on cardiac cells, and K_{ATP} channels on smooth muscle cells, by binding with sulfonylurea receptor SUR2A that causes cardiovascular complications, is also mentioned. Gliclazide causes reduced hepatic glucose output, with anti-oxidant and antiplatelet effect. Gly in turn, aggravates blood pressure due to sympathetic activation [89].

2.4.1.3 Efficacy

All SUs are equally efficacious at equipotent doses. Therapy is initiated from a lower dose range, on the basis of glycaemic control. Longer-acting SUs are administered as a single dose daily and rest is available in extended-release dosage forms (glipizide) or micronized tablets (glyburide), to prolong the duration of action and the dose is kept lower. SUs reduce glycated haemoglobin by 1.5% to 2%, with a fasting plasma glucose (FPG) decrease of up to 60-70mg/dL. Usually, primary failure of SU monotherapy is seen in patients with low C-peptide levels and high FPG levels (>250 mg/dL). In such patients, SUs cause less than 30mg/dl decrease in FPG levels. Almost 75% of the patients come under secondary failure on SU monotherapy, initially responding well (>30mg/dL reduction in FPG), however failing to reach acceptable glucose control [87,90].

2.4.1.4 Adverse effects

Older SU drugs (glimepiride, Gly, glipizide, gliclazide) are reported to induce weight gain of 1.8-2.6kg in previous studies [91]. Modern SUs (glimepiride, gliclazide) are widely preferred over SUs due to less risk of hypoglycaemia, weight gain, and cardiovascular complications. The Scottish Intercollegiate Guidelines Network, International Diabetes Federation and National Institute for Health and Care Excellence recommend SUs use in patients who are not obese. Weight neutrality is reported with glimepiride extended release and gliclazide modified release during the period of 1

year. Regular consumption of glimepiride produces weight neutrality for about 1.5 years [89]. Due to the narrow therapeutic index, SUs even in small doses can induce hypoglycaemia in paediatrics and geriatrics. High doses can cause chronic hypoglycaemia (less than 60 mg/dL), rarely leading to death due to neuroglycopenia and cardiotoxicity [92].

2.4.2 Glinides (Meglitinides /D-Phenylalanine analogs)

This class of anti-diabetic drugs includes repaglinide and nateglinide, which act as ATP-sensitive potassium channel blockers. They are also insulin secretagogues, and are sometimes named as prandial glucose regulators. They have similar mechanism of action (MOA) as SUs but are structurally unrelated. The first agent of this class, repaglinide was approved by FDA in 1997, and nateglinide in 2000. They are rapidly absorbed and have a short duration of action, in contrast to second-generation SUs, thus flexible dosage can be designed [93]. They are contraindicated in diabetic ketoacidosis, hypersensitivity, renal and liver diseases. Repaglinide is contraindicated in patients on lipid-lowering gemfibrozil, as it can increase repaglinide blood levels by 28.6 folds [94].

2.4.2.1 Mechanism of action

Both meglitinides, analogously to SUs, block ATP-dependent potassium ion channels, causing insulin release from pancreatic beta-cells. Repaglinide is derived from benzoic acid, while nateglinide is derived from d-phenylalanine [87]. Meglitinides bind to sulfonylurea receptor SUR1, and are also reported to bind at a separate site on beta-cells. Nateglinide shows larger selectivity for SUR1 over SUR2, in contrast to repaglinide and SUs. Nateglinide remains binded to the receptor for a very limited period of about 2 secs, contrasting with repaglinide which stays for 3min, whereas the dissociation from the receptor is 90 times greater than repaglinide. Therefore nateglinide has a very limited on-off impact on insulin discharge [95].

2.4.2.2 Efficacy

These agents are reported to treat long term hyperglycaemic stages in patients with T2DM. In a 3.6 months' clinical trial, repaglinide (0.5-4 mg/meal) reduced glycosylated haemoglobin levels by 1.57%, while nateglinide (60-120 mg/meal) achieved 1.04% decrease. Repaglinide reduced pre-prandial glucose values by 57 mg/dL while nateglinide by 18 mg/dL, in a period of 16 weeks [96].

2.4.2.3 Adverse effects

Patients on repaglinide suffer weight gain of 1.8 kg and with nateglinide 0.7 kg, after 3.6 months of therapy [96]. Meglitinides are indeed associated with minor to moderate weight gain, as per a report by the American Association of Diabetes Educators 2016 [31]. Meglitinides are associated with hypoglycaemia (16 to 31%) and weight gain, however less remarkably than SUs [97].

2.4.3 Biguanides

Guanidine is the active ingredient in *Galega officinalis*, a small tree found in Europe and Western Asia, which was prescribed in primitive times for diabetic patients. However, guanidine and derivatives showed toxicity. First generation biguanides (phenformin and buformin) were introduced for diabetes pharmacotherapy in 1950. In 1970 phenformin was withdrawn due to cardiac mortality and lactic acidosis. Metformin appeared as a safer alternative and was approved in the USA in 1995. Now it is one of the most widely prescribed antidiabetic agents [98]. Caution is advised for patients liable to display metabolic acidosis including renal insufficiency, hepatic failure, alcoholism, congestive heart failure (CHF), sepsis, and surgery. Certain studies reported the safety of metformin with stable CHF, resulting in reduced mortality rates [2].

2.4.3.1 Mechanism of action

Metformin is an AMPK (AMP-dependent protein kinase) activator. When cellular energy stores are reduced, AMPK is stimulated by phosphorylation. Stimulated AMPK initiates the process of fatty acid oxidation and glucose uptake, reducing lipid production and gluconeogenesis. The net outcome of such actions is decreased hepatic glucose output, enhanced insulin sensitivity in fat cells and muscles, enhanced storage of glycogen in skeletal muscles and reduces blood glucose levels. The exact mechanism by which metformin stimulates AMPK is unknown. Metformin has shown reduced cellular respiration by selectively affecting mitochondrial complex I. It does not disturb the discharge of any islet hormones, and hardly causes hypoglycemia [87].

2.4.3.2 Efficacy

Metformin decreases glycosylated haemoglobin levels by 1.5%-2%, with FPG reduction by 60-80 mg/dL. It is acceptable even in cases of extremely high post prandial glucose (PPG) (>300 mg/dL), and is also able to reduce TGs and LDL-C by 8%-15%, with a slight increase in HDL-C by 2%. It stimulates plasminogen activator inhibitor-1, and induces decrease in weight by 2 to 3kg [90].

2.4.3.3 Adverse effects

Metformin is recommended for diabetes patients on account of suppression of hepatic gluconeogenesis, increased insulin sensitivity in peripheral tissue, and some degree of anorexia. Approximately 31% reduction in episodes of T2DM in highly obese patients has been achieved by metformin as stated by Diabetes prevention program (DPP) clinical trial [99]. Combination of metformin with lifestyle modification has shown improvement in gestational diabetes [91]. Gastrointestinal symptoms (10-25%) can include dyspepsia, diarrhoea, nausea, and intestinal muscle spasm. Dosage tapering or intake with meal can be helpful. Reduced levels of cobalamin (20-30%) in malabsorption is a possibility. Overdose, or regular use of metformin for years, can rarely precipitate metabolic acidosis (3-6 /100,000 patients) [87].

2.4.4 Thiazolidinediones (TZDs)

TZDs (insulin sensitizers) were approved for clinical use by FDA in 1997, though controversies surrounded the first agent of this class, troglitazone. Troglitazone was withdrawn from the market due to liver toxicity [86]. Pioglitazone is the only widely used TZD, as rosiglitazone was also withdrawn in some countries in terms of cardiovascular safety [91]. In patients with New York Heart Association (NYHA) class III and IV cardiac failure, and even in class I and II patients, caution is advised [90].

2.4.4.1 Mechanism of action

TZDs or glitazones are the selective synthetic ligands of nuclear peroxisome-proliferator-activated receptor gamma (PPAR γ) [100]. Such types of receptors are a subfamily of 48-member nuclear γ -receptors, and regulate transcription of genes linked to glucose and lipid metabolism [87,100]. PPAR γ is mainly expressed in adipocytes, with minor findings on skeletal, cardiac, smooth muscle cells, pancreatic β -cells, macrophages, and vascular endothelial cells [87]. Hence adipose tissue is the main target of PPAR γ agonists. However, there is no evidence whether TZDs reduces insulin resistance by directly acting on to the target tissues, or indirectly through the release of secreted products by adipocytes such as adiponectin, that increases insulin sensitivity. TZDs binding with PPAR γ receptor induce a conformational change, and form a heterodimer with another nuclear receptor (retinoid X receptor), which then further binds with peroxisome proliferator response element. Such activation causes adipocyte differentiation, increases subcutaneous fat cells, FFA oxidation, FFA uptake into adipocytes, and storage from extra-adipose tissues to adipose tissues. Such effects enhance insulin sensitivity at fat cells, muscles, and liver. [87,90,100].

2.4.4.2 Efficacy

Pioglitazone or rosiglitazone therapy for 6 months, decreases glycosylated haemoglobin by 1.5%, and PPG level by 60-70 mg/dL at a higher dose. TZDs slowly reduce blood glucose levels for about 3-4 months, after which the highest glucose response is seen. Patients must be counselled regarding such point, so that they continue therapy without any drop-out [87,90].

2.4.4.3 Adverse effects

A weight gain of 3.6 kg after 35 months has been registered in a large trial [101]. TZDs lead to weight gain of up to 3-4 kg in 6 months and 5kg in 3-5 years as per UKPDS [102]. Weight gain varies on the basis of dose regimen used [103]. These agents also affect lipid parameters such as TGs, LDL-C and HDL-C. Pioglitazone reduces triglyceride levels by 10% to 20% while rosiglitazone has a neutral effect. Rosiglitazone increases LDL-C up to 5% to 15%, whereas pioglitazone is devoid of such effect. Both are able to alter minor, dense LDL-C particles to bulky soft particles, which are less dense and less atherogenic, and also increase HDL-C up to 3 to 9 mg/dL [90].

TZDs as single oral anti-diabetic agents do not produce hypoglycaemia, whereas combination with SUs can slightly increase the risk [104]. Other adverse effect includes edema (2-4%) due to sodium/water retention and enhanced vascular permeability, cardiac failure and weight gain. The severity of edema (approx. 15%) increases in combination with insulin. Edema is dose-dependent so, by dropping the dose and using diuretics, alleviation could follow, especially if edema is not severe [90].

2.4.5 GLP-1 receptor agonists (Injectable drugs)

These are also called incretin mimetics. Incretins are hormones produced by epithelial intestinal L-cells, in response to food ingested: GIP (glucose-dependent insulinotropic polypeptide) and GLP-1 (glucagon-like peptide 1). GLP-1 administration reduces blood glucose levels by mediating insulin release, and also inhibits it when the glucose level is normal, while GIP is not clinically effective in T2DM patients. [87,105,106].

Pancreatic α -cells produce and split proglucagon into glucagon and a large peptide (C-terminal) comprising GLPs (GLP-1 and GLP-2), whereas intestinal L-cells transform proglucagon into a large peptide (N-terminal) comprising glucagon or GLPs. GLP-2 is of little importance for diabetes management. It mainly influences epithelial cell proliferation in the digestive tract, hence it has been approved as an orphan drug (teduglutide; GLP-2 agonist) for the treatment of short bowel syndrome, by both the

FDA and the European Medicine Agency [87]. Family history of medullary carcinoma of the thyroid, and patients with multiple endocrine neoplasias, should avoid such therapy. Caution is advised in the presence of gastroesophageal reflux [105].

2.4.5.1 Mechanism of action

There are two GLP-1 receptor agonists (exenatide and liraglutide) prescribed intravenously for type 2 diabetic subjects. These agents increase insulin secretion which is glucose-dependent, inhibit glucagon, slow gastric emptying, reduce appetite and body weight, and normalize pre-prandial and postprandial glucose levels, by stimulating GLP-1 receptor [87,107]. These receptors are G-protein coupled receptors (GPCR) expressed in pancreatic alpha-cells, beta-cells, specific neurons in hindbrain, intestinal cells, and other structures.

Beta-cell functioning is required for incretin-based therapy; else it could lead to failure [108]. GLP-1 as such has limited therapeutic potential, due to rapid degradation by dipeptidyl peptidase 4 enzyme (DPP-4), consequently half-life is just 2-3min. The enzyme is mainly expressed in luminal capillary endothelial cells, kidney, gastrointestinal mucosa, and immune cells. To increase the half-life, DPP-4 resistant GLP-1 agonists have been produced. Use of DPP-4I potentiates the pharmacological action of incretin-based therapy [87,108].

2.4.5.2 Exenatide

It is a synthetic exendin-4, potent, DPP-4 resistant, GLP-1 agonist which is short-acting. It is injected subcutaneously twice daily, with a plasma half-life of 3 hours, and acts for about 6-10 hrs. It can be used as monotherapy or in combination with metformin, SUs, or TZDs if required. It reduces glycosylated haemoglobin by 1% in patients with T2DM, after 6.9-18.8 months [87,108,109].

2.4.5.3 Liraglutide

It is rigidly bound to a plasma protein that accounts for increased plasma half-life of > 12h, and thus acts for > 24hrs. Due to its prolonged plasma half-life, it is given subcutaneously once daily. It reduces glycosylated haemoglobin by 30%, which is greater than exenatide. It can be used as monotherapy, or in combination with metformin, SUs, or TZDs [87,108,109].

2.4.5.4 Adverse effects

Patients on exenatide show weight reduction of 2.5 kg to 4 kg within 30 to 82 weeks of therapy, whereas liraglutide can be followed by weight reduction of 5.6 kg, in obese non-diabetic or diabetic patients. Therefore, it can also be used as an anti-obesity drug

[87,108,109]. Nausea, vomiting, and diarrhoea are common (40-50%) and dose-related. Hypoglycaemia is rarely reported with GLP analogues, except when used in combination with SUs [87,108].

2.4.6 DPP-4 inhibitors

DPP-4 belongs to the family of prolyl oligopeptidases. It is a serine protease highly expressed on intestinal epithelial cells, brush-border renal cells, pancreatic cells, hepatic cells, endothelial cells, glandular epithelium, and T-cells. It is also called as T-cell differentiation antigen (CD26). DPP-4 protein consists of an extracellular domain, with the catalytic site in the C-terminal attached to the transmembrane protein, and an intracellular tail at the N-terminal. When it is cleaved it discharges the extracellular domain in the blood, in the form of soluble DPP-4, and also circulates in body fluids (seminal and cerebrospinal fluids) [110].

The extracellular domain of the protein also contains glycosylation and cysteine-rich sites, that contribute to non-enzymatic actions of DPP-4. Such sites are believed to interact with adenosine deaminase, streptokinase, plasminogen, and are also a binding site for chemokines. The antidiabetic effect of DPP-4I was evaluated after the investigations about inactivation of incretin hormones by DPP-4 [110]. DPP-4I are identified to enhance plasma half-life of incretin-based therapy. The first DPP-4I sitagliptin was approved by FDA in 2006. After this saxagliptin was approved in the US and vildagliptin in Europe and America, as monotherapy or combination therapy with other anti-diabetics. DPP-4I linagliptin and alogliptin are also available [111]. Hypersensitive persons, and those with chronic pancreatitis and renal diseases are not safe candidates for such therapy [112].

2.4.6.1 Mechanism of action

Due to the essential role of DPP-4 enzyme in inactivation of incretin hormones, orally active inhibitor drugs of this enzyme have been produced. These are indirectly acting insulin-secreting agents and are mostly used in combination therapy [87,108]. DPP-4I such as sitagliptin, vildagliptin, and saxagliptin are selective competitive inhibitors of DPP-4, with high affinity for the enzyme. The concentration of physiologically produced GLP-1 and GIP after food intake was doubled with DPP-4I. Such selective inhibition of enzyme provides an extended safety profile and allows prolonged treatment with DPP-4I.

It indirectly increases insulin secretion and inhibition of glucagon in patients with T2DM. DPP-4I are also reported to counter-regulate glucagon release by pancreatic

alpha-cells under hypoglycaemia. Thus, these agents do not cause alpha-cell dysfunction, and improve alpha-cell sensitivity to glucose without affecting appetite. Experimental beta-cell neogenesis was demonstrated, and genetically DPP-4 deficient rats showed resistance to streptozotocin (STZ) induced beta-cell destruction. These drugs also improve TGs and FFA levels [87,113].

2.4.6.2 Efficacy

Sitagliptin has been shown to reduce glycosylated haemoglobin by 0.65% to 1.0% within 2 to 7 months, and 0.67% upon 12 months of therapy. Saxagliptin reduces glycosylated haemoglobin by 0.43 to 1.17%, while vildagliptin reduces by 1.4% in 24 weeks of therapy. In terms of anti-hyperglycaemic effect, DPP-4I were found to be slightly less effective than SUs, and equivalent to metformin and TZDs [111,114].

2.4.6.3 Adverse effects

Sitagliptin during 12 months triggered weight reduction of 1.5 kg, up to weight gain of 1.8kg. Vildagliptin and saxagliptin were not much different: weight shifts of - 1.8 kg to +1.3 kg, and -1.8 kg to + 0.7 kg, respectively, after 5 months. In a meta-analysis of 13 studies they were considered to be weight neutral [111].

A slight effect on *in-vitro* immune cell functions has been seen with DPP-4I, and allergic reactions such as anaphylaxis, angioedema, Stevens-Johnson syndrome, flu-like symptoms, and skin reactions are reported. Hypoglycaemia is observed during combination therapy of DPP-4I with SUs and insulin [87,111,115].

2.4.7 α -glucosidase inhibitors

The α -glucosidase enzyme is released by the chorionic epithelium of enterocytes, with the function of digestion of carbohydrates and glucose production. Due to its important role in glucose production, various alpha-glucosidase inhibitors were produced as a new class of oral hypoglycemic agents in 1980s. They are obtained from natural sources including plants and micro-organisms. The alpha-glucosidase enzymes from rodent intestine and from yeast are employed for pharmacological purposes. They include acarbose, miglitol and voglibose [116]. Diabetic ketoacidosis, inflammatory bowel disease, other gastrointestinal conditions, and hypersensitivity are contraindications [117].

2.4.7.1 Mechanism of action

α -glucosidase inhibitors retard intestinal absorption of carbohydrates by preventing alpha-glucosidase action in enterocytes of the brush border of the mucosa. Mouth to cecum transit time is reduced and leads to larger evacuation of carbohydrates via stools. Acarbose, produced by actinobacteria *Actinoplanes utahensis*, as well as voglibose, are reversible inhibitors. These agents also cause the release of GLP-1 in systemic circulation which adds on to the therapeutic action, while miglitol is a powerful inhibitor of the enzyme sucrase [87,108]. Acarbose also inhibits glucoamylase and alpha-amylase enzymes, thus impairing carbohydrate digestion and absorption [118].

2.4.7.2 Efficacy

Post-prandial glucose concentration diminishes by 1-3 mmol/L and pre-prandial glucose concentration by 1 mmol/L. Also glycated haemoglobin can be lowered by 0.5% to 0.8%, and even can exceed 1% at higher doses, however proper maintenance of diet is a must. Body wt. and lipid parameters remain unchanged. Long term administration of these agents in prediabetes can prevent the onset of T2DM and heart disease. Both monotherapy and combination protocols are available [87,119].

2.4.7.3 Adverse effects

Flatulence (78%) and loose stools (14%) are dose-related. In certain cases, hepatitis is reported, that reverts when therapy is stopped [118].

2.4.8 Sodium-glucose co-transporter-2 inhibitors/Gliflozins

These are the FDA-approved latest class of anti-diabetics. Primarily introduced in 2013, sodium-glucose co-transporter-2 (SGCT-2) inhibitors consist of canagliflozin, dapagliflozin, ertugliflozin, and empagliflozin, which can be used as monotherapy, or in combination with metformin and linagliptin. These agents are reported to reduce the incidence of mortality due to cardiac diseases in patients with T2DM [120–122]. These are contraindicated in patients with kidney diseases or nephropathy (GFR < 45 mL/min/1.73m²) [122].

2.4.8.1 Mechanism of action

The glomerulus of the kidney filters all the circulating glucose, which is reabsorbed into the blood via SGCT-2 of the proximal convoluted tubule. These transporters cause 90% reabsorption of filtered glucose, so these are an interesting target for T2DM. Inhibition of this co-transporter promotes glucouresis, and lowers blood glucose levels along with weight reduction [108,122]. Empagliflozin has maximum specificity for SGCT-2, while canagliflozin is least specific.

These drugs can also be used in obese individuals, due to their weight reduction effect [122].

2.4.8.2 Efficacy

They are useful in all the stages of T2DM because the mechanism of action is independent of beta-cell function. Hypoglycaemia can occur if these agents are used in combination with an insulin secretagogue [123]. SGCT-2 inhibitors showed 9.1% reduction of glycated haemoglobin at baseline, 0.9% in 1 month and 0.8% in 6 months of therapy [124].

2.4.8.3 Adverse effects

Weight loss of 2.6 kg in 6 months of therapy is documented, due to glucouresis and loss of adipose mass. Apart from body fat these agents also reduce epicardial fat. Extracellular fluid diminishes after 28 days, and return to baseline after 3 to 6 months of therapy [124]. Therefore, SGCT-2 therapy is associated with conspicuous weight loss. They can increase the risk of serious genital anaerobic infections (Fournier's gangrene), and urinary tract infections in diabetic patients [121,122]. The overall properties of the oral anti-hyperglycaemic drugs used in the management of T2DM is presented in **Table 2.2**. In addition, the status of various anti-diabetic drugs under clinical trials are presented in **Table 2.3**.

Table 2.2: Properties of Anti-diabetic agents used in the treatment of T2DM [125]

Class	Drugs	Trade name	Dosage range	HbA1c reduction (%)	Weight changes	Hypoglycaemia	Duration of action
Oral							
Biguanide	Metformin	Glucophage	500-3000 mg	1-2%	Neutral	No	24 h
SGCT-2 inhibitors	Dapagliflozin	Froxiga	5-10 mg	0.6-1.2%	Loss	No	t _{1/2} ~12.9 h
	Canagliflozin	Invokana	100-300 mg				24 h
	Empagliflozin	Jardiance	10-25 mg				t _{1/2} ~12.4 h
	Ertugliflozin	Steglatro	5-15 mg				t _{1/2} ~16.6 h
Meglitinides	Repaglinide	Prandin	0.5-16 mg	1-2%	Gain	Yes	2-6 h
	Nateglinide	Starlix	180-360 mg				2-4 h
DPP-4I	Sitagliptin	Januvia	100 mg	0.5-1%	Neutral	No	24 h
	Vildagliptin	Galvus	50-100 mg				12-24 h
	Saxagliptin	Onglyza	2.5-5 mg				24 h
	Alogliptin	Nesina	25mg				24 h
	Linagliptin	Tradjenta	5 mg				>24 h
TZDs	Pioglitazone	Actos	15-45 mg	0.5-1.4%	Gain	No	24 h
	Rosiglitazone	Avandia	4-8 mg				24 h
Sulfonyl ureas (2 nd generation)	Glyburide	Diabeta	1.25-20mg	1-2%	Gain	Yes	12-24 h
	Glipizide	Glucotrol	5-40mg				12-18 h
	Gliclazide	Bilxona MR	40-320 mg				12-24 h
	Glimepiride	Amaryl	1-8mg				24 h
Alpha-glucosidase inhibitors	Acarbose	Glucobay	25-50/100 mg	0.5-0.8%	Neutral/minor loss	No	1-3 h
	Miglitol	Glyset	25-50/100 mg				1-3 h
Parenteral							
GLP-1 RAs	Exenatide	Bydureon	2mg s.c	0.9-1.6%	Loss	No	6-10 h
	Liraglutide	Victoza	1.2-1.8 mg s.c				24 h

Table 2.3: Drug therapy under investigation for the treatment of diabetes/T2DM

Drug	Sponsor	Phase	Status	Study title/objective	Completion date	References
Trodusquemine (MSI-1436)	Genaera Corporation	I	Completed	Single dose, tolerance and pharmacokinetic study in obese T2DM patients	April 2009	[126]
SAR425899	Sanofi	I	Completed	Safety and tolerability in overweight to obese and T2DM patients	Oct 2018	[127]
KRP-104 (novel DPP-4I)	ActivX Biosciences, Inc.	II	Completed	Randomized, double-blind, placebo-controlled trial to assess safety and effectiveness in T2DM patients	Aug 2008	[128]
Oral ORMD-0801 (oral insulin)	OraMed, Ltd.	II	Completed	Randomized, double blind, placebo controlled, parallel group trial to evaluate safety and efficacy.	April 2016	[129]
LX4211	Lexicon Pharmaceuticals	II	Completed	Assessment of safety, efficacy and tolerability in T2DM patients	Dec 2009	[130]
HOE901-U300 (new formulation of insulin glargine)	Sanofi	III	Completed	Consideration of efficacy between HOE901-U300 and lantus in T2DM patients	March 2014	[129]
Sitagliptin and metformin therapy	The University of Texas Health Science Center at San Antonio	IV	Completed	Assessment of sitagliptin and metformin effects alone and in combination contrast to placebo on liver gluconeogenesis.	Oct 2012	[131]

2.5 Oral/Nasal insulin

Insulin therapy can be used in all modalities of diabetes, including T1DM, T2DM and gestational diabetes. It can be taken subcutaneously, intravenously, intramuscularly, and more recently also orally. The subcutaneous route is classic for long term management of glycaemic control, notably in patients with T1DM [87]. Oral insulin is a long-acting, basal insulin analogue. When target with combination therapy of oral hypoglycaemic agents is not achieved, oral insulin therapy is instigated to control glycosylated haemoglobin levels (A1C) > 7% in type 2 diabetic patients [132].

Oral insulin at high dose, in insulin naive patients with T2DM, seems to be effective in controlling FPG (7.1 mmol/L) levels after 8 weeks, comparable to subcutaneous insulin glargine (6.8 mmol/L), with the absence of any serious adverse effects or hypoglycaemia [132]. Only nasal insulin (Afrezza®), for both T1DM and T2DM patients, is already FDA approved. Afrezza is rapid-acting inhaled insulin and is not a substitute of long-acting insulin. It is taken before a meal or within 20 minutes of starting a meal and can be used along with long-acting insulin in patients with T1DM [133]. The FDA has also approved the first glucagon therapy (Baqsimi® nasal powder) for the emergency management of severe hypoglycaemia [134].

2.6 Pharmacological approaches of the American Diabetes Association (ADA)

Metformin is recommended as the first-line agent for the treatment of T2DM. Metformin therapy should be continued if it is tolerated and not contraindicated. In the long run it causes vitamin B12 deficiency, especially in patients with anaemia or peripheral neuropathy. Therefore, vitamin B12 levels should be monitored [31].

Initially, insulin can be added with anti-diabetic drugs in case of weight loss, hypertriglyceridemia, ketosis, and hyperglycaemia (≥ 300 mg/dL), or glycated haemoglobin (>10%) [135]. Along with active pharmacological agents, lifestyle modification should be considered to improve health. For T2DM patients affected by atherosclerotic cardiovascular disease, SGCT-2 inhibitors and GLP-1 receptor agonists are recommended. For patients at risk of cardiac failure, SGCT-2 inhibitors are ideal. T2DM patients with chronic renal disease should receive SGCT-2 inhibitors and GLP-1 receptor agonists, to prevent the progression of kidney or cardiovascular disease [28].

Among the parenteral drugs to achieve extreme blood glucose reduction, GLP-1 receptor agonists are considered over insulin. After every 3-6 months, anti-diabetic drug regimen should be assessed and adjusted based on clinical assessment [28].

The combination of new anti-diabetic agents with initial therapy should be recommended, to reduce glycated haemoglobin level by 0.7-1%. If glycated haemoglobin levels are not controlled in 3 months without atherosclerotic cardiovascular disease or chronic kidney disease, SUs, TZDs, SGCT-2 inhibitors, GLP-1 agonists, DPP-4I and basal insulin can be combined with metformin, with emphasis on patient factors and treatment selective effects [28].

For obese patients, selection of anti-diabetic drug should be based on effect of body wt. Initially diet modification should be recommended, and can be further combined with exercise and anti-obesity agents ($BMI \geq 27 \text{ kg/m}^2$). Patients receiving anti-obesity agents with weight loss $< 5\%$ in 3 months, or any safety or tolerability issues, should have the prescription discontinued and alternative pharmacological approaches should be taken into account. Anti-diabetic agents having an influence on body weight includes metformin, α -glucosidase inhibitors, SGCT-2 inhibitors, GLP-1 receptor agonists, and amylin mimetics [91].

DPP-4I are weight neutral, while insulin secretagogues, thiazolidinediones, and insulin induce weight gain. For short term and long-term management of obesity ($BMI \geq 27 \text{ kg/m}^2$), all FDA approved agents for weight loss are found to be associated with glycemic control in T2DM patients, or patients at risk of T2DM. Five weight-reducing drugs (or combination of drugs), namely Orlistat, Lorcaserin, Phentermine/ Topiramate (ER), Naltrexone/ Bupropion ER and Liraglutide have been approved by FDA for long term use in patients with obesity-associated T2DM, dyslipidemia, or elevated blood pressure [136]. Therefore, overall approach of oral hypoglycemic agents for the treatment of T2DM by ADA is presented in **Fig 2.2**.

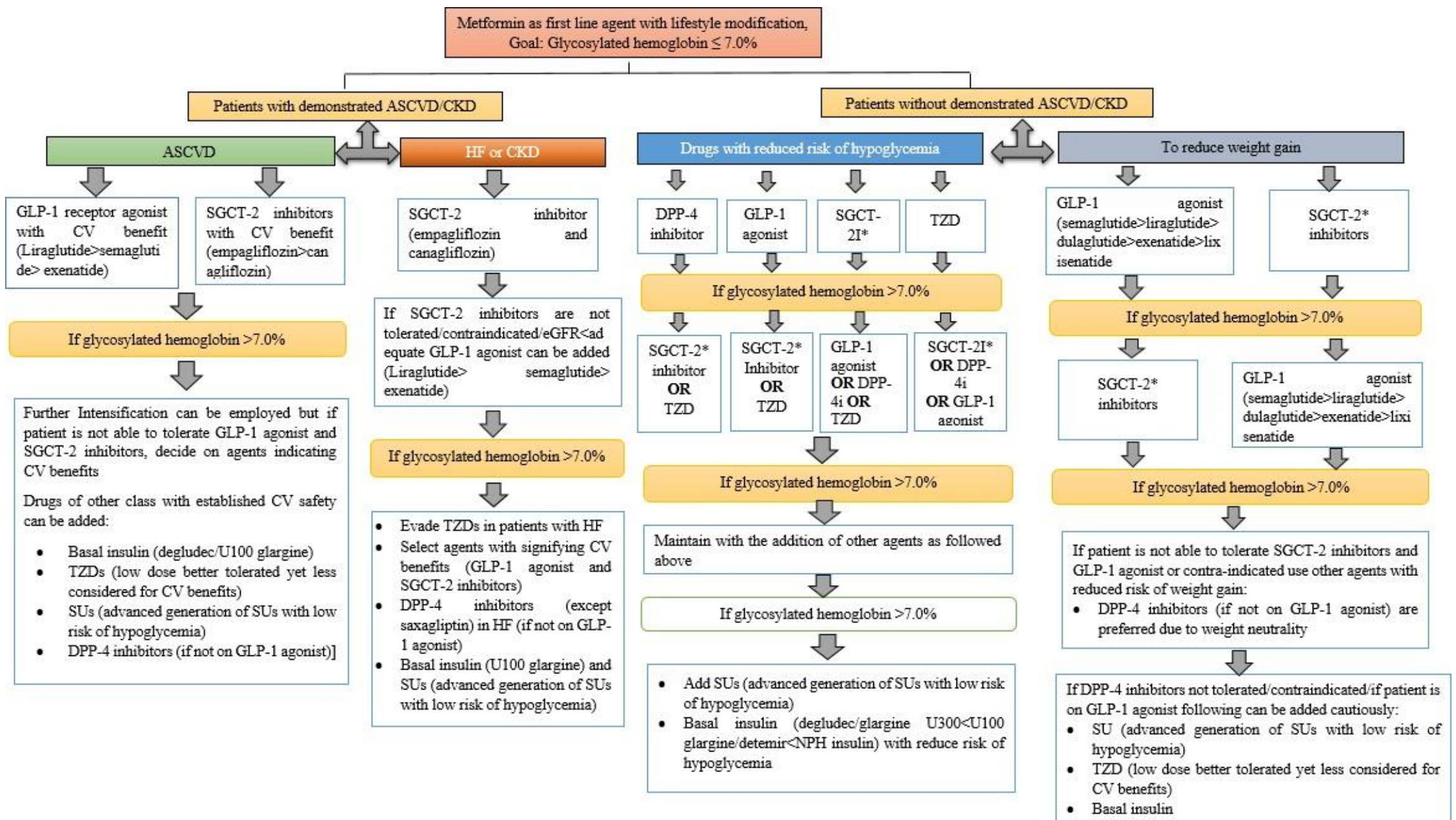


Fig 2.2: Pharmacological approaches based on oral anti-hyperglycemic drugs employed for the management of T2DM by ADA

Abbreviation: eGFR, Estimated glomerular filtration rate; ASCVD, Atherosclerotic vascular disease; HF, Heart failure; CKD, Chronic kidney disease; SGCT-2I, Sodium glucose cotransporter-2 inhibitor, CV, cardiovascular; GLP-1, Glucagon like peptide-1; TZD, Thiazolidinedione's; SU, Sulfonyl urea; DPP-4, Dipeptidyl peptidase -4; SGCT-2I*, Individual agents differ based on zone with respect to specified level of eGFR for commencement and persistent use.

2.7 Advanced treatment strategies for T2DM

The complexity of T2DM i.e., the interplay between genetic, epigenetic and environmental factors, has made its treatment a complicated. Various approaches based on lifestyle modification, anti-diabetic medications and insulin therapy indicated potential in managing T2DM. Here in, the emphasis is on the one of the extensively discovered approaches i.e., nanotechnology based approaches, which are discussed in the subsequent sections.

2.7.1 Nanocarrier-based approaches

The modern developments made in the nanocarrier-based strategies are discussed here in, that primarily includes lipid-based nanocarrier, polymeric micelles (PMs), polymeric nanoparticles, and nanocrystals for the effective treatment of T2DM. A few of the relevant case studies with respect to the above-mentioned delivery systems are presented in *Table 2.4* after section 2.6.1.5.

2.7.1.1 Lipid-based nanocarriers

Lipid based drug delivery systems (LDDS) have gained importance due to their ability to deliver poorly water-soluble drugs. LDDS are widely preferred over conventional dosage forms because of their multifunctional role, good biocompatibility and biodegradability, and in augmenting oral bioavailability of lipophilic drugs [137]. In addition, offers desire release kinetics such as controlled, sustained or extended [138]. These lipid-based oral formulations are generally composed of water-insoluble excipients, triglycerides, surfactants, co-surfactants, co-solvents, simple oils or mixture of oils and many lipids [137]. LDDS enhance the absorption of drug by reducing the particle size to molecular level, and increases drug transport to systemic circulations by altering enterocyte-based transport [137]. Apart from this, LDDS can be solidified into powder or pellets using various techniques pertaining to its stability for oral delivery [137]. The most commonly explored and established LDDS include liposomes [139], niosomes [140], self-nanoemulsifying drug delivery system (SNEDDS), and solid lipid nanoparticles (SLN) [141].

2.7.1.1.1 Liposomes

Liposomes are spherical vesicular nanostructures composed of one or more partially substituted phospholipid bilayers along with cholesterol. It consists of hydrophilic aqueous core and hydrophobic phospholipid tail due to which it can encapsulate both hydrophilic and lipophilic drugs. This composition of liposomes facilitates its use in encapsulating various categories of payloads, due to which its application in drug

delivery systems are increasing rapidly. In addition to this, liposomes have gained importance as potential drug delivery systems owing to their stable lipid bilayer membrane, minimized enzymatic degradation and biocompatibility and cell-specific targeting [142]. One such application of liposomes is that they can be used in increasing the oral bioavailability of drugs [143].

Niu *et al.* (2012), reported that the liposomes composed of different bile salts successfully encapsulated insulin for oral delivery. The different bile salts used for the formation of insulin-loaded liposomes were sodium glycocholate, sodium taurocholate, sodium deoxycholate, and cholesterol. Amongst the different bile salts, sodium glycocholate-liposomes showed the highest increase in the oral bioavailability of insulin, which was 11% in diabetic mice. The developed formulation in *in vivo* study, showed size-dependent antihyperglycemic effect. Sodium glycocholate-liposomes of size > 100 nm exhibited rapid decrease in blood glucose levels and < 100 nm exhibited slower and prolonged antihyperglycemic activity in diabetic mice. Thus, no significant difference ($p > 0.05$) was noted between the antihyperglycemic action of insulin solution administered subcutaneously and oral sodium glycocholate-liposomes in diabetic mice [144].

Agrawal *et al.* (2014), developed liposomes functionalized with folic acid for the successful entrapment of insulin molecule. The developed formulation was made from alternate coating of poly (acrylic acid) and poly (allyl amine) hydrochloride. The developed functionalized formulation increased the oral bioavailability of insulin up to 20% in comparison to insulin solution. Also, remarkably decreased the severity of hyperglycaemia with respect to oral-insulin and insulin liposomes [145].

Zhang *et al.* (2014), developed insulin loaded oral liposomal formulation modified with targeted ligand biotin for the effective treatment of hyperglycaemia. The developed liposomes enhanced the oral bioavailability of insulin up to 5.28-folds in comparison to conventional formulation, attributed to biotin-mediated endocytosis in Caco-2 cells. Also, reduced the blood glucose levels up to 1.5- and 1.3-folds in comparison to base control and insulin solution [146].

Yazdi *et al.* (2020), developed liposomes composed of phospholipid with high transition temperature along with PEGylation and a targeting moiety folic acid. This formulation successfully encapsulated insulin and improved its (19%) oral bioavailability. The PEGylation of insulin loaded liposomal oral formulation provided protection against harsh conditions of GIT and its targeting moiety led to increased

absorption via intestinal epithelium. In *in vivo* study, this formulation (50 IU/kg) reduced the plasma sugar profile and enhanced the plasma insulin levels in diabetic rats ($p < 0.001$) in comparison to regular insulin injection. The targeting ligand folic acid in the liposomal formulation enhanced the cellular uptake in Caco-2 cells by 1.5-folds with respect to liposomal formulation without folic acid [143].

2.7.1.1.2 Niosomes

Niosomes are colloidal nanocarriers that are bilayered structures (unilamellar or multilamellar vesicles) composed of lipid and non-ionic surfactants incorporated in aqueous phase. Lipid component mostly include cholesterol or L- α -soya phosphatidylcholine that imparts stability to niosomes in biological fluids [147]. Whereas amongst non-ionic surfactants spans and Brij are widely used, due to which niosomes are also referred as “non-ionic surfactant vesicles” [148]. Recently, various ionic amphiphiles like dicetyl phosphate, sodium deoxycholate, stearyl amine etc. are also used to augment the stability of vesicular suspension by inducing negative or positive charge [149]. The size of niosomes ranges between 10 to 1000 nm and are preferred as drug delivery vehicles over liposomes due to its more chemical stability and low cost [149]. These nanocarriers are amphiphilic in nature and can encapsulate hydrophilic drug in core region and lipophilic drug in non-polar region of bilayer membrane [149]. These nanocarriers can be functionalized to obtain desired physicochemical property and for targeted delivery of drugs. In addition, niosomes offer drug sustainability resulting into prolonged drug's effect, lower toxic-effects, change in the distribution profile of drugs, and increased bioavailability of the encapsulated drug [147,149]. For example, metformin as first-line antidiabetic agent is widely administered i.e., 2-3 times/day by T2DM patients. However, the drug is associated with number of side effects.

Sankhyan *et al.* (2013), reported that the dosing frequency and associated side effects of metformin could be reduced by sustaining the drug release. For which the non-ionic surfactant vesicles was used as a novel drug delivery vehicle. In this study, 12 batches of metformin loaded niosomes was prepared to study the influence of varying molar concentration of cholesterol: surfactant (span 60/span40), type of surfactant, presence of dicetyl phosphate and volume of hydration on to the stability, entrapment efficiency and *in-vitro* drug release profile. Higher entrapment efficiency i.e. 84% was resulted from the use of 15 ml of hydration volume, which provided ample space for vesicle formation. In addition, cholesterol at optimized ratio with span 60 (100:100) provided

sufficient rigidity to the bilayer and cemented the leakage points that resulted in higher entrapment of drug in core. The type of surfactant used i.e. span 60 provided more sustained release and higher entrapment efficiency due to difference in the alkyl chain length. The dicetyl phosphate used had great impact onto the stability as it provided uniformity and prevented the aggregation and fusion of vesicles. Therefore, the optimized formulation composed cholesterol: span 60 (100:100) with 5 mg dicetyl phosphate and 15 ml of volume of hydration exhibited most sustained metformin release i.e. 69% up to 8h in pH 6.8 and was stable up to 3 months in refrigerator temperature [150].

Similarly, Kumar *et al.* (2017), developed formulation of niosomes containing span 60 and cholesterol in 1:1 ratio for the sustained release of entrapped metformin and gliclazide. The results of *in vitro* release study revealed 1.4-folds decrease in metformin release and 1.6-folds decrease in gliclazide release profile in comparison to pure drugs. Almost 40.1% of metformin and 45.7% of gliclazide was released in sustained manner in pH 6.8 over 8h [140].

In the next study, Mohsen *et al.* (2017), developed cholesterol and span 60 based niosomes to increase the oral bioavailability and therapeutic efficacy of glimepiride. The formulation resulted in sustained release of drug i.e. 39.5% for 24h that was slower than the free drug. In agreement with the drug release results, formulation showed 1-fold lower C_{max} and 3-folds higher T_{max} than free drug respectively. This indicated that the drug required more time to reach maximum concentration in plasma. Further, the $AUC_{0-48hrs}$ of the glimepiride released from formulation was 7-folds higher than the free drug that indicated increase in relative bioavailability of glimepiride. This resulted in higher blood glucose level reductions by 2.1-folds and 2-folds in comparison to free drug and marketed product respectively [151].

2.7.1.1.3 SNEDDS

SNEDDS are liquid-lipid nanocarriers, composed of isotropic mixtures of oils, surfactants, and co-surfactants/co-solvents that forms fine oil in water nanoemulsion upon mild agitation in GI media [152,153]. The production of SNEDDS is thermodynamically spontaneous, as they require very low free energy. In comparison to other nanocarrier systems, production of SNEDDS is facile and cost-effective [152]. These nanocarriers orient nanoemulsions in the range of 20 to 200 nm upon dilution [152]. These nanocarriers provide improved drug oral bioavailability, permeability, enzymatic and chemical stability [152,153].

However, because of larger interfacial area for drug adsorption, SNEDDS are claimed to be suitable nanocarrier for increasing the oral bioavailability of lipophilic drugs [152].

In addition, its ease of functionalization offers controlled and targeted delivery of wide range of drugs [152]. These nanocarriers can be easily modified for their incorporation in soft/hard gelatin capsules via drying techniques for better patient compliance [154]. Further, Rashid *et al.* (2018), reported the formation of SNEDDS composed of Capmul MCM, Kolliphor HS and PEG 400 to enhance the oral bioavailability of embelin and gliclazide. In *in vitro* dissolution study, the dissolution rate of embelin and gliclazide loaded in SNEDDS was increased up to 3.4- and 2.8-folds in PBS pH 7.4 over 70 min than plain drugs respectively. This increase in dissolution profile of both the drugs is attributed to the ability of SNEDDS to keep drugs in the solubilized state. This has led to increase in the therapeutic efficacy of the drugs. In *in vivo* study, co-loaded SNEDDS with 10 mg/kg of gliclazide and 30 mg/kg of embelin exhibited significant reduction in blood glucose levels, body weight, cholesterol and triglycerides levels ($p < 0.05$) in comparison to their respective pure drugs respectively [155].

Ameeduzzafar *et al.* (2019), reported the formation of solid SNEDDS using eucalyptus oil, tween 80, polyethylene glycol 400 and biocompatible adsorbent avicel PH-101 for the successful loading of poorly water-soluble drug dapagliflozin for its oral delivery. In *in vivo* study, drug loaded solid SNEDDS exhibited 1.2-folds ($p < 0.05$) increase in the antihyperglycemic action of dapagliflozin than the unprocessed dapagliflozin in diabetic rats [156].

Kazi *et al.* (2021), reported that the SNEDDS composed of black seed oil, Capmul MCM, and Cremophor EL not only enhanced the oral bioavailability of the loaded drugs but exhibited moderate antioxidant activity mainly attributed to the main constituent in black seed oil thymoquinone. The developed SNEDDS was used for the loading of two antidiabetic drugs sitagliptin and dapagliflozin. The developed SNEDDS upon co-loading the model drugs retained the antioxidant activity and exhibited 4-folds increase in the total antioxidant activity as compared to blank SNEDDS. The oral bioavailability of the loaded dapagliflozin was increased up to 2-folds in comparison to commercial drug. This increment in the oral bioavailability of dapagliflozin led to decrease in blood glucose levels up to 1.4- and 1.6-folds than commercial and pure drug in diabetic mice respectively.

Whereas, the loaded sitagliptin exhibited 1.1-folds greater reduction in blood glucose levels in comparison to pure drug in diabetic mice. However, this study has not reported the pharmacokinetic data of the loaded drug sitagliptin [157].

2.7.1.1.4 Solid-lipid nanoparticles (SLNs)

SLNs are composed of biodegradable solid lipid matrix and a surfactant layer that are spherical in shape with mean size of 40-1000 nm [158,159]. Lipids used in the formation of SLNs include triglycerides, sterols, fatty acids, and waxes whereas the surfactants include bile salts, lecithin, and copolymers [158]. Solid lipid matrix of SLNs can be mixture of solid and liquid lipids used in the range of 0.1%-30% w/w concentration for their dispersion in aqueous medium. While, the stability of SLNs is ensured by surfactant used in range of 0.5%-5% w/w concentration and can be used in the loading of both hydrophilic and lipophilic drugs [158].

In addition, of improving bioavailability of drugs, SLNs for oral delivery offer good stability, improved epithelium permeability, prolonged half-life, tissue-targeting and minimal side effects. Further, for the drug mucosal or lymphatic transport (GI permeation), the physicochemical properties of SLNs can be tailored by engineering SLNs using various nontoxic excipients and sophisticated materials [160]. In order to reduce the dosing frequency, side effects and to enhance overall therapeutic efficacy of antidiabetic drugs, SLNs as prolonged release formulation has been widely explored. With this context, in one of the studies, Rawat *et al.* (2010), made SLNs using glyceryl mono stearate and tris-tearin as lipid core and Pluronic F68 to enhance the oral dissolution of repaglinide. The developed SLNs increased the AUC of repaglinide by 12.8-folds than free drug respectively. This led to increase in relative bioavailability of drug in SLNs by 14-folds in comparison to free drug. Thus, indicated increased drug intestinal absorption from SLNs than free drug. These results were in direct co-relation with its antihyperglycaemic effect in *in vivo* study. The formulation at dose 0.286 mg/kg exhibited higher glucose/lipid lowering effect (TGs and CHL) ($p < 0.05$) than free drug at same dose respectively. The formulation showed 30.8-folds increase in area under the effect curve than free drug respectively. In addition, showed maximum nadir effect i.e. 1.1-folds higher with increased t_{Nadir} (h) i.e. 13.3-folds higher than free drug respectively. Thus, the formulation showed controlled release with prolonged antihyperglycemic effect [161].

Ebrahimi *et al.* (2015), prepared SLNs composed of stearic acid and glyceryl mono stearate as lipid phase and various surfactants/stabilizers such as phosphatidylcholin, Tween80, Pluronic F127, poly vinyl alcohol (PVA) and polyvinyl pyrrolidone (PVP) to study their influence on physicochemical parameters of SLNs in oral delivery of repaglinide. The use of surfactant phosphatidylcholine in drug loaded SLNs exhibited increased zeta potential i.e. -54 mV than other surfactant based SLNs due to their ionic nature that formed electric double layer on nanoparticles surface and resulted in good stability. In case of particle size, tween 80-based SLNs formed smaller particles (83 nm) than other surfactant based SLNs attributed to their low molecular weight that covers interfacial surfaces more rapidly than high molecular surfactants. However, phosphatidylcholine based SLNs were of intermediate size i.e. 203 nm that was reduced by 2.2- and 1.2-folds when used along with tween 80 and Pluronic F127 [141].

Further, loading parameters exhibited linear relationship with particles size i.e. 3.1-folds increase in loading efficiency was observed with increase in size up to 203 nm due to higher drug repulsion. However, PVA and PVP based SLNs having size greater than 250 nm exhibited reduced loading efficiency. However, the drug release rate was controlled in all surfactant based SLNs i.e. 1.12-1.49% over 1h with difference in burst release. The burst release rate showed inverse relationship with particle size. Therefore, mixture of Pluronic F127 with phosphatidylcholine was considered to modify the properties of repaglinide loaded in SLNs to improve its bioavailability for which further *in vivo* studies are required [141].

2.7.1.2 Micelles

Micelles are nanoscopic supramolecular structures formed from biocompatible and biodegradable amphiphilic block copolymers, which above critical micelle concentration in water self-assembles in spherical micellar form [162]. The size of these nanoparticles ranges between 10 to 100 nm that offer increase in bioavailability and penetration of drugs. These are also referred as “amphiphilic polymeric micelles” due to their amphiphilic nature [163]. These nanomicellar structures provide good metabolic stability and prolonged blood circulation time due to which these are widely used in the oral delivery of wide range of drugs [163].

In addition to this, micelles offer good stability due to low CMC value (0.1-1 μ M), controlled drug release, ease of functionalization, minimized side effects, stimuli-sensitivity, high surface to volume ratio, low production cost, target selectivity, and enhanced permeation as well as retention effect [20].

In this regard, to enhance the oral antidiabetic effect, Kassem *et al.* (2017), developed micelles based on phospholipid complexation for the oral delivery of repaglinide. The drug loaded micelles offered sustained release profile over 24 hours due to the hydrophobic nature of the micellar core. The drug release from micelles was greater in PBS pH 1.2 than in pH 6.8 respectively. In *in vivo* study, oral administration of drug-loaded micelles of dose 2 mg/kg for 7 days resulted in 2.5-folds decrease in blood glucose levels in comparison to marketed tablet respectively. In addition, increased the serum insulin levels by 1.97-folds and HDL levels by 1.3-folds in comparison to marketed tablet. Whereas, decreased the serum triglycerides, cholesterol, low density lipoprotein, and total lipid levels by 1.2-, 1.0-, 1.1-, and 1.2-folds in comparison to marketed tablet respectively [164].

Further, the stimuli-sensitive property of micelles has been widely explored in the oral delivery of insulin, which makes them intelligent oral drug delivery carrier. With this context, Hu *et al.* (2019), reported the formation of pH-responsive cationic polymeric micelles (PCPMs) formed from poly(methyl methacrylate-co-methacrylic acid)-block-poly(2-amino ethyl methacrylate) for oral insulin delivery. The developed PCPMs exhibited sharp pH-sensitive behaviour with change in particle size, which allowed increased absorption of insulin in the GIT alkaline environment. Increase in pH from 1.8 to 6.0 exhibited decrease in size while further increment in pH from 6.0 to 7.4 resulted in increased size. This was attributed to increased ionization of methacrylic acid segment with increase in alkaline pH that favoured swelling of PCPMs and further, favoured release of insulin in pH 7.4. The PCPMs released more than 50% of the insulin in a sustained manner while released less than 35% insulin in pH 1.2 over 6h respectively. Also, exhibited more than 80% cell-viability in Caco-2 cell line study [165].

Similarly, Bahman *et al.* (2020), reported that the pH-sensitive micelles composed of poly(styrene-co-maleic acid) loaded with insulin at concentration of 100 μ M increased the 2-deoxyglucose uptake by 15% in HepG-2 cells in comparison to free insulin over 1h respectively. Further, larger amount of fluorescent 2-deoxyglucose was accumulated in HepG-2 cells while free insulin failed to accumulate fluorescent 2-deoxyglucose. The loaded insulin in micelles released almost 23% of insulin in pH 7.4 over 36h in a sustained manner. Further, exhibited low burst release i.e., 21% in simulated gastric fluid. The developed micelles exhibited higher transport efficacy of insulin across intestinal ileum segment i.e., by 2-folds than duodenum and 3.6-folds than jejunum

segment respectively. These results were in agreement with *in vivo* data. The oral administration of the insulin-loaded micelles at dose 72 mg/kg significantly reduced the blood glucose levels by 1.5-folds in comparison to diabetic control and was found more effective than free oral insulin. Further, the repeated oral administration of insulin loaded micelles exhibited higher glucose reduction ($p < 0.05$) in comparison to single dose respectively. In addition, the reduction in blood glucose levels by oral insulin loaded micelles was 4-folds less in comparison to subcutaneously administered insulin loaded micelles respectively. Therefore, formulation optimization is required to enhance the oral efficacy of the insulin [166].

2.7.1.3 Polymeric nanoparticles

Polymeric nanoparticles are self-assembled structures formed from biodegradable or biocompatible amphiphilic molecules either natural or synthetic (ionic or non-ionic) that acts as a stabilizing agents as well. During the self-assembly process, these nanoparticles encapsulates the drug molecules within the core or at the surface of the polymeric core based on their affinity (Pridgen). These nanoparticles have advantages of controlled drug release, metabolic stability, improved bioavailability and therapeutic index [167].

In addition, these nanoparticles have ease of surface modification that employ their use in drug targeting and helps in improving their *in vivo* performance [168]. The size of these nanoparticles ranges from 1 to 1000 nm [169,170]. Due to small size, these nanoparticles possess larger specific surface area that allow their interaction with epithelial surface to reach at the target site [168]. These nanoparticles are flexible to design and the physicochemical properties can be tailor made based on the choice of polymer and self-assembly conditions [168]. For example, to deliver GLP-1 via oral route and in order to enhance their metabolic stability and absorption via GIT, polymeric nanoparticles can be developed as a dual-drug delivery vehicle for oral peptide delivery by incorporating DPP-4 inhibitor. This approach along with functionalization property of polymeric nanoparticles can increase the therapeutic efficacy of GLP-1 in comparison to conventional GLP-1 and DPP-4 inhibitor solution respectively [171].

In this regard, Araujo *et al.* (2013), functionalized the PLGA nanoparticles with chitosan and a cell penetrating peptide. These nanoparticles were designed to increase the cellular uptake by facilitating higher interaction with intestinal cells or to increase the transcellular transport of the nanoparticles. In *in vivo* study, oral delivery of these

functionalized polymeric nanoparticles co-loaded with GLP-1 and DPP-4 inhibitor at dose 200 µg/kg greatly reduced the plasma glucose levels by 44.3% ($p < 0.001$) in a sustained manner for 8h than GLP-1 plus DPP-4 inhibitor solution and GLP-1 loaded nanoparticle respectively. Thus, the co-loaded nanoparticles showed 2.1- and 1.9-folds decrease in blood glucose levels than GLP-1 loaded nanoparticles and GLP-1 plus DPP-4 inhibitor solution respectively. Also, increased pancreatic insulin content ($p < 0.001$) after 8h of oral administration than GLP-1 plus DPP-4 inhibitor solution respectively. The plasma insulin levels were increased by 1.4-folds after 6h of oral administration of co-loaded nanoparticles in comparison to GLP-1 loaded nanoparticles and GLP-1 plus DPP-4 inhibitor solution respectively [171].

In another study, Shrestha *et al.* (2016), developed chitosan-modified porous silicon nanoparticles coated by gastro-resistant polymer hydroxyl propyl methyl cellulose acetate succinate for the dual oral delivery of GLP-1 and DPP-4 inhibitor. The developed co-loaded polymeric nanoparticles due to its polycationic and mucoadhesive nature exhibited good adhesion efficacy in ligated intestinal loop study. The pharmacokinetic study revealed 1.2- and 2.2-folds increase in AUC and C_{max} of the co-loaded nanoparticles in comparison to GLP-1 plus DPP-4 inhibitor solution respectively. This indicated that the DPP-4 levels were significantly higher for co-loaded nanoparticles ($p < 0.01$) than GLP-1 and DPP-4 inhibitor solution respectively. Thus, the co-loaded nanoparticles reduced the plasma DPP-4 levels by 2-folds within 6h of its oral administration in comparison to GLP-1 plus DPP-4 inhibitor solution respectively. In *in vivo* study, the oral administration of co-loaded nanoparticles at dose 250 µg/kg reduced the blood glucose levels by 45% in sustained manner for 8h in comparison to GLP-1 plus DPP-4 inhibitor solution respectively. In addition, the co-loaded nanoparticles increased the pancreatic insulin content by 6- and 3.4-folds as compared to GLP-1 plus DPP-4 inhibitor solution and blank nanoparticles respectively [172].

2.7.1.4 Nanocrystals

Nanocrystals are nanosized range carrier-free colloidal delivery system. These are nanoscopic crystals composed of 100% parent compounds that are stabilized with surfactants or polymeric steric stabilizers [173]. In comparison to other carrier-based nanoparticles, nanocrystals are advantageous in drug loading (50-90% w/w) and stability [174]. The higher specific surface and curvature of nanocrystals via nanosizing offers increased oral bioavailability of lipophilic drugs [174].

In addition, nanocrystals can be chemically modified for the controlled release of antidiabetic drugs in order to minimize the side effects and to enhance their therapeutic efficacy for prolonged periods. This controlled release system helps in maintaining the required drug levels within the therapeutic range of plasma for extended periods and prevents unwanted toxicity of the drugs [175].

In agreement to this, Abo-Elseoud *et al.* (2018), developed cellulose nanocrystals incorporated in chitosan nanoparticles (CNC-CHNPs) by ionotropic gelation method for the controlled release of repaglinide. Further, to study the influence of CNC on drug release profile, they were chemically modified by oxidation process (OXCNC) and incorporated in CHNPs. In *in vitro* drug release study, OXCNC-CHNPs caused slower release rate over 8h in pH 1.2 and pH 6.8 in comparison to CNC-CHNPs respectively. The drug release rate was 1.4-folds slower in pH 1.2 for 2h followed by 1.7-folds in pH 6.8 in last 6h than CNC-CHNPs respectively. In addition, OXCNC-CHNPs exhibited 2.2- and 1.7-folds slower drug release in pH 1.2 and pH 6.8 in comparison to free drug over 8h respectively [176].

Such difference in drug release profile was attributed to the presence of carboxylic group on CNC surface that provided stronger hydrogen bonding between functional groups of drug molecules (amide and carboxyl groups) and OXCNC (hydroxyl and carboxyl groups) than CNC (hydroxyl group) respectively. However, further studies in higher animals and human beings is required for the commercial application of this antidiabetic controlled drug delivery system [176].

2.7.1.5 Miscellaneous

The nanocarrier such as gold nanoparticles and dendrimers have also shown its potential in the delivery of antidiabetic drugs/peptides for managing T2DM and its associated comorbidities. Both of these nanoparticles have gained attention as antidiabetic nanomaterials from past few years due to their glucose lowering effect [177]. Recently, plant mediated synthesis of gold nanoparticles as antidiabetic nanomaterial have gained attention to treat hyperglycemia and associated complications [178].

For example, gold nanoparticles synthesized using *Chamaecostus cuspidatus* (insulin plant) exhibited 2.2- and 2-folds increase in blood glucose reduction and insulin levels in comparison to diabetic control respectively. Further, reduced the total cholesterol levels and wound size in diabetic rats by 1.4-folds in comparison to diabetic control respectively [178].

In addition, amongst various dendrimic forms, PAMAM poly(amidoamine) G4 is quite popular as antidiabetic nanomaterial because of their unique molecular architecture and easy functionalization with desire ligands that offers potential to reduce long-term markers of hyperglycemia [177]. This makes them perfect nanocarriers for the longterm management of hyperglycemia and in increasing the efficacy of antidiabetic drugs/peptides to treat T2DM.

Gold nanoparticles as non-invasive drug carriers have been extensively used for targeting drugs to their site of action [179]. Over the past few years, their unique colors, tunable surface Plasmon resonance or typical electronic properties led their use in biomedical applications [177]. Further, their chemical inertness and minimum toxicity makes them suitable agents for drug delivery purposes [177]. Drug conjugated gold nanoparticles have been intensively investigated as a carrier system [180].

For example, Perez-Ortiz *et al.* (2017), used gold nanoparticles for the functionalization of incretin GLP-1 analog to enhance their stability and absorption by coating with PEG. The functionalization was accomplished by modifying the C-terminal region of GLP-1 analog by using cysteine residues. The GLP-1(7-37)-Lys(PEGCys)-NH₂ conjugated gold nanoparticles delivered higher proportions of peptide by exhibiting good permeability across Caco-2 cells. In *in vivo* study, the developed nanoconjugate reduced the blood glucose levels by 1.1-and 1.2-folds after 2h of intraperitoneal administration in comparison to unconjugated GLP-1(7-37) Lys(PEGCys)-NH₂ and native GLP-1 respectively [181].

In addition, dendrimers are polymeric globular hyperbranched macromolecules with tree-like morphology in 3D nanostructure composed of a central core and branched monomers with different reactive end groups on its corona. Its size ranges between 1-100 nm [182]. Their ease of functionalization and control over its synthesis for desired physicochemical properties makes them an interesting and effective nanocarrier for desire molecules. Their unique physiochemical properties based on the modification of functional end groups of dendrimers such as change in hydrophilicity, size, molecular weight etc. contributes to its wide usage in pharmaceutical and biochemical applications [183].

The family of dendrimers consists of poly (amidoamine) (PAMAM), poly (propylenimine) (PPI), liquid crystalline (LC), core shell (tecto), peptide, glycol and hybrid dendrimers [183]. Particularly, PAMAM dendrimers have been recently investigated for their application in the delivery of drugs and therapeutic genes.

As these offers optimized controlled drug release and itself provide antihyperglycemic action in sustained manner as discussed above [177].

For example, Pyung-Hwan Kim *et al.* (2013), developed arginine-grafted poly (cystamine bisacryl amide diamino hexane) (ABP)-conjugated PAMAM dendrimer (PAM-ABP) using two-step transcription amplification (TSTA) plasmid system to improve incretin-based therapy. In *in vivo* study, PAM-ABP/chimeric DNA polyplex increased the expression of exendin-4 in diabetic mice by 1.5-, 1.3- and 2-folds than PEI/chimeric DNA, ABP/chimeric DNA or PAM-ABP/TSTA DNA respectively after third day of i.v administration. The upregulation of exendin-4, induced cAMP mediated protein kinase-A signalling stimulation in β -cells, that was 1.3-folds higher than other DNA systems. This led to better insulinotropic effect in diabetic mice i.e. 1.3-folds higher in comparison to PAM-ABP/TSTA DNA system. In addition, exhibited 1.3-folds higher reduction in blood glucose levels than PEI/chimeric and ABP/chimeric DNA respectively after three days of its i.v administration. It was also successful in reducing free fatty acid levels by 1.1-folds than other DNA systems respectively [184]. However, studies pertaining to its use in the oral delivery of antidiabetic drugs with poor bioavailability has not been explored so far. Thus, dendrimer delivery of antidiabetic drugs/peptides/proteins can provide feasible pharmacotherapy for the better control of hyperglycaemia and its associated markers in T2DM patients in future.

Table 2.4: A brief list of advanced delivery systems used for improving the bioavailability and antidiabetic effect of the drugs used to treat T2DM

Delivery system	Drug	Outcome	Reference
Lipid Nanosystem			
Glycerolphosphate– Chitosan Microcomplexation based liposomes	Metformin	-In <i>in vivo</i> study, microcomplexes showed 1.6- and 2.5-folds increase in AUC/D and T_{max} than aqueous solution of metformin. -Offered controlled drug release due to reduced swelling of polymer in GIT that led to reduced drug diffusion from microcomplexes and resulted in sustained antihyperglycemic action	[185]
Anionic liposomes containing DSPE- PG8G, DPPC, Cholesterol and DPPG	GLP-1	-In pharmacokinetic studies, GLP-1 liposomes (100 nmol/kg) upon i.v administration in rats increased the plasma GLP-1 levels by 3.6-folds than GLP-1 injection. -Further, increased the insulinotropic effect by 1.7-folds than GLP-1 solution. -Exhibited highest antihyperglycemic effect by reducing the $AUC_{0-120 \text{ min}}$ of glucose by 49.2% than control respectively	[139]
Niosomes containing Span 40/cholesterol dicetyl phosphate and DOTAP	Metformin	-In <i>in vivo</i> study, oral administration of niosomes increased the glucose reduction effect of loaded metformin by 1.9-folds within 4h (T_{max}) than free drug. -The antihyperglycemic effect of loaded drug extended to 6-8h than free drug. -Further, the area above the blood glucose levels-time curve increased by 2-folds than free drug respectively	[186]
Niosomes containing Span 60 and cholesterol	Gliclazide	-In <i>in vivo</i> study, gliclazide niosomes exhibited sustained antihyperglycemic effect for 12h in comparison to free drug. -Further maintained significant hypoglycaemic effect of 25% for 12 h in comparison to free drug for 2-3h, due to prolonged duration of drug absorption from niosomes.	[187]
SNEDDS containg Miglyol, Tween 80, PEG and Aerosol 200	Glyburide	-The loaded drug in SNEDDS showed complete drug release in 30 min, in contrast to 16% by pure drug in the same time interval. - <i>In vivo</i> studies revealed 1.82-and 1.93-folds increase in $AUC_{(0-24h)}$, for S-SNEDDS and L-SNEDDs respectively when compared with pure drug.	[188]
SNEDDS containing Cremophor RH 40, propanediol and Miglyol 812	Glyburide	-In <i>in vivo</i> pharmacokinetic studies, SNEDDS increased the AUC and C_{max} of glyburide by 1.5- and 1.4-folds after oral administration in comparison to glyburide micronized tablets respectively.	[189]

SLNs containing Compritol® 888 ATO and tween 80	Pioglitazone	-In <i>in vivo</i> study, oral administration of SLNs increased the blood glucose lowering effect of pioglitazone by 1.1-folds in sustained manner up to 12h than free drug respectively.	[190]
Precirol-based SLNs containing lecithin	Glyburide	-In <i>in vivo</i> study, drug loaded SLNs reduced the blood glucose levels by 1.2-folds upon oral administration within 4h in comparison to free drug. -The effect of drug loaded in SLNs was significantly higher and more prolonged than free drug alone.	[191]

Micelles

Phospholipid complex enriched micelles	Repaglinide	-The formulation demonstrated sustained release pattern i.e. 99% in 24h in comparison to free drug with rapid release pattern in acidic pH 1.2. - <i>In vivo</i> studies revealed 1.4-folds higher reduction in blood glucose levels and 2.1-folds higher insulin secretion in diabetic rats upon oral administration than free drug respectively. -Further, reduced the overall plasma lipid profile by 1.1.-folds than free drug	[164]
Zwitterionic micelles (freeze dried powder into enteric coated capsule)	Insulin	-The formulation exhibited greater oral bioavailability of insulin i.e. 43.4%, which was higher than polysorbate 80/insulin capsule i.e. 8.53% respectively. - <i>In vivo</i> studies revealed 4-folds higher pharmacological activity (glucose reduction) than polysorbate 80/insulin capsule respectively while native insulin (oral) exhibited similar effects to that of saline. -Further, exhibited 1.0-folds higher reduction in glucose levels in sustained manner than native insulin (s.c.) respectively	[192]
Glucose responsive complex micelles	Insulin	- <i>In vivo</i> studies revealed self-regulated insulin release that maintained normoglycemia (0.9-2.0g/L) for longer duration due to “on-off” controlled release of insulin i.e. for 16h upon s.c. administration in comparison to native insulin (for 5h) and simple micelles (10h) respectively	[193]
mPEG-PCL based micelles	Gliclazide	- <i>In vivo</i> studies revealed, 1.1-folds higher reduction in blood glucose levels upon oral administration of drug loaded micelles in comparison to free drug in sustained form (21 days)	[23]
Benzoboroxole-containing multi-armed poly(ethylene glycol)	Insulin	- <i>In vivo</i> studies revealed 20% reduction in blood glucose levels upon oral administration of the formulation after 2h in comparison to insulin (s.c) that rapidly reduced glucose levels by 20% in 1h	[194]

amphiphilic dendrimer based micelles		-Further, maintained normoglycemia for up to 10h due to increased permeation of insulin through the mucus layer that eventually led good absorption by villi	
Polymeric nanoparticles			
Pectin nanoparticles	Metformin	- <i>In vitro</i> cell line studies revealed 1.5-folds increase in glucose uptake in red blood cells and L6 skeletal muscle cells in comparison to free drug respectively	[195]
Eudragit L100 and Pluronic F-68 based nanoparticles	Glyburide	<i>In vivo</i> studies revealed 1.7-folds increase in blood glucose reduction in comparison to free drug upon oral administration respectively Further, reduced the t_{min} and glucose AUC_{0-10h} by 1- and 3.8-folds in comparison to free drug	[196]
Nanocrystals			
Solidified nanocrystals	Glyburide	- <i>In vivo</i> pharmacokinetic studies of nanocrystal tablet dosage form revealed 5.6-and 2.2-folds increase in C_{max} and AUC_{0-24h} upon oral administration in comparison to marketed tablets respectively	[197]
Nanocrystals containing Lipoid S100, PVPK 30, and PEG 6000	Glimepiride	- <i>In vivo</i> pharmacokinetic studies revealed 1.1-,1.8- and 1.5-folds increase in C_{max} , AUC_{0-36h} and T_{max} upon oral administration in comparison to marketed tablets respectively	[198]
PLGA second generation nanocrystals	Gliclazide	- <i>In vivo</i> pharmacokinetic studies revealed 3.2- and 5.6-folds increase in C_{max} and AUC_{0-24h} in comparison to pure drug respectively -Further, revealed 2.2-folds increase in blood glucose level reduction in sustained manner (biphasic pattern) after 24 hours of oral administration in diabetic rats comparison to pure drug respectively	[199]
Miscellaneous			
Dendronized chitosan using PAMAM	Insulin	- <i>In vivo</i> studies revealed relative oral bioavailability of ~9.19% i.e. 1.7-folds higher than native chitosan/insulin nanoparticles -Further, exhibited sustained antihyperglycemic effect for 8h in comparison to subcutaneously administered insulin for 2h respectively without any systemic toxicity in diabetic mice	[200]
Chondroitin sulfate-capped gold nanoparticles	Insulin	- <i>In vivo</i> studies revealed 6.6-folds increase in insulin concentration after 120 min of oral administration of insulin loaded gold nanoparticles in comparison to insulin solution	[201]

Gold nanoparticle conjugate	Vildagliptin	-Further, reduced the blood glucose levels by 1.4-folds after 4h than insulin solution respectively - <i>In vitro</i> studies revealed increased DPP-IV inhibitory activity by 2-folds in comparison to reference solution via non-competitive mode of inhibition -Exhibited stability under GIT harsh microenvironment that indicated safety and long term bioavailability	[180]
-----------------------------	--------------	---	-------

2.8 Glyburide

Gly is a first generation sulfonylurea drug, which upon ingestion binds with sulfonylurea receptor type 1 subunit of the ATP-sensitive potassium (K^+) ion channel that are present on pancreatic membrane of β -cells and suppress it. This causes increase in the K^+ ions concentration in β -cells that ultimately results in depolarization or activation of the calcium ion channels in β -cells. This increase in the influx of calcium ions further elicits exocytosis of insulin producing granules and causes release of insulin into systemic circulation [12,87]. The diagrammatic presentation is shown in **Fig 2.3**. Different physicochemical properties of Gly are presented in **Table 2.5**.

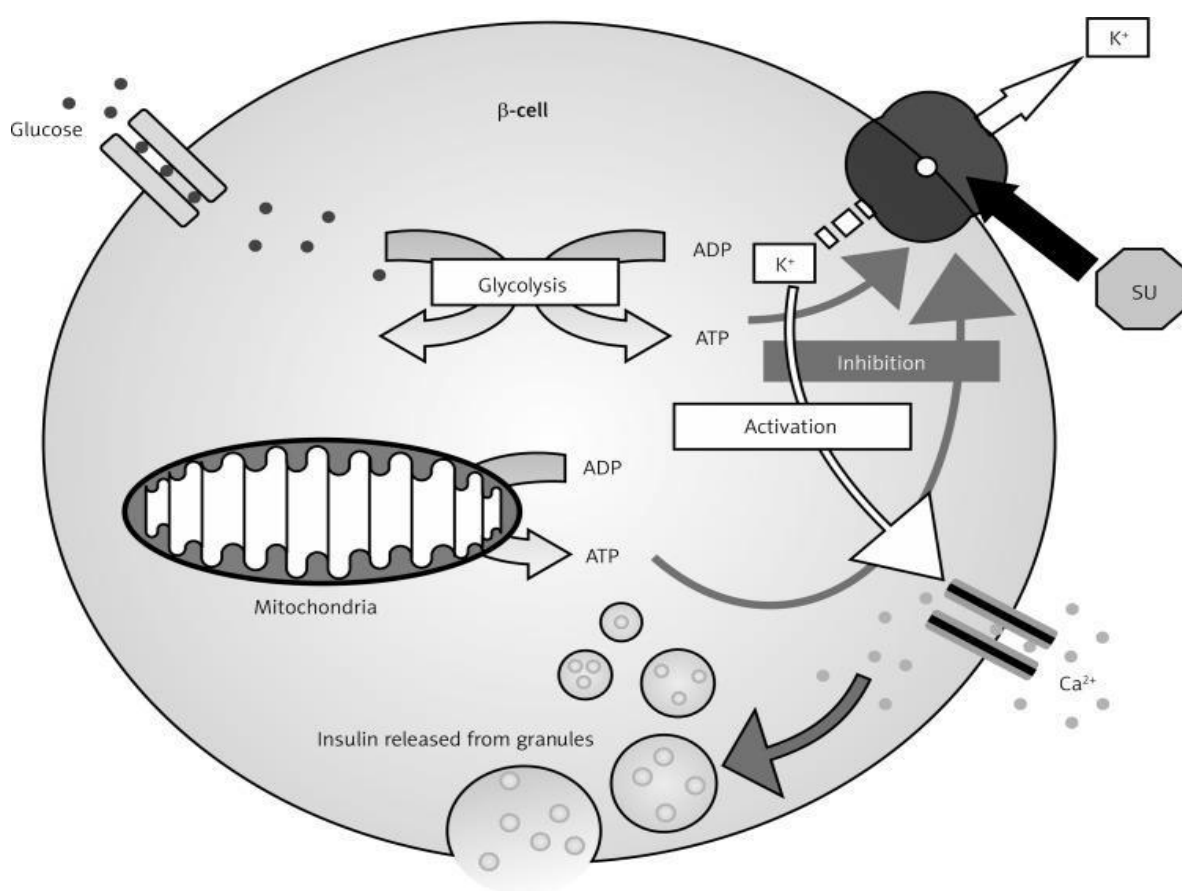
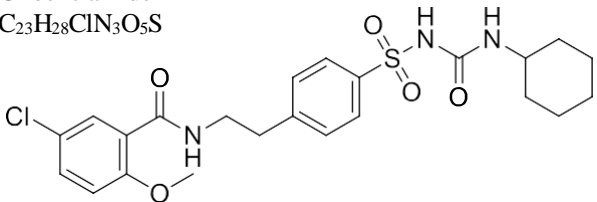


Fig 2.3: Mechanism of action of Gly

Table 2.5: Physicochemical properties of Gly

Property	Outcome
Description	White colored crystalline solid powder
IUPAC Name	5-chloro-N-[2-[4-(cyclohexylcarbamoylsulfamoyl)phenyl]ethyl]-2-methoxybenzamide
Additional Name	Glibenclamide
Molecular Formula	C ₂₃ H ₂₈ ClN ₃ O ₅ S
Chemical Structure	 <p>The chemical structure of Glibenclamide consists of a central benzamide core. The benzamide ring has a chlorine atom at the 5-position and a methoxy group at the 2-position. The amide nitrogen is attached to a 2-ethyl chain, which is further connected to a para-substituted phenyl ring. This phenyl ring is linked via a sulfamoyl group (-SO₂NH-) to another amide group (-NH-CO-), which is finally attached to a cyclohexane ring.</p>
Molecular weight	494.0 g/mol
Melting point	169-170 °C
Solubility	0.01 mg/mL (Practically insoluble)
Log P	3.75
PKa	5.3

Being a BCS Class II drug it possess low solubility and high permeability [202]. Its poor aqueous solubility hinders them to reach the systemic circulation at a desired concentration upon oral administration. This urge the need for frequent dosing of this potent drug or the commencement of multidrug therapy, which causes unwanted adverse effects especially GIT related in T2DM patients. Extensive work has been done to improve dissolution and bioavailability of Gly as presented in aforementioned **Table 4** highlighted in bold.

For instance, Cirri *et al.* (2007), reported 100% dissolution of Gly fast dissolving tablets containing ternary solid dispersion. The best product was the 10:80:10 w/w ternary dispersion with PEG 6000 and sodium lauryl sulphate, with dissolution efficiency 5.5-fold greater than the reference tablet formulation and 100% drug dissolution after only 20 min [203]. Bachhav and Patravale, 2009, reported more than 90% Gly release from Gly-SMEDDS in 5 min in both pH 1.2 and 7.4. However, stability studies indicated substantial degradation of Gly in the developed SMEDDS [204].

Devireddy and Veerareddy, 2013, reported that solid dispersion of the Gly with vitamin E TPGS at 1:0.3 (W/W) ratio showed increase in Gly dissolution within 25 min and increase in the oral bioavailability (4.5-folds increase in AUC_{0-∞}) compared to pure Gly respectively.

Patil *et al.* (2017), prepared sustained release Gly loaded silica nanoparticles (250-590nm) without any incompatibility. The results showed drug release in the range of 68.8– 87.8% over 24h respectively [205]. Mukherjee *et al.* (2020), prepared Gly loaded glyceryl monostearate solid lipid nanoparticles which showed 87.82% drug release for 14 hours. It enhanced the dissolution profile of Gly but stability was not achieved with the use of solid-lipid matrix [206]. However, the complete dissolution of Gly is still an issue and in no case, exhaustive formulation studies have been performed. However, despite the numerous attempts, concrete satisfactory results were not still achieved and no commercial Gly products arising from these approaches are available.

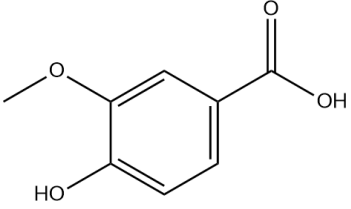
2.9 Vanillic acid

VA is an aromatic phenolic acid, which is an oxidized form of vanillin and gives off a pleasant odour [207]. It is used as flavouring agent in food industries [208]. VA has been extracted from a variety of medicinal plants, amongst which, its higher amount has been obtained from the roots of *Angelica sinensis* [207]. It is formed by secondary metabolism in plants. Its traces have been identified in olives, cereals, whole grains, fruits, green tea, juices, beers, and wines [209].

These are the constituents of regular diet consumed on daily basis. Thus, VA helps to manage/reduce the oxidative stress on due to its antioxidant potential. Commercially, it is used in argan oil, wine and vinegar because of its acidity. Amongst the dietary sources, its highest content is found in dried fruits (4.13 mg/100g) and in sweet basil (14 mg/100 g) (<http://phenol-explorer.eu/contents/polyphenol/414>) (Accessed on 25 October 2021).

It is also a metabolic byproduct of caffeic acid and its traces have been identified in human urine. Ebinger, in 1976, identified VA as one of the endogenous biochemicals derived from catecholamines. It was also identified in various parts of the human brain (cortex, striatum, thalamus, cerebellum, brain stem and hypothalamus) and cerebrospinal fluid (CSF) [210]. Its natural antioxidant and antimicrobial property caught attention of researchers of food and therapeutic science. The physiochemical properties of VA are presented in **Table 2.6**.

Table 2.6: Physicochemical properties of VA

Property	Outcome
Description	Slightly/pale yellow crystalline solid powder
IUPAC Name	4-hydroxy-3-methoxybenzoic acid
Additional Name	Acide vanillique, Benzoic acid
Molecular Formula	$C_8H_8O_4$
Chemical Structure	 <p>The chemical structure shows a benzene ring with a carboxylic acid group (-COOH) at the 1-position, a hydroxyl group (-OH) at the 4-position, and a methoxy group (-OCH₃) at the 3-position.</p>
Molecular weight	168.15 g/mol
Melting point	211.5 °C
Solubility	1.5 mg/mL at 14 °C (slightly soluble in water; soluble in organic solvents)
Log P	1.43
PKa	4.5

2.9.1 Botanical sources of VA and their geographical distribution

Phenolic acids are the aromatic natural phytochemicals, which consist of a phenolic ring and a carboxylic functional group in their chemical structure. These are found in abundance in many plant species and are largely consumed via diet. Phenolic acids are broadly classified into two types i.e. hydroxybenzoic acid derivatives and hydroxycinnamic acid derivatives. Each phenolic acid varies chemically, depending on the number and position of a hydroxyl group at the aromatic ring. VA is an example of hydroxybenzoic acid [3]. It is identified in many plant species, vegetables, fruits and several kinds of cereals [211]. Various botanical sources of VA and their geographical distribution are discussed in the subsequent sections.

2.9.1.1 Actinidia species

Traces of VA are found in *Actinidia deliciosa* and *Actinidia eriantha*, which belong to family *Actinidiaceae* [212,213]. Both the species are native to southern China (colder regions) and the genus has wide geographic distribution in eastern Asia [214]. *A. deliciosa* (kiwi fruit) is the most common and is commercially available natural source of VA. It is cultivated and commercialized in New Zealand, India and Italy [214]. The fruits of *A. deliciosa* plant contain VA as a major bioactive compound. “Hayward” cultivar of *A. deliciosa* from New Zealand is of the best quality due to its higher nutritional value [215].

However, the highest proportion of VA is obtained from the fruits of *A. eriantha* and its cultivar “Bidan”, which is largely cultivated in Korea [212,216,217].

2.9.1.2 *Angelica decursiva*

This plant belongs to family *Umbelliferae* and is widely distributed in Korea, Japan, and China [218]. It is a rich source of coumarin derivatives but the dried methanol extract of the whole plant has been reported to contain VA [219,220]. Mainly, it was isolated in the ethyl acetate fraction during the extraction from the whole plant [220].

2.9.1.3 *Leonurus sibiricus*

This plant is commonly known as “honey weed”. It belongs to the family *Lamiaceae*. It is native to China, Russia and Mongolia. Besides, it is also widely distributed in Japan, Korea, Vietnam, and southern Siberia. VA has been identified in the transformed root extract of this plant [221].

2.9.1.4 *Berberis orthobotrys*

This plant belongs to the family *Berberidaceae* [222]. It is cultivated in the eastern and southern regions of Iran [223]. The presence of VA with other bioactive constituents has been identified in aqueous methanol extract of *B. orthobotrys* [224].

2.9.1.5 *Angelica sinensis*

Angelica sinensis (Oliv.) Diels is a popular medicinal plant in China which belongs to the family *Umbelliferae* [207]. This plant is cultivated at high-altitude mountainous regions especially in outlying areas of China i.e. Qinghai, Gansu, Sichuan, and Yunnan. Among these, Gansu produces the highest yield of VA i.e., 90% of the total Chinese *A. sinensis* production [225]. The highest fraction of VA is obtained from the roots of this plant. Some of the recent studies have identified the presence of VA in *Angelica* stem as well [207].

2.9.1.6 *Cucurbita pepo*

This plant belongs to family *Cucurbitaceae*, and is commonly known as “pumpkin” [226]. This plant is native to America and got distributed to other countries via transoceanic voyagers [227]. The pumpkin seeds have traditional value due to their high nutritional and medicinal properties and have been recently reported as a rich source of VA [226]. The amount of VA identified in the different parts of afore-mentioned medicinal plants with appropriate extraction techniques is presented in **Table 2.7**. The extraction methods reported so far for the isolation of VA have been summarized in **Fig 2.4**.

Table 2.7: Amount of VA isolated from different parts of medicinal plants

Botanical source	Parts/extract	Extraction/Isolation technique	Quantification	Yield (µg/g)	References
<i>A. deliciosa</i>	Fruit	Aqueous extraction	HPLC	5.41	[212]
<i>A. deliciosa</i>	Pulp extract	Organic solvent extraction	GC-MS	34000	[228]
<i>A. eriantha</i>	Fruit	Aqueous extraction	HPLC	7.15	[212]
<i>A. decursiva</i>	Whole plant	Organic solvent extraction	HPLC	39.3	[220]
<i>L. sibiricus</i>	Transformed root extract	Ultrasonic extraction	HPLC-ESI-MS/MS	3390	[229]
<i>B. orthobotrys</i>	Crude extract	Cold maceration process	HPLC	4.4	[224]
<i>A. sinensis</i>	Roots	Ultrasonic extraction	GC-MS	1300	[207]
<i>A. sinensis</i>	Stem	Ultrasonic extraction	GC-MS	1160	[207]
<i>C. pepo</i>	Seeds	Vacuum filtration	HPLC	18000	[226]

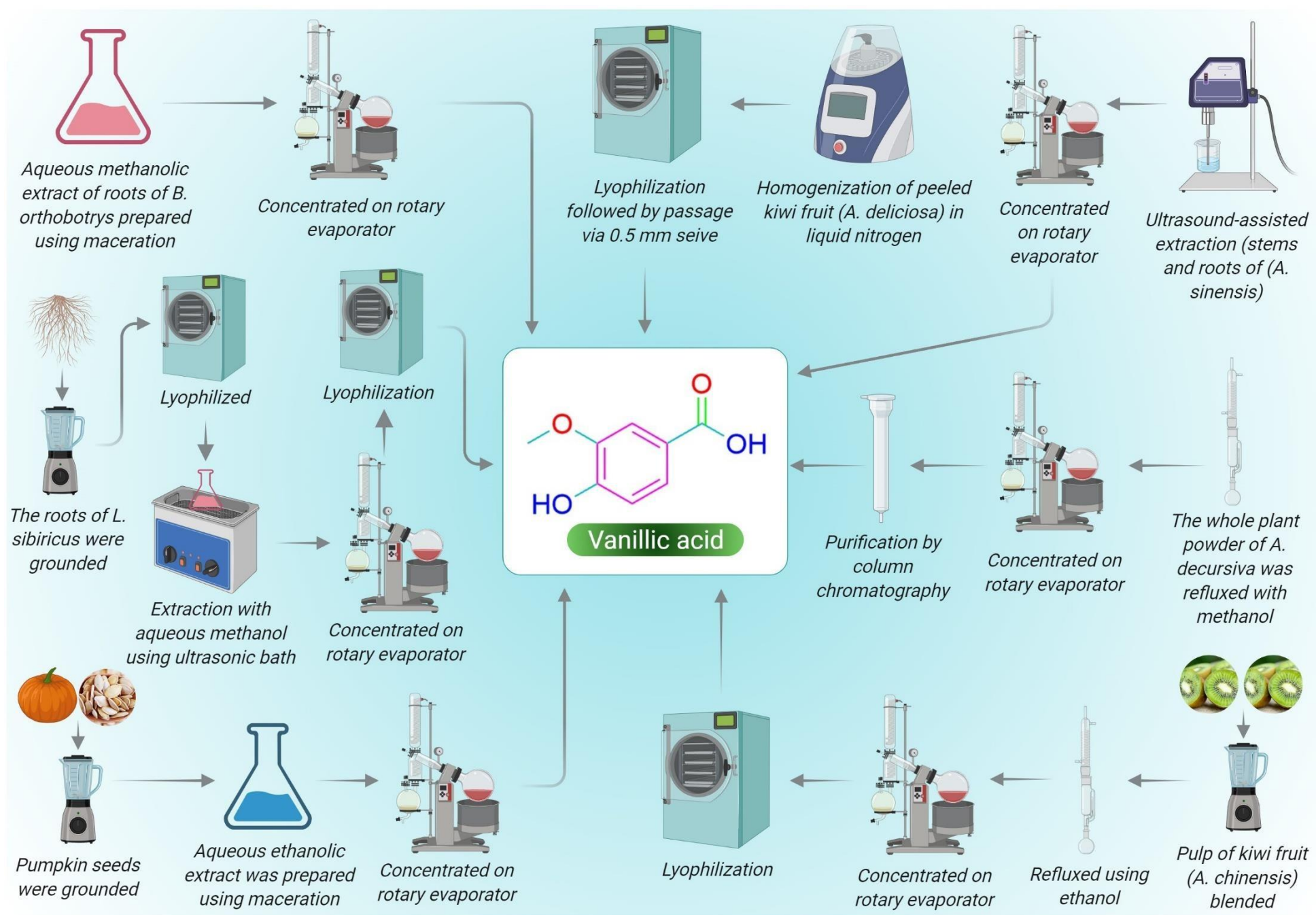


Fig 2.4: Methodologies used for the extraction of VA from natural sources

2.9.2 Pharmacological activity of VA in T2DM

Several studies have demonstrated the role of VA in ameliorating obesity condition by reducing lipid and inflammatory markers. Further, indicated the potential for its use in obesity associated hepatic insulin resistance. For instance, Feng *et al.* (2007), revealed that VA derivative from *Cladophora socialis* suppressed protein tyrosine phosphatase 1B, which is involved in negative modulation of insulin signalling in cell and its inhibition enhances insulin sensitivity [230]. Another study demonstrated the antihyperglycemic effect of VA in high-fat diet (HFD) fed rat model (**Fig 2.5**). The results showed that four-week treatment of VA-induced down-regulation of COX-2 and MCP-1 protein expression in HFD fed rats. It also increased the hepatic phosphorylated ACC protein expression with reduced hepatic non-esterified fatty acid (NEFA) levels [17].

Treatment of VA for 112 days was reported to ameliorate the hepatic insulin resistance by increasing the expression of insulin receptor, PI3K and glucose transporter 2 (GLUT-2) protein in HFD fed rats [25].

Jung *et al.* (2018), reported the anti-obesity effect of VA in an *in vivo* study. It stimulated AMPK α - and thermogenesis in obese mice and reduced two major adipogenic markers, peroxisome proliferator-activated receptor γ (PPAR γ) and CCAAT/enhancer-binding protein α (C/EBP α) [18]. In another similar study, VA stimulated thermogenesis in adipocyte by increasing the mRNA expression of thermogenic gene uncoupling protein 1 (UCP1) and mitochondrial specific proteins (ATP5A, NDUFB8, NRF2). Besides, it activated transcription factors in beige cells and upregulated the expression of brown like adipocyte marker [231].

Mahendra *et al.* (2019), in an *in vitro* study, reported that VA exhibited glucose-stimulated insulin release in INS-1 cell line and in quarantined rat pancreatic β -cells via the activation of cyclic adenosine monophosphate-protein kinase A pathway, followed by phosphorylation of extracellular signal-regulated kinase $\frac{1}{2}$ [232].

VA has also been explored in the effective management of DM associated complications such as diabetes associated oxidative stress, inflammation, neuropathic pain, and cardiovascular complications. For instance, Ji *et al.* (2020), reported that oral administration of VA at dose 50 mg/kg in STZ-induced diabetic rats reduced HbA1c and glucose levels, increased insulin levels near to glyburide and reduced the levels of inflammatory markers. This indicated potential role of VA in managing diabetes associated oxidative stress and inflammation [233]. In one of the studies, oral administration of VA at dose at dose 100 mg/kg ameliorated neuropathic pain by inhibiting neuroinflammatory responses, increasing the levels of glutathione, and improving

motor neuron conduction [234]. In another study, VA (50 mg/kg) treatment in HFD fed rats for 8 weeks resulted in a significant decrease in FGLs, insulin and blood pressure levels in comparison with diabetic control group. The antioxidant activities were significantly increased and the levels of lipid peroxidation markers were significantly decreased in diabetic hypertensive rats treated with VA [25].

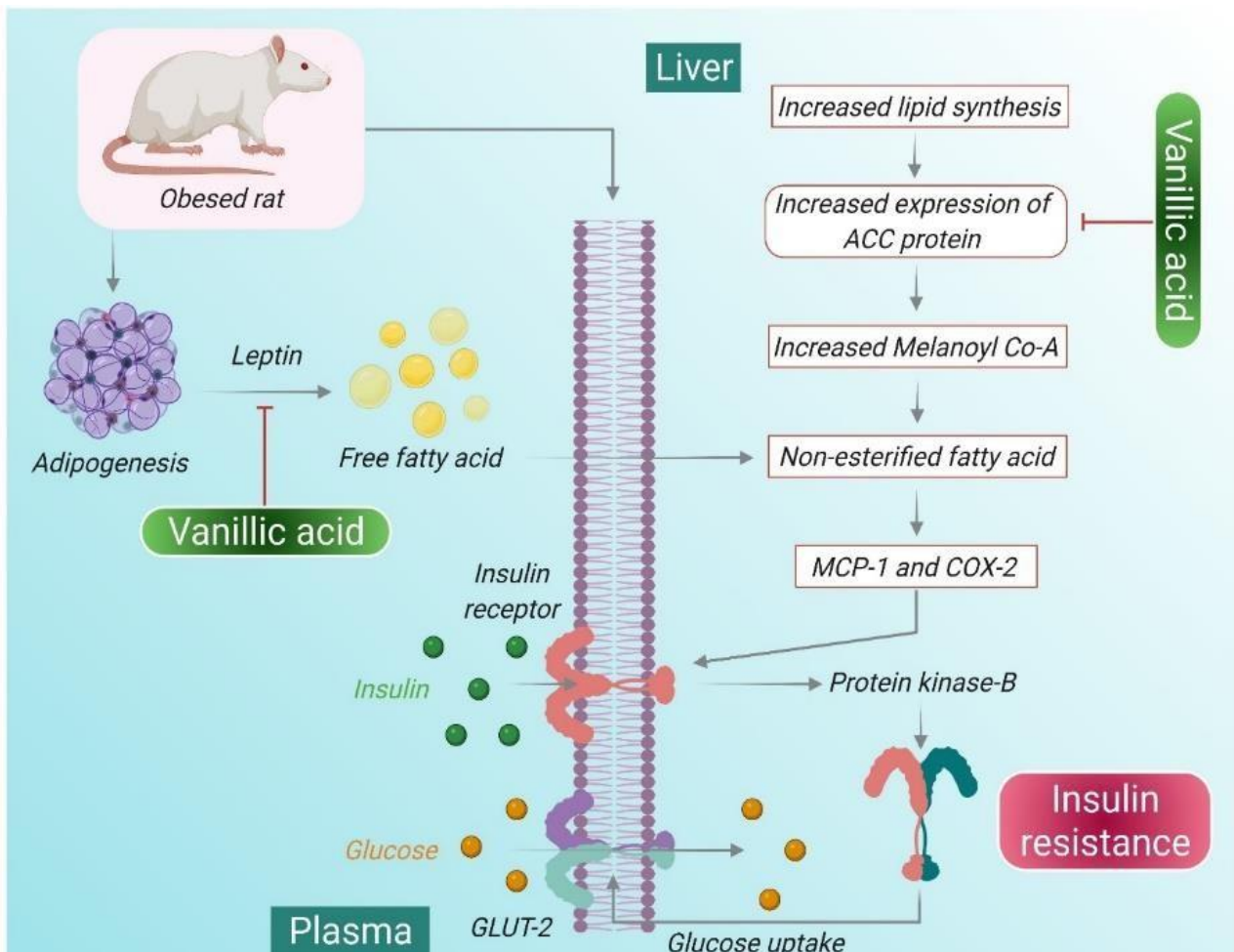


Fig 2.5: Proposed mechanism of action of VA in improving insulin resistance

Abbreviations: ACC, Acetyl CoA carboxylase; NEFA, Non-esterified fatty acid; MCP-1, Monocyte chemoattractant protein-1, GLUT-2, Glucose transporter-2, COX-2, Cyclooxygenase-1.

2.9.3 Safety studies of VA

Toxicity potential of VA needs to be evaluated to rule out any harmful effects caused by it. Administration of VA (1000 mg/kg) for 14 days, was reported to be devoid of toxicity and mortality in Wistar rats. The lethal dose (LD₅₀) of VA in rats and mice was reported to be 5020 mg/kg and 2691 mg/kg respectively upon intraperitoneal administration [235]. Erdem *et al.*

(2012) reported dose-dependent toxicity of VA in human peripheral lymphocytes. It was observed that VA, at a dose of 2 µg/mL, exhibited genotoxic effect (DNA damage) and upon combination with mitomycin C, its genotoxic effect was enhanced. Whereas, at lower dose (1 µg/mL), it was found safe when administered alone or in combination with mitomycin C [236]. In another study, four days' treatment of VA (100 µM) showed non-cytotoxic effect on *Rattus norvegicus* hepatoma cells, whereas at higher dose (500 µM), it induced DNA breakdown in MTT assay [237]. Similarly, it displayed no cytotoxic and genotoxic effect in Chinese hamster ovary cells and human lymphocytes at a dose of 168 mM [238]. In another study, VA at a dose of 50 µM in one-day treatment was found safe on rat hippocampus embryonic cells [239].

2.9.4 Future direction

Herbal drugs have been used since ancient times to treat various diseases and they are still being used as traditional and alternative systems of medicines such as Ayurveda. Their therapeutic potential has attracted people for using them as nutraceuticals for prophylaxis of many metabolic diseases that occur due to oxidative stress, such as obesity, diabetes, cardiovascular diseases etc. As per the report of 2019, it has been reported that the global herbal medicine market size was estimated to be US\$ 83 billion and this is expected to reach US\$ 550 billion by 2030 at a compound annual growth rate of 18.9% by the end of 2030 [<https://www.globenewswire.com/en/news-release/2021/02/16/2176036/0/en/Herbal-Medicine-Market-Global-Sales-Are-Expected-To-Reach-US-550-Billion-by-2030-as-stated-by-insightSLICE.html>] (Accessed on 26 October, 2021). VA is one such potent nutraceutical that is commercially isolated from kiwi fruits and *A. sinensis*. It is being used since many decades as flavoring agent in bakery items as well as beverages. Though it is reported to possess excellent antioxidant, anti-inflammatory, anticancer, neuroprotective, antidiabetic, cardioprotective as well as hepatoprotective properties, its commercial application as a therapeutic agent is relatively unexplored due to lack of awareness about its therapeutic potential among public. Various mechanistic pathways through which VA can offer therapeutic effect in treating neurological and cardiovascular disorders, cancer, diabetes, as well as other diseases have been deciphered. These include upregulation of p53 expression and stimulation of apoptosis via mitochondrial caspase activation, interruption in protein expression levels involved in HIF-1 α activation in tumor cells, inhibition of biological targets that are involved in disease's pathophysiology etc. The favorable safety profile of VA as reported in the scientific literature strengthened by the fact that it has been used for centuries as a flavoring agent make VA a potential therapeutic candidate. The various

mechanistic pathways of its actions, as discussed above, particularly make it an ideal candidate to synergize the therapeutic potential of the existing drugs.

However, its dissolution rate limited oral bioavailability due to its poor aqueous solubility needs to be enhanced to explore its full potential. Hence, it is important to develop novel approaches for improving its aqueous solubility. These may include nanosuspension, lipid based nanoformulations such as liposomes, nanoemulsions, solid lipid nanoparticles, nanostructured lipid carriers and polymeric micelles. Moreover, clinical trials must be designed to explore its synergistic potential along with existing drugs for the treatment of infectious as well as lifestyle diseases.

2.10 Amphiphilic Block Copolymers

The ABCs consisting of both hydrophilic and hydrophobic blocks connected through covalent bond with an ability to self-assemble in a specific solvent are able to mimic the biological systems [240]. These are generally made of biocompatible, non-immunogenic, biodegradable lipophilic blocks i.e., polyesters or poly (amino acids) attached with biologically compatible hydrophilic blocks usually PEG [241]. In recent years, significant progress has been made to design various ABCs with different combinations and varying block length by controlled/living radical polymerization techniques [242,243]. This technique further includes atom transfer radical polymerization, reversible addition-fragmentation chain transfer or nitroxide mediated polymerization. Such techniques are widely employed in the synthesis of copolymers. These techniques are preferred over conventional polymerization techniques based on the parameters presented in ***Table 2.8***.

Table 2.8: Conventional polymerization Vs. controlled radical polymerization techniques [242,244–252]

Parameters	Conventional polymerization techniques	Controlled radical polymerization techniques
Chemical compatibility	<ul style="list-style-type: none"> ➤ Chemically incompatible with various monomers ➤ Sensitive to functional groups 	<ul style="list-style-type: none"> ➤ Offer compatibility with various chemically distinct monomers ➤ Resistant to functional groups
Purity	<ul style="list-style-type: none"> ➤ Presence of impurity in designed ABCs 	<ul style="list-style-type: none"> ➤ Eliminates impurity from designed ABCs
Degree of polymerization	<ul style="list-style-type: none"> ➤ Provide uncontrolled polymerization of monomer unit 	<ul style="list-style-type: none"> ➤ Offer controlled degree of polymerization
Polydispersity	<ul style="list-style-type: none"> ➤ Other side reactions provide multimodal distribution (Dispersity>2) 	<ul style="list-style-type: none"> ➤ Offer narrow molecular weight distributions (Dispersity <1.1)
Molecular weight	<ul style="list-style-type: none"> ➤ Provide no control over molecular weight 	<ul style="list-style-type: none"> ➤ Provide control over molecular weight
Chain termination	<ul style="list-style-type: none"> ➤ Irreversible chain termination 	<ul style="list-style-type: none"> ➤ Reversible chain termination

The ABCs produced by polymerization of more than one type of monomer result in generation of molecule having opposite affinities in aqueous medium. Thus, broad range of ABCs with unique characteristics can be formed depending on the type of monomer and variable block numbers. Production of two monomers with different chemical characteristics forms di-block copolymer and production of three distinct monomers in which either two monomers can be chemically same (ABA type) or all the three monomers can be chemically different (ABC type), form tri-block copolymer [249,253]. In addition to this, graft copolymers are also available. These consist of backbone chains with several branches of different macromolecular chains having distinct chemical composition bounded by covalent bonds. These are randomly distributed along the backbone chain as presented in *Fig 2.6* [254].

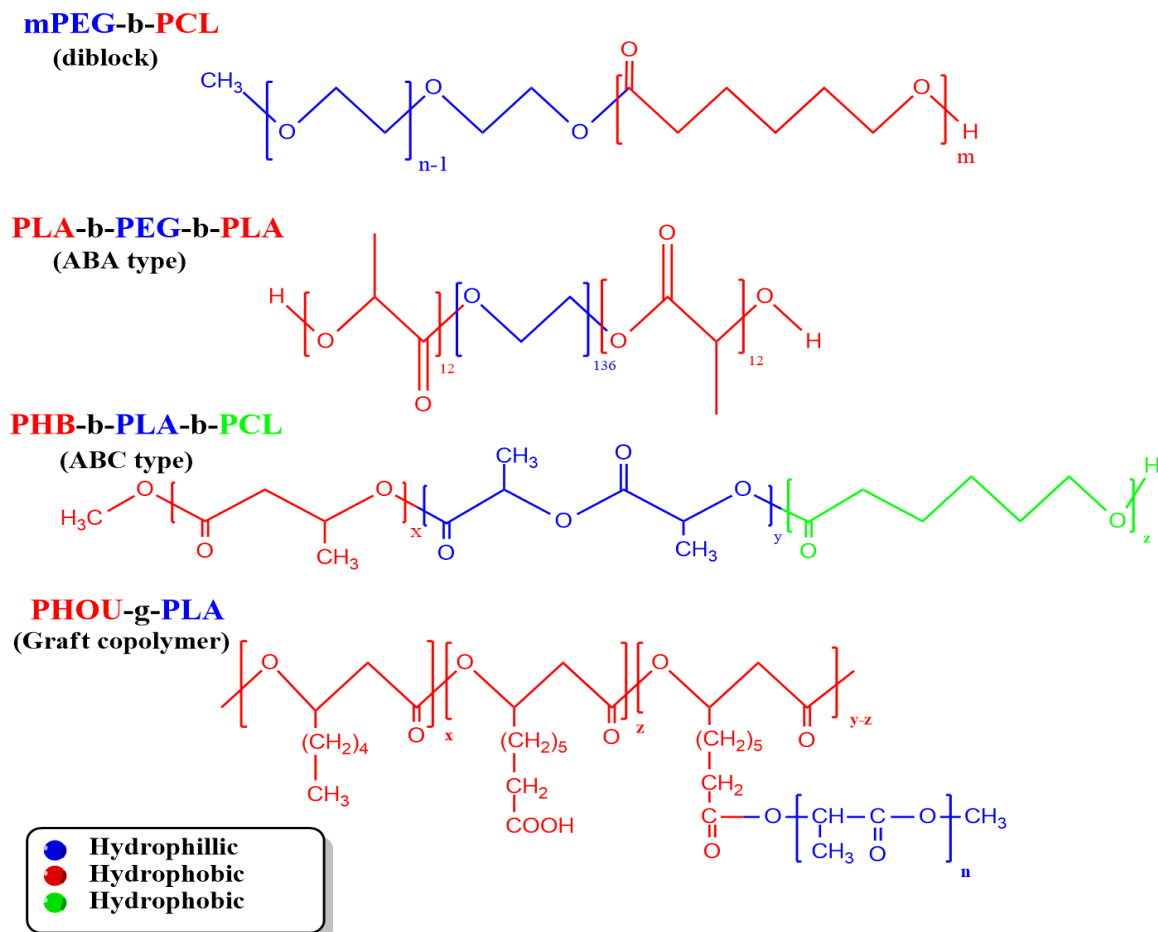


Fig 2.6: Chemical structures of different amphiphilic molecules

Self-assembly of amphiphilic molecules involves weak forces such as hydrogen bonding, hydrophobic effects, electrostatic interaction and van der Waals forces. However, overall strength of each interaction results in strong interaction, which is sufficient to embrace the different amphiphile molecules together and ensure stability in solution as well. These weak forces make the self-assembled structure more flexible and impart resistance for minor perturbation. These impart reversibility to the self-assembled structures upon their preservation [240].

2.10.1 Amphiphilic Polymeric Micelles

The APMs are formed from amphiphilic block copolymers (ABCs) that consist of hydrophilic and hydrophobic segments. These ABCs above their critical micelle concentration (CMC) self-assemble into nanoscopic supramolecular configuration i.e., micellar structure containing corona formed from hydrophilic block and core formed from hydrophobic block respectively as shown in **Fig 2.7** [241,255–261]. The ABCs undergo reversal of orientation in hydrophobic media to form reverse micelle as well [262]. The size of APMs ranges from 10-100 nm [263], which prohibits their accumulation in organs [264]. Core of APMs has potential to encapsulate

more than one lipophilic drugs at a time with targeting ability at site of interest. PEGylated corona of APMs exhibits prolonged circulation time in the blood offering enhanced intracellular accumulation, controlled and sustained drug release [265,266].

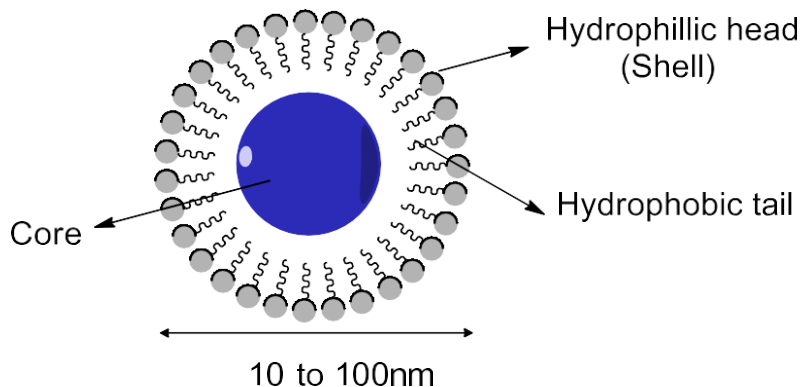


Fig 2.7: Self-assembly of ABCs into APMs

APMs owe their clinical advantages due to their low CMC (0.1-1 μ M) [267,268], metabolic stability, and enhanced solubilization of lipophilic drugs [269–273]. APMs can overcome limitations of the oral delivery of lipophilic drugs by acting as carriers that can enhance drug absorption, by providing protection to the loaded drugs from the harsh environment of the GI tract, release of the drug in a controlled manner at target sites, prolongation of the residence time in the gut by mucoadhesion, and inhibition of efflux pumps to improve the drug accumulation [274]. This is achieved by the hydrophilic corona that confers aqueous solubility upon exposure to the aqueous environment of the GIT.

The core of PMs provide protection to the entrapped therapeutic drug (depending on to the nature and physicochemical properties) from the harsh environment of the GIT via hydrophobic interactions [275]. Further, improves the drug absorption by enhancing the intestinal permeability owing to the ABCs that increases the fluidity of the membrane or loosen the tight junctions for paracellular passage [276].

For instance, Dian *et al.* (2014), reported increase in the oral bioavailability of quercetin by 286% with 2.1-folds longer half-life upon loading it in Polaxamer 407 and Soluplus® based mixed PMs [277]. In another study, Zhang *et al.* (2016), reported 2.0-folds increase in the AUC and C_{max} of the PTX upon loading in Solutol HS 15 and D- α -tocopheryl polyethylene glycol succinate based PMs. This resulted in increase in the antitumor efficacy ($p < 0.05$) of the drug against breast cancer than that of free drug respectively [278].

Therefore, PMs can be designed to cross the intestinal barriers by using permeation enhancers such as cationic polymers (e.g., chitosan and its derivatives), anionic polymers (e.g., polyacrylic acid and its derivatives), or calcium chelators (e.g., ethylenediaminetetraacetic acid) in the copolymer network. Further, PMs can be designed for active transcellular transport to enhance the oral bioavailability of the loaded cargo. This mainly involves phagocytosis, macropinocytosis, clathrin-mediated endocytosis, and caveolin-mediated endocytosis [279].

2.10.2 Factors affecting physicochemical properties of APMs

There are various factors, which govern the physicochemical properties of APMs. These include size, shape, CMC and surface charge. Size is an important parameter to govern the bioavailability, penetration and site-specific delivery of APMs. APMs of small size increase the bioavailability and penetration of drug [280] and offer passive targeting to tumors by enhanced permeation and retention effect [281,282].

The size of APMs can be optimized by controlling ABCs based factors, formulation and processing parameters. ABCs based factors include molecular weight and effect of block length/hydrophobicity while formulation and processing-based parameters include drug to copolymer ratio, temperature, composition of solvent/co-solvent system, concentration of copolymer and type of solvent used.

Size of APMs is influenced by change in molecular weight of blocks in ABCs. Increase in the molecular weight of both the hydrophilic and hydrophobic blocks is reported to increase the size of APMs. Bas *et al.* (2012), reported that increase in the molecular weight of hydrophilic block (PHPMA) of copolymer PHPMA-b-PDMS-b-PHPMA increases size by 2.1-folds [283]. Bagheri *et al.* (2018), reported that increase in molecular weight of the hydrophobic block (HPMA) of copolymer MPEG-b-p(HPMA-Bz) increases size by 1.6-folds [284].

Increase in core to corona block length of copolymer increases aggregation number of copolymers, and reduces CMC of amphiphilic molecules. This ultimately reduces the size of APMs. Change in any of the above-mentioned parameter affects the size of APMs. Li *et al.* (2011), reported that increase in core to corona block length (PBMA/PAM) by 7.7-folds resulted in increase in the aggregation number of copolymers by 5-folds. This reduced the CMC value by 2.6-folds, and ultimately decreased the size by 1.7-folds. However, increase in corona block length (PAM) in copolymer with constant core block length increased size by 1.7-folds [285].

Glavas *et al.* (2013), reported that the length of core forming block is a dominating factor in controlling the size of APMs. PEG-PεDL copolymer with increased core block length increased

the size of APMs as compared to PEG-PCL respectively. PEG-P ϵ DL copolymer with amorphous core (higher CMC) increased the size of APMs by 2-folds with increase in core block length than PEG-PCL with semi-crystalline core. However, despite of difference in core crystallinity, no significant difference in size was observed by keeping core block length constant [286].

Shape of APMs primarily affects their solubilization efficiency i.e., it depends on to the locus of drug solubilization in APMs. Solubilization of drugs in core increases with increase in asymmetry of APMs, as it leads to an increase in the relative volume of core [287]. APMs are mostly spherical in shape and can exist in other morphological forms, which depends on ABC based parameters. This include (i) hydrophilic volume fraction, f , (ii) block length and (iii) heterogeneity in block structure.

APMs formed from copolymer with corona block content more than 30% at physiological temperature and f greater than 45% exist in spherical shape [288]. Spherical morphology intensely reduces the exposure of hydrophore to the bulk aqueous solution with steric stabilization and shows shear thinning rheological property [289,290]. Copolymer with longer core block chain forms APMs of cylindrical (worm and rod like) shape. Branched or even brush like corona promotes the formation of unimolecular star micelle by lowering the aggregation number [291,292].

The ABCs of different shapes such as cyclic, tadpole and linear are able to form various micellar topologies [293]. This include prolate and oblate ellipsoid micelles, respectively as presented in **Fig 2.8**. Cvejic *et al.* (2014), reported 4.6-folds increase in the resveratrol solubilization in sodium $3\alpha,12\alpha$ -dihydroxy-7-oxo- 5β -cholanoate based APMs of longitudinal shape as compared to that in sodium dodecyl-sulfate based APMs of spherical shape [294].

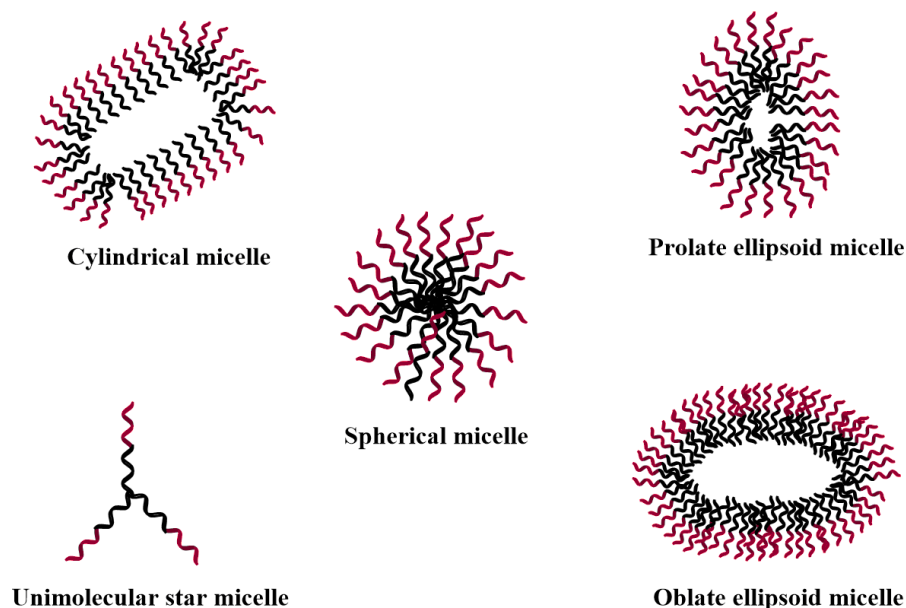


Fig 2.8: Various topologies of micelles obtained by amphiphilic block copolymer

Surface charge of APMs has strong impact on the stability of APMs and in targeting the delivery of drugs [295,296]. PEG-b-PCL based APMs with attached NH_2 functional group displayed aggregation behavior in the presence of bovine serum albumin due to strong electrostatic interaction between oppositely charged APMs and serum albumin protein.

On the other hand, no aggregation behavior was reported in APMs composed of negatively charged carboxyl group, neutral methoxy group and mixed charged APMs composed of carboxyl and amino group. In order to combine the advantages of both the positively and negatively charged APMs, the design of mixed charged APMs is also reported. This offers excellent stability, prolonged circulation time in blood and efficient cell uptake [296].

CMC of ABCs govern the stability of APMs. The lower the CMC value, the higher will be the stability of APMs. CMC of ABCs is primarily affected by properties of core forming blocks such as hydrophobicity, degree of crystallinity, and core/corona ratio [270]. Increase in hydrophobicity of core forming block results in improved thermodynamic stability to APMs [297].

The crystallinity of core forming blocks plays an important role in the stability of APMs. The semicrystalline nature of core forming blocks provides higher thermodynamic stability than that of the amorphous ones [298]. Increase in core/corona ratio at fixed corona block length has been reported to reduce the CMC value of copolymer. This leads to the formation of stable APMs [270,299].

2.10.3 Methods of preparation of APMs

There are various methods used in the formation of APMs, which include chemical conjugation, and physical methods. These methods are commonly used and widely accepted for the development of micellar drug delivery systems. The detailed description of each method and the challenges associated are discussed in subsequent sections.

2.10.3.1 Chemical conjugation method

Helmut Ringsdorf in 1975 introduced the concept of covalently bound polymer-drug conjugates for the delivery of small lipophilic molecules. He proposed the model of pharmacologically active polymers, which were highly biocompatible and used for three different purposes, i.e., (i) as solubilizers for imparting hydrophilicity, (ii) for drug binding via bonds, and (iii) as targeting moiety for delivery of drugs to desired destination. The aqueous solubility of lipophilic drugs gets improved by their conjugation with water-soluble polymers.

In addition to this, the polymer-drug conjugates offer targeted delivery of drugs, which further improves efficacy and reduces toxicity [300,301]. This concept of polymer-drug conjugates has been widely explored in the formulation of nanomicellar based drug delivery systems. In this, the covalent conjugation of drugs to hydrophobic segment of copolymer of choice leads to successful encapsulation upon their self-assembly in aqueous medium.

2.10.3.2 Physical methods

These methods were developed in late 1980s. Physical method of APMs formation allows incorporation of drug and copolymer in a specific organic solvent/aqueous buffer having complete solubility in it. Selection of solvents depends on the HLB value of the ABCs. Most of the methods under this category require the use of organic solvent and their subsequent removal from the micellar solution enabling the formation of drug loaded APMs in aqueous medium. This method is preferred over chemical conjugation, as it does not require modification of drugs for conjugation.

Several materials can be physically incorporated into the core of APMs, such as contrast agents, fluorophore, hydrophobic dyes etc. This method allows modification of both molecular parameters of copolymer and critical process parameters for the formation of APMs of required physicochemical property [298]. Methods, which are commonly used for the formation of drug-loaded APMs are discussed in the subsequent sections with diagrammatic presentation as shown in *Fig 2.9*.

2.10.3.2.1 Direct dissolution method

It allows easy formation of drug loaded APMs by directly dissolving both drug and copolymer (high HLB value) in aqueous solvent (**Fig 5A**) [302–305]. This method provides good solubilization of lipophilic drugs in APMs. However, it is associated with low EE [306].

2.10.3.2.2 Dialysis method

It requires copolymers with less HLB value to form APMs by solubilizing them and the drug in water-miscible organic solvent. This solution is dialyzed against water. This favors formation of APMs after complete removal of organic solvent (**Fig 5B**) [302,304,307]. This method is advantageous in terms of ease of controlling process parameters. However, this method has serious limitations such as extended period of dialysis to ensure complete removal of organic solvent, low EE, low yield, poor stability and large size [288,302,304,307,308].

2.10.3.2.3 Thin film hydration method

In this method, both the drug and copolymer (low HLB value) are dissolved in a common organic solvent in a round bottom flask. A thin film of drug-copolymer is formed after evaporation of organic solvent by rotary vacuum evaporation. Hydration of dry thin film facilitate the formation of APMs (**Fig 5C**). The major advantages of this method include easy experimental set-up and suitability for small to mid-size batches [297,309,310]. However, the associated limitations include poor scalability due to size restrictions of round bottom flask and rotary evaporator capacity [311,312].

2.10.3.2.4 o/w emulsion solvent evaporation method

The method is also known as “liquid antisolvent precipitation method”. In this, the drug and copolymer are dissolved in organic solvent and added to water in a controlled manner. Here, water serves as an antisolvent. This mixture is emulsified using high-speed homogenizer. The evaporation of organic solvent leads to the formation of APMs (**Fig 5D**) [313,314]. The major advantages of this method include its scalability potential and better control of processing parameters. This method is associated with poor control over size [311].

2.10.3.2.5 Direct freeze-drying method

It involves the use of organic solvent/water system to dissolve drug and copolymer. *Tert*-butanol is commonly used as organic solvent in this method. Both drug and copolymer are dissolved in mixture of organic and aqueous solvent and lyophilized to form dried powder that forms APMs upon reconstitution (**Fig 5E**). The advantages of this method include good drug loading efficiency, sterility assurance, better stability and large-scale production of APMs [87,110]. The main limitation of this method is the risk of the presence of residual organic solvent in the final product [311].

2.10.3.2.6 Fast heating method

The method is generally applied for thermosensitive block copolymer. Its solubilization in distilled water or aqueous buffer with heating at temperature below to above critical micelle temperature leads to the formation of APMs (***Fig 5F***). The major advantages of this method is its simplicity, scalability, and requirement of very less organic solvent to solubilize drug of interest. However, this method is rarely used for the formation of APMs, as its application is limited to thermosensitive polymers. Moreover, the issue regarding the thermodynamic stability of polymers is the major drawback of this method [315,316].

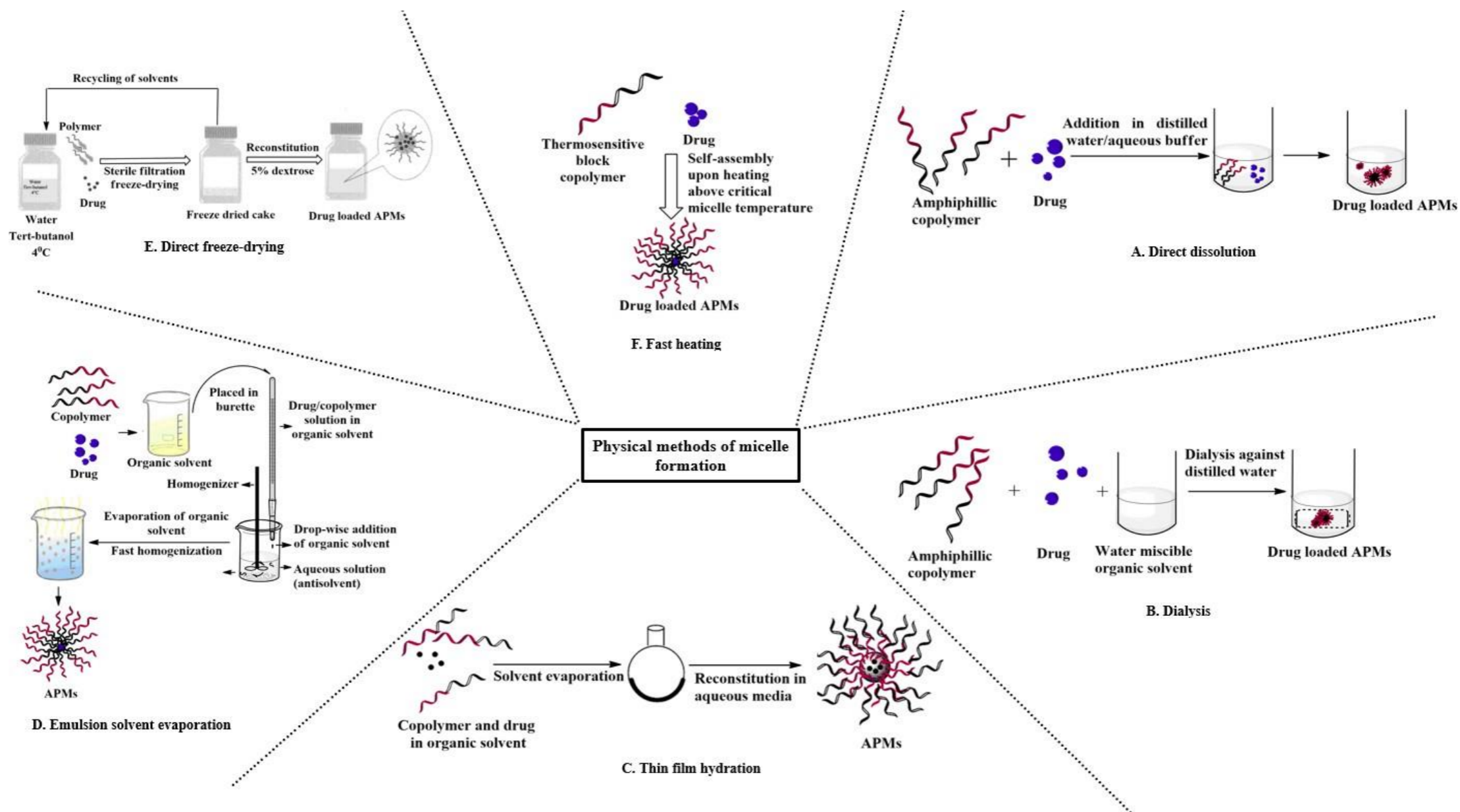


Fig 2.9: Physical methods used in the formation of drug loaded APMs

2.11 Therapeutic applications of APMs in T2DM

2.11.1 Oral drug delivery

APMs have been widely explored in improving the oral bioavailability of poorly water-soluble drugs especially chemotherapeutic drugs with controlled release properties [317]. This has attracted the attention of many researchers for their further exploration in the delivery of synthetic anti-diabetic drugs having poor pharmacokinetic profiles [318]. Despite extensive advancements in drug delivery systems, the frequent dosing of synthetic anti-diabetic drugs due to immediate release profile offers an increased risk of side effects in long run [7,178,319]. This has shifted the focus of researchers on micellar-based drug delivery systems that offer controlled release property. As a result, augment the therapeutic efficacy of loaded cargoes with reduced dosing frequency and safety in long run [19]. In addition, these protect drugs from their burst release due to strong hydrophobic interaction with the micellar core, which increases their availability in systemic circulations. Further, they offer improved intestinal permeability to enhance the absorption of loaded drugs into systemic circulations upon oral delivery [320–323].

For instance, Danafar *et al.* (2018), developed gliclazide loaded PMs composed of methoxy poly (ethylene glycol)-polycaprolactone to enhance the therapeutic efficacy of the drug. The PMs released more drug at pH 5.5 i.e., (78 %) than at pH 7.4 (72 %) over a period of 120 h in a sustained manner. The sustained pattern of drug release from PMs was attributed to the strong hydrophobic interaction of the drug with the micellar core. The *in vivo* studies revealed about 1.1-folds higher reduction in blood glucose levels upon oral administration of drug-loaded PMs in comparison to the free drug in sustained form (21 days) [7].

Han *et al.* (2020), developed zwitterionic betaine PMs composed of polycarboxybetaine and 1,2-distearoyl-*sn*-glycero-3-phosphoethanolamine for *in vivo* oral insulin delivery. The *in vitro* study revealed higher penetration of the developed PMs across intestinal epithelium via proton-assisted amino acid transporter-1 (PAT-1) that is responsible for the penetration of betaine and its derivatives. These PMs did not disrupt the integrity of tight junctions upon exposure to monolayer Caco-2 cells while the blank PMs disrupted the tight junction protein ZO-1. In addition, the developed PMs decreased the blood glucose levels by 1.2-folds in diabetic mice in comparison to native insulin. This indicated improved intestinal absorption of the developed PMs for oral insulin delivery. Therefore, these PMs exhibited 4-folds higher *in vivo* pharmacological activity in comparison to non-zwitterionic PMs [324].

2.11.2 Stimuli-triggered insulin delivery

To improve the patient compliance and glucose homeostasis of insulin, the oral route is considered a convenient administration route, which is safe and non-invasive [8]. However, the poor permeation across intestinal mucus, low absorption and bioavailability of oral insulin formulations hamper their clinical translation [325,326]. To resolve this issue, PMs as an effective nanocarrier have been reported to increase the absorption of insulin in the gastrointestinal tract and facilitated insulin uptake via transcellular/paracellular pathway upon oral administration [279].

In addition to this, PMs have been reported to provide targeted delivery of insulin at intestinal and neutral pH without opening tight junctions with high controlled release than that at gastric pH [165]. This indicated good stability of PMs in the gastric environment and stealth property in systemic circulations [327]. Thus, PMs resulted in efficient delivery of insulin upon oral administration.

For instance, Hu *et al.* (2013), reported the formation of pH-responsive cationic polymeric micelles (PCPMs) formed from poly(methyl methacrylate-co-methacrylic acid)-block-poly(2-amino ethyl methacrylate) for oral insulin delivery. The developed PCPMs exhibited sharp pH-sensitive behaviour with change in particle size, which allowed increased absorption of insulin in the alkaline environment of the gastrointestinal tract. An increase in pH from 1.8 to 6.0 exhibited a decrease in size while further increment in pH from 6.0 to 7.4 resulted in increased size. This was attributed to increased ionization of methacrylic acid segment with an increase in alkaline pH that induced swelling of PCPMs. The swollen PCPMs released the loaded insulin at pH 7.4 in a sustained manner (more than 50%) than at pH 1.2 (30%) for a period of 6h respectively. This indicated low burst release of loaded insulin at acidic pH without any cytotoxicity [328].

Similarly, Bahman *et al.* (2020), reported that the pH-sensitive PMs composed of poly(styrene-co-maleic acid) loaded with insulin increased the 2-deoxyglucose uptake by 15% in HepG-2 cells in comparison to free insulin over a period of 1h respectively. Further, it led to a larger accumulation of fluorescent 2-deoxyglucose in HepG-2 cells while free insulin failed to accumulate fluorescent 2-deoxyglucose. The PMs exhibited low burst release in simulated gastric fluid and released almost 23% of loaded insulin in pH 7.4 over 36 h in a controlled manner. In addition, PMs enhanced the transport efficiency of insulin across the intestinal ileum by 2-folds than duodenum and by 3.6-folds than jejunum segment respectively [166].

The *in vivo* study revealed 1.5-folds higher decrease in blood glucose levels by insulin loaded PMs in comparison to diabetic control upon oral administration. Moreover, the repeated oral administration of insulin loaded PMs exhibited higher blood glucose reduction ($p < 0.05$) in comparison to a single dose over 4h. However, the reduction in blood glucose levels by oral insulin loaded PMs was 4-folds lower in comparison to subcutaneously administered insulin loaded PMs respectively. Therefore, optimization of PMs is required to enhance the oral efficacy of insulin [166].

Based on the aforementioned properties, APMs have reached clinical trials and currently there is one insulin formulation based on APMs named as “*Oral-lyn*TM” (Generex Biotechnology Corporation). It has a size of 7 nm designed for oral insulin delivery via local trans-mucosal absorption and is under phase III clinical trial to treat T1/T2 DM [143].

2.11.3 “On-Off” insulin release

Recently, various types of APMs composed of two hydrophilic blocks have been designed for self-regulated insulin delivery in response to physiological blood glucose levels and temperature (stimuli-triggered “on-off” insulin release) [329]. This includes, zwitterionic dialdehyde starch-based APMs, pH-responsive cationic APMs, complex APMs etc. [330–333].

For instance, Zhao *et al.* (2012), developed glucose-responsive polypeptide PMs composed of phenylboronic acid-functionalized block copolymer i.e., monomethoxy poly(ethylene glycol)-*b*-poly(L-glutamic acid-co-N-3-L-glutamylamidophenylboronic acid) for self-regulated insulin delivery. These PMs exhibited 1.5-folds increase in insulin release in phosphate buffer (pH 7.4) in 14h in comparison to PMs containing lower units of phenylboronic acid units in its side chain [334].

This was attributed to a higher fraction of poly glutamylamidophenylboronic acid units in the PMs that led to an increase in permeation of glucose molecules to form a hydrophilic complex in the micellar core. This resulted in swelling of the micellar core followed by disassembly of PMs that favoured faster insulin payloads [334].

In addition to this, these PMs exhibited glucose-responsive insulin release at pH 7.4 with an increase in glucose concentration in the medium. About 1.6-folds higher insulin release was observed in the medium containing 10mg/mL of glucose than in medium containing 5mg/mL of glucose concentration. Further, the bioactivity of released insulin in the medium was retained after being released from the developed PMs and was found hemocompatible and non-toxic [334].

Wen *et al.* (2018), developed zwitterionic dialdehyde starch-based complex APMs composed of sulfobetaine as corona attached with dialdehyde starch backbones with 3-aminophenylboronic acid (SB-DAS-APBA) as a glucose-responsive group for triggered oral insulin delivery with reduced macrophage response. The developed APMs got disaggregated in response to varying glucose concentration in phosphate buffer (pH 7.4) as measured by the change in particle size of the APMs [331].

However, in response to increased glucose concentration, the size was increased by 1.0-fold by the developed APMs in comparison to nonionic APMs with mPEG and dialdehyde starch groups. This indicated enhanced disintegration of the APMs because of the hydrolysis of dialdehyde starch in response to glucose with higher selectivity in comparison to APMs without sulfobetaine. Such results were in correlation with the *in vitro* release study, which exhibited 3.0-folds higher insulin release from the developed APMs in the phosphate buffer, (pH 7.4) containing glucose (1 g/L) in comparison to the medium without glucose in 2 days [331].

In addition to this, the cellular uptake of developed APMs by macrophage cells was 2.6- and 2.3-folds lower than mPEG based nonionic APMs upon incubation for 1 and 4h with lower cytotoxicity respectively. The results indicated great potential for glucose-responsive APMs for insulin delivery [331].

Chapter 3
***Rationale and
plan of work***

Chapter 3

3.0 The rationale of the study

T2DM is a serious lifelong condition. It is mainly characterized by hyperglycaemia that can damage the other parts of the body i.e., the heart, eyes, kidneys, feet, nerves etc. These are the serious complications that can worsen the life of diabetic patients if hyperglycaemia is not controlled [1]. In addition to this, obesity has become an exaggerating factor in such metabolic alteration and in past few years, the prevalence of T2DM has paralleled that of obesity [30]. Increased body mass index and central adiposity are in a strong relationship with insulin resistance and are believed to be the key factor involved in the incidence of T2DM. This is chiefly because of the secondary lifestyle that results in IR [91].

To overcome such serious conditions, oral anti-hyperglycaemic drugs are prescribed by the physician according to the patient-related factors. Among these sulfonylureas are the first oral antihyperglycemic drugs approved by FDA in 1956 to treat T2DM. These are insulin secretagogues that stimulate insulin release from pancreatic β -cells [335].

Gly is a potent synthetic drug, which is the second most widely prescribed drug by the physician that can be used with a proper diet and exercise program to control hyperglycaemia. Its mechanism of action is well known and depends on the functioning pancreatic β -cells. It also acts on broad-spectrum sulfonylurea receptors [12,336]. In addition to this, it possesses anti-inflammatory action as well, which is one of the factors involved in insulin resistance. Gly therapy is initiated from a lower dose range to high based on glycemic control. Generally, the oral antihyperglycemic drugs that are rapidly absorbed by the gastrointestinal tract (GIT) are required to prevent a sudden increase in blood glucose levels after food ingestion in T2DM. However, the poor oral bioavailability of Gly due to its poor dissolution via GIT impedes its clinical performance [337]. It is also associated with higher hypoglycemic episodes i.e., by 80% than other sulfonylureas with a maximum of 20 mg daily dose [12].

It can also be used in the form of combination therapy with other anti-diabetic drugs that result in unwanted side effects upon consumption in long run. Therefore, the co-administration of natural antioxidants with improved toxicity profiles could be a suitable alternative option for increasing the therapeutic efficacy of Gly [13].

VA is a benzoic acid, which is popular as a flavoring agent, natural antioxidant anti-hyperglycemic and anti-obesity effect [14]. Despite its therapeutic potential, VA has not been explored well, especially in the form of combination therapy with other anti-diabetic drugs to treat T2DM. Being a plant-derived product it is reported to act via multiple pathways to control

IR i.e., by increasing the hepatic phosphorylated ACC protein expression with reduced hepatic non-esterified fatty acid (NEFA) levels, increases the expression of the insulin receptor, PI3K and glucose transporter 2 (GLUT-2) protein in HFD fed rats [17]. However, its poor oral bioavailability due to its rapid elimination from systemic circulations upon oral administration is the major challenge in oral drug delivery [14].

The APMs formed from ABCs are excellent candidates for entrapping multiple lipophilic drugs in their hydrophobic core. This formulation as a nanocarrier for co-delivery of drugs has been selected over conventional nanoparticles owing to its low CMC value (stability), self-assembly (ease of particle formation) and controlled-release property (prolonged residence time) that fulfils the objectives of the presented state of the artwork [19]. Further, the micellization process in water due to the balance of intermolecular forces such as hydrophobic electrostatic, hydrogen etc. increases the solubilisation of lipophilic drugs in GIT upon oral delivery. This contributes to the release of loaded drugs from the core in a controlled manner (depending on the hydrophobic interactions with the core) that provides the possibility to improve the dose regimen [19]. Therefore, in the presented work, a nano combination therapy has been developed by co-loading VA with Gly in the core-corona based self-assembled nanoparticles i.e., APMs (*Fig 3.1A and B*).

3.1 Hypothesis

- To optimize the design of controlled release micellar nano-formulation i.e., APMs for the oral delivery of both the drugs (Gly and VA) upon their entrapment in the core.
(The mPEG-b-PCL is a diblock copolymer that self-assembles into nanoparticles with core-corona supramolecular configuration: PCL forms the core and mPEG forms the corona).
- To improve the common challenges associated with existing drug regimens including adverse effects, increased regimen complexity or dosing frequency
(Entrapment of Gly and VA in mPEG-b-PCL APMs will possibly improve the constancy, higher absorption from GIT, systemic distribution of drugs and release of drugs at sustained time intervals)
- Synergistic interaction between both the drugs upon co-loading in APMs owing to an increase in the oral bioavailability of both the drugs in the form of nano-combination therapy
- The schematic presentation of the proposed hypothesis using APMs is presented in *Fig 3.1C*

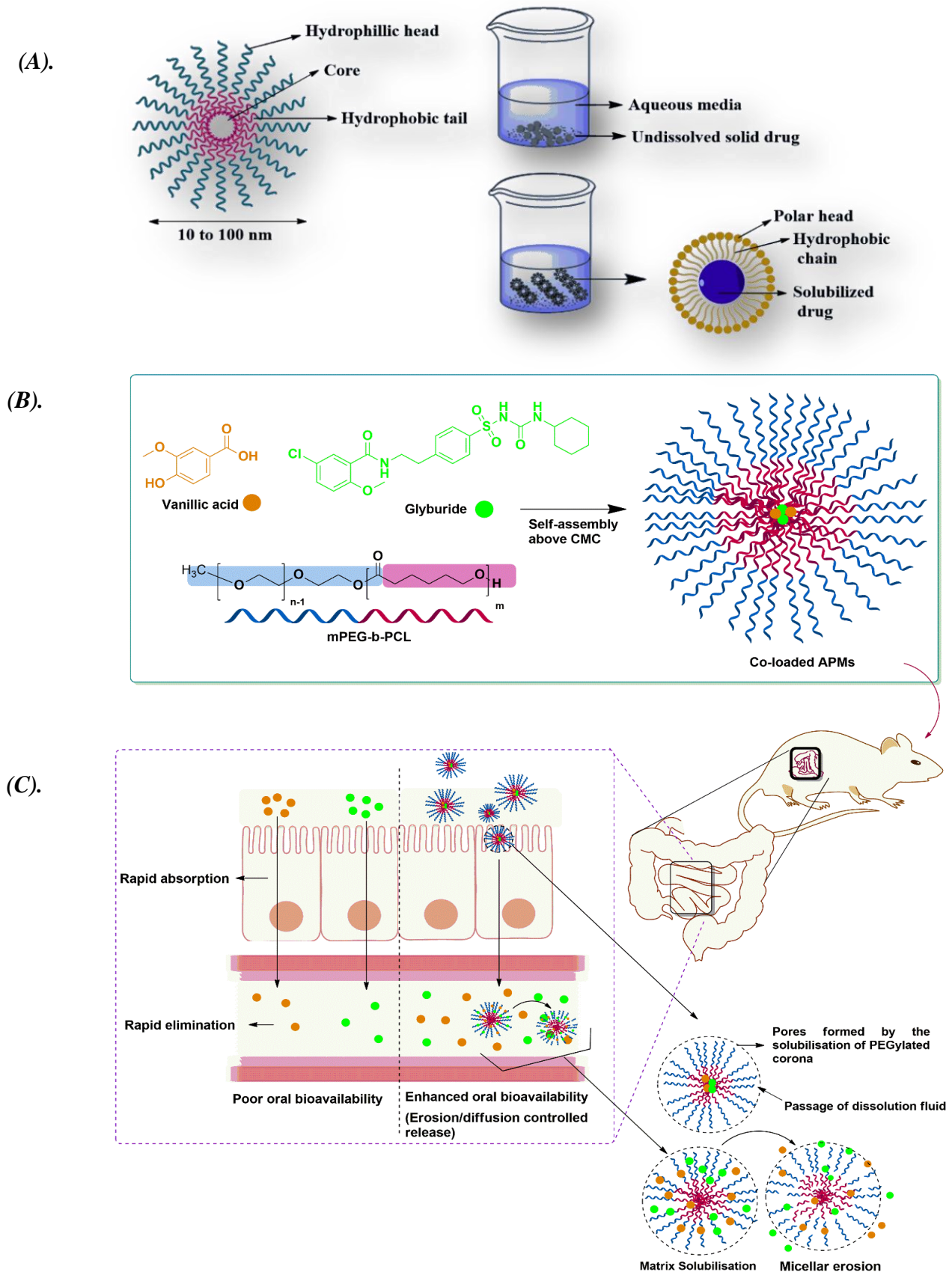


Fig 3.1: (A) Micellization process, (B) Co-loading of drugs in APMs, (C) Proposed hypothesis of the research work

3.2 Aim

Development and optimization of polyethylene glycol methyl ether-polycaprolactone based glyburide and vanillic acid co-loaded amphiphilic polymeric micelles for the management of type-2 diabetes mellitus.

3.3 Objectives

The brief objectives of the research are as follows:

- Development and optimization of the Gly and VA co-loaded APMs
- Characterization of the co-loaded APMs
- Pharmacokinetic evaluation of the optimized co-loaded APMs
- Cell-line studies of the developed formulation
- Pharmacodynamics evaluation of the optimized co-loaded APMs

3.4 Plan of work

Present research work was carried out as per the following steps:

- Literature review on T2DM, conventional drug therapy, and NPs based approaches
- Selection of anti-diabetic drug Gly and natural product VA in the present study
- Challenges associated with the selected drugs that hinder their clinical performance
- Structural characterization of raw Gly and VA for formulation development
- Development of an analytical method for the simultaneous estimation of both the selected drugs in the formulation
- Preformulation studies of both the drugs
- Selection of polymer-based nanotechnology over other NPs
- Synthesis of the amphiphilic diblock copolymer mPEG-b-PCL for the formation of APMs
- Characterization of the synthesized diblock copolymer mPEG-b-PCL
- Selection of a method for physical loading of both the drugs in the core of APMs
- Formation of initial batches for the screening of physicochemical traits of the prepared APMs
- Optimization of the developed co-loaded APMs using DoE expert software 2.0
- Characterization of the optimized co-loaded APMs
- Development of a bioanalytical method for the simultaneous estimation of both the drugs in rats' plasma
- Pharmacokinetic evaluation of the developed formulation
- *In vitro* study: MTT assay and glucose uptake (%) potential of the prepared optimized formulation on Caco-2 and HepG2 cells

- Selection of appropriate animal model for evaluation of the anti-diabetic activity of both the drugs co-loaded in APMs
- *In-vivo* study: High-fat diet (HFD) plus a low dose of streptozotocin (STZ) model was selected to carry out the pharmacodynamics study of the developed formulation for T2DM. SD rats were procured from Punjab University, Chandigarh; the institutional animal ethics committee (IAEC) approved the protocol. The studies were passed out as per the guideline of the council for control and supervision of experiments on animals (CPCSEA).
- Biochemical estimation: Oral glucose tolerance test (OGTT), fasting insulin levels, plasma glucose levels, inflammatory and antioxidant markers
- Histopathological study of liver and pancreas
- Compilation of the results obtained from the aforementioned study

Chapter 4
Experimental Work

4.1 Experimental

4.1.1 Equipments

The list of equipment and chemicals used to carry out the research work is presented in **Tables 4.1** and **4.2**.

Table 4.1: List of equipments used in the research work

Equipment's	Manufacturer
Analytical balance (AX200)	Shimadzu Analytical Pvt. Ltd., Mumbai, India
Cooling Centrifuge	Remi instruments, India
Deep freezer	Blue star ltd., India
Differential Scanning Calorimetry	DSC 6000 PerkinElmer, USA
Digital weighing balance	Contech instruments ltd., India
Electrospray ionization-mass spectroscopy	<i>Q-Tof micro</i> TM
Erba Transasia biochemistry analyzer	<i>Erba, EM360, Germany</i>
Fourier transformer infrared	Perkin Elmer, USA
Hot air oven	Cadmach Drying Oven, Cadmach Machinery Ltd., Ahmadabad, India
High-performance liquid chromatography	HPLC LC-20AD, Shimadzu Co. Ltd., Kyoto, Japan
High resolution-Transmission electron microscopy	JEOL, JEM 2100 Plus
High-speed homogenizer	Thomas Scientific, USA
Magnetic stirrer	Remi 5MLH, Vasai, Mumbai, India
Mechanical shaker	Labfit, Ambala, India
Melting point apparatus	Labotach, Mumbai, India
Micropipettes	Himedia Laboratories Pvt. Ltd.; Mumbai, India
pH meter	Phan, Lab India, Mumbai, India
Proton nuclear magnetic resonance	¹ H NMR, Bruker, Avance-II 500 MHZ, Switzerland
Rotary vacuum evaporator (RV-8) with vacuum pump (MPV10), water bath (HB10) and chiller (IC201T)	IKA, Bengaluru, India
Scanning electron microscopy	JSM7610, JEOL India Pvt. Ltd
Shaking water bath	LabFit, India
Sonicator	Lobachemie, Mumbai, India
Tissue homogenizer	REMI instruments, India
UV-Visible spectrophotometer	Shimadzu corporation, Japan
Vacuum pump	Tarson Products Pvt.Ltd.
Vortex mixer	REMI CM101, Delhi, India
X-ray diffractometer	Bruker D8 Advance, USA
Zeta sizer	Malvern Zetasizer, Nano ZS90, UK

4.1.2 Chemicals

Table 4.2: List of chemicals used in the research work

Chemicals	Manufacturer
Acetone	Loba Chemie Pvt.Ltd., India
Acetonitrile	HPLC grade Rankem
Carboxy methyl cellulose	Loba Chemie Pvt.Ltd., India
Casein	Loba Chemie Pvt.Ltd., India
Cetyltrimethyl ammonium bromide	Loba Chemie Pvt.Ltd., India
Diethylene triamine penta acetic acid	CDH chemicals Pvt.Ltd., India
5,5-dithiobis (2-nitrobenzoic acid)	Sigma Aldrich, Switzerland
Epsilon-caprolactone	TCI, Chemicals, Japan
Ethanol	CDH chemicals Pvt.Ltd., India
Formaldehyde	CDH chemicals Pvt.Ltd., India
Gallic acid	TCI, Chemicals, Japan
Glutathione	Loba Chemie Pvt.Ltd., India
Glyburide	TCI, Chemicals, Japan
Hexane	Loba Chemie Pvt.Ltd., India
Hydrochloric acid	Loba Chemie Pvt.Ltd., India
Hydrogen peroxide	Loba Chemie Pvt.Ltd., India
L-methionine	CDH chemicals Pvt.Ltd., India
Methanol	CDH chemicals Pvt.Ltd., India
Methyl Polyethylene glycol ether	TCI, Chemicals, Japan
Nitro blue tetrazolium	CDH chemicals Pvt.Ltd., India
Octanol	Loba Chemie Pvt.Ltd., India
Orthophosphoric acid	Loba Chemie Pvt.Ltd., India
Polyvinyl alcohol	CDH chemicals Pvt.Ltd., India
Polyvinyl pyrrolidone K90	Loba Chemie Pvt. Ltd, India
Potassium biphthalate	Loba Chemie Pvt. Ltd, India
Potassium chloride	Loba Chemie Pvt. Ltd, India
Potassium dihydrogen orthophosphate	CDH chemicals Pvt.Ltd., India
Sodium chloride	CDH chemicals Pvt.Ltd., India
Sodium hydroxide	Loba Chemie Pvt. Ltd, India
Sodium Lauryl Sulphate	CDH chemicals Pvt.Ltd., India
Stannous octoate	TCI, Chemicals, Japan
Streptozotocin	SRL, laboratories Pvt. Ltd
Thiobarbituric acid	Finar Chemicals Pvt.Ltd., India
Vanillic acid	TCI, Chemicals, Japan
Yeast extract	CDH chemicals Pvt.Ltd., India

4.1.3 Computer programs and software

Table 4.3: List of computer software packages used during the research work

Material	Manufacturer
BioRender®	Crunchbase Pvt. Ltd., Toronto, Canada
Chem Draw Ultra 12.0 Software	CambridgeSoft Corp., Cambridge, USA
Design Expert® (ver. 11.0.5.0)	Stat-Ease, Inc., Minneapolis, USA
DD solver	China pharmaceutical university, Nanjing, China
GraphPad Prism®	GraphPad Inc., La Jolla, USA
Mendeley® Dekstop (ver. 1803)	Elsevier, London, UK
Origin Pro®(ver. 8.5)	OriginLab Corporation, Northampton, USA
Phoenix Winnonlin® (ver. 8.2)	Certara™ Company, USA

4.2 Preformulation studies

4.2.1 Identification of raw drugs and excipients

4.2.1.1 Physical examination

The physical examination was performed by visually analysing the drug samples in terms of colour, aroma, crystals, any precipitation and the presence of impurities. To carry out this, both the raw drugs (1000 mg) were distributed uniformly on a watch glass for the confirmation of their identity and the determination of their quality and purity [338].

4.2.1.2 Melting point analysis

The melting point of both the raw drugs was determined using the capillary melting method. This method is used to measure the melting range of the solid drug samples. The drug samples are filled in a capillary tube sealed from the side. The melting range is observed in the capillary melting point apparatus with the help of a thermometer [338].

4.2.1.3 Differential Scanning calorimetry (DSC) analysis

Apart from the capillary melting method, DSC was used to determine the melting point (T_m) of the raw drugs. Both the raw drugs (3 mg) were packed and heated inside an aluminium crucible in the range of 10 to 100°C at a heating rate of 10°C/min in the presence of nitrogen with a flow rate of 50 mL/min. A separate empty aluminium pan was used as a reference [232].

4.2.1.4 Fourier transformer infrared (FTIR) spectroscopy

In this study, 5 mg of raw drugs (Gly and VA) were separately triturated with potassium bromide (100 mg) using mortar and pellets were prepared. The drug samples were scanned over a wavenumber range of 4000–500 cm^{-1} in an FTIR spectrophotometer for structural confirmation in terms of sharp bands displayed by the different functionalities present in the drug samples [198].

4.2.1.5 X-ray diffraction (XRD) analysis

The evaluation of X-ray diffraction patterns of raw Gly and VA powder was performed by using an X-ray diffractometer with Cu line as the radioactivity source. The carefully prepared samples were placed in the sample slot and pushed efficiently with iced glass. Thereafter, the samples were placed inside the powder X-ray diffractometer and the scanning was performed at the adjusted speed of $0.010^{\circ}\text{min}^{-1}$, over a 2θ range of 10–90 degrees, The X-Ray beams at 40 kV voltage and 40 mA current were made incident on the sample [338].

4.2.1.6 Partition coefficient (Log P)

The partition coefficient of both the raw drugs (Gly and VA) was determined using the shake-flask method. Both the raw drug (10 mg) was separately dissolved in one of the phases (n-octanol: water: 20:20), and the solution was shaken with other corresponding liquid for 30 minutes in a separating funnel. Both the liquids were allowed to stand for 24 hours and then the lower water layer was collected and individually assayed at 228 nm (Gly) and 261 nm (VA) using UV spectroscopy. The amount of drug assayed was subtracted from the total drug added initially, which provided the amount of drug in the organic phase as presented in equations (1) and (2) [338].

$$\text{Drug in organic phase} = \text{Total drug} - \text{Drug assayed in water phase} \quad \text{Equation (1)}$$

$$\text{Log } P = \text{Log} \frac{(\text{Drug in organic phase})}{(\text{Drug in aqueous phase})} \quad \text{Equation (2)}$$

4.2.2 Solubility study

The solubility study of both the raw drugs was carried out in different surfactants including CTAB, sodium lauryl sulfate (SLS), polyvinyl alcohol (PVA), and polyvinyl pyrrolidone-K90 (PVP-K90), solvents (distilled water, ethanol, methanol, and acetone) and various buffer systems (0.1N hydrochloric acid buffer pH 1.2 and 0.1M phosphate buffer of pH 4.5, 6.8, and 7.4) respectively at their respective reported lambda max [338].

4.2.2.1 Solubility in surfactants

Different surfactants including SLS, CTAB, PVA and PVP-K90 were used and taken in varying concentrations of 0.5, 1.0, 1.5, and 2.0% w/v to determine the concentration for maximum solubility of raw drugs. Both the raw drugs (20 mg each) was added separately in 250 mL of the volumetric flask containing varying concentration of surfactants and the final volume was adjusted to 250 mL using deionised water. These solutions were agitated for 48h at the temperature $37 \pm 0.2^{\circ}\text{C}$ with a speed of 50 rpm on a shaking water bath.

Thereafter the samples were centrifuged at 5000 g for 30 minutes to remove the undissolved part of drugs from the saturated solutions. The concentration of both the drugs in the supernatant was determined using UV spectroscopy at their respective reported lambda max. The percentage solubility of raw drugs was determined by using the formula given below [338].

$$\text{Percentage solubility} = \frac{\text{Practical Concentration}}{\text{Theoretical Concentration}} \times 100 \quad \text{Equation (3)}$$

4.2.2 Solubility in buffer systems and organic solvents

The solubility study in various buffer systems was performed using the direct absorption method. For this, 20 mg each of raw Gly and VA was dissolved in 250 mL of volumetric flasks containing distilled water and various buffers. These samples were kept for 48h with a speed of 50 rpm on a mechanical shaker. After 48h, the samples were centrifuged at 5000 g for 30 min. The clear supernatant obtained was analysed using UV spectroscopy at a wavelength of 234 nm respectively. The fraction of drugs got solubilized in each buffer were obtained using a calibration curve with a regression equation. In addition to this, the solubility of the drugs in organic solvents were determined by dissolving 10 mg of each drug in 10 mL of each solvent to make 1000 µg/mL of the solution named as solution A. Further from solution A, 1 mL was withdrawn and added into 10 mL of the solvent to make concentration of 100 µg/mL named as solution B. From this solution B, various dilutions were made in a concentration range of 10-50 µg/mL and their absorbance was recorded using UV spectroscopy at their respective reported lambda max. The unknown sample of both drugs was prepared and kept for 72h to determine their solubility in each solvent [338].

4.3 Development of RP-HPLC analytical method

4.3.1 Selection of chromatographic conditions

The HPLC system with PDA detector (SP20AD; Shimadzu, Japan) was utilised to develop the chromatogram. Rheodyne injector with 20 µL sample injector loop was used to inject samples. Nucleodur C18 column with dimension 250 mm × 4.6 mm, i.e., 5µ, was used for estimation of drugs. The chromatograms were recorded on LC solution software. During selection of the particular mobile phase for the method development, various solvents such as acetonitrile (ACN), methanol, water and orthophosphoric acid (OPA), acetic acid were used in varying ratios. The final absorbance maxima were selected as 234 nm (isosbestic point) based on the obtained chromatogram based on the observations from the initial trails, the specific mobile phase and the ratio was finalized along with the retention time and flow rate [238].

4.3.2 Preparation of stock and sample solution

Raw VA and Gly (10 mg each) were dissolved in 10 mL of ACN in standard volumetric flask (100 mL), and then volume was adjusted to 100 mL in order to get final concentration 100 µg/mL (Solution A). An aliquot (10 mL) of solution A was withdrawn and the final volume was diluted up to 100 mL to get solution of concentration 10 µg/mL (Solution B) [232].

4.3.3 Development of calibration curve

A solution B (100 µg/mL) was prepared from a standard solution (solution A) from which a significant amount of volume was withdrawn to make concentration in the range of 2 to 10 µg/mL using ACN. This concentration range was used to develop calibration curve of both the drugs in ACN by inserting each concentration 5 times in HPLC.

4.3.4 Validation

The validation of the method was performed in terms of specificity, linearity and range, accuracy and precision, sensitivity (LOQ and LOD), and robustness according to ICH Q2 (R1) guideline.

4.3.5 Linearity and range

The standard plot was prepared between concentration Vs. mean area and the regression equation and, coefficient was determined.

4.3.6 Accuracy

The method accuracy was determined by recovery studies at three different concentration levels, i.e., 80%, 100% and 120% (10.8 µg/mL [LQC], 12 µg/mL [MQC] and 13.2 µg/mL [HQC]), and six samples from each of the prepared concentration were analysed. Percentage recovery of VA and Gly was calculated by using equation 4 [232].

$$\text{Recovery (\%)} = \frac{\text{Actual cocentration recovered}}{\text{Theoritcal Concentration}} \times 100 \quad \text{Equation (4)}$$

4.3.7 Precision

Six samples from each concentration levels, i.e., 80%, 100% and 120% were injected on the day 1 to determine precision of the method. For intermediate precision, six samples from each solution at three concentration levels on day 1-3 (Inter-day) and by different analyst (inter-analyst) were injected using the same experimental conditions. The %RSD of the obtained results was calculated to obtain repeatability in the results using the following formula [256].

$$\%Relative\ standard\ deviation = \frac{Standard\ deviation\ of\ peak\ area}{Average\ peak\ area} \times 100 \quad Equation\ (5)$$

4.3.8 Robustness

Robustness study of the method was performed by making minor alterations in experimental conditions employed for the method development. This include flow rate (0.8, 1 and 1.2 mL/min), ratio of mobile phase (A: B) i.e. ACN: OPA 0.1% in water v/v (68:28 v/v, 70:30 v/v, and 72:32 v/v), pH (1.3, 1.5, and 1.7 pH) and isosbestic point (232, 234, and 236 nm). The changes were made to observe their influence on the method. The results achieved were determined by calculating percentage recovery [198].

4.3.9 System suitability and assessment of LOD and LOQ

System suitability was determined by recording peak purity index, height equivalent to theoretical plate (HETP), theoretical plate and, tailing factor. The calculation of Limit of detection (LOD) and Limit of quantification (LOQ) were done by standard deviation of the response (sigma) and the slope of calibration curve(s). Standard deviation of Y intercepts of the regression line was selected as the standard deviation. The calculations were done according to equation 6 and 7 respectively [198].

$$LOD = 3.3 \times \frac{\sigma}{S} \quad Equation\ (6)$$

$$LOQ = 10 \times \frac{\sigma}{S} \quad Equation\ (7)$$

4.4 Formulation Development

4.4.1 Synthesis of mPEG-b-PCL copolymer

A previously published method i.e., ring open polymerization reaction was employed to synthesize mPEG-b-PCL [339]. The mPEG (8.5mmol) was melted in a 50 mL round

bottom flask followed by the addition of epsilon-CL (170 mmol) and $\text{Sn}(\text{Oct})_2$ (0.617 mmol) under anaerobic condition using nitrogen gas. The reactant mixture was sustained at 160 °C for 6 hours at a constant supply of nitrogen. Afterwards, the mixture was kept unshaken overnight to get a white color solid product. The obtained product was purified by adding warm acetone followed by precipitation due to hexane. The resultant product was isolated by vacuum filtration and stored in an airtight container at ambient temperature [339].

4.4.2 Liquid antisolvent precipitation (LAP) method for formation of APMs

This is one of the widely used physical methods used in the formation of ultrafine nanoparticles (NPs) by precipitating them in an aqueous medium. This method includes the simple step of mixing solvent and antisolvent followed by achievement of supersaturation process, nucleation and aggregation [340]. The extent of supersaturation (rapid and high) is one of the essential steps or main energy required for precipitation of NPs that can tailor the particle size, topology, appearance, or structural integrity of the NPs. The density of the NPs in the antisolvent is also one of the critical steps that regulate the particle growth and if it continues to grow it leads to agglomeration [340]. Thus, various critical parameters such as interfacial surface energy and supersaturation are responsible to control the precipitation method. Therefore, critical variables associated with such parameters can be fine-tuned to develop particles of desirable characteristics. Such as the concentration of the copolymer that self-assembles in nanoparticles, the addition of surfactant to form a heterogeneous system, and the ratio of solvent to antisolvent have a significant impact on the yield, drug entrapment, stability, and particle size.

4.4.3 Design of experiment (DoE)

DoE is a powerful tool utilized by industries to save manufacturing costs by reducing the process variation and enhancing the product quality at the same time via optimization. Therefore, the consideration of the associated process variables is very important to improve either the manufacturing process or its scale-up and product characteristics [341,342]. DoE has emerged as a systemic, efficient, and economical method for analysing and interpreting various critical factors that control the product quality. It also enables to study of the interaction between the multiple variables [343]. George Box and Donald Behnken first introduced Box-Behnken design (BBD) in the year 1960 [344]. It is a quadratic design that is autonomous and does not involve factorial design. BBD involves three levels (-1, 0, +1) of all independent variables/factors and the designs are rotatable [341,345]. Initial screening trials were carried out for evaluating the formulation and processing aspect of the APMs. Results from the initial screening trials revealed that the drug to copolymer ratio, drug to surfactant ratio, and solvent to antisolvent ratio were the main factors that significantly affected the formulation characteristics such as size and charge. In agreement with this, these factors were further explored to study their influence at three levels (-1, 0, +1)

onto the various responses i.e., particle size (nm), entrapment efficiency (%), charge (mV), and polydispersity index (PDI) as presented in **Table 4.4**.

Table 4.4: Variables for Box–Behnken study for bottom up technology

Independent factors	Design level			
	Uncoded	Coded	Uncoded	Coded
Drug to copolymer ratio (mg)	A	1-0.2	-1	
		1-0.4	0	
		1-0.6	+1	
Drug to surfactant ratio (mg)	B	1-0.25	-1	
		1-0.5	0	
		1-0.75	+1	
Solvent to antisolvent ratio (mL)	C	0.1-1	-1	
		0.2-1	0	
		0.3-1	+1	

A set of 17 experiments using BBD was adopted to develop GV-APMs using LAP method. The synthesized mPEG-PCL, Gly and VA were dissolved in the organic phase (acetone) of varying concentrations and further added into an aqueous phase containing CTAB to obtain ratios as per DoE using a high-speed homogenizer (REMI, India) to obtain a suspension. The resulting suspension was kept open to air for overnight to allow the slow evaporation of acetone from the formulation. The residual acetone was removed using a rotary evaporator that led to the formation of APMs in distilled water. The composition of the batches prepared and their responses achieved is discussed in section.

4.5 Characterization of synthesized mPEG-b-PCL and APMs

4.5.1 Product yield

The percentage yield of the synthesized diblock copolymer mPEG-b-PCL was calculated using the formula given below.

$$\% \text{ Yield} = \frac{\text{Actual yield}}{\text{Theoretical yield}} \times 100 \quad \text{Equation (8)}$$

E
q
u
a

Here, the actual yield is the weight of the resultant product obtained after the completion of ring open polymerization reaction whereas, the theoretical yield is the total weight of the reactants incorporated before the start of the experiment.

4.5.2 CMC determination

The CMC of the synthesized mPEG-b-PCL copolymer was estimated using iodine UV absorption method. A standard solution was made by adding 250 mg of iodine and 500 mg of potassium iodide in 25 mL of distilled water. On the other hand, a stock solution of the synthesized diblock copolymer was prepared by adding 0.02 g of mPEG-b-PCL in 1000 mL of distilled water. The copolymer solution was kept for 24h for complete dissolution before dilution. Further, a standard iodine solution (25 μ L) were incorporated into each dilution made (1.1 to 2.2 μ g/mL) from the stock solution. These solutions made was kept overnight in dark for their further analysis at 255 nm UV spectrophotometer. A graph was plotted between the concentration of the diblock copolymer and corresponding absorbance. A particular point exhibiting a sudden and sharp increase in the absorbance indicated the CMC value of the diblock copolymer [346].

4.5.3 FTIR

The FTIR spectrum reveals the characteristic peaks of all functional groups present in a sample. In FTIR spectroscopic study, 5 mg each of the mPEG (M_w 2000), epsilon-CL, and mPEG-b-PCL were triturated with KBr (100 mg) using mortar and pellets were prepared. The samples were scanned over a wavenumber range of 4000–500 cm^{-1} in an FTIR spectrophotometer. The FTIR spectrum of Gly, VA, and CTAB was recorded similarly by individually mixing them with potassium bromide and subjecting them to IR analysis. However, for GV-APMs, the liquid sample cell holder was used.

4.5.4 ^1H NMR

The ^1H NMR was used to determine the chemical structure of mPEG-b-PCL based on the number of protons present in NMR spectrum using TOPSPIN NMR data system. The study was carried out in deuterated DMSO solution at 500 MHz using the tetramethyl silane proton signal as a reference.

4.5.5 DSC

mPEG-b-PCL (3mg) was packed and heated inside an aluminium crucible in the range of 10 to 100°C at a heating rate of 10°C/min in the presence of nitrogen with a flow rate of 50 mL/min. A separate empty aluminium pan was used as a reference. Similarly, the DSC analysis of the CTAB, and the GV-APMs was also carried out. The data were recorded from 10 to 500°C.

4.5.6 ESI-MS

The ESI-MS was used to determine the molecular weight of the synthesized diblock copolymer mPEG-b-PCL using an electrospray ionization-mass spectrometer (with a mass range of 4000 amu in quadruple and 20,000 amu in time of flight). The instrument is equipped with an HPLC system having quaternary pumping configured for flow rates from 0.05-5.0 mL/min. An ionization voltage

of 2–3 kV was applied to the outlet of the stainless-steel nozzle and the GV-APMs were infused by a syringe pump at a constant flow rate of 1 μ L/min.

4.5.7 SEM

The surface morphology and shape appearances of GV-APMs were carried out using SEM by drop-casting method along with other excipients i.e., CTAB and mPEG-b-PCL. A descent amount of the formulation was dropped on a glass slide and allowed to air-dry for water evaporation. Further, it was layered with gold by sputter coater for 40 s in a vacuum at a current intensity of 30 mA after preparing the sample. The other samples were dispersed by scattering them on an adhesive carbon tape placed over an aluminum stub. Afterwards, the samples were layered twice with gold and scanned at 10 mV of voltage.

4.5.8 Particle size and zeta potential

The PS and ZP of 1-17 batches and the optimized batch of GV-APMs were analyzed using a zeta sizer. The samples were dispersed in standard 1 mL disposable polystyrene cuvettes followed by exposure to the laser light at 25°C. Afterwards, their hydrodynamic radius as well as PDI was determined.

4.5.9 High resolution-Transmission electron microscopy (HR-TEM)

The imaging of the GV-APMs were performed using HR-TEM, a 120 kV illumination system, highest magnification of 500K, and resolution of <1 nm. Briefly, small amount of APMs were distributed onto a carbon-coated copper grid and were exposed to HR-TEM after fully drying.

4.5.10 Entrapment efficiency (EE %)

An aliquot (1 mL) was withdrawn from the GV-APMs into a epindroff and centrifuged for 20 min at 15000 g. The clear liquid obtained was withdrawn using micropipette and injected to HPLC after passing via. 0.2 μ m syringe filter. The EE % of both the drugs was calculated using the formula given below.

$$\%EE = \frac{(\text{Conc of drug added} - \text{Conc of drug in supernatent})}{\text{Conc of drug added}} \times 100 \quad \text{Equation (9)}$$

4.5.11 Drug loading (DL %)

The GV-APMs (1 mL) were taken in a epindroff followed by centrifugation at 15000 g over 20 min. The clear liquid was collected and the sample (20 μ L) was injected into HPLC. The amount of drugs got entrapped in the formulation was used to determine the DL % using the formula presented below.

$$\%Drug\ loading = \frac{Amount\ of\ drug\ entrapped}{Total\ weight\ of\ the\ formulation} \times 100 \quad \text{Equation (10)}$$

4.5.12 *In vitro* release study

This study was performed by making a sac with dialysis membrane-110 (DM) (Mw 14kDa). The pH-gradient method was used to examine the release behavior from the prepared GV-APMs. The DM was drenched in a sufficient amount of PB pH 7.4 for 24 h before its use for stimulation. GV-APMs (1 mL) was transferred in the sac and then immersed in 50 mL of the HCL buffer (pH 1.2) over 2 h at 37±0.2°C with constant agitation using a magnetic stirrer at 50 rpm. Then for the next 4 hours, the volume of the medium was made up to 50 mL using PB to maintain a pH of 6.8. Lastly, the pH of the medium was adjusted to pH 7.4 using sodium hydroxide solution. This study was further continued at pH 7.4 for 48h respectively. At pre-determined time intervals (0.5, 1, 2, 4, 8, 16, 24, 32, 40, and 48 h), the dialysate was withdrawn from each pH solutions and replaced by 1mL of the fresh medium [347]. The % drug dissolution (%DD) of both the drugs were determined using HPLC at 234 nm using the formula given below. Further their release kinetics was studied using DD solver software.

$$\%DD = \frac{Sample\ area}{Standard\ area} \times \frac{Sample\ dilution}{Standard\ dilution} \times 100 \quad \text{Equation (11)}$$

4.6 *In vitro* cell line study

The *in vitro* cell line toxicity for raw drugs (Gly and VA), their APMs and placebo APMs was performed using Caco-2 cell lines. Whereas, the glucose uptake study for the above-mentioned samples were carried out using HepG2 cells. A detailed description of these studies is provided below.

4.6.1 *Caco-2* cytotoxicity study

The cytotoxicity of free drugs (Gly and VA), their physical mix, individual drug loaded APMs, GV-APMs and blank APMs to the Caco-2 cell line were evaluated by 3-(4,5-dimethylthiazol-2-yl)-2,5-diphenyltetrazolium bromide (MTT) method. Caco-2 cells were plated at a density of 5 x 10³ cells per well in 100 mL of Dulbecco's Modified Eagle Medium containing 10% FBS in 96-well plates and grown for 24 h. Cells were then exposed to a series of raw drugs, their physical mix, individual drug loaded APMs, GV-APMs and blank APMs at different concentrations viz. 0.9, 1.9, 3.9, 7.8, 15.6, 31.2, and 62.5 µg/mL for 48 h. The cell viability was determined as a measure of succinate dehydrogenase released by the viable cells, which reduces tetrazolium salt of MTT into formazan. The percentage cell viability was calculated using the formula given below [341].

$$\%Cell\ viability = \frac{OD\ of\ tested\ compound}{OD\ of\ control} \times 100 \quad \text{Equation (12)}$$

4.6.2 Passive glucose uptake study

To test whether HepG2 cells can take up glucose passively, 1×10^4 cells were seeded in 96 well plate in 100 μ L MEM (Himedia, India) supplemented with 20% FBS (Gibco, USA) and 1g/L glucose. Cells were allowed to grow for about 36h, and the spent media was exchanged with fresh 100 μ L MEM containing 20% FBS and 1g/L glucose. The concentration of glucose in the media was measured at 6h, 12h and 24h respectively. Glucose in the media was estimated using glucose oxidase and peroxidase assay (Agappe Diagnostics Ltd.) [348].

4.6.3 Insulin-resistant HepG2 cell model

To test whether HepG2 cells exhibit resistance to insulin, the exponentially growing cells were starved of FBS for 12h by growing in MEM supplemented with 1% FBS instead of 20% FBS; and exposed to increasing concentration of insulin beginning from 0.005 to 50 μ M for 6h, 12h and 24h. To avoid any interference by 1% FBS, the insulin-treated groups were grown in a medium prepared without FBS [348,349]. Therefore, insulin resistance was confirmed as a measure of glucose uptake by the HepG2 cells.

4.6.4 Selection of non-cytotoxic concentration

To select a concentration that does not affect cell growth, the viability of exponentially growing HepG2 cells was determined by sulforhodamine B assay and percentage growth inhibition/viability was calculated [349]. Experimentally, 1×10^4 HepG2 cells were seeded in 96 well plates in 100 μ L MEM supplemented with 20% FBS and 1g/L glucose. Cells were allowed to grow for about 36h and treated with increasing concentration of raw drugs, their physical mix, Gly APMs, VA APMs, GV-APMs, and blank APMs for 24h. Percentage growth inhibition was calculated by comparing the optical density value of treated cells with that of control untreated cells by using the following equation.

$$\%Cell\ inhibition = \frac{OD\ of\ control - OD\ of\ test}{OD\ of\ control} \times 100 \quad \text{Equation (13)}$$

4.6.5 Glucose uptake in insulin-resistant cells

A time-dependent glucose uptake assay was carried out to evaluate the glucose uptake ability of the developed GV-APMs in insulin-resistant HepG2 cells [348]. Experimentally, 1×10^4 HepG2 cells were seeded in 96 well plates in 100 μ L MEM supplemented with 20% FBS and 1g/L glucose. The spent media was exchanged with fresh 100 μ L MEM containing 20% FBS and 1g/L glucose for control of untreated cells. However, the media in treated groups was devoid of FBS. Cells were

treated with the test compounds for 6h and 24h. The concentration of the test compounds possessing minimal cytotoxicity (<15% cell growth inhibition compared to control cells treated with vehicle) was selected based on the cytotoxicity profile as discussed above. Percentage glucose uptake was calculated based on the glucose that remained in the media using the formula given below.

$$\%Glucose\ concentration = \frac{(G)\ blank - (G)\ cells}{(G)\ blank} \times 100 \quad \text{Equation (14)}$$

(G)blank = Glucose in the media but no cells

(G) cells = Glucose in the media collected from untreated cells / treated cells

Further, the interaction between both the tested drugs used in combination was determined by calculating the combination index (CI) using the equation given below.

$$\text{Combination index (CI)} = \left[\frac{Ca}{ICa} \right] + \left[\frac{Cb}{ICb} \right] \quad \text{Equation (15)}$$

Where, C_a and C_b are the concentrations of Gly and VA used in combination to achieve a fixed effect (i.e., percentage of glucose uptake). IC_a and IC_b are the concentrations of both the drugs required to achieve the same effect when used alone. A CI value less than, equal to, or more than 1 indicates synergistic, additive and antagonistic interaction, respectively, between the two compounds [27].

4.7 In vivo studies

4.7.1 Animals

Healthy SD rats of either sex (270-300 g) of age 10-12 weeks were procured from Punjab University, Chandigarh, India for the pharmacokinetic study. The animals were kept in cages in the central animal house of the School of Pharmaceutical Sciences, Lovely Professional University (Phagwara, Punjab) at an ambient temperature of 25 ± 2 °C and relative humidity of 65 % with a 12 h light/dark cycle. The experimental protocol was duly approved by the institutional animal ethics committee (Protocol no: LPU/IAEC/2021/5/73).

4.7.2 Development of bioanalytical method

4.7.2.1 Chromatographic conditions

Similar chromatographic conditions were used for development of bioanalytical method as mentioned in section 4.3.1.

4.7.2.2 Extraction of plasma from rats' blood samples

The blood was collected using the orbital sinus technique with the help of a capillary tube. In this technique, a rat is scruffed with the thumb and the forefinger of the non-dominant hand is used to pull the skin around the eye. A fine capillary is inserted into the medial canthus of the eye and slight pressure is applied to puncture the sinus. Once, the sinus is punctured, blood comes out via capillary and is collected in EDTA (ethylene diamine tetraacetic acid) vials. Once the required amount of blood is collected, the capillary is removed and the eye of the rat is wiped with sterile cotton. The collected blood is centrifuged at 5632 g for 15 min and the clear supernatant is withdrawn and is stored at a -20 °C for further processing.

4.7.2.3 Preparation of blank plasma

An adequate amount of plasma (1mL) was taken in epindroff followed by the addition of 2 mL of ACN. The mixture was vortexed for about 5 min to precipitate the plasma proteins. The clear supernatant was collected in separate epindroff and was further centrifuged at 5782 g for 15 min. After this, the obtained supernatant was transferred in a 100 ml volumetric flask and the volume was made up to 100 mL.

4.7.2.4 Preparation of standard stock solution

Both the raw drugs (VA and Gly) of 10 mg each were dissolved in 1 mL of plasma followed by vortexing the mixture for about 10 min. Further, 2 mL of ACN was added in the spiked plasma

containing both the drugs and vortexed for 10 min for protein precipitation. Once the proteins got precipitated, the mixture was centrifuged at 5782 g for 15 min to obtain a clear supernatant. The obtained supernatant was added in a 100 mL volumetric flask and the volume was made up to 100 mL to make a stock solution of concentration 100 µg/mL (solution A).

4.7.2.5 Preparation of internal standard (IS)

The GA (10 mg) was incorporated in a 100 mL volumetric flask with 20 mL ACN followed by sonication for about 10 min. Once the GA got dissolved completely, the volume was made up to 100ml with ACN to make a stock solution of 100 µg/mL. Further, 1mL of aliquot was withdrawn from 100 µg/mL stock solution in a 10 mL of volumetric flask and the volume was made up to 10 mL using ACN to get 10 µg/mL of GA solution.

4.7.2.6 Method specificity

To confirm the method specificity, both the drugs (VA and Gly) and blank plasma were injected to HPLC consisting ACN and 0.1% OPA (70:30 v/v) as a mobile phase. These were analysed at 234 nm to identify any interference between the drugs and plasma peaks.

4.7.2.7 Development of calibration curve

Dilutions were made in the concentration range of 100-500 ng/mL from the stock solution of 10 µg/mL (solutions B) containing a mixture of VA and Gly in plasma. In each dilution, 1mL of GA (100 µg/mL) was added to get the final concentration of 10 µg/mL of IS GA. Each dilution was injected into HPLC in five replicates and analysed at 234 nm. Similarly, the calibration curve of both the drugs was developed in the concentration range of 100-500 ng/mL in mobile phase along with the addition of 1mL of GA (100 µg/mL). In addition, a calibration curve was also plotted between area ratio of analyte/IS versus concentration of both the drugs in plasma and in mobile phase.

4.7.2.8 Accuracy study

The accuracy of the developed method was determined by calculating the absolute recovery of drugs from the plasma samples. The samples were made by determining the lower quantifiable concentration (LQC, 80%), middle quantifiable concentration (MQC, 100%) and higher quantifiable concentration (HQC, 120%) of the mid concentration of the calibration curve. The LQC, MQC, and HQC values were found to be 0.24, 0.30, and 0.36 µg/mL. Further, the IS 1 mL of GA (100 µg/mL) was added to the prepared solutions. The prepared samples were injected to HPLC in six replicates and their mean, standard deviation (SD), and percentage relative standard deviation (% RSD) were noted. The absolute recovery (%) of each prepared sample was calculated using formula given below.

$$\text{Absolute recovery (\%)} = \frac{\text{Actual concentration recovered}}{\text{Theoretical concentration}} \times 100 \quad \text{Equation (16)}$$

4.7.2.9 Precision studies

To carry out the precision study, LQC, MQC, and HQC solutions containing 10 µg/mL of GA as IS being injected in six replicates on the same day (intraday), on different days (interday), and by different analysts on the same day under the same experimental conditions. The mean, SD, and % RSD were determined for each injected sample.

4.7.2.10 Determination of LOD and LOQ

LOD and LOQ for both the drugs were determined using the standard deviation of response (σ) and the slope of the calibration curve (S). The SD of the Y-intercept of the regression line was used as SD. The given below equations were used for calculating LOD and LOQ.

$$LOD = 3.3 \times \frac{\sigma}{S} \quad \text{Equation (17)}$$

$$LOQ = 10 \times \frac{\sigma}{S} \quad \text{Equation (18)}$$

4.7.2.11 System suitability

The system suitability was determined by injecting the lower concentration of the calibration curve (100 ng/mL) in six replicates. Their system suitability parameters including theoretical plate, tailing factor, resolution of both the peaks, and height equivalent to a theoretical plate (HETP) were determined.

4.7.2.12 Stability study

The stability of both the drugs (VA and Gly) in plasma samples was determined upon exposure to freeze-thaw cycles, short-term stability at room temperature for 3 h, and long-term stability at -70°C over 3 weeks. 3 mL of the plasma were extracted from the blood sample followed by precipitation and centrifugation. Both the drugs (10 mg each) were added in plasma, vortexed for 5 min, and stored at -70°C for 1 hour. One aliquot (1 mL) was withdrawn from plasma sample (freeze-thaw 1) and centrifuged to obtain clear supernatant. Post-precipitation and centrifugation, the obtained clear supernatant was diluted with ACN to make up the volume upto 100 ml (100 µg/mL). Rest of the samples were re-frozen at -70°C for 1 hour. Further, the LQC, MQC and HQC (0.24, 0.30 and 0.36 µg/mL) solutions were prepared from 100 µg/mL solution. Similarly, the aliquots (1 mL) were withdrawn from the left over frozen plasma sample i.e., freeze-thaw 2 and freeze-thaw 3 under same experimental conditions to prepare LQC, MQC and HQC. 1 mL of IS GA (100 µg/mL) were added into each prepared samples to make concentration of 10 µg/mL. All the prepared samples were injected in triplicate and analysed at their respective RT at 234 nm to determine their mean, SD and %RSD [350].

For short-term stability study, 3 mL of the plasma containing 10 mg of each drug were kept at room temperature. An aliquot (1mL) was withdrawn from the plasma to process it for the preparation of LQC, MQC and HQC along with the addition of 1 ml of 100 µg/mL of GA. Each sample were injected in triplicate after every 1 hour of interval for upto 3 h. The mean, SD, %RSD were noted [351]. To determine the long-term stability of both the drugs in plasma, 10 mg of each drug were added in three vials containing 1 mL of plasma. These vials were vortexed for few min and stored at -70°C. The samples were taken out from the freezer after 1, 2 and 3 weeks to process it for the preparation of LQC, MQC and HQC with 10 µg/mL of the GA. These solutions were injected to HPLC in triplicate after every week for the determination of peaks at their respective RT at 234 nm. The mean, SD and %RSD were noted [352]

4.7.3 Pharmacokinetic study

The parallel study was carried out using 42 rats that were divided into seven groups, each containing six rats. The rats were kept under fasting conditions for 12h before the start of the experiment. Rats received raw drugs (Gly and VA), their physical mixture, Gly-APMs, VA-APMs, and GV-APMs at a dose containing 0.5 mg/kg of Gly and 7.5 mg/kg of VA each respectively. However, placebo APMs were used as control. To each rat, 1mL formulation containing Gly and VA equivalent to 0.125 and 1.801 mg were administered orally using oral gavage. The pharmacokinetic study design is presented in **Table 4.5**. Both the raw drugs were dispersed in 0.1% w/v carboxy methylcellulose (CMC) suspension. The respective treatments were administered to rats via oral route using oral gavage.

Blood was withdrawn via tail vein (0.2 mL) at 0, 1, 2, 3, 4, 5, 6, 8, 10, 12, 18, and 24 h in EDTA vials respectively. Plasma was collected and further processed to extract drugs via protein precipitation method and the supernatant was collected by performing centrifugation at 5782 g for 15 min at 4°C. The area under the curve (AUC) was calculated by using Phoenix winnonlin 8.2 software (USA).

Table 4.5: Pharmacokinetic study design

Groups	Treatment	Animals used	Dose
1	Raw Gly	6	0.5 mg/kg p.o
2	Raw VA	6	7.5 mg/kg, p.o
3	Raw Gly + VA	6	0.5 mg/kg + 7.5 mg/kg, p.o
4	Gly APMs	6	0.5 mg/kg, p.o
5	VA APMs	6	7.5 mg/kg, p.o
6	GV-APMs	6	0.5 mg/kg + 7.5 mg/kg, p.o
7	Placebo Control of APMs	6	Without drugs

Abbreviations: APMs, Amphiphilic polymeric micelles; Gly, Glyburide; VA, Vanillic acid; GV-APMs, Gly and VA co-loaded APMs

4.7.4 *In vitro/ In vivo correlation (IVIVC) studies*

The level A (point-to-point) IVIVC co-relation between *in vitro* percent drug dissolved and *in vivo* percent drug absorbed was studied. The correlation was studied at the corresponding time-points for the developed APMs i.e., VA-APMs, Gly-APMs and GV-APMs, raw drugs and their physical mixture from the concentration-time dependent data obtained by Wagner-Nelson method. The statistical significance of each correlation was determined from the respective values of F-ratios [353,354].

4.7.5 *Pharmacodynamics study*

The pharmacodynamics study is divided into two sections describing the induction of T2DM using HFD plus low dose of STZ, and the pharmacodynamics screening of the tested compounds.

4.7.5.1 *HFD plus low dose of STZ model*

This model is commonly used for the induction of T2DM as it replicates the natural history and metabolic characteristics of human T2DM. The T2DM rat model was developed as per Srinivasan *et al.* (2005) [355]. High lipid rich regimen consisting of huge caloric quantity supports obesity triggered glucose intolerance and insulin resistance rather than frank hyperglycemia, which displays typical characteristics of T2DM [355]. HFD administration primarily induces excessive insulin discharge from the pancreatic β -cell, which is then reduced by the fractional destruction of the functioning β -cells and frank hyperglycemia upon low dose of STZ administration in non-genetic SD rats [355].

SD rats of either sex were randomly divided into 12 groups based on dietary regimen i.e., normal pellet diet (NPD) and HFD (58% fat, 25% protein, and 17% carbohydrate, as a percentage of total kcal) *ad libitum*, respectively. The HFD was prepared according to Srinivasan *et al.* (2005) as presented in **Table 4.6**. Group 1 received NPD while the rats allocated to rest of the other groups received HFD for the initial period of 14 days. The treatment groups employed in the pharmacodynamics study is specified in the **Table 4.7**. The total duration of the *in vivo* study was of 48 days.

All the ingredients of HFD were weighed, powdered and triturated in melted desi ghee. Further, the semi-solid mixture obtained was made in pellets and stored at -70°C temperature until use. In general, six pellets were given to each experimental groups at least two times/day. After the 14 days of dietary manipulations (on day 15th), oral glucose tolerance test (OGTT) was performed to determine the response of the rat's body towards higher blood glucose levels i.e., to confirm insulin resistance and glucose intolerance upon consumption of HFD and NPD [356]. Further, the increase in body weight and lipid profile was determined at the end of 14 days.

Table 4.6: Composition of HFD

Ingredients	Diet (g/kg)
NPD	365
Desi ghee	310
Casein	250
Cholesterol	10
Vitamin and mineral mix	60
DL-methionine	03
Yeast powder	01
Sodium chloride	01

4.7.5.2 OGTT

The OGTT was performed on rats in all groups after an overnight fasting on 14th day. On 15th day the rats were orally administered (16G oral feeding cannula) with 2.0g of glucose/kg body weight. The blood samples were taken by slightly pricking the rat's tail with the help of a needle before 0 min and after 0.5, 1, 1.5, 2, 3, 4, 5 and 6 h of glucose administration. The blood glucose levels at each time intervals were determined using glucometer (Dr. Morepen, BG-03) based on glucose oxidase method. The obtained values of blood glucose levels were plotted against time to develop a curve showing the changes in glucose levels with time [356].

4.7.5.3 Body weight and lipid markers

After OGTT, increase in body weight and the serum lipid markers such as triglycerides (TGs), cholesterol (CHL), low-density lipoprotein (LDL), very low density lipoprotein (VLDL), high density lipoprotein (HDL), CHL/HDL ratio and LDL/HDL ratio was determined on 15th day at the end of

HFD consumption. For the estimation of serum lipid levels, blood samples were withdrawn from the rat's retro-orbital plexus using a fine sterilized capillary tube and was collected in plain Eppendorf tubes.

4.7.5.4 STZ injection

After the confirmation of HFD induced-insulin resistance (on day 16th), the rats from HFD-fed group was injected with a single low dose of STZ (35 mg/kg; i.p.) in ice cold 0.1 M sodium citrate buffer (pH 4.5) upon overnight fasting while NPD-fed group received an equivalent amount of sodium citrate buffer. Four days after STZ injection i.e., on 20th day, blood glucose levels were estimated and rats having non-fasting value above 200 mg/dL were identified and further divided into different treatment groups for pharmacological screening. The respective treatments in each divided groups was initiated from 21st day for a consecutive period of 4 weeks as presented in **Table 4.7**. The blood glucose levels and body weight of each groups were determined on weekly basis during the treatment protocol of 28 days. Furthermore, at the end of the 28 days of study, serum lipid levels of each groups were determined.

Table 4.7: Pharmacodynamics study design

Groups	Treatment	Dose (Route of Administration)
Oral NPD treatment		
I	Normal control (NC)	Ice cold 0.1 M sodium-citrate buffer (pH 4.5), p.o.
STZ (35 mg/kg) in ice cold 0.1 M sodium-citrate buffer (pH 4.5) intraperitoneal + oral HFD treatment will be given to rats of groups II to XII		
II	Experimental control (EC)	HFD+ STZ, i.p.
III	Placebo of APMs (P-APMs)	Placebo APMs (without drugs), p.o.
IV	Raw VA in 0.5% w/v in CMC at high dose 7.5 mg/kg [R-VA(H)]	(R-VA)-H, p.o.
V	Raw Gly in 0.5% w/v CMC at high dose 0.50 mg/kg [R-Gly (H)]	(R-Gly)-H, p.o.
VI	High dose of raw Gly (0.50 mg/kg)-VA (7.5 mg/kg) in 0.5% w/v CMC [R-Gly-VA(H)]	(R-Gly-VA)-H, p.o.
VII	VA APMs in 0.5% w/v CMC at low dose 3.7 mg/kg [VA-APMs(L)]	(VA-APMs)-L, p.o.
VIII	Gly APMs in 0.5% w/v CMC at low dose 0.25 mg/kg [Gly-APMs (L)]	(Gly-APMs)-L, p.o.
IX	VA APMs in 0.5% w/v CMC at high dose 7.5 mg/kg [VA-APMs(H)]	(VA-APMs)-H, p.o.
X	Gly APMs in 0.5% w/v CMC at high dose 0.50 mg/kg [Gly-APMs (H)]	(Gly-APMs)-H, p.o.
XI	Low dose of Gly (0.25 mg/kg)-VA (3.7 mg/kg) APMs in 0.5% w/v CMC [GV-APMs(L)]	(GV-APMs)-L+(D), p.o.
XII	High dose of Gly (0.50 mg/kg)-VA (7.5 mg/kg) APMs in 0.5% w/v CMC [GV-APMs(H)]	(GV-APMs)-H+(D), p.o.

4.7.6 Parameters for evaluation

Following parameters were evaluated before the initiation, during and at the end of the study for the pharmacological evaluation of the test compounds in T2DM rat model.

4.7.6.1 Body weight

The body weight of the rats was determined in triplicates on 0th, 15th, 20th, 27th, 33rd, 39th, and 45th day of the treatment protocol.

4.7.7 Biochemical parameters

4.7.7.1 Blood glucose levels

The blood glucose levels were determined in triplicate using glucometer on 20th, 27th, 33rd, 39th, and 45th day of the treatment protocol. The blood drop was taken by slightly pricking the rat's tail using a sterilized needle and was subjected to glucometer strip for the determination of blood glucose levels.

4.7.7.2 Serum lipid markers

Serum lipid markers such as CHL, HDL, TGs, were determined using Erba EM360 automated chemistry analyzer instrument while the VLDL, LDL, CHL/HDL, and LDL/HDL ratios were calculated from the values obtained with aforementioned markers using the formula as discussed in the subsequent sections. The concentration of serum lipid markers was determined on 0th, 15th and at the end of the 28th day of the treatment protocol.

4.7.7.2.1 Serum cholesterol

Increased CHL levels indicates impaired hepatic functions. It involves the estimation of CHL after the conversion of cholesterolester to CHL and fatty acid in the presence of CHL esterase. Free CHL, including that originally present, is then oxidized by cholesterol oxidase to cholest-4-en-3-one and H₂O₂. In presence of peroxidase, the formed H₂O₂ affects the oxidative coupling of phenol and 4-aminoantipyrine to form a red-colored quinoneimine dye. The 10µL of blood serum of fasted animals was used after centrifugation of the fresh clotted blood at 2500-3000 rpm. The clear supernatant was used for the determination of CHL in the rat's sample by running them in an automated biochemistry analyzer equipment erba EM360 based on photometric analysis using MultiXL v2017.02 (EM360) software upon selection of the working reagent mode. The XL results was calculated automatically by the instrument.

4.7.7.2.2 Serum HDL

The assay is based on a modified polyvinyl sulfonic acid (PVS) and polyethylene glycol-methyl ether (PEGME) coupled classic precipitation method. When the serum reacts with PEGME present in the precipitating reagent, all the LDL, VLDL and chylomicrons are precipitated. The HDL remains in the supernatant and is assayed as a sample for CHL using the CHL reagent. The

cholesterol oxidase and cholesterol esterase selectively react with HDL to produce H₂O₂ which is detected via a trinder reaction. The serum HDL levels in the rat's sample was determined after the centrifugation of the fresh clotted blood at 2500-3000 rpm to obtain a clear supernatant. The clear supernatant obtained is runned in an automated erba EM360 analyzer by selecting the working reagent mode. The XL results was calculated automatically by the instrument.

4.7.7.2.3 Serum Triglycerides

Triglycerides (TGs) belongs to the family of lipids that are absorbed from diet and is measured for the diagnosis and management of hyperlipidemia. The serum TGs levels was determined based on glycerol phosphate oxidase method. In this assay system, a series of reaction take place, initially the TGs are hydrolyzed by lipase to produce free acids and glycerol. The glycerol is phosphorylated by adenosine triphosphate with glycerol kinase to produce glycerol-3-phosphate and adenosine diphosphate. Glycerol-3-phosphate is oxidized to dihydroxy-acetone phosphate by glycerol phosphate oxidase producing H₂O₂. In a trinder type reaction catalyzed by peroxidases the H₂O₂ reacts with 4-aminoantipynne and N-Ethyl-N-Sulphohydroxy propyl-m-Toluidine to produce a dye. The absorbance of the dye is directly proportional to the concentration of TGs present in the sample. Such measurement was done by running the sample (clear supernatant) in automated erba EM360 analyzer. The XL results was calculated automatically by the instrument.

4.7.7.2.4 Others

The serum VLDL, LDL, CHL/HDL, and LDL/HDL ratios were calculated using the formula presented below:

$$\text{VLDL} = \text{TGs (mg/dL)} \div 5 \quad \text{Equation (19)}$$

$$\text{LDL} = \text{CHL} - \text{HDL} - \text{VLDL (mg/dL)} \quad \text{Equation (20)}$$

$$\text{CHL/HDL ratio} = \text{CHL/HDL (mg/dL)} \quad \text{Equation (21)}$$

$$\text{CHL/HDL ratio} = \text{CHL/HDL (mg/dL)} \quad \text{Equation (22)}$$

4.7.8 Serum inflammatory markers

Increased uptake of dietary fat causes fat accumulation in the peripheral organs including liver and activates hepatic pro-inflammatory cytokine levels. This results in alteration of glucose homeostasis by the liver [357]. Therefore, several studies reported overexpression of TNF- α by the liver cells during HFD-induced obesity [358]. In addition to this, chronic HFD consumption in rats induces glucose intolerance due to hepatic IL-6 resistance [357]. This is considered as one of the contributing factors involved in the occurrence of obesity-associated IR [357]. The levels of TNF- α and IL-6 in rat's serum sample were estimated using ELISA Invitrogen kits.

The blood samples were taken on the terminal day after the completion of the treatment period i.e., on 29th day and were stored at 4°C until processing. After 30 min, the collected blood samples were centrifuged at 8000 rpm for 15 min using cooling centrifuge. Supernatant was withdrawn in a separate Eppendorf tube and were stored at -20°C until analysis. Quantification of TNF- α and IL-6 in the blood serum was performed using an ELISA Invitrogen kit according to the manufacturer's protocol. Briefly 100 μ L of each standards and samples were added to respective wells containing pre-coated monoclonal antibody. Detection antibodies (biotinylated anti-Rat IL-6/TNF- α) and substrate solution (3,3',5,5'-tetramethylbenzidine). A blue color was produced upon the addition of the substrate solution which turned yellow upon addition of the stop buffer. The assay range was 40.96-10,000 pg/mL for IL-6 and 82.3-20,000 pg/mL for TNF- α . The OD of samples were compared to the standard curve and their concentration were determined [359].

4.7.9 Serum hepatic and renal markers

On the terminal day i.e., on 48th day, blood was withdrawn from rats of each group (G1-G12) via retro-orbital plexus for the determination of the effect of different treatments on serum glutamic pyruvic transaminase (SGPT), Serum glutamic oxaloacetic transaminase (SGOT), alkaline phosphatase (ALP), Creatinine and urea as a measure of hepatic and renal function. The blood withdrawn was centrifuged at 2500-3000 rpm to obtain serum. The clear supernatant was used for the determination of hepatic/renal markers in the rat's sample by running them in an automated biochemistry analyzer equipment erba EM360 based on photometric analysis using MultiXL v2017.02 (EM360) software upon selection of the working reagent mode. The XL results was calculated automatically by the instrument.

4.7.10 Euthanasia

The technique used to euthanize the experimental rats were overdose of general anesthesia that was performed at the terminal day of the treatment protocol i.e., on 49th day. The experimental rats from each groups were administered with ketamine hydrochloride (22-24 mg/kg) via intravenous route. Furthermore, to ensure the death of the animal cervical dislocation was employed. The liver and pancreas were isolated and preserved in 10% v/v formaldehyde at -20°C until analysis.

4.7.11 Determination of pancreatic oxidative stress

The extent of oxidative stress in the pancreas of diabetic rats were determined by measuring the levels of antioxidant enzymes viz, catalase (CAT), glutathione (GSH) and thiobarbituric acid reactive substances (TBARS) in the isolated pancreas of diabetic euthanized rats. After sacrificing the rats, their pancreas was quickly isolated, weighed, and washed for blood removal with PBS (pH=7.4). The isolated pancreas was cut into pieces for their homogenization. For the preparation of homogenate (10% w/v), the pancreatic tissue was mixed independently with 0.1M PBS. Then the

mixture was homogenized and centrifuged at 1000 rpm at 4°C for 20 min to obtain clear supernatant (Vade et al., 2009). The supernatant obtained was used for the assessment of CAT, GSH and TBARS respectively.

4.7.12 Histological study

The organs (liver and pancreas) were carefully removed and fixed in 10% v/v formaldehyde, cleaned up in xylene and embedded in a paraffin wax. Tissue sections were prepared and stained with eosin/hematoxylin. Photomicrographs were taken at × 400 magnification using a digital camera.

4.7.13 Statistical analysis

Data were presented as mean ± SEM of the respective replicates. Means of different groups were compared using analysis of variance (ANOVA). *P* values ≤ 0.05 (95% confidence interval) was considered significant. Graph Pad Prism 7.0 version, USA was employed to carry out the statistical analysis.

Chapter 5

Results and discussion

5.0 Results and discussion

5.1 Physical examination

Both the drugs (Gly and VA) was visually analyzed for physical changes. Gly was found to be odorless white crystal powder and VA was found to be pale-yellow free flowing powder with vanilla aroma without any precipitation observed.

5.2 Melting point analysis

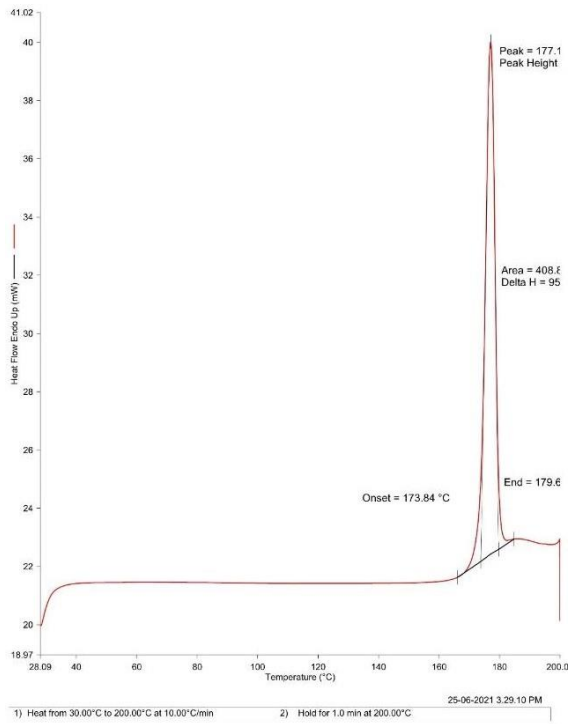
This method is used to measure the melting range of the solid using the procedure mentioned in Lachman and Lieberman, 2009. The solid is filled in a capillary tube sealed from a side. The melting range is observed in the capillary melting point apparatus with the help of a thermometer. The melting point of Gly was found in the range of 170-172°C (reference 169-174°C) while for VA it was found to be 210-211°C (reference 211.5°C).

5.3 DSC, XRD, FTIR analysis

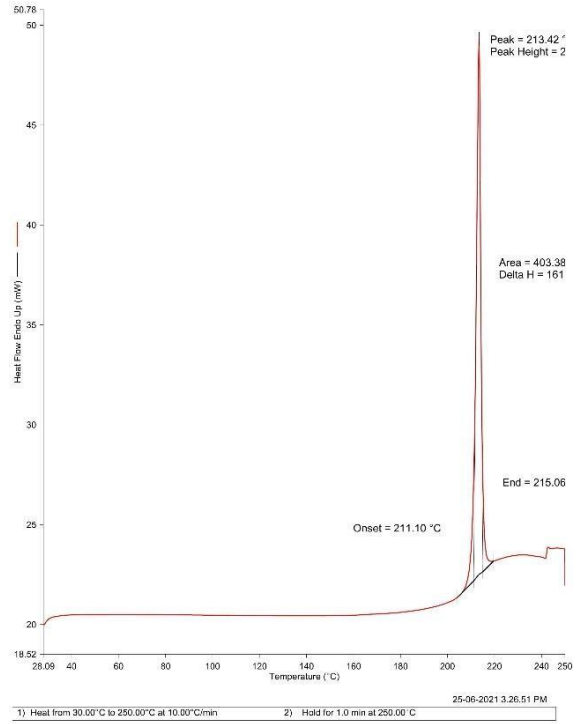
The thermogram of both the raw drugs are presented in **Fig 5.1 (A and B)**. The melting point of raw Gly was found to be 169°C and raw VA was found to be 218°C respectively. The results of XRD indicated sharp crystalline peaks for raw Gly and VA as presented in **Fig 5.1 (C and D)**. The FTIR spectrum of raw Gly reveal the presence of C=O group at 1712.8 cm⁻¹ of frequency, S=O group at 1340.5 cm⁻¹, amide group at 3331 cm⁻¹ and C=C-H stretching at 1614.4 cm⁻¹. Whereas FTIR spectrum of raw VA showed the presence of C=O at a frequency of 1672.3 cm⁻¹, O-C-O group at 1024.2 cm⁻¹ and O-H functionality at 3477.7 cm⁻¹ as presented in **Fig 5.1(E and F)**.

5.4 Partition coefficient (Log P)

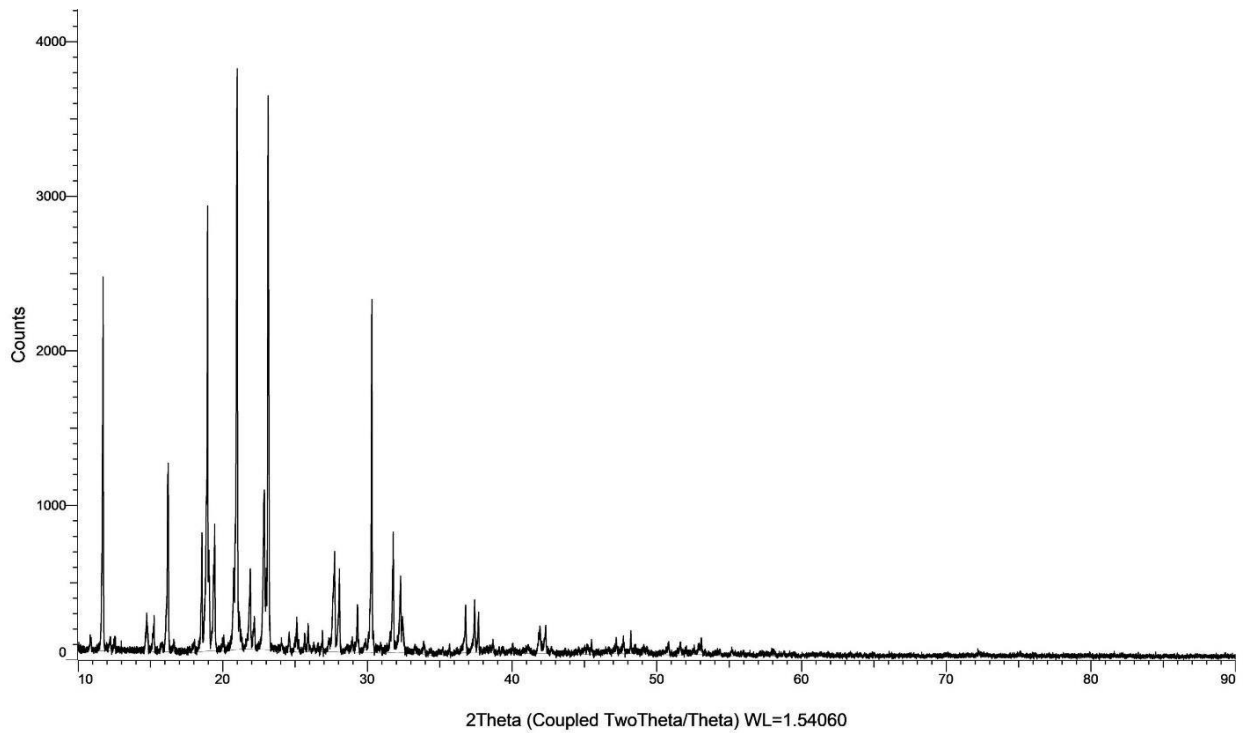
The log P of both the drugs raw Gly and VA were determined using shake-flask method. The amount of both the drugs present in the aqueous phase was estimated using UV spectroscopy at λ_{max} 261 nm for VA and 229 nm for Gly respectively. The total amount of drugs added was 10 mg each and the amount of drugs assayed in aqueous phase was 0.042 mg/mL (VA) and 0.001 mg/mL (Gly) after 24 hours of continuous shaking. The value of log P for both the drugs was calculated using **equation (1) and (2)**. The log P value of VA was found to be 1.02 while for Gly it was found to be 2.69 respectively. The reference log P values for VA and Gly was reported to be 1.43 and 3.70 respectively (Pub chem).



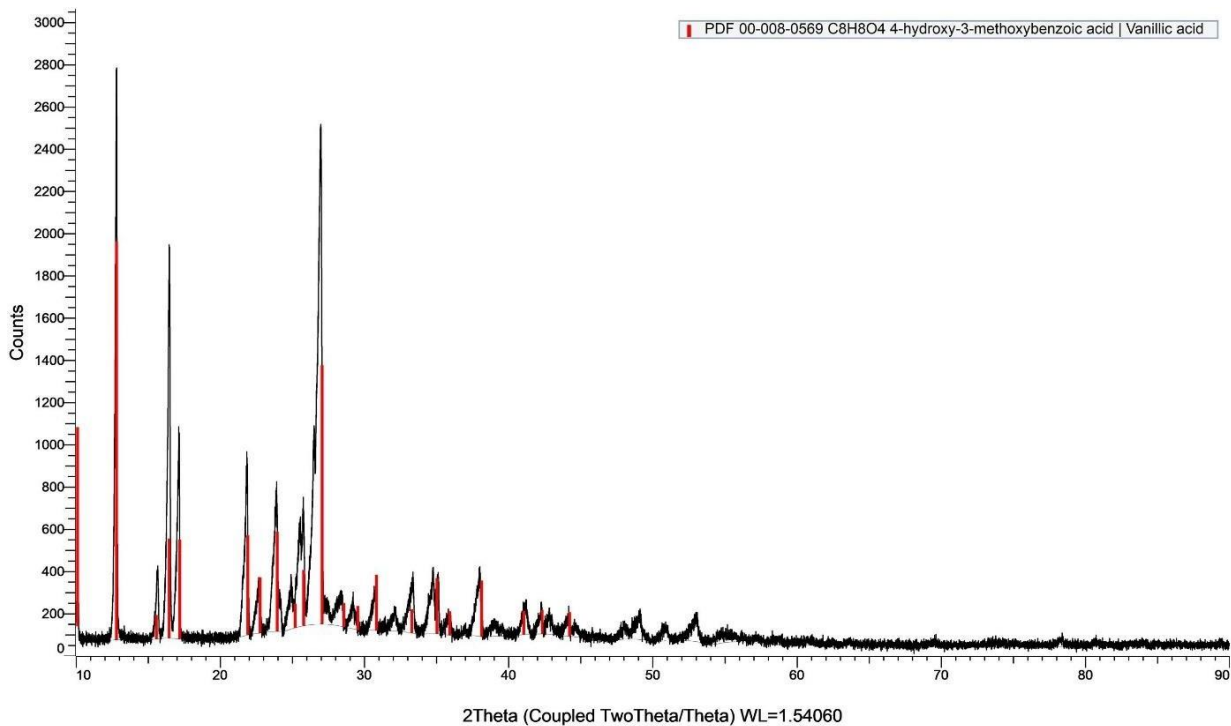
(A)



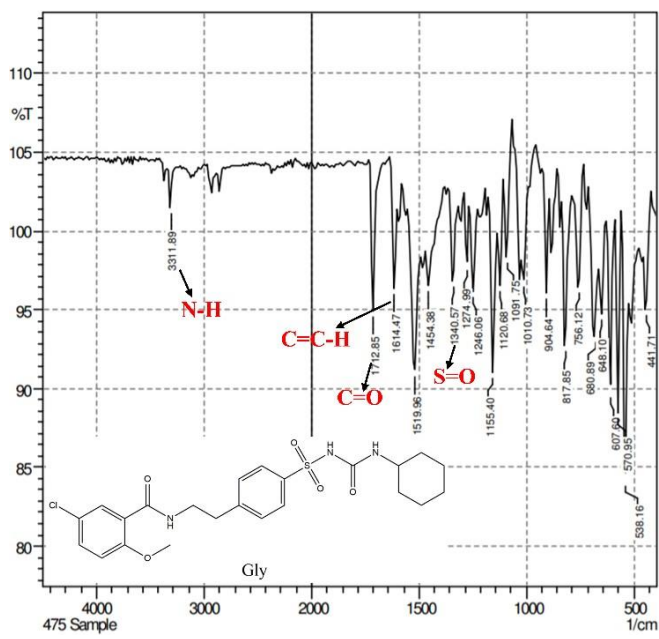
(B)



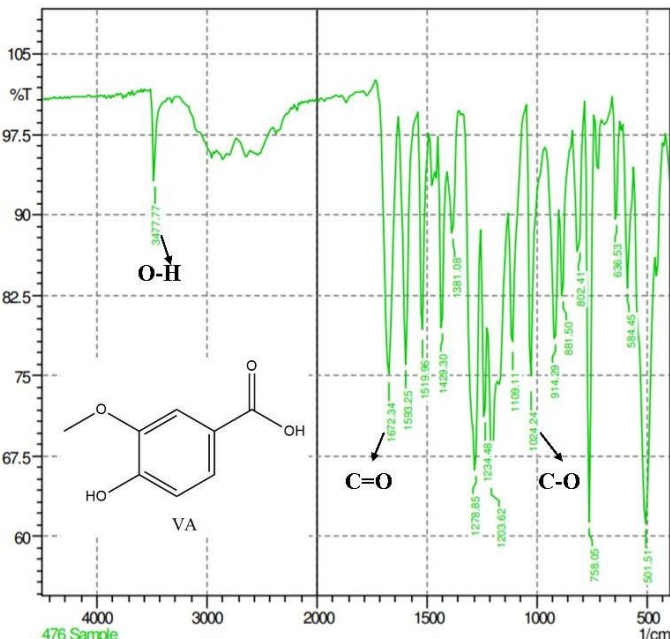
(C)



(D)



(E)



(F)

Fig 5.1: DSC thermogram (A) Gly, (B) VA; XRD Graph (C) Gly, (D) VA; IR spectra (E) Gly, (F) VA

5.5 Solubility in surfactants

The solubility of Gly and VA was evaluated in different surfactants with objective to select a conventional low molecular weight ionic or non-ionic surfactant together with the synthesized mPEG-b-PCL copolymer for the good stabilization of APMs. The results are presented in **Table 5.1**. It was observed that the Gly was found highly soluble at the lowest concentration of CTAB i.e., 0.5% w/v ($61 \pm 0.37 \mu\text{g/mL}$) followed by SLS ($48 \pm 1.00 \mu\text{g/mL}$), PVA ($32 \pm 0.11 \mu\text{g/mL}$), and PVP-K90 ($11 \pm 0.35 \mu\text{g/mL}$). Similarly, the highest solubility of VA was observed at the lowest concentration of CTAB i.e., 0.5% w/v ($63 \pm 0.42 \mu\text{g/mL}$) followed by PVA ($59 \pm 0.30 \mu\text{g/mL}$), SLS ($49 \pm 0.51 \mu\text{g/mL}$), and PVP-K90 ($48 \pm 0.51 \mu\text{g/mL}$). The percentage solubility of both the drugs in the rest of the other concentrations is shown in **Fig 5.2A** and **B**.

Table 5.1: Solubility of raw drugs in different surfactants (each value represents the mean \pm SD, n=3)

Surfactant	Concentration of surfactant (%w/v)	Solubility of Gly ($\mu\text{g/mL}$)	Solubility of VA ($\mu\text{g/mL}$)
SLS	0.5	48 ± 1.00	49 ± 0.51
	1	61 ± 0.50	46 ± 0.37
	1.5	54 ± 1.00	52 ± 0.13
	2	45 ± 0.71	63 ± 0.11
CTAB	0.5	61 ± 0.37	63 ± 0.42
	1	50 ± 0.12	42 ± 0.15
	1.5	33 ± 0.22	40 ± 0.10
	2	26 ± 0.17	49 ± 0.05
PVA	0.5	32 ± 0.11	59 ± 0.30
	1	18 ± 0.01	48 ± 0.46
	1.5	24 ± 0.18	45 ± 0.30
	2	16 ± 0.05	63 ± 1.10
PVP-K90	0.5	11 ± 0.35	48 ± 0.51
	1	4 ± 0.42	46 ± 0.02
	1.5	3 ± 0.73	38 ± 0.18
	2	0.8 ± 0.55	41 ± 0.03

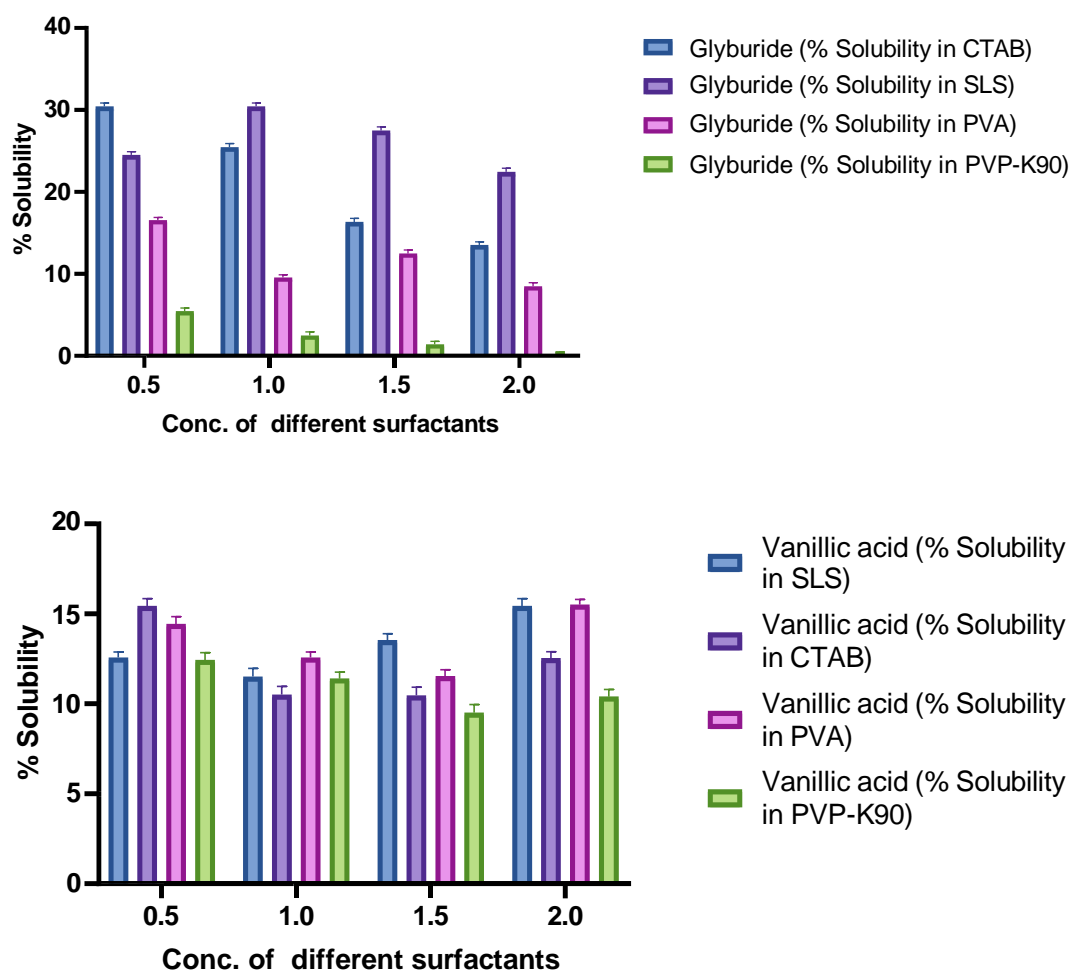


Fig 5.2: Percentage solubility of (A) Gly and (B) VA in varying concentrations of surfactants

5.6 Solubility in solvents and buffer systems

The solubility of both the drugs were determined in various organic solvents to select them for formulation development and in buffers as well. The highest solubility of both the drugs were observed in acetone. The solubility of VA in distilled water, ethanol, and in acetone was found to be 13.0, 817000, and 982000 $\mu\text{g/mL}$ respectively. The solubility of VA in phosphate buffer pH 1.2, 4.5, 6.8 and 7.4 were found to be 15.0 $\mu\text{g/mL}$ irrespective of the pH range. On the other hand, the solubility of Gly in distilled water, ethanol and acetone was found to be 7.6, 7768, and 852671 $\mu\text{g/mL}$ while in phosphate buffers it was found to be pH-dependent. An increase in the solubility profile of Gly was observed with increase in the pH value. With this agreement, the solubility of Gly in pH 1.2, 4.5, 6.8, and 7.4 were found to be 1.40 $\mu\text{g/mL}$, 1.67 $\mu\text{g/mL}$, 14.0 $\mu\text{g/mL}$, and 15.0 $\mu\text{g/mL}$ respectively. The percentage solubility of both the drugs were determined using *equation (3)* and is presented in *Table 5.2*.

Table 5.2: Solubility of raw drugs in different buffers (each value represents the mean \pm SD, n=3)

Solvent	Solubility VA ($\mu\text{g/mL}$)	Solubility Gly ($\mu\text{g/mL}$)	%Solubility VA	%Solubility Gly
Distilled water	13.0	7.6	16.2	9.5
HCL buffer (pH 1.2)	15.1	1.4	18.8	1.7
Phosphate buffer (pH 4.5)	15.0	1.6	18.0	2.0
Phosphate buffer (pH 6.8)	15.0	14.0	18.0	17.5
Phosphate buffer (pH 7.4)	15.0	15.0	18.0	18.7

5.7 Development of RP-HPLC analytical method

5.7.1 Selection of chromatographic conditions

Different ratios of varying mobile phase compositions were explored and the results were analysed. It was observed that the peak of VA and Gly appears at different retention times in all the mobile phase compositions **Fig. 5.3**. However, the shape of peaks was not acceptable as in these peaks tailing and broadening were observed. It was observed that when ACN and OPA 0.1% w/v were used in the ratio of 70:30 v/v at a 1 mL/min flow rate, sharp peaks of both the drugs were observed at the retention times of 2.6 and 5.4 min (**Fig. 5.3G**). Hence, this chromatographic condition was finalized for further development of the calibration curve and validation of the method.

5.7.2 Linearity and range

The developed calibration curve was found to be linear in the range of 2 to 10 $\mu\text{g/mL}$ with a regression coefficient (r^2) of 0.999 as presented in **Fig 5.4**.

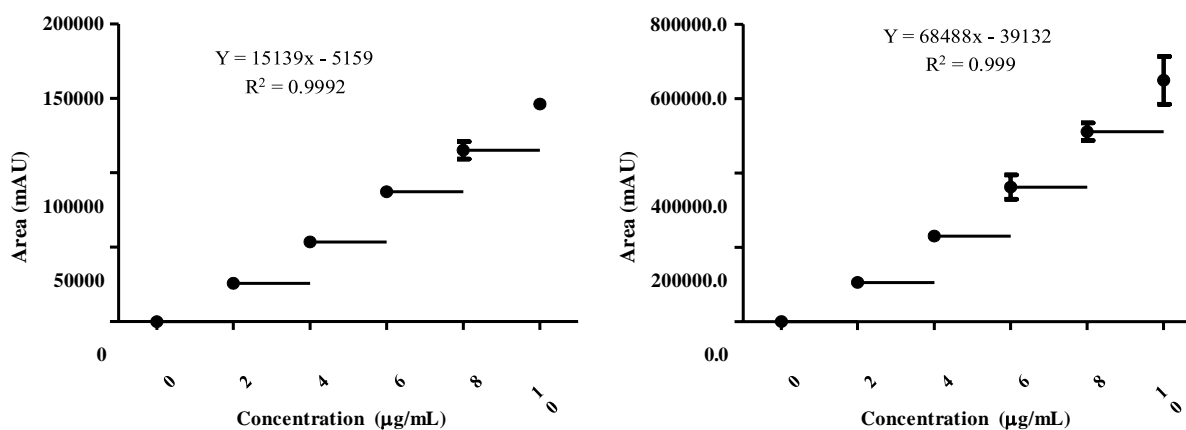


Fig 5.4: (A). Calibration Curve of VA (B). Calibration curve of Gly

5.7.3 Accuracy

The results of the accuracy study showed percentage recovery at all three levels in the range of 95-105% that was calculated using *equation (4)*. The data revealed that for all the three levels the mean percentage recovery was within the acceptable limits as shown in **Table 5.3**. This indicates that the developed method was accurate.

5.7.4 Precision

The results of method precision showed that the method is precise within the acceptable limits. The %RSD, tailing factor, and the number of theoretical plates were calculated for each solution; all the results are within limits. It was observed that the %RSD calculated using *equation (5)* and tailing factor was < 2%, and the number of plates was more than 1000 as presented in **Table 5.4 (A and B)**.

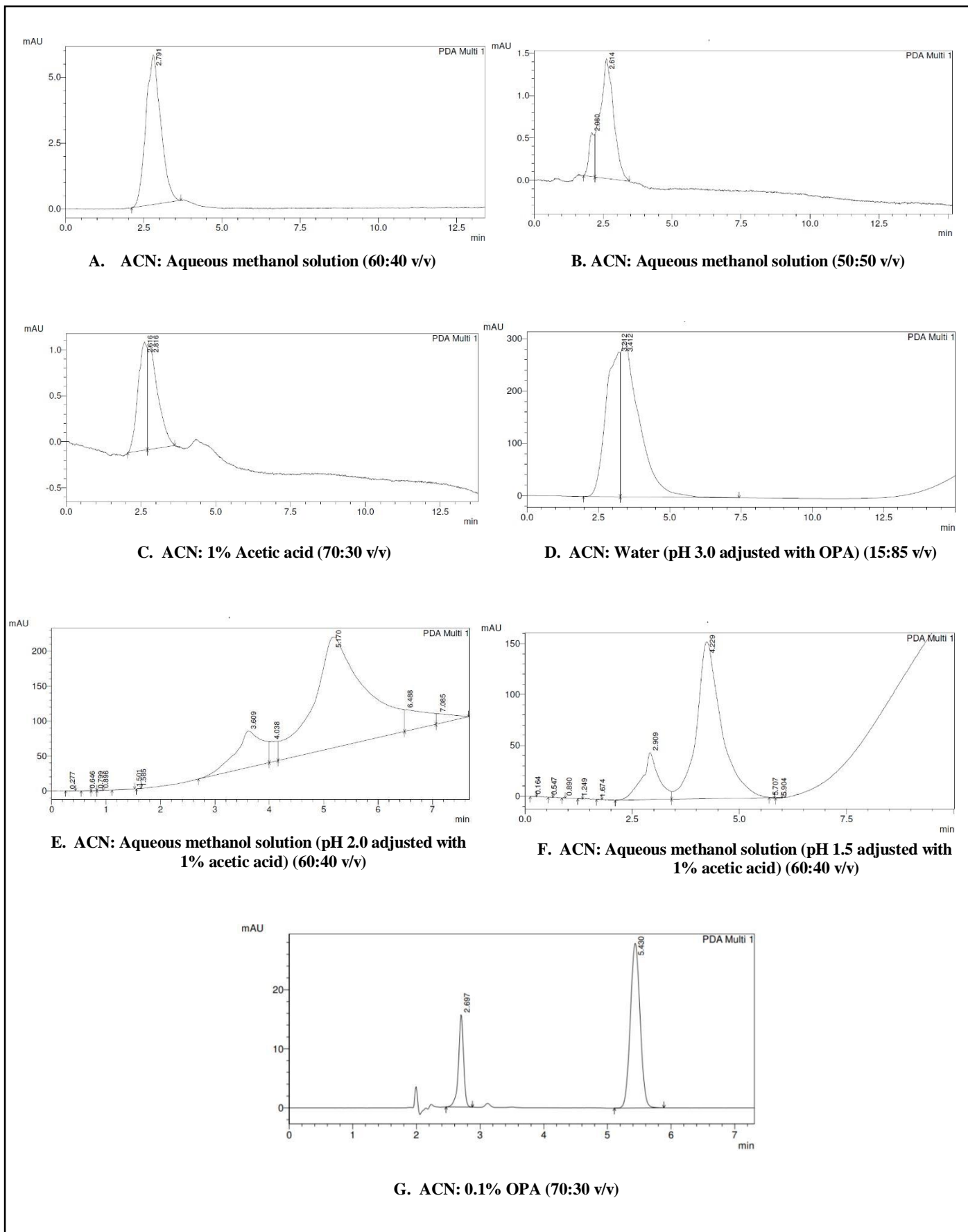


Fig. 5.3: Chromatogram of VA and Gly with different mobile phases

Table 5.3: Results of accuracy study

Level	Conc. (µg/mL)	VA						Mean±SD	%Recovery
		1	2	3	4	5	6		
LQC	4.8	65102.5	66113.5	67188.0	68410.3	69584.4	68542.4	67490.1±1674.9	99.9%
MQC	6	86504.0	85488.0	88127.1	85101.7	86332.0	85470.0	86170.4±1101.3	100.5%
HQC	7.2	108406.3	108889.8	108252.9	106530.3	107876.8	107573.4	107921.6±817.4	103.7%
Level	Conc. (µg/mL)	Gly						Mean±SD	%Recovery
		1	2	3	4	5	6		
LQC	4.8	278113.3	295943.3	289621.5	284018.8	280373.9	287938.0	286001.5±6534.8	98.9%
MQC	6	383244.8	374680.5	371664.0	372179.7	374232.7	371298.0	374550.0±4477.5	100.6%
HQC	7.2	442257.9	441352.4	446755.7	460402.9	448279.4	453245.4	448715.6±7170.2	98.9%

5.7.5 Robustness

The results of percentage relative standard deviation after doing minor changes in the flow rate, the ratio of mobile phase and pH was less than 2% and its value was calculated using *Equation (5)*. This indicates that the developed method was robust (**Table 5.5**).

5.7.6 System suitability

The values of the system suitability parameters are presented in **Table 5.6**. The absence of any extra peak in the chromatogram of indicated the specificity of the method to estimate VA and Gly (**Fig 5.6**). The LOD and LOQ were determined using *equation (6)* and *(7)*.

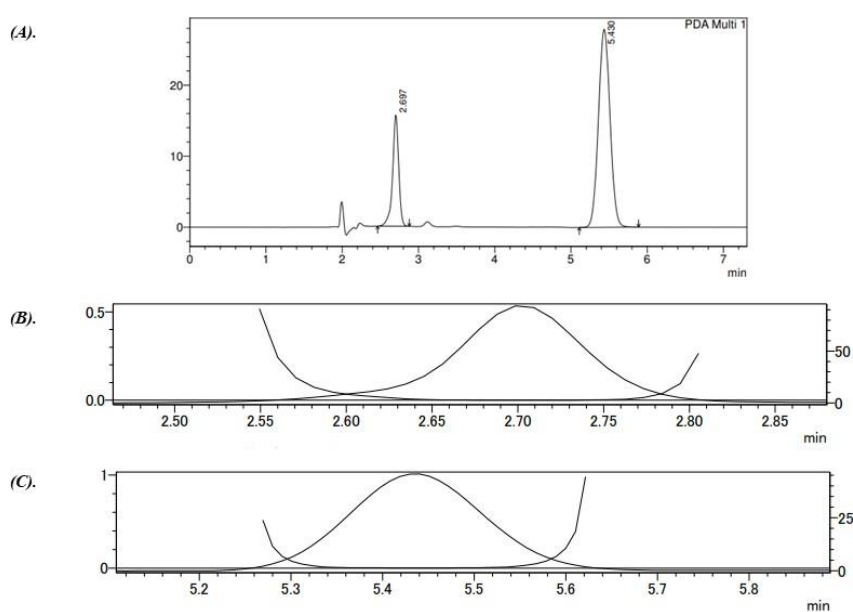


Fig 5.6: (A). Chromatogram of Unprocessed VA and glyburide, (B). The peak of Purity of VA, (C). The peak of Purity of Gly

Table 5.4A: Results of Precision Study of VA

Parameter	Level	Conc. (ng/mL)	Area (cm ²)						Mean area (cm ²)	Standard deviation	% RSD
			1	2	3	4	5	6			
Intra-day											
	LQC	4.8	67692.2	66927.5	68097.4	67830.9	66676.5	66879.2	67350.6	593.4	0.8
	MQC	6.0	86600.1	85425.9	85102.7	86706.1	85970.5	86442.5	86041.3	660.3	0.7
	HQC	7.2	101130.7	101181.5	102028.7	102248.3	101544.1	101196.4	101555.0	480.2	0.4
Inter-day											
Day 1	LQC	4.8	67992.6	68050.0	67350.6	67288.5	67799.6	67839.2	67720.1	324.4	0.4
	MQC	6.0	85604.0	84689.0	84137.1	84101.7	84322.0	84550.0	84567.3	557.1	0.6
	HQC	7.2	105153.2	106613.3	107230.0	107882.0	106997.0	106512.5	106731.3	916.0	0.8
Day 2	LQC	4.8	64806.6	64483.6	64147.9	65432.5	74476.0	74609.5	67992.6	228.3	0.3
	MQC	6.0	81024.4	81068.1	81430.9	81654.1	81189.6	82718.5	81604.2	597.0	0.7
	HQC	7.2	107973.0	108428.0	101717.2	101671.2	102819.6	102310.1	104153.2	321.7	0.3
Day 3	LQC	4.8	67899.1	67793.6	67010.0	68847.3	68729.4	68022.7	68050.3	673.5	0.9
	MQC	6.0	82429.5	82782.8	82312.3	83297.5	83157.1	82155.4	82689.1	467.3	0.5
	HQC	7.2	104306.3	107979.8	107192.9	106530.3	106986.8	106683.4	106613.3	1239.0	1.1
Intermediate precision (inter analyst)											
Analyst 1	LQC	4.8	68102.5	69113.5	69188.0	69410.3	69584.4	69442.4	69140.1	536.9	0.7
	MQC	6.0	87231.5	87544.0	86234.3	87222.3	87032.0	86611.5	86979.2	476.3	0.5
	HQC	7.2	102663.0	102118.2	101503.2	101239.0	101445.8	101623.5	101765.4	528.8	0.5
Analyst 2	LQC	4.8	69058.2	69634.0	69632.7	69298.1	69552.5	70848.1	69670.6	619.1	0.8
	MQC	6.0	85734.1	86779.8	85031.1	86683.2	86543.8	87413.9	86364.3	846.4	0.9
	HQC	7.2	101197.8	101396.5	101204.2	101250.0	102773.8	102678.8	101750.2	760.0	0.7
Analyst 3	LQC	4.8	68111.4	69298.1	69812.2	68185.1	69007.4	69513.5	68987.9	702.1	1.0
	MQC	6.0	87483.9	88978.0	88544.1	88087.0	88411.0	89193.3	88449.5	617.5	0.6
	HQC	7.2	101703.3	101189.7	102228.2	101169.4	101279.7	101706.1	101546.1	413.6	0.4

Table 5.4B: Results of Precision Study of Gly

Parameter	Level	Conc. (ng/mL)	Area (cm ²)						Mean area (cm ²)	Standard deviation	% RSD	%Recovery
			1	2	3	4	5	6				
Intra-day												
	LQC	4.8	287182.5	284970.1	283128.2	289915.1	289915.1	287331.3	287073.7	2691.3	0.9	99.2
	MQC	6.0	363964.2	360581.4	363509.5	363604.3	360721.9	371414.2	362685.0	2392.0	0.6	97.0
	HQC	7.2	434322.3	431403.1	410816.2	424028.6	429590.6	422594.6	432862.7	2064.1	0.4	95.7
Inter-day												
Day 1	LQC	4.8	283113.3	283843.3	282221.5	286026.8	280133.9	286726.0	283677.5	2442.0	0.8	98.0
	MQC	6.0	372144.8	377880.5	372554.0	371069.7	371212.7	372399.0	372876.8	2527.4	0.6	100.0
	HQC	7.2	442311.6	451606.4	439990.7	443393.0	441588.8	441257.0	443357.9	4195.5	0.9	97.8
Day 2	LQC	4.8	284114.7	284859.2	280332.9	286829.6	286647.5	284421.2	284534.2	2352.8	0.8	98.4
	MQC	6.0	363132.6	358216.1	375366.0	375582.9	379821.1	375606.8	371287.6	3476.4	0.9	99.8
	HQC	7.2	410852.9	414755.7	406230.5	406092.4	411697.1	415941.6	410928.3	4143.2	1.0	91.2
Day 3	LQC	4.8	286211.2	287460.3	286105.6	287094.2	287288.2	288120.5	287046.7	770.5	0.2	99.2
	MQC	6.0	378980.1	377609.3	374334.0	377829.8	375943.1	372070.5	376127.8	2566.7	0.6	100.0
	HQC	7.2	445177.9	443381.4	445645.7	450801.9	449389.4	449155.4	447258.6	2920.8	0.6	98.2
Intermediate precision (inter analyst)												
Analyst 1	LQC	4.8	290086.1	294620.3	295620.1	297025.0	297833.4	293740.6	294820.9	2763.9	0.9	100.0
	MQC	6.0	371084.3	369307.5	365234.7	375487.1	373199.8	371529.1	370973.7	3503.1	0.9	99.0
	HQC	7.2	452551.5	457092.8	453462.2	451628.3	455661.8	451721.6	453686.4	2233.4	0.4	99.0
Analyst 2	LQC	4.8	290781.4	295094.6	298268.6	297509.1	299716.6	297133.9	296417.4	3147.4	1.0	100.0
	MQC	6.0	376738.5	372304.7	371154.0	379647.8	379107.6	378585.8	376256.4	3658.9	0.9	100.0
	HQC	7.2	458522.9	461517.3	457139.6	452324.5	458005.5	453253.8	456793.9	3446.6	0.7	100.0
Analyst 3	LQC	4.8	289390.8	294146.1	292971.5	296540.9	295950.1	290347.2	293224.4	2909.1	0.9	100.0
	MQC	6.0	365430.0	366310.3	359315.3	371326.4	367291.9	364472.3	365691.0	3921.9	1.0	98.5
	HQC	7.2	446580.0	452668.4	449784.8	450932.1	453318.0	450189.3	450578.7	2398.6	0.5	100.0

Table 5.5: Results of Robustness Study of VA and Gly

Variable	Value	Conc. ($\mu\text{g/mL}$)	Peak area (Mean \pm SD) (*N=6)	%Recovery (Mean \pm SD) (*N=6)	Retention time (Mean \pm SD) (*N=6)
VA					
Flow rate (mL/min)	0.8	6.0	80636.1 \pm 761.1	93.3 \pm 0.1	2.1 \pm 0.2
	1.0	6.0	84567.2 \pm 557.1	98.8 \pm 0.3	2.6 \pm 0.1
	1.2	6.0	81865.3 \pm 585.9	95.8 \pm 0.2	2.4 \pm 0.2
Ratio of mobile phase (A:B) v/v	68:28	6.0	86161.2 \pm 1108.4	95.4 \pm 0.2	2.4 \pm 0.2
	70:30	6.0	88449.5 \pm 617.5	103.0 \pm 0.1	2.6 \pm 0.1
	72:32	6.0	90070.4 \pm 998.2	104.8 \pm 0.2	2.8 \pm 0.2
pH	1.3	6.0	87890 \pm 1127.1	102.4 \pm 0.3	2.5 \pm 0.3
	1.5	6.0	88449.5 \pm 617.5	103.0 \pm 0.3	2.6 \pm 0.2
	1.7	6.0	87700.6 \pm 1153.3	102.2 \pm 0.1	2.5 \pm 0.1
Isosbestic point (wavelength in nm)	232	6.0	82685.4 \pm 1547.9	96.7 \pm 0.3	2.2 \pm 0.3
	234	6.0	86041.3 \pm 660.3	100.0 \pm 0.2	2.6 \pm 0.2
	236	6.0	84315.1 \pm 751.5	98.5 \pm 0.3	2.4 \pm 0.3
Gly					
Flow rate (mL/min)	0.8	6.0	354639.0 \pm 3603.4	95.8 \pm 0.3	5.3 \pm 0.3
	1.0	6.0	372876.8 \pm 2527.4	100.2 \pm 0.2	5.4 \pm 0.1
	1.2	6.0	348030.3 \pm 4704.5	94.2 \pm 0.4	5.2 \pm 0.2
Ratio of mobile phase (A:B) v/v	68:28	6.0	363875 \pm 6978.7	98.0 \pm 0.2	5.3 \pm 0.3
	70:30	6.0	362685 \pm 2392	97.7 \pm 0.3	5.4 \pm 0.2
	72:32	6.0	375646.4 \pm 607.1	100.9 \pm 0.2	5.5 \pm 0.1
pH	1.3	6.0	357292.1 \pm 6155.2	96.4 \pm 0.3	5.1 \pm 0.3
	1.5	6.0	371287.6 \pm 3476.4	99.8 \pm 0.4	5.4 \pm 0.2
	1.7	6.0	348078.5 \pm 3596.1	94.2 \pm 0.3	5.3 \pm 0.4

Isosbestic point (wavelength in nm)	232	6.0	366599.7 ± 6575.6	98.7 ± 0.4	5.3 ± 0.1
	234	6.0	376127.8 ± 2566.7	101.0 ± 0.2	5.4 ± 0.2
	236	6.0	368094.2 ± 5071.5	99.0 ± 0.4	5.3 ± 0.2

Table 5.6: Parameters of system suitability

Sr. no	Parameter	VA value	Gly value
1	LOD	0.34 µg/mL	0.38 µg/mL
2	LOQ	1.04 µg/mL	1.17 µg/mL
3	Theoretical Plates	4588.82	5478.50
4	HETP	32.68	27.38
5	Tailing factor	0.9	1.0
6	Peak purity index	1.000	1.000

5.8 Formulation Development

5.8.1 Synthesis and characterization of mPEG-b-PCL copolymer

The diblock copolymer mPEG-b-PCL was synthesized using ring open polymerization reaction as reported previously [339]. In this reaction, the hydroxyl terminal groups of mPEG as presented in **Fig 5.7** initiated the ring-opening of the epsilon-CL. The final weight of the synthesized mPEG-b-PCL copolymer obtained was 32 g. The product yield was calculated using **equation (8)** and it was found to be 86.9%. The characteristics of the synthesized diblock copolymer are presented in **Table 5.7**.

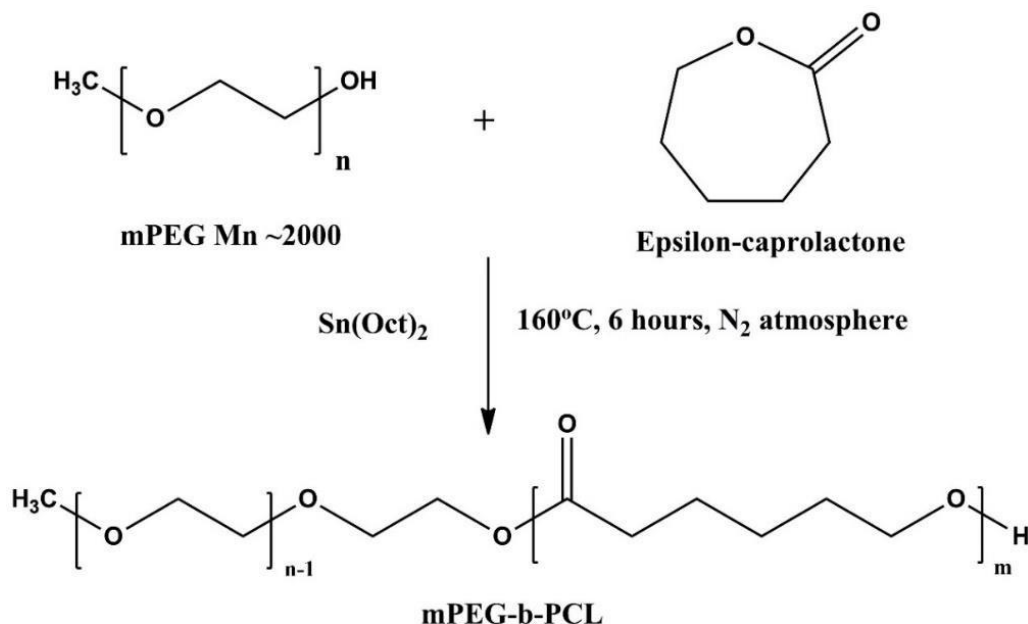


Fig 5.7: Diagrammatic presentation of the synthesis of diblock copolymer mPEG-b-PCL

Table 5.7: Molecular characteristics of the synthesized diblock copolymer

Copolymer	PEG/PCL feed ratio	^a M _w (Da)	^b M _n (Da)	^c PDI	T _m (°C)	^d DP(PEG)	^d DP (PCL)	^e HLB
mPEG-b-PCL	1:20	2115.7	2105.1	1.0	55	34.1	14.3	10.0

^a Determined using ESI-MS spectroscopy

^b Determined by multiplying DP with molecular weight of the repeating units

^c M_w/M_n = Polydispersity Index of the copolymer

^d Determined by dividing the M_w of copolymer with molecular weight of the repeating units in polymer chain

^e HLB value calculated by 20 * M_n (PEG)/M_n mPEG-b-PCL

Abbreviations: M_w, Average molecular weight; M_n, Number average molecular weight; PDI, Poly dispersity index; DP, Degree of polymerization; HLB, Hydrophilic-lipophilic balance

5.8.2 CMC determination

CMC is an essential critical factor that influences the stability and solubilisation characteristics of APMs. To assess the CMC of the synthesized mPEG-b-PCL, we used iodine as a hydrophobic probe that easily solubilizes in the micellar core. The conversion of triatomic I₃⁻ into I₂ in the presence of potassium iodide maintained the saturated solution of I₂. The absorption intensity of I₂ was plotted against different concentrations of copolymer (log scale) as presented in **Fig 5.8**. The CMC value was obtained from the point on the curve representing an abrupt increase in absorbance. From this curve, the CMC value was found to be i.e., 1.7 µg/mL.

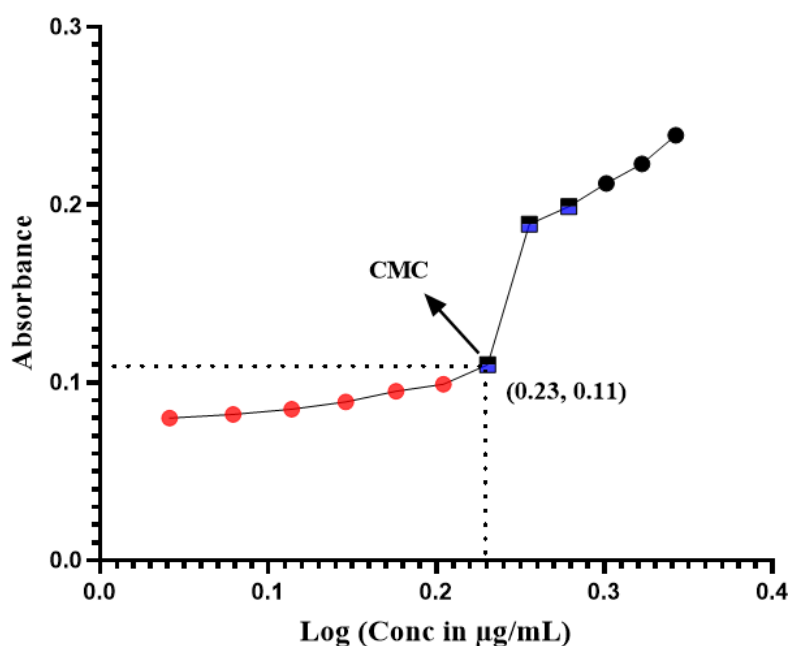


Fig 5.8: Determination of CMC value of mPEG-b-PCL copolymer

5.8.3 FTIR

FTIR spectrum of mPEG-b-PCL is presented in **Fig 5.9** and was compared with the FTIR spectra of mPEG polymer and epsilon-CL. In comparison to the mPEG and epsilon-CL, FTIR spectra with mPEG-b-PCL copolymer represented sharp and intense bands at 1724.4 cm^{-1} and 1103.2 cm^{-1} that were showing the presence of carboxylic ester (C=O) and ether (C-O) groups. This indicated the successful synthesis of mPEG-b-PCL .

5.8.4 NMR

The structure and composition of the synthesized mPEG-b-PCL was assessed by ^1H NMR spectroscopy in DMSO as presented in **Fig 5.10A**. The presence of methylenes of PCL and PEG have observed around 1.2 -1.3 ppm (a, 2H), 1.4-1.5 ppm (b. 4H), 2.28 ppm (c, 2H), 3.3 ppm (f, 3H), and 3.5 ppm (d, 10H) while methyl of PEG was observed at 3.9 ppm (e, 3H). The presence of triplet at 3.9 ppm (3 protons) arising from the terminal methyl of the PEG block as it links to the ester group in the PCL indicated the successful synthesis of mPEG-b-PCL.

5.8.5 DSC

The thermogram of the synthesized mPEG-b-PCL is presented in **Fig 5.10B**. In the thermogram, the melting point of mPEG-b-PCL was observed at $55\text{ }^\circ\text{C}$ as a measure of the appearance of the endothermic peak observed in the thermogram. This indicated the melting of the semi-crystalline PCL block of the synthesized copolymer.

5.8.6 ESI-MS

The ESI-MS spectrum of mPEG-b-PCL contains very rich information since there is one peak for each molar mass (**Fig 5.10C**). Within the displayed m/z range where singly charged ions were observed, homologue series could be defined from each peak by adding or subtracting 62.07 or 114.14 Da i.e., the mass of the ethylene glycol and caprolactone respectively that corresponds to one ethylene glycol unit and for each caprolactone unit. It allowed checking against the presence of by-products, particularly unreacted mPEG or PCL.

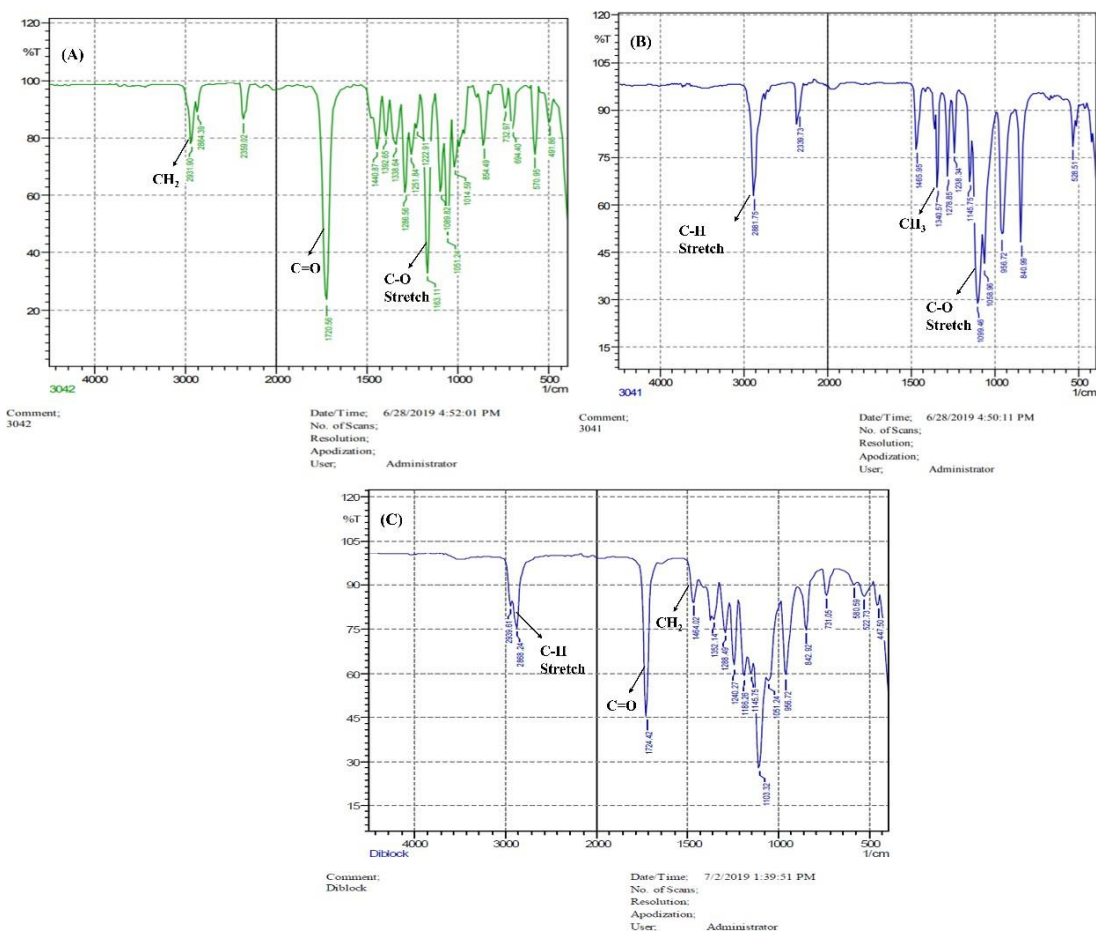
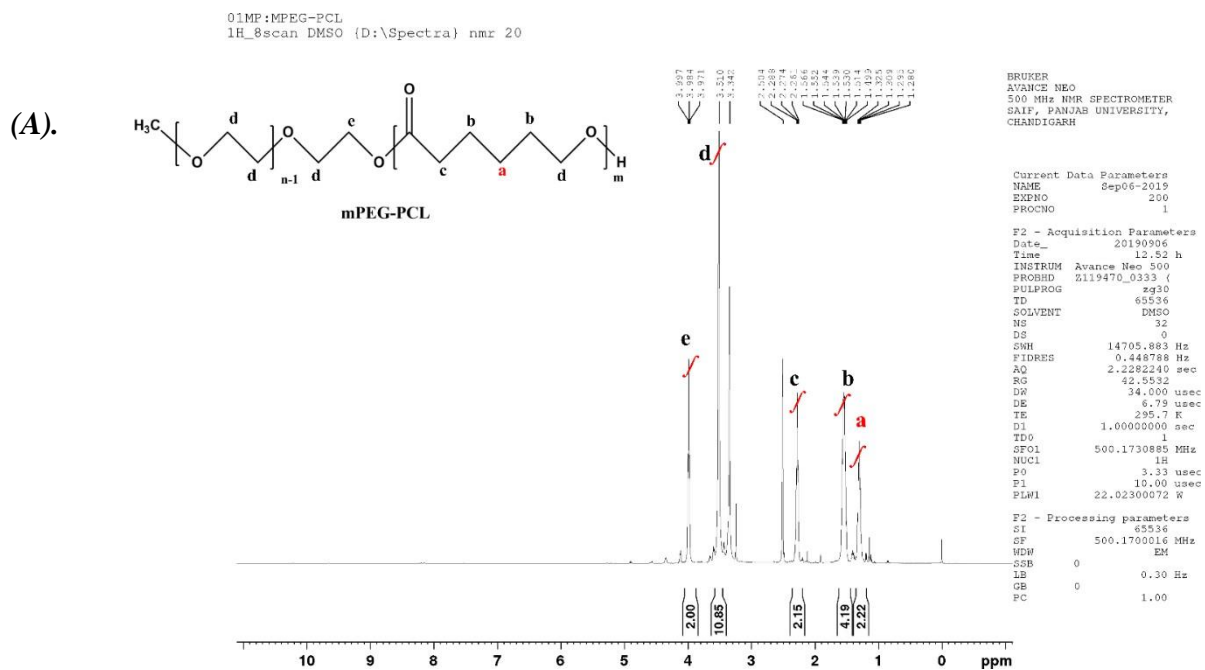
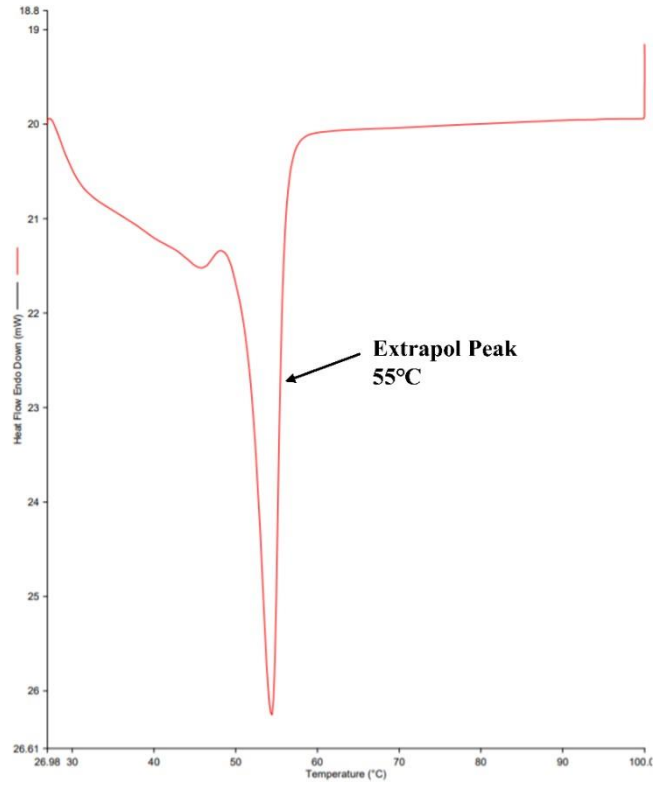


Fig 5.9: FTIR spectra (A) Epsilon-CL (B) mPEG (C) mPEG-b-PCL



(B).



(C).

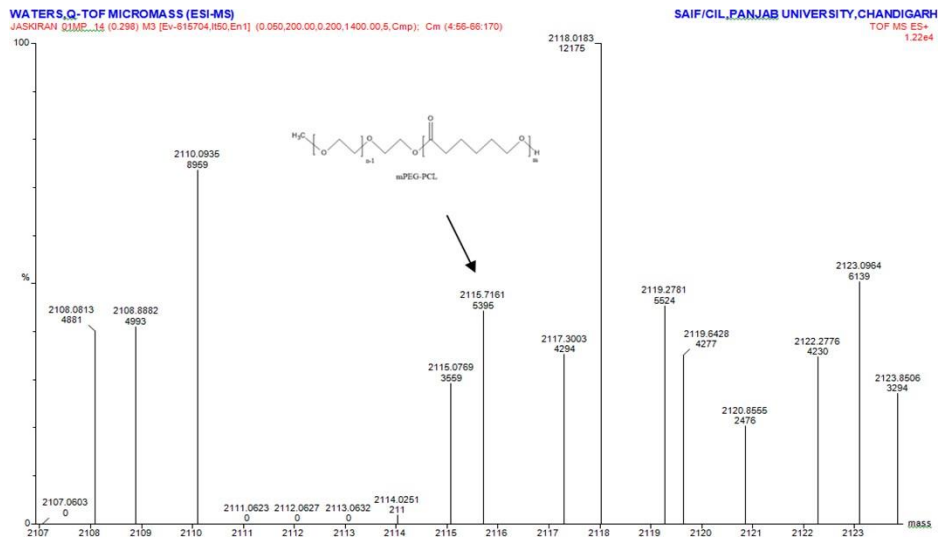


Fig 5.10: (A) ¹HNMR spectra, (B) DSC thermogram (C) Mass spectra of mPEG-b-PCL copolymer

5.8.7 Examination of process variables for optimization of formulation

As per BBD, 17 batches were prepared to evaluate the influence of independent variables coded as A, B, C on the responses viz. particle size (R1), EE of VA (R2), EE of Gly (R3), zeta potential (R4) and PDI (R5) respectively. The results of these 17 batches are presented in the aforementioned **Table 5.8**. The lowest particle size (R1) was observed in run 10 (44.6 nm) while the highest (80.6 nm) was for run 14. Likewise, for EE of VA (R2), the highest value (99.3%) was obtained in run 8 while the lowest value (80.7%) was observed in run 13. On the other hand, EE of Gly (R3), the highest value (99.9%) was obtained in run 8 and the lowest value (90.0%) was observed for run 12.

In the case of zeta potential (R4), the highest value (25.7 mV) was found for run 9 while the lowest value (9.1 mV) was observed in run 2. Similarly, the lowest value (0.247) of PDI (R5) was found in run 1 and the highest value (0.454) was observed for run 8. The higher to the lower ratio for R1, R2, R3, R4 and R5 was found to be 1.8, 1.2, 1.1, 2.8, and 1.8 respectively. The power of transformation was not required since all the values of higher to lower ratio were below 10. The results of the statistical analysis of the responses using DoE tools is presented in Table 5. The lower value of standard deviation and predicted residual error sum of square (PRESS), the high value of R-square and $P < 0.0001$ suggested a quadratic model for all the responses obtained. The significant effect and the interaction among the variables were determined using ANOVA as presented in **Table 5.9**. The F value for all responses was found as follows: R1: 8.16, R2: 6.61, R3: 88.0, R4: 4.10, and R5: 3.61. The *P*-value was found less than 0.05 in all cases demonstrating the significance of the model. In addition, the adequate precision values were found to be greater than 4 (R1: 9.56, R2: 8.51, R3: 32.5, R4: 7.91 and R5: 6.57) This specified that the used model is adequate. For all responses, the R-squared value was found above 0.500.

Table 5.8: Factor level and experimental data for BBD

Run	Factor 1 (Drug to copolymer ratio)	Factor 2 (Drug to surfactant ratio)	Factor 3 (Solvent to antisolvent ratio)	R1 (Particle Size) nm	R2 (EE of VA)%	R3 (EE of Gly)%	R4 (Zeta potential) mV	R5 (PDI)
1	0.6 (+)	0.25(-)	0.2(0)	67.5	97.4	95.2	11.3	0.247
2	0.2 (-)	0.5(0)	0.1(-)	50.7	87.2	92.9	9.1	0.27
3	0.4 (0)	0.5(0)	0.2(0)	46.6	98.7	95.1	16.4	0.323
4	0.4 (0)	0.5(0)	0.2(0)	46.6	98.7	95.6	16.4	0.323
5	0.4 (0)	0.5(0)	0.2(0)	46.6	98.7	95.2	16.4	0.323
6	0.4 (0)	0.5(0)	0.2(0)	46.6	98.7	95.3	16.4	0.323
7	0.4 (0)	0.75(+)	0.1(-)	47.9	98.7	99.6	21.5	0.296
8	0.6 (+)	0.75(+)	0.2(0)	46.3	99.3	99.9	23.2	0.454
9	0.4 (0)	0.75(+)	0.3(+)	69.7	97.7	99.2	25.7	0.367
10	0.6 (+)	0.5(0)	0.1(-)	44.6	99.1	98.9	11.2	0.372
11	0.2 (-)	0.5(0)	0.3(+)	51.6	94.6	95.2	14.1	0.367
12	0.4 (0)	0.25(-)	0.1(-)	52.1	95.4	90	25.5	0.361
13	0.2 (-)	0.75(+)	0.2(0)	50.9	80.7	99.7	22.8	0.349
14	0.6 (+)	0.5(0)	0.3(+)	80.6	96.8	98.6	15.1	0.295
15	0.4 (0)	0.25(-)	0.3(+)	72.9	94.3	94.1	21.3	0.343
16	0.2 (-)	0.25(-)	0.2(0)	65.2	83.9	88.6	14.2	0.325
17	0.4 (0)	0.5(0)	0.2(0)	46.6	98.7	95.1	16.6	0.323

Table 5.9: Fit summary and ANOVA using DOE tools

Summary															
Source	Sequential <i>P</i> value					Lack of fit <i>P</i> value					Adjusted R-squared				
	R1	R2	R3	R4	R5	R1	R2	R3	R4	R5	R1	R2	R3	R4	R5
Linear	0.021	0.019	<0.0001	0.504	0.495	-	-	0.0008	<0.0001	-	0.399	0.409	0.848	-0.034	-0.030
2FI	0.268	0.720	0.0009	0.883	0.017	-	-	0.0085	<0.0001	-	0.465	0.323	0.959	-0.263	0.494
Quadratic	0.018	0.016	0.0474	0.0078	0.781	-	-	0.022	<0.0001	-	0.801	0.759	0.980	0.636	0.375
Cubic	-	-	0.022	<0.0001	-	-	-	-	-	-	1.000	1.000	0.996	0.999	1.000
Source	Predicted R-squared					F-value					<i>P</i>-value				
Linear	0.137	0.107	0.751	-0.765	-0.739			54.9	4725.3		-	-	0.0008	<0.0001	-
2FI	-0.063	-0.704	0.903	-3.002	-0.564			16.5	6657.5		-	-	0.0085	<0.0001	-
Quadratic	-0.391	-0.684	0.874	-1.542	-3.370			10.5	2680.1		-	-	0.0228	<0.0001	-
Cubic	-	-	-	-	-						-	-	-	-	-

Sequential model sum of squares (type I)

Source	Sum of squares					Df					Mean square				
Mean vs total	51205.2	1.541E+05	1.559E+05	5195.7	1.89	1	1	1	1	1	51205.2	1.541E+05	1.559E+05	5195.7	1.89
Linear vs mean	1073.1	271.5	153.1	64.5	0.0056	3	3	3	3	3	357.7	90.5	51.0	21.5	0.0019
2FI vs linear	320.1	30.0	16.9	20.6	0.0179	3	3	3	3	3	106.7	10.0	5.66	6.89	0.0060
Quadratic vs 2FI	518.8	165.7	2.92	255.2	0.0015	3	3	3	3	3	172.9	55.2	0.973	85.0	0.0005
Cubic vs quadratic	182.1	54.9	1.36	64.3	0.0094	3	3	3	3	3	60.7	18.3	0.452	21.4	0.0031
Residual	0.00	0.00	0.172	0.0320	0.00	4	4	4	4	4	0.00	0.00	0.0430	0.0080	0.00
Total	53299.4	1.546E+05	1.561E+05	5600.5	1.92	17	17	17	17	17	3135.2	9096.0	9183.4	329.4	0.1129

Lack of fit tests

Source	Sum of squares					Df					Mean square				
Linear	1021.1	250.7	21.2	340.2	0.0288	9	9	9	9	9	113.4	27.8	2.36	37.8	0.0032
2FI	700.9	220.7	4.28	319.5	0.0108	6	6	6	6	6	116.8	36.7	0.713	53.2	0.0018

Quadratic	182.1	54.9	1.36	64.3	0.0094	3	3	3	3	3	60.7	18.3	0.452	21.4	0.0031
Cubic	0.00	0.00	0.00	0.00	0.00	0	0	0	0	0	-	-	-	-	-
Pure error	0.00	0.00	0.172	0.032	0.00	4	4	4	4	4	0.00	0.00	0.043	0.008	0.00

Model summary statistics

Source	Std. Dev.		R ²					Adjusted R ²							
Linear	8.86	4.39	1.28	5.12	0.047	0.51	0.51	0.87	0.15	0.16	0.39	0.40	0.84	-0.03	-0.03
2FI	8.37	4.70	0.66	5.65	0.032	0.66	0.57	0.97	0.21	0.68	0.46	0.32	0.95	-0.26	0.49
Quadratic	5.10	2.80	0.46	3.03	0.036	0.91	0.89	0.99	0.84	0.72	0.80	0.75	0.98	0.63	0.37
Cubic	0.00	0.00	0.20	0.08	0.00	1.00	1.00	0.99	0.99	1.00	1.00	1.00	0.99	0.99	1.00

Model summary statistics

Source	Predicted R ²		PRESS				Adjusted R ²								
Linear	0.13	0.10	0.75	-0.74	-0.73	1806.7	466.2	43.4	706.9	0.059	0.39	0.40	0.84	-0.03	-0.03

2FI	-0.06	-0.70	0.90	-3.00	-0.56	2226.4	890.0	16.8	1620.0	0.053	0.46	0.32	0.95	-0.26	0.49
Quadratic	-0.39	-0.68	0.87	-1.54	-3.37	2914.2	879.6	21.9	1029.2	0.150	0.80	0.75	0.98	0.63	0.37
Cubic	-	-	-	-	-						1.00	1.00	0.99	0.99	1.00

The results of ANOVA obtained indicated that the responses have been influenced significantly concerning the independent variables. The polynomial equation for different responses is presented from equation (23) to (27).

$$\text{Particle size, (R1)} = +2.58 * A - 5.36 * B + 9.94 * C - 1.73 * AB + 8.78 * AC + 2.500 * BC + 3.55 * A^2 + 7.32 * B^2 + 6.73 * C^2 \dots \text{Equation (23)}$$

$$\text{EE of VA, (R2)} = +5.78 * A + 0.6750 * B + 0.3750 * C + 1.27 * AB - 2.42 * AC + 0.0250 * BC - 5.24 * A^2 - 3.14 * B^2 + 0.9625 * C^2 \dots \text{Equation (24)}$$

$$\text{EE of Gly, (R3)} = +2.03 * A + 3.81 * B + 0.7125 * C - 1.60 * AB - 0.6500 * AC - 1.12 * BC + 0.6325 * A^2 - 0.0425 * B^2 + 0.5075 * C^2 \dots \text{Equation (25)}$$

$$\text{Zeta potential, (R4)} = +0.0750 * A + 2.61 * B + 1.11 * C + 0.8250 * AB - 0.2750 * AC + 2.10 * BC - 4.84 * A^2 + 6.28 * B^2 + 0.7800 * C^2 \dots \text{Equation (26)}$$

$$\text{PDI, (R5)} = +0.0071 * A + 0.0237 * B + 0.0091 * C + 0.0458 * AB - 0.0435 * AC + 0.0222 * BC \dots \text{Equation(27)}$$

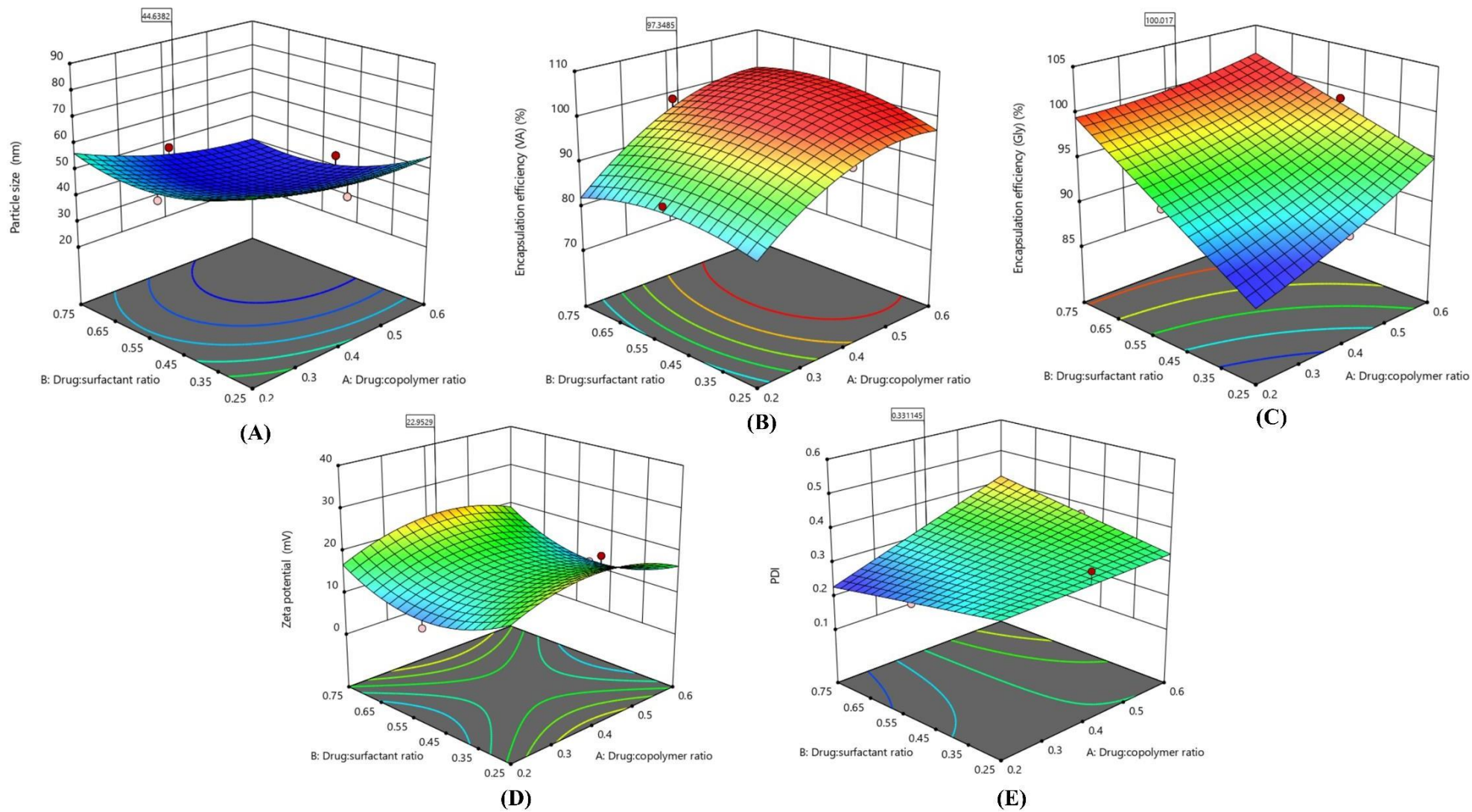
The positive sign in the obtained polynomial equations indicated the synergistic effect of factors on the responses. Whereas the negative sign specified the antagonistic effect of the factors on the responses. For particle size (R1), an increase in the value was observed with an increase in factor A, C, and with an increase in the combination of factors AC, BC, B² and C² and decrease in the value with an increase in factor B, and with an increase in the combination of factors AB. Similarly, EE of VA increased with an increase in factors A, B, C and with an increase in the combination of factors AB, BC, and C², and decreased with an increase in the combination of factors AC, A², and B². The EE of Gly increased with an increase in factors A, B, C, and with a combination of factors A², and C², and decreased with an increase in the combination of factors AB, AC, BC, and B². The zeta potential of APMs increased with an increase in factors A, B, C, and with an increase in the combination of factors AB, BC, B², and C², and decreased with an increase in the combination of factors AC and A².

Despite having an antagonistic or synergistic effect of factors on responses, the effect may not be so significant. To determine the significance of the effect of different factors on responses, a perturbation plot is used. This reveals the significant influence of the factors dominating a specific response. The perturbation plot graphs for all factors are shown in **Fig 5.11**. **Fig 5.11A** indicated that factor C was having more dominant effect than factors A and B on the particles size. Similarly, **Fig 5.11B** showed that the effect of factor A was more dominant than factor B and C. In **Fig 5.11C**, it was found that the effect of factor B was more dominant than factor A and C on EE of Gly. Similarly, in **Fig 5.11D** it was observed that the effect of factors B and

C was equally dominant than factor C on the zeta potential of APMs. Lastly, *Fig 5.11E* indicated that both factors B and C was equally dominant over that of factor C.

Further, these polynomial equations generated 3D response surface plots for a more detailed understanding of the design i.e., the effect of interaction of three different factors (A, B, C) onto the three different responses (R1, R2 and R3) as presented in *Fig 5.12 22, 5.13 23 and 5.14 24*. *Fig 5.12A* indicated that with an increase in factor A (drug to copolymer ratio) and B (drug to surfactant ratio), particle size (R1) decreases. The effect of factors A and C on R1 is presented in *Fig 5.13A*, indicating increase in particle size (R1) with an increase in factor A and factor C respectively. The effect of factor B and C on R1 is presented in *Fig 5.14A*, indicating decrease in particle size (R1) with an increase in factor B and increase in particle size (R1) with an increase in factor A respectively. *Fig. 5.12B* represents that with an increase in factor A (drug to copolymer ratio); an increase in EE of VA (R2) was observed. Whereas, with an increase in factor B (drug to surfactant ratio), a decrease in EE of VA (R2) was seen. The increase in EE of VA was observed with increase in factor A while decrease in EE of VA was seen with an increase in factor C respectively as presented in *Fig 5.13B*. Furthermore, decrease in EE of VA was observed with an increase in factor B and C up to a certain level followed by increase in EE of VA as presented in *Fig 5.14B*. *Fig. 5.12C* indicated an increase in EE of Gly (R3) with an increase in factor B (drug to surfactant ratio) while an increase in factor A (drug to copolymer ratio) decrease in EE of Gly (R3) was noted. An increase in EE of Gly (R3) was observed with an increase in factor A and C as presented in *Fig 5.13C*. The EE of Gly (R3) was increased at a greater extent with an increase in factor B than factor C as presented in *Fig 5.14C*. *Fig 5.12D* presents an increase in zeta potential (R4) with the increase in factor B (drug to surfactant ratio) while an increase in factor A (drug to copolymer ratio) decrease in zeta potential (R4) was observed. Increase in zeta potential (R4) was observed with an increase in factor A and C up to a certain level as presented in *Fig 5.13D*. Similarly, an increase in factor B and C indicated increase in zeta potential (R4) as presented in *Fig 5.14D*. Lastly, *Fig 5.12E* indicated a decrease in PDI (R5) with the increase in factor B (a drug to surfactant ratio) whereas an increase in factor A (drug to copolymer ratio) increase in PDI (R5) of APMs was seen. Increase in PDI (R5) was observed with an increase in factor A and C as presented in *Fig 5.13E*. Further, decrease in PDI (R6) was seen with increase in factor C while increase in R6 was observed with an increase in factor B as shown in *Fig 5.14E*.

This signifies that both factors A and B have an antagonistic effect on the particle size (R1) as its value was decreased. An increase in the ratio of drug to copolymer and surfactant formed small APMs, which could be due to increased hydrophobicity of the micellar core that was able to form compact APMs. This resulted in a decrease in the particle size of drug co-loaded APMs with the increase in factor A and B. Factor A have a synergistic effect on EE of VA (R2) that could be because of the availability of the more amphiphilic molecules that led to the formation of APMs with higher EE. However, factor A shows an antagonistic effect on EE of Gly (R3) that could be because of the presence of CTAB, which provide more compatible hydrophobicity to entrap Gly. As a result, factor B showed a synergistic effect on the EE of Gly. Factor B have a synergistic effect on zeta potential (R4) because of the cationic surfactant CTAB which provide a more steric hindrance between the particles. In agreement with this, factor B have an antagonistic effect on the PDI (R5) as the incorporation of CTAB provided improved homogeneity in the micellar system.



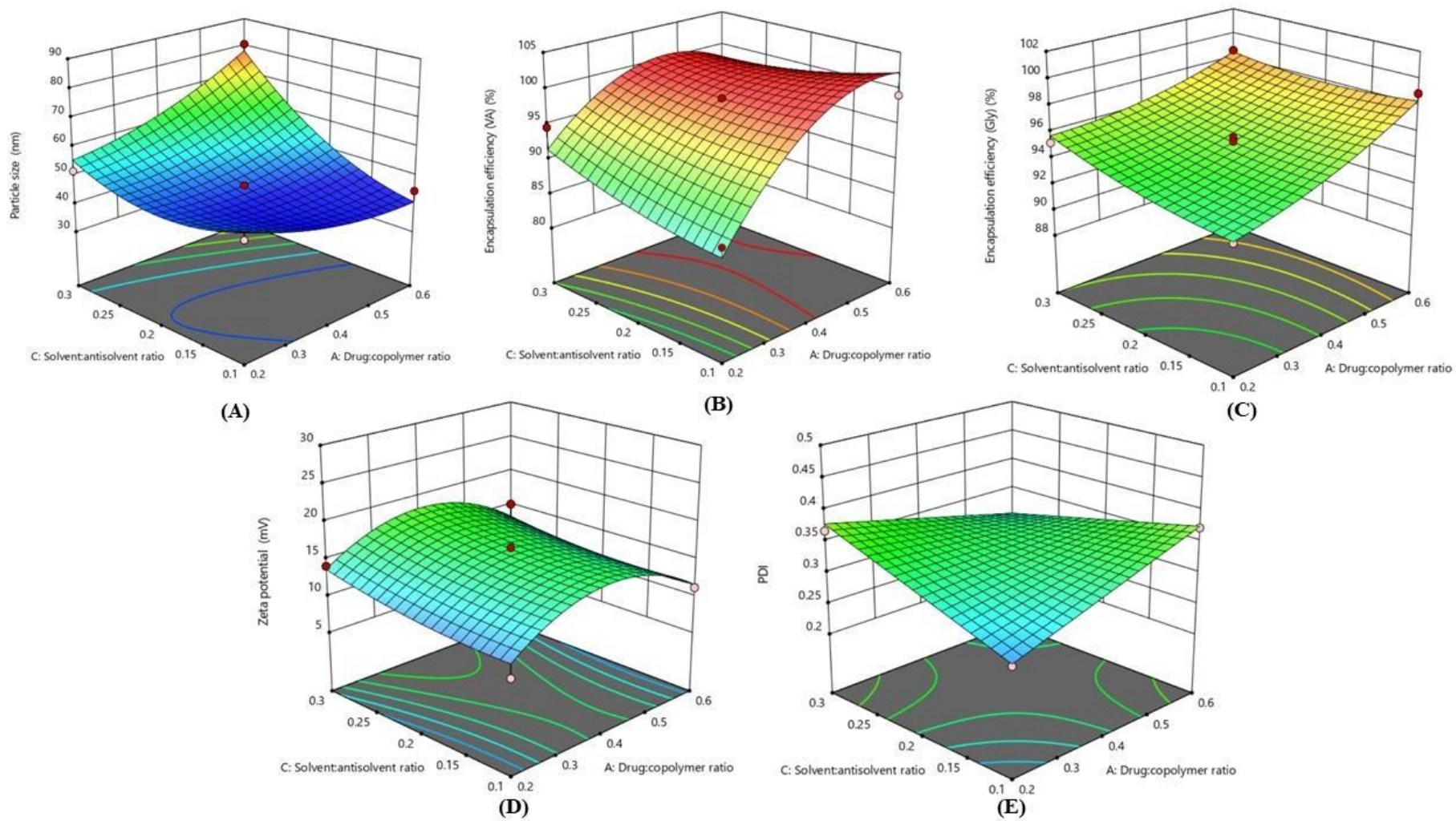
1

2

Fig 5.12: 3D-response surface plots for effect of factor A and B on A) particle size; B) EE of VA(%); C) EE of Gly (%); D) Zeta potential; E) PDI

3

4



5

6

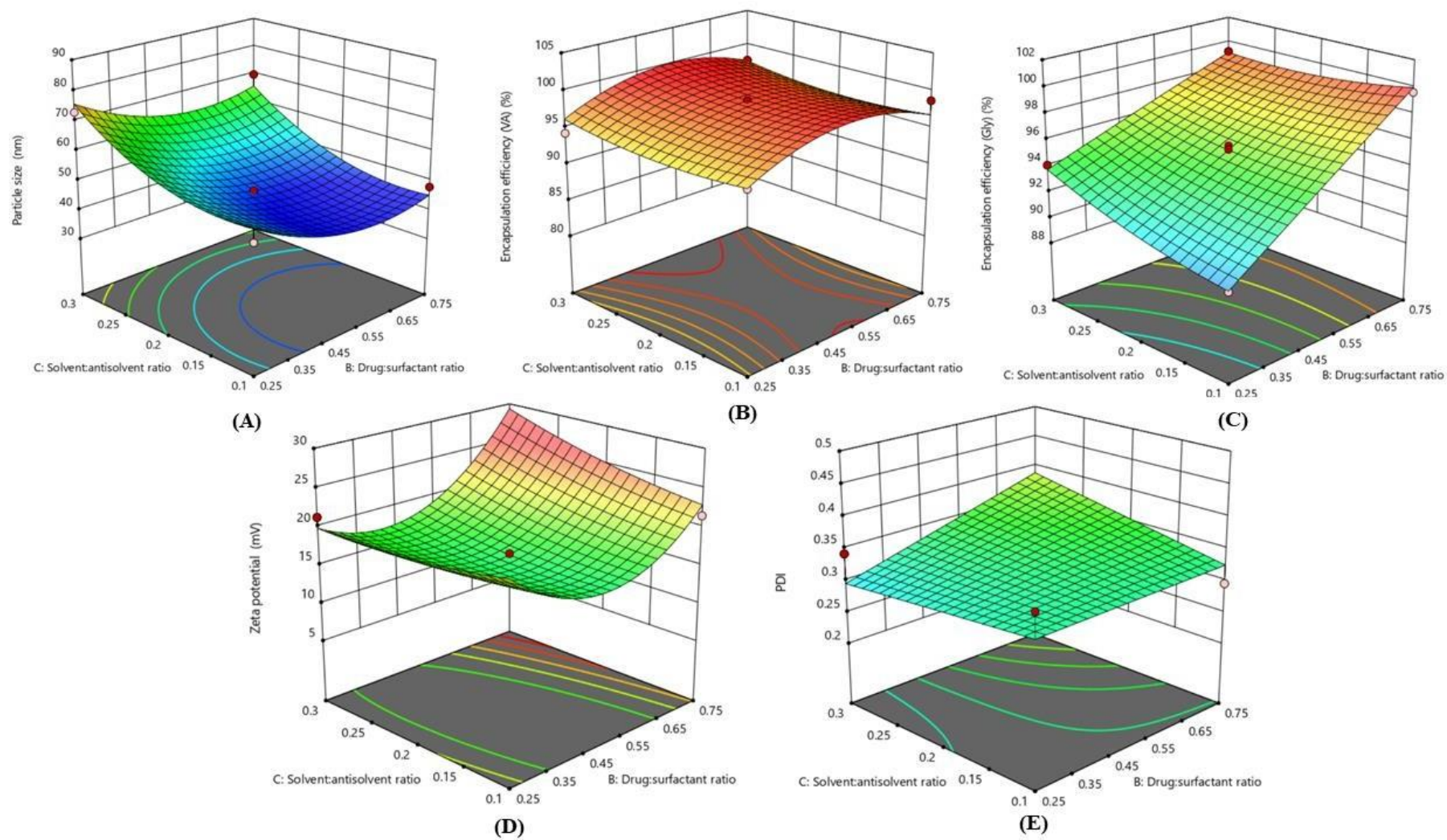
7

Fig 5.13: 3D-response surface plots for effect of factor A and C on A) particle size; B) EE of VA(%); C) EE of Gly (%); D) Zeta potential; E) PDI

8

9

10



11

12

13

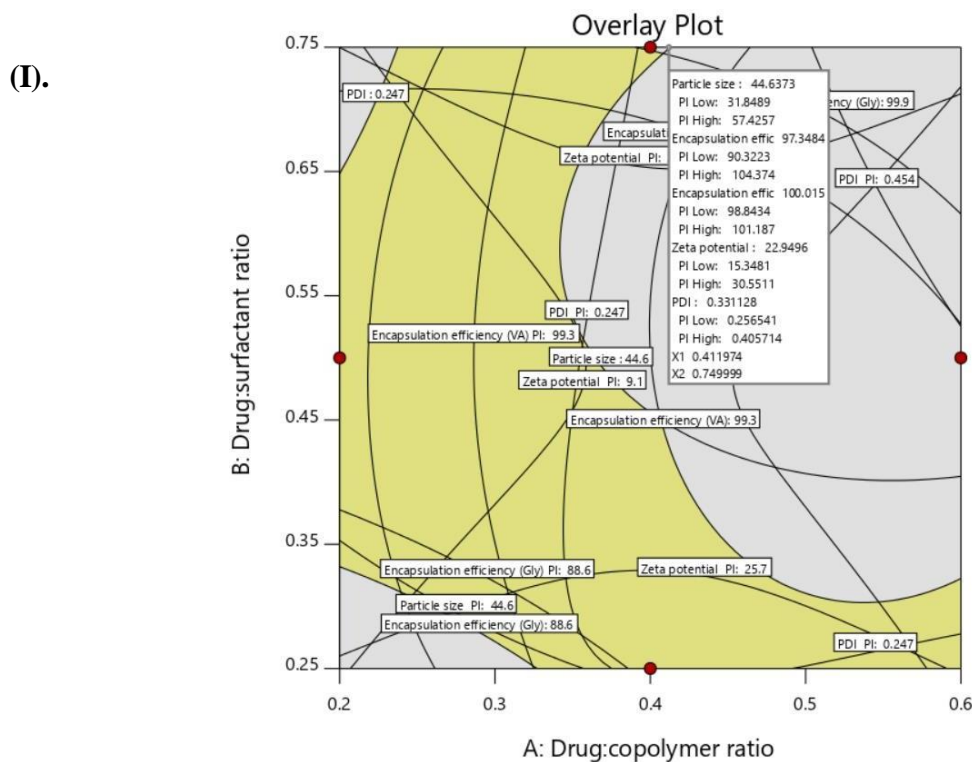
14

15

Fig 5.14: 3D-response surface plots for effect of factor B and C on A) particle size; B) EE of VA(%); C) EE of Gly (%); D) Zeta potential; E) PDI

5.8.8 Graphical optimization

To find out the levels of factors A to C, graphical optimization of the formulation was carried out which showed particle size (R1) in the range of 31.8-57.4 nm, EE of VA (R2) in the range of 90.3-100.0, EE of Gly (R4) in the range of 98.8-100.0, zeta potential (R5) in the range of 15.3-30.5, and PDI (R6) in the range of 0.256-0.405 respectively. The predicted values obtained through BBD for the three factors were 0.40 (A), 0.75 (B) and 0.1 (C) (**Fig 5.15**). These predicted values of factors were used to develop the optimized batch of the co-loaded APMs. Hence, the final formula composition as per BBD for 100 mL of GV-APMs was 12.5 mg of Gly, 180 mg of VA, 481.2 mg of copolymer, 256.6 mg of CTAB and water quantity sufficient to 100 mL. This implied that for 1mL of formulation that was to be administered to rats orally contained 0.5 mg/kg of Gly, 7.5 mg/kg of VA, 19.2 mg/kg of copolymer, and 10.2 mg/kg of CTAB once daily. The ratio of Gly and VA in the APMs was 0.07. It is pertinent to add that the amount of CTAB used in the APMs (1mL) was about 10 mg/kg daily, which comes under the safety limits of CTAB concentration (i.e., 20 mg/kg) [360]. The experimental value of particle size was 46.82 nm, EE of VA was 93.4%, EE of Gly was 97.9%, the zeta potential was 12.5 mV, and PDI was 0.281. All these values were found to lie within the predicted values (i.e., R1=44.6 nm, R2=97.3%, R3=100%, R4=22.9 mV, R5=0.331). This specified the reproducibility of the optimization method.



(II).

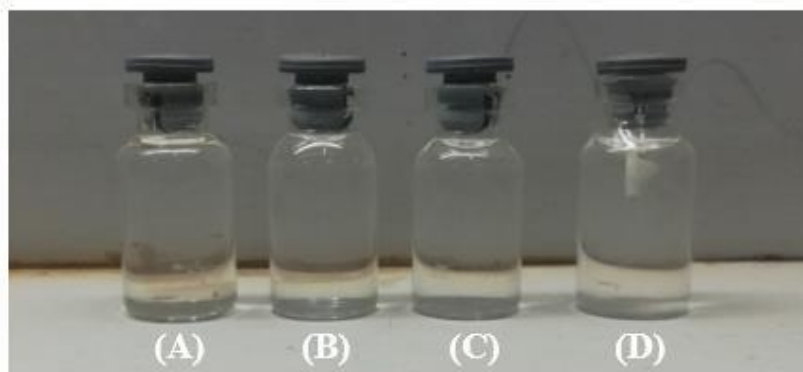


Fig 5.15: (I). The overlay plot representing optimized composition for GV-APMs, (II). (A) Blank APMs; (B) VA-APMs; (C) Gly-APMs; (D) GV-APMs

5.9 Characterization of optimized GV-APMs

5.9.1 FTIR

The FTIR spectra of raw Gly, raw VA, CTAB, mPEG-b-PCL and GV-APMs is presented in **Fig 5.16**. The FTIR spectrum of raw Gly reveal the presence of C=O group at 1712.8 cm^{-1} of frequency, S=O group at 1340.5 cm^{-1} , amide group at 3331 cm^{-1} and C=C-H stretching at 1614.4 cm^{-1} . Whereas FTIR spectrum of raw VA showed the presence of C=O at a frequency of 1672.3 cm^{-1} , O-C-O group at 1024.2 cm^{-1} and O-H functionality at 3477.7 cm^{-1} . The FTIR spectrum of CTAB exhibited C-H stretching at 1478.4 cm^{-1} of frequency, symmetric and asymmetric CH_2 stretching vibrations at a frequency of 2848 and 2918 cm^{-1} . The mPEG-b-PCL spectrum showed the alkyl C-H stretch at 2868.2 cm^{-1} , and 2939.6 cm^{-1} along with C=O functionality at 1724.4 cm^{-1} . In agreement with the data obtained above, GV-APMs spectrum shows the presence of raw Gly and VA characteristic peaks, which express the proper loading of both the drugs in the APMs. The remarkable trait of the FTIR spectra of APMs was the blue shift of the C=O vibration, from 1724.4 to 1644.1 cm^{-1} for GV-APMs in comparison to the mPEG-b-PCL spectrum. The shift in the co-loaded APMs indicated the existence of some form(s) of interaction between raw drugs and the C=O functional group of the copolymer.

5.9.2 DSC

The DSC thermograms corresponding to raw Gly, raw VA, CTAB, mPEG-b-PCL copolymer and GV-APMs exhibiting a sharp endothermic peak at $169\text{ }^\circ\text{C}$, $218\text{ }^\circ\text{C}$, $100\text{ }^\circ\text{C}$ and $55\text{ }^\circ\text{C}$ is presented in **Fig 5.17**. As it is clear, there was no peak visible near the melting point of raw drugs (Gly and VA) for co-loaded APMs thermogram, which can be indicative of successful loading of both drugs in APMs. The developed GV-APMs showed two endothermic peaks at 46.2°C and 96.1°C representing the melting of mPEG-b-PCL and

CTAB co-relation in the form of APMs. This endothermic peak of APMs probably confirmed the physical interaction between mPEG-b-PCL-CTAB systems upon entrapping both the drugs in APMs, since the melting point of GV-APMs was lower than the melting point of both mPEG-b-PCL (55°C) and CTAB (100 °C).

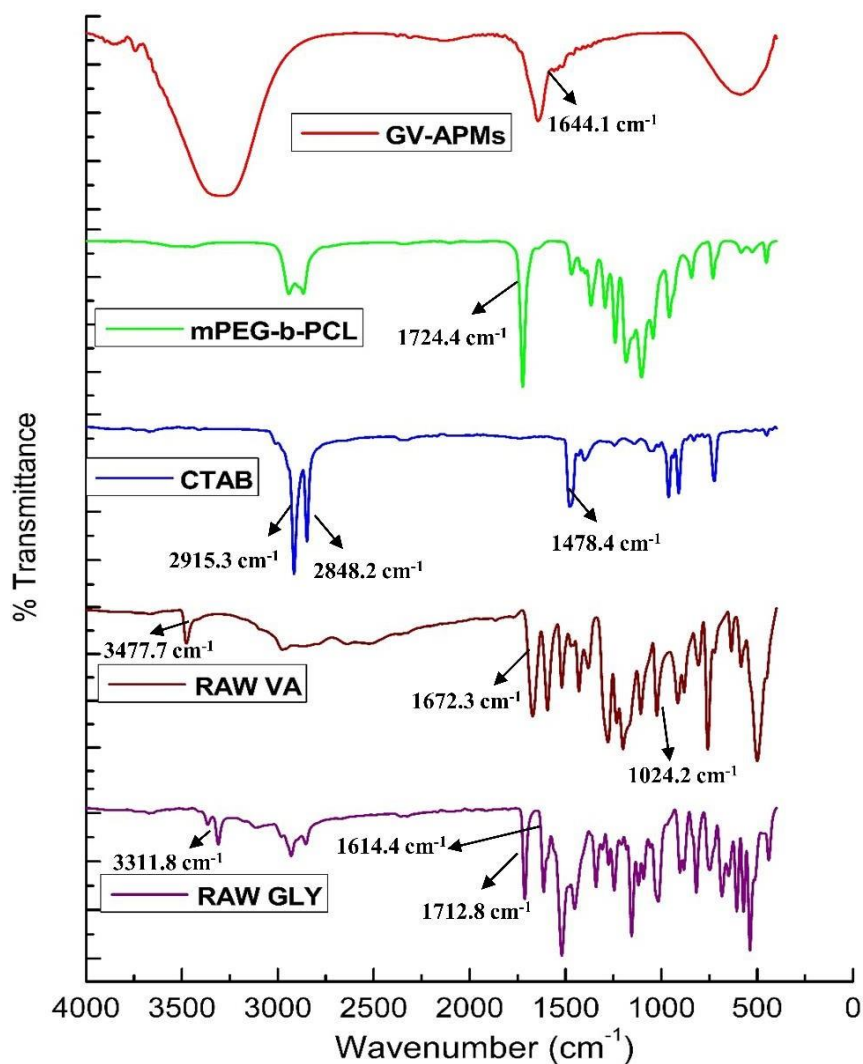


Fig 5.16: (A) FTIR spectra and (B) DSC thermogram of raw Gly, raw VA, CTAB, mPEG-b-PCL, GV-APMs

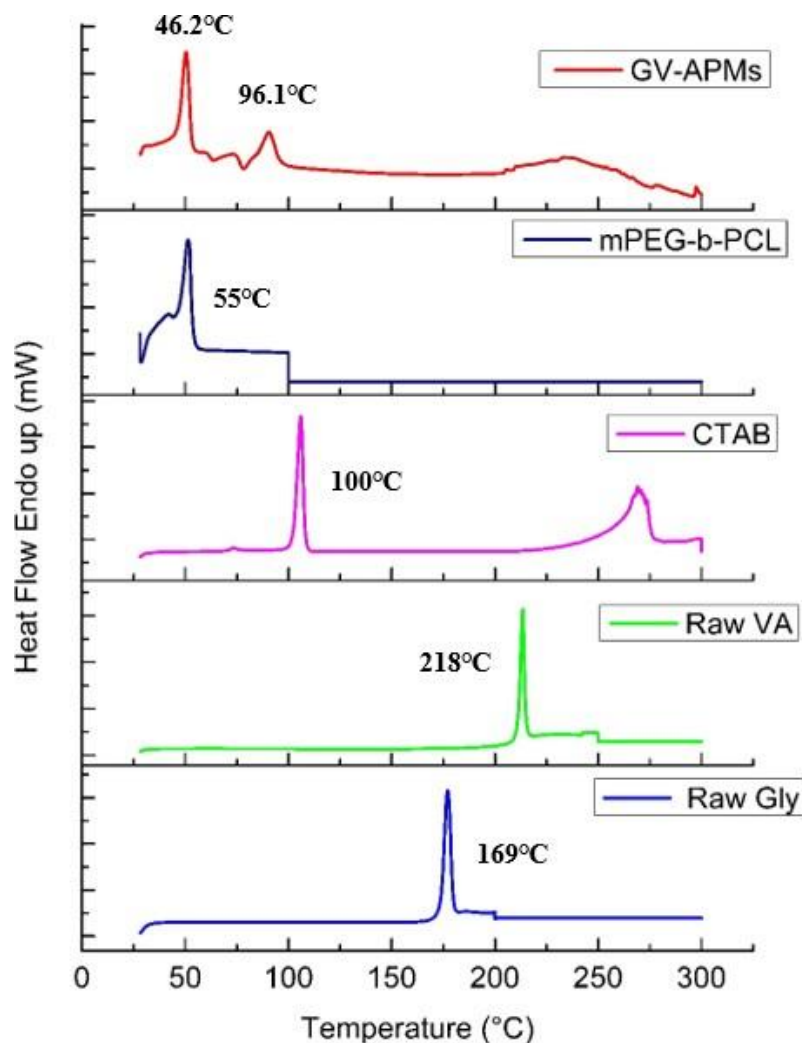


Fig 5.17: DSC thermogram of raw Gly, raw VA, CTAB, mPEG-b-PCL, GV-APMs

5.9.3 SEM analysis

The SEM images of raw drugs (VA and Gly), CTAB, and GV-APMs is presented in *Fig 5.18*. *Fig 5.18A* presents flat and long crystals of VA with sharp edges and filiform habit. Raw Gly appeared as a rectangular smooth blade-like crystal as presented in *Fig 5.18B*. The synthesized mPEG-b-PCL copolymer appeared waxy with an irregular shape as presented in *Fig 5.18C*. Similar to the shape of VA, CTAB appeared as a long cylindrical structure with needle shape ends as presented in *Fig 5.18D*. GV-APMs present a semi-crystalline structure with waxy and irregular edges with spherical morphology as shown in *Fig 5.18E*.

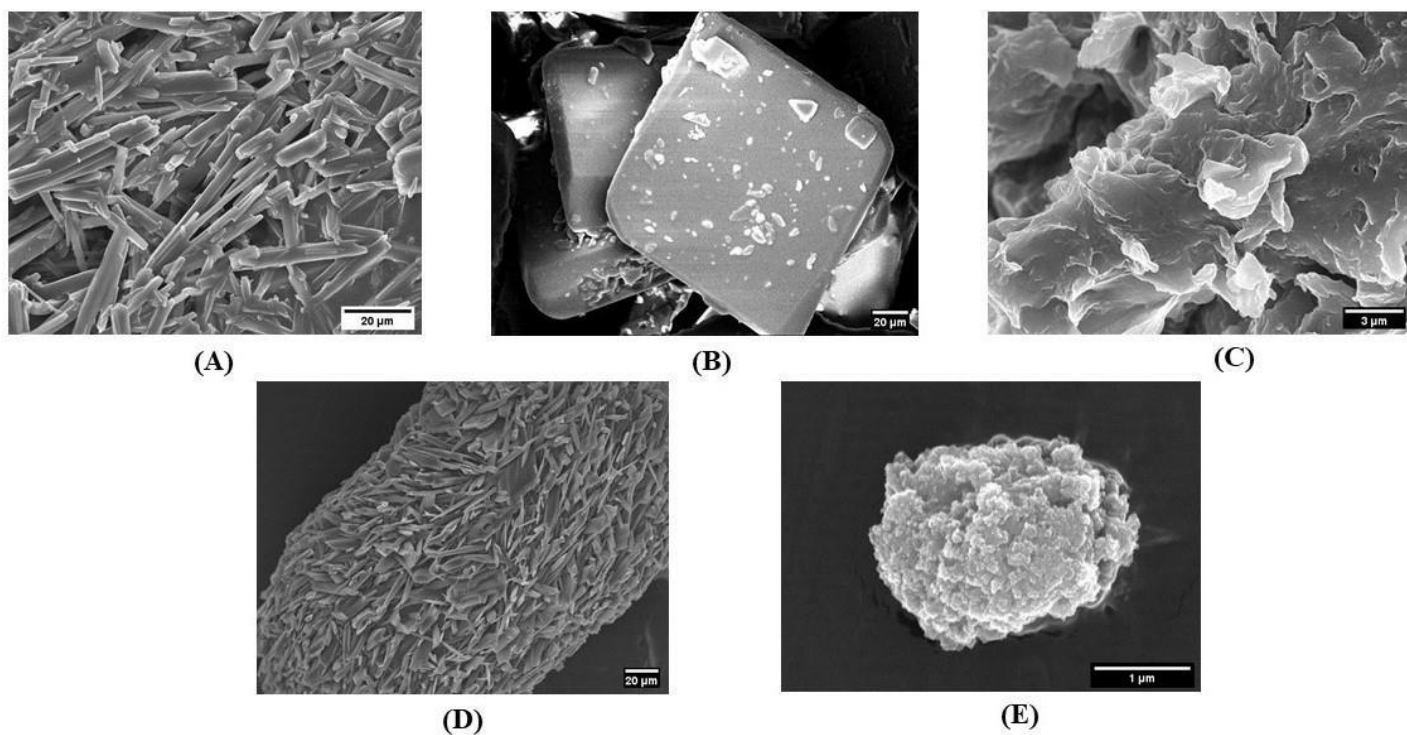


Fig 5.18: SEM images of A) VA; B) Gly; C) mPEG-b-PCL; D) CTAB; E) GV-APMs

5.9.4 Particle size and zeta potential

The optimized GV-APMs revealed a unimodal size distribution with an average particle size of 46.82 ± 2.1 nm and an average zeta potential of 12.5 ± 3.1 mV. The polydispersity index (PDI) of GV-APMs was 0.281 ± 0.2 . The results of the particle size and zeta potential are presented in **Fig 5.19A** and **B**. All the values were found near the range predicted by DoE software.

5.9.5 HR-TEM analysis

The TEM image of optimized GV-APMs is presented in **Fig 5.19C**. It demonstrates that the GV-APMs are spherical with a smooth surface and having an average particle size of 34.3 nm. TEM analysis revealed less particle size in comparison to the DLS particle size analysis [361]. DLS measure the hydrodynamic particle size; however, the loss of water during TEM analysis can be credited for a decrease in the particle diameter [362].

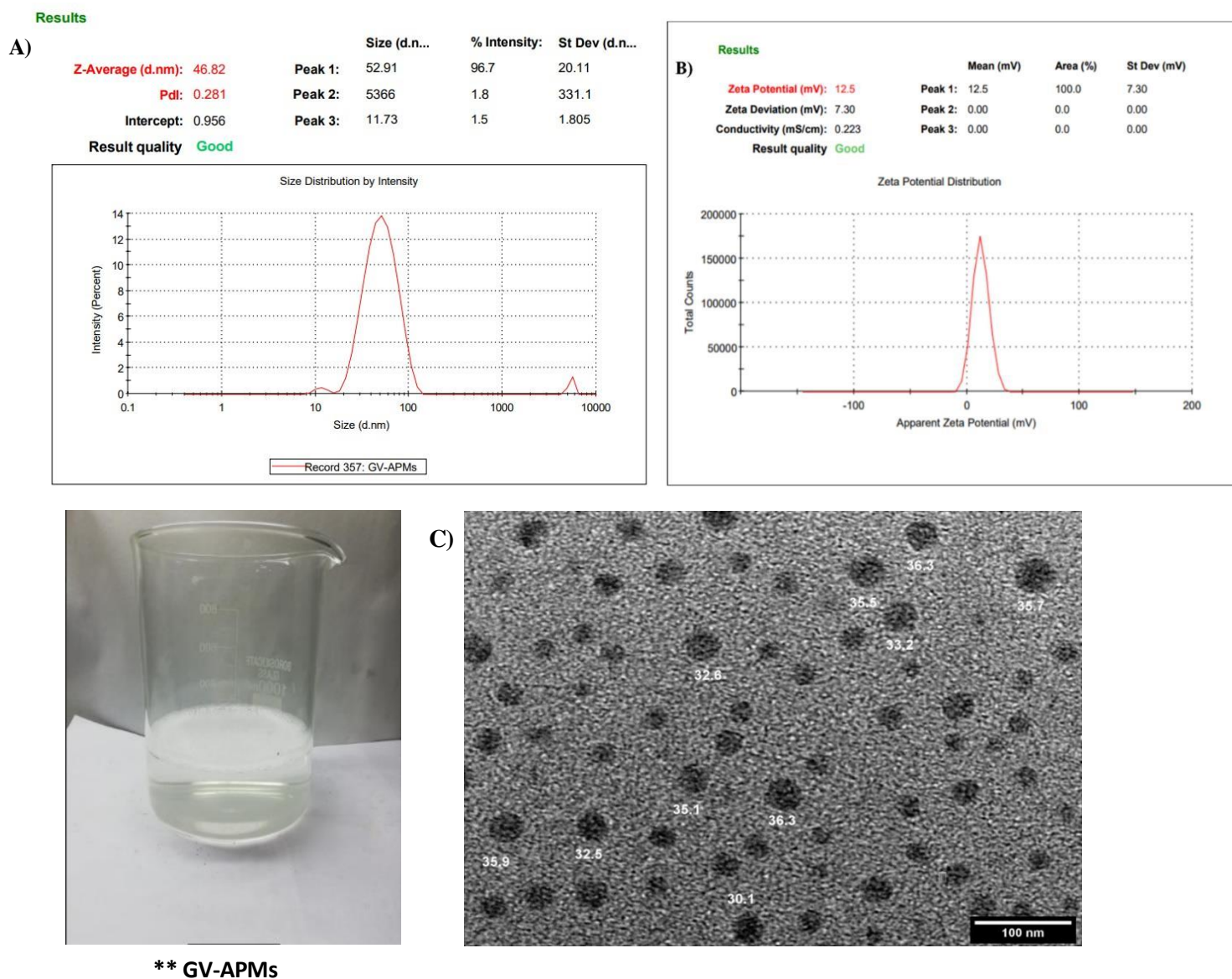


Fig 5.19: GV-APMs (A) Average particle size (B) Zeta potential (C) TEM

****Appearance of optimized GV-APMs**

5.9.6 EE and DL of GV-APMs

The EE% and DL% of Gly and VA in the optimized co-loaded APMs (GV-APMs) were calculated using *equations (9) and (10)* as per the previously published method [347]. For this, the concentration of both the drugs untrapped in the formulation was determined using HPLC with the developed analytical method for the simultaneous estimation of both the drugs. The mean AUC for Gly and VA was found to be 249433 and 1624862 cm^{-1} and their concentration in the supernatant was obtained using calibration equation of the developed analytical method. The EE% and DL% of Gly were found to be $97.9 \pm 0.24\%$ and $1.62 \pm 0.32\%$ whereas, for VA it was found to be $93.4 \pm 0.15\%$ and $19.3 \pm 0.20\%$ respectively.

5.9.7 In vitro drug release kinetic modelling studies

To study the impact of the various release media on the release profile of both the drugs from co-loaded APMs, the release study was carried out in PB solutions of varying pH. The DD% of both the drugs co-loaded in APMs at pH 1.2, 6.8 and 7.4 was calculated using *equation (11)* (**Fig 5.20**). As shown in **Fig 5.20A** the release of Gly loaded in APMs was found to be pH-dependent with enhanced DD% compared to the raw Gly and its physical mixture with VA. The release of Gly from APMs was found to be 16.2% in pH 1.2 over 2h, 28.5% in pH 6.8 over 4h and 89.5% in pH 7.4 over 48h in a controlled manner. This controlled-release pattern of Gly can be attributed to the entrapment of Gly in the core of the APMs. Similarly, a pH-dependent release pattern was observed in the case of raw Gly owing to its pH-dependent solubility (weak acid) but the DD% was extremely poor due to its poor oral bioavailability. However, in the physical mixture, the DD% of Gly was observed to be increased by 1.2-folds ($P < 0.01$) than raw Gly. This could be due to the ability of the hydroxyl group of the VA to form hydrogen bonds, which ultimately increased the water solubility of the hydrophobic drug Gly. With this agreement, the DD% of Gly from co-loaded APMs was found to be higher i.e., 20.9% in pH

1.2 over 2h, 32.4% in pH 6.8 over 4h and 94.5% in pH 7.4 over 48h than that of Gly-APMs. Overall the %DD of Gly in GV-APMs was enhanced by 1.9-folds ($p < 0.001$) and 1.6-folds ($p < 0.001$) than that of raw Gly and Gly in physical mixture respectively.

However, the release of VA from APMs was found to be 62.5% in pH 1.2 for 2h, 86.5% in pH 6.8 for 4h and 100% in pH 7.4 over 8h respectively. Similar to Gly, it displayed pH-dependent solubility. The developed APMs successfully sustained the VA release more than that of raw VA however; the sustainability offered by the micellar core was less than Gly. This could be due to the amphiphilic nature of the VA that resulted in weaker hydrophobic interaction with the PCL core. In the physical mixture, the release of VA was observed to be delayed i.e., by 1.2-folds ($p < 0.01$) than raw VA which could be due to the hydrophobic influence of the drug Gly as presented in **Fig 5.20B**. In co-loaded APMs, the DD% of VA was found to be 33.8% in pH 1.2 for 2h, 57% in pH 6.8 for 4h and 100% in

pH 7.4 for 16h respectively. The co-loaded APMs sustained the release of VA by 1.8-folds ($p < 0.01$) in pH 1.2, 1.5-folds ($p < 0.001$) in pH 6.8, and 1.2-folds ($p < 0.001$) in pH 7.4 than VA-APMs respectively. Therefore, the developed APMs can be regarded as highly attractive nanocarriers for both time-controlled drug deliveries for the drugs with poor bioavailability to achieve different therapeutic objectives. The various dissolution model fitting parameters computed are summarized in **Table 5.10 (A and B)**.

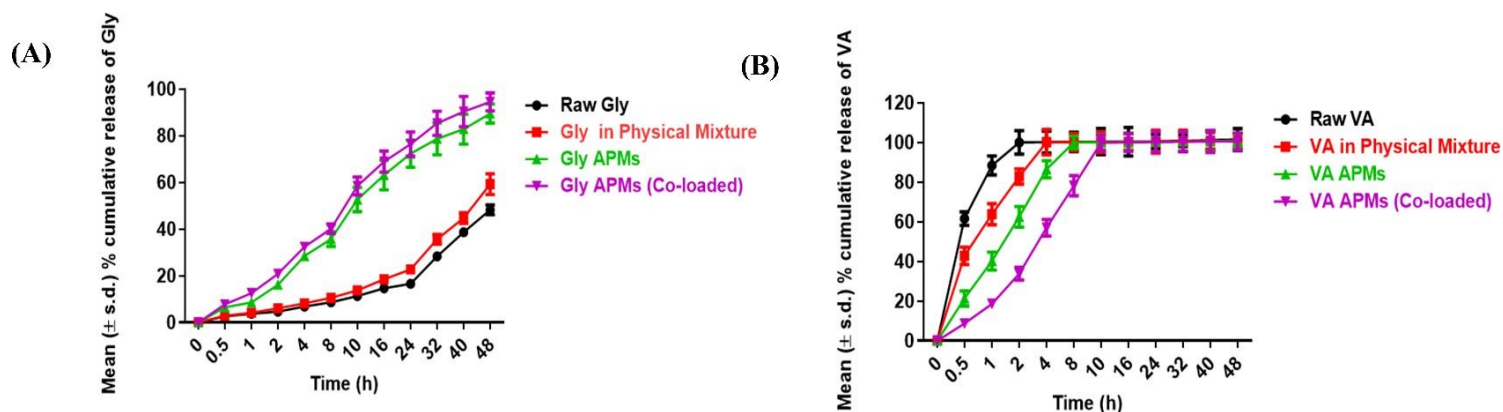


Fig 5.20: Release profiles of Gly and VA from co-loaded GV-APMs in different release media (A) Gly release in pH 1.2 over 2h, pH 6.8 over 4h and pH 7.4 for 48h; (B) VA release in pH 1.2 over 2h, pH 6.8 over 4h and pH 7.4 for 48h

Table 5.10A: Drug release kinetic model fitting in various dissolution models

Drug release model	Raw Gly		Raw VA		Gly-APMs		VA-APMs	
	R	AIC	R	AIC	R	AIC	R	AIC
Zero-order	0.983	55.4	0.795	32.7	0.847	99.1	0.774	49.9
First-order	0.974	60.2	0.999	11.0	0.986	70.6	0.999	12.3
Higuchi	0.922	73.4	0.978	24.1	0.987	69.8	0.981	35.6
HC	0.978	58.5	0.999	6.5	0.969	80.7	0.997	24.4
BL	0.911	74.9	0.996	16.6	0.987	70.0	0.982	35.4
KP	0.983	57.3	0.994	20.5	0.988	71.3	0.995	30.4

Table 5.10B: Drug release kinetic model fitting in various dissolution models

Drug release model	Physical mix Gly		Physical mix VA		GV-APMs (Gly)		GV-APMs (VA)	
	R	AIC	R	AIC	R	AIC	R	AIC
Zero-order	0.983	55.4	0.727	41.7	0.816	102.4	0.884	64.4
First-order	0.978	63.0	0.998	43.6	0.988	70.5	0.995	62.9
Higuchi	0.931	76.6	0.981	28.9	0.986	72.1	0.862	103.3
HC	0.982	60.6	0.990	25.8	0.974	79.8	0.927	96.1
BL	0.918	78.6	0.997	19.4	0.990	67.9	0.961	56.0
KP	0.987	58.2	0.996	23.0	0.989	71.2	0.980	52.7

The dissolution efficiency (DE) of Gly in the physical mix with VA and in GV-APMs was increased by 1.2- and 3.1-folds than the raw Gly respectively. Whereas, DE of VA in GV-APMs was retarded by 1.0-folds along with more sustained release profile, and indicated potential in enhancing its residence time in the body. The developed formulation indicated significance in overcoming the challenges associated with VA i.e., rapid dissolution. Similar, profile of VA in terms of DE was observed in physical mix with Gly.

According to the release kinetic fitting models, both the individual drug loaded APMs (Gly APMs/VA-APMs) followed zero-order kinetic model as a measure of highest AIC value obtained. Therefore, this indicated that the release of both the drugs loaded in APMs was found independent of their concentration. Similar to the release kinetics in Gly-APMs, the release of Gly loaded in GV-APMs followed zero-order kinetics whereas, the release of VA from GV-APMs followed Higuchi model.

5.9.8 *In vitro* Caco-2 toxicity study

The results revealed that the raw Gly and VA were nontoxic to the cells in contrast to the drugs loaded in APMs. The higher concentration of raw Gly (62.5 µg/mL) exhibited highest cell inhibition of 15%, which indicated more than 80% of the cell viability. Whereas raw VA (62.5 µg/mL) exhibited highest cell inhibition of 7.8% at its highest concentration which revealed more than 90% of the cell viability, which was calculated using *equation (12)*. In the case of APMs, concentration-dependent toxicity was observed on cells. Both the Gly and VA loaded individual APMs at the highest concentration (62.5 µg/mL) displayed 70% of the cell viability. Similarly, in the case of co-loaded APMs, the cell viability (%) was observed to be 70%. The highest cell viability (%) of more than 90% was observed at the lowest concentration of the developed APMs (0.9 µg/mL). According to the International Organization for Standardization (ISO 10993-5), 70% is commonly accepted as the threshold for cell viability [363]. The cytotoxicity profile of

the blank APMs at all the concentrations that correspond to drug-loaded APMs showed no potential cytotoxicity to the cells; the cell viabilities were up to 70%. The IC₅₀ value of the raw drugs and their value upon loading in APMs was obtained using Graph pad prism 2.0 software. The IC₅₀ value of the raw Gly was found to be 1.42 µg/mL while upon loading in APMs it was found to be 1.10 µg/mL. In the case of VA, the IC₅₀ value was found to be 1.17 µg/mL and 1.03 µg/mL upon its loading in APMs. However, in co-loaded APMs the IC₅₀ value was found to be 0.96 µg/mL. This indicated that both the drugs are effective at the lowest concentrations in APMs and will exhibit lower systemic toxicity upon oral administration. The results of the cytotoxicity study are presented in **Fig 5.21A**.

5.9.9 Passive glucose uptake study

The HepG2 cells showed a time-dependent increase in the glucose uptake profile i.e., 25% at 6h, 45% at 12h and 100% at 24 h respectively as shown in **Fig 5.21B**. This indicated normal physiological functioning of the cultured HepG2 cells in response to higher exposure of glucose in the medium or kinetics of glucose absorption.

5.9.10 Insulin-resistant HepG2 cell model

IR is one of the factors responsible for metabolic diseases such as hyperglycaemia, hyperinsulinemia and hypertriglyceridemia, which are common features of T2DM. This condition primarily affects hepatic cells in which glycogen synthesis becomes altered. As a result, excessive hepatic glucose production occurs [348]. Such event contributes to hyperglycaemia. To establish an *in vitro* insulin-resistant model of hepatic cells and to determine the influence of different insulin concentrations on glucose metabolism in the cell model, HepG2 cells were incubated with insulin (0.005 µM -50 µM) to build an insulin-resistant cell model. Analysis of the data showed no significant increase (p<0.01) in the glucose uptake compared to starved cells growing in MEM with 1% FBS at all the time points, confirming that the HepG2 cells are resistant to insulin. As presented in **Fig 5.21C**, the most significant decrease in the glucose uptake by HepG2 cells was observed with 500nM of insulin after incubation for 6h.

5.9.11 Selection of non-cytotoxic concentration

To determine the cytotoxic effect of the different treatments on HepG2 cells, percentage growth inhibition was measured by comparing the optical density value of treated cells with that of control untreated cells by using the **equation (13)**. Results of HepG2 cytotoxicity data showed a dose-dependent growth inhibition with raw Gly, raw VA, their physical mix, Gly-APMs, VA-APMs, and GV-APMs. Amongst the various treatments, raw VA was found to be the safest drug on HepG2 cells. The results are presented in **Fig 5.21D**. Based on this study, the concentration

with minimal cytotoxicity (<30% cell growth inhibition compared to control cells treated with vehicle) was selected for further glucose uptake study in insulin-resistant cells.

5.9.12 Glucose uptake study in insulin-resistant HepG2 cells

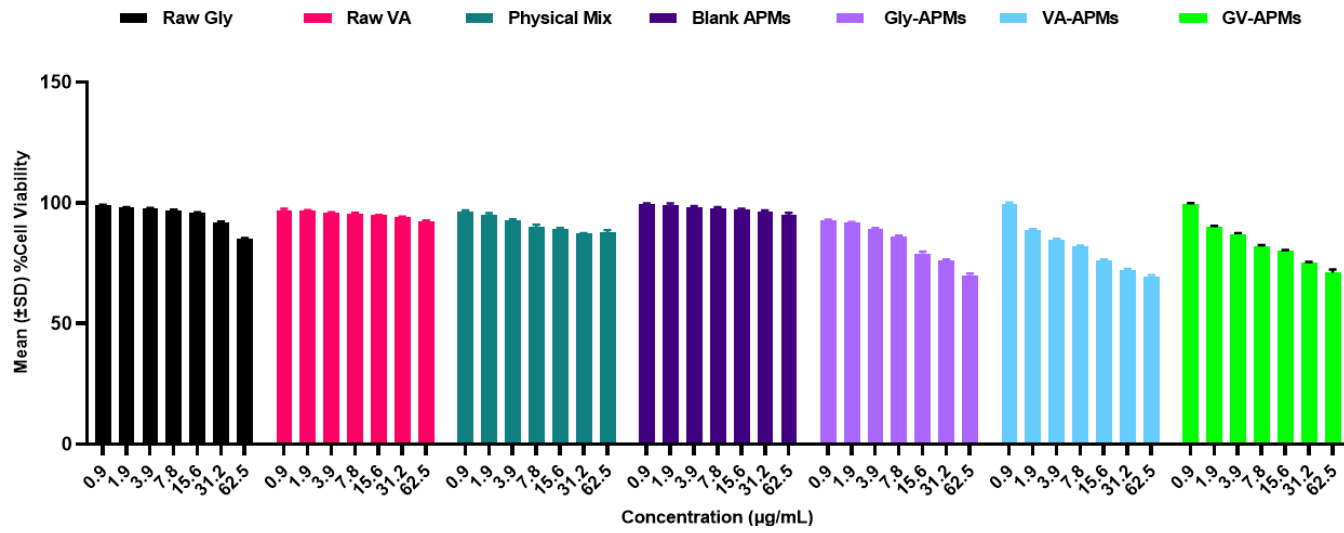
Based on the aforementioned study, the least cytotoxic concentration range for each treatment was selected i.e., from 0.9 to 31.2 µg/mL for all the test compounds. The sampling was done at 6h and 24h to measure changes in the glucose concentration using *equation (14)* when the passive uptake is minimal and maximal. The results revealed a significant difference ($p < 0.001$) in the reduction of glucose concentration (%) by the exposed treatments in a dose-dependent manner upon incubation for 6h than that of 24h respectively using paired student t-test. The highest glucose-lowering effect by the treatments was observed at 31.2 µg/mL. However, the developed APMs showed improvement in glucose consumption at 24h as well in comparison to the raw drugs and their physical mix.

Analysis of the data at 6h revealed 1.7-folds ($p < 0.05$) and 2.0-folds higher glucose reduction by the physical mix than that of raw drugs at an equivalent concentration of 31.2 µg/mL respectively. The loading of Gly in Gly-APMs increased the glucose lowering action by 1.8-folds ($p < 0.05$) than that of raw Gly while VA-APMs increased the glucose lowering action by 1.9-folds ($p < 0.05$) than that of its raw form respectively at the highest concentration. The co-loading of both the drugs in optimized GV-APMs resulted in 3.3-folds ($p < 0.01$) and 4.0-folds ($p < 0.05$) higher glucose lowering action than the raw Gly and raw VA respectively (**Fig 5.21E**). In addition to this, GV-APMs increased the glucose consumption by 1.9-folds ($p < 0.05$) than that of physical mix respectively.

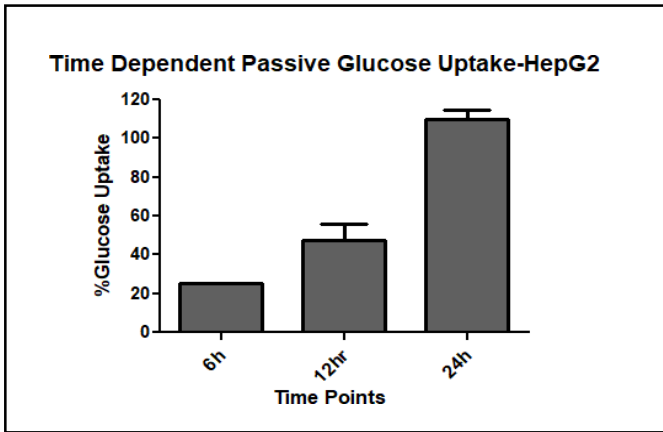
Further, the similar results were obtained with all the treatment at 24h as presented in **Fig 5.21F**. The exposure of physical mixture at the highest concentration resulted in 1.2-folds ($p < 0.05$) and 1.4-folds ($p < 0.05$) higher glucose consumption by the insulin-resistant HepG2 cells than that of the raw Gly and raw VA respectively upon incubation after 24h. Furthermore, the developed optimized GV-APMs exhibited 2.0-folds ($p < 0.05$) higher glucose lowering action than that of its physical mix.

The interaction between the natural product VA with the marketed drug Gly was determined by calculating the CI using *equation (15)*. The CI for Gly with VA in GV-APMs at a concentration of 31.2 µg/mL was found equal to 1, indicating additive interaction between both the drugs.

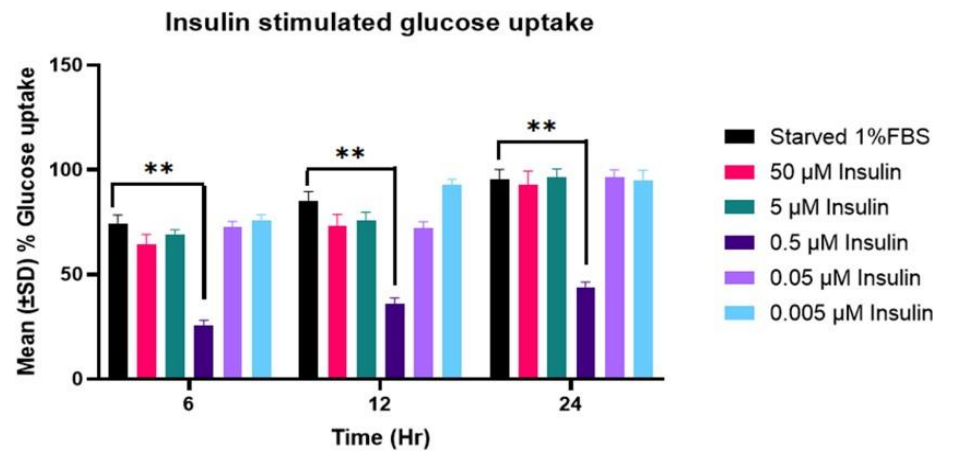
(A.)



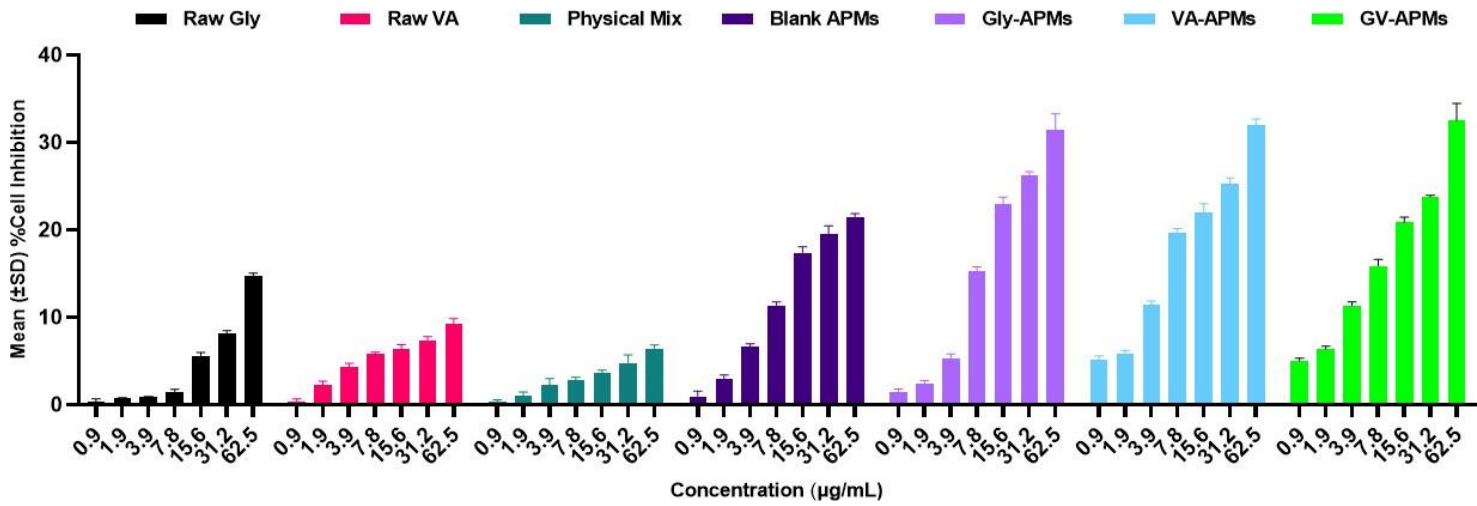
(B.)



(C.)



(D.)



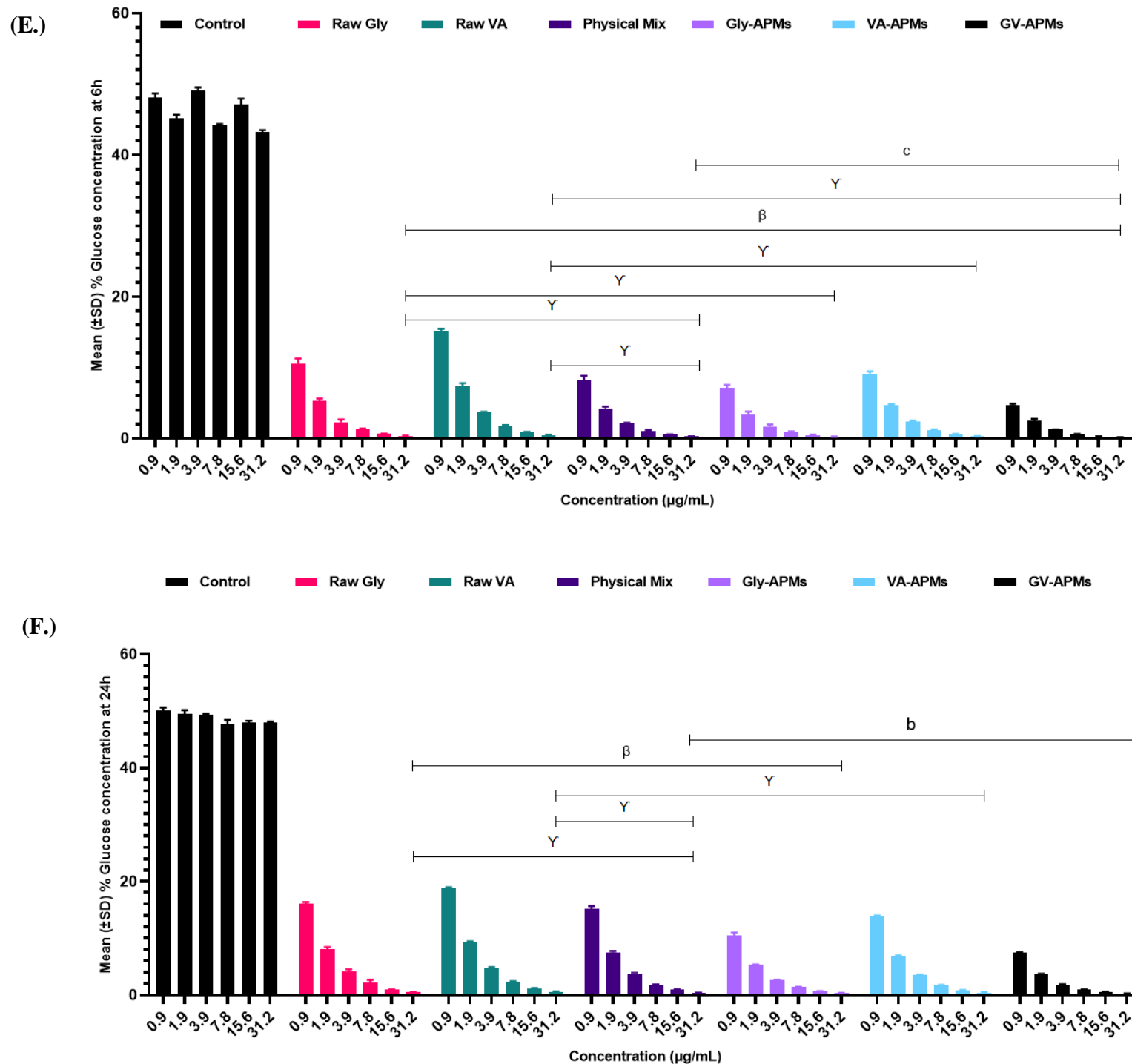


Fig 5.21: (A) Cell line cytotoxicity study of raw drugs (Gly and VA), Gly-APMs, VA-APMs, GV-APMs; (B) Time-dependent increase in the passive glucose uptake profile by HepG2 cells; (C) Insulin-stimulated glucose uptake in HepG2 cell line. Data are expressed as mean \pm SEM, $n=3$, level of significance was considered as $P < 0.05$ (one-way ANOVA), ** compared to the control; (D) Cytotoxicity of different treatments in insulin-resistant HepG2 cells; (E) Effects of the raw drugs and drug-loaded/co-loaded APMs on glucose consumption by HepG2 cells after 6h. Data are expressed as mean \pm SEM, $n=3$, α indicates $P < 0.001$; β indicates $P < 0.01$ and γ indicates $P < 0.05$ with respect to raw drugs, a indicates $P < 0.001$; b indicates $P < 0.01$ and c indicates $P < 0.05$ with respect to physical mix, using one-way ANOVA for different treatment groups; (F) Effects of the raw drugs and drug-loaded/co-loaded APMs on glucose consumption by HepG2 cells after 24h. Data are expressed as mean \pm SEM, $n=3$, α indicates $P < 0.001$; β indicates $P < 0.01$ and γ indicates $P < 0.05$ with respect to raw drugs, a indicates $P < 0.001$; b indicates $P < 0.01$ and c indicates $P < 0.05$ with respect to physical mix, using one-way ANOVA for different treatment groups

5.10 Development of bioanalytical method

5.10.1 Chromatograms of mixture

The chromatogram of both the drugs (VA and Gly) and GA as IS is presented in **Fig 5.22B** along with their respective RT i.e., 2.3 min for GA, 2.6 min for VA and 5.6 min for Gly respectively.

5.10.2 Specificity studies

Specific method was developed as the chromatogram of blank plasma did not show interference with any peak of two drugs at RT as presented in **Fig 5.22A** and **C**. The chromatogram of both drugs in plasma solution with GA also indicated method specificity without any peak interference at RT of both drugs as shown in **Fig 5.22B**.

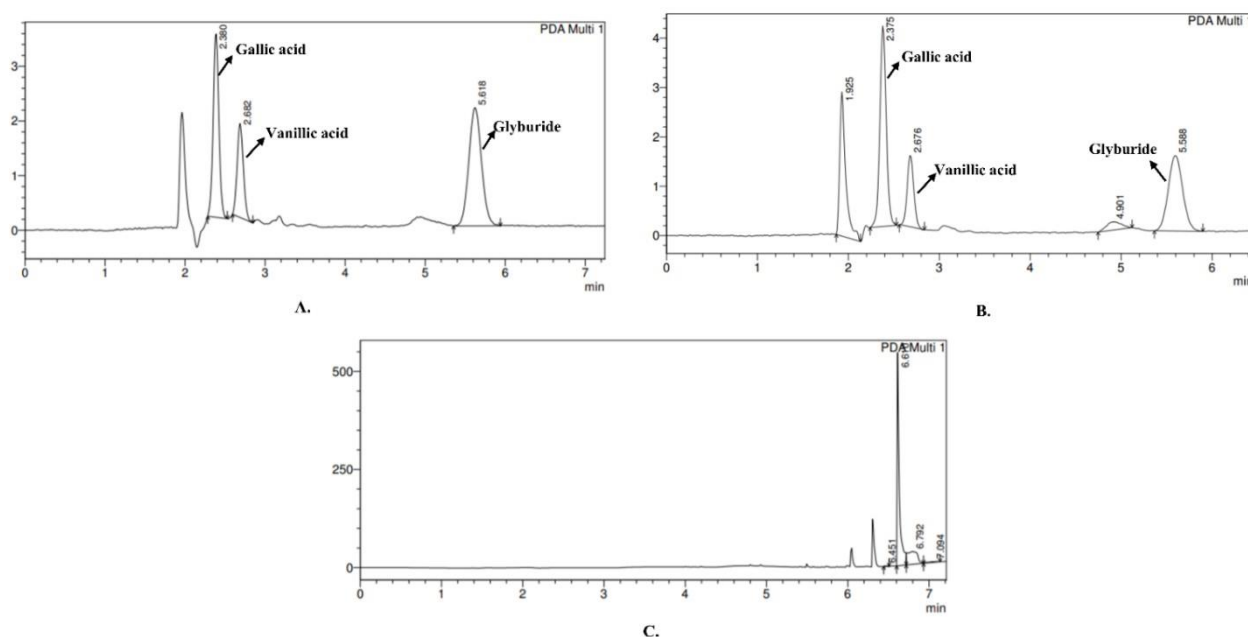


Fig 5.22: A). Chromatograms of GA, VA and Gly in mobile phase, B). Chromatogram of GA, VA and Gly in plasma, C). Chromatogram of blank plasma

5.10.3 Calibration curve development

Developed calibration curve of two drugs in mobile phase and plasma was linear in the decided range of 100 to 500 ng mL⁻¹ with R² values more than 0.999 as shown in **Fig 5.23A** to **D**. The results of area ratio of analyte/IS versus concentration calibration curve were also found linear with R² values of 0.9991 and 0.9992 for VA in plasma and in mobile phase. Similarly, for Gly R² values were found to be 0.9993 in plasma and 0.9995 in mobile phase. The results are shown in **Fig 5.23E** to **3H**.

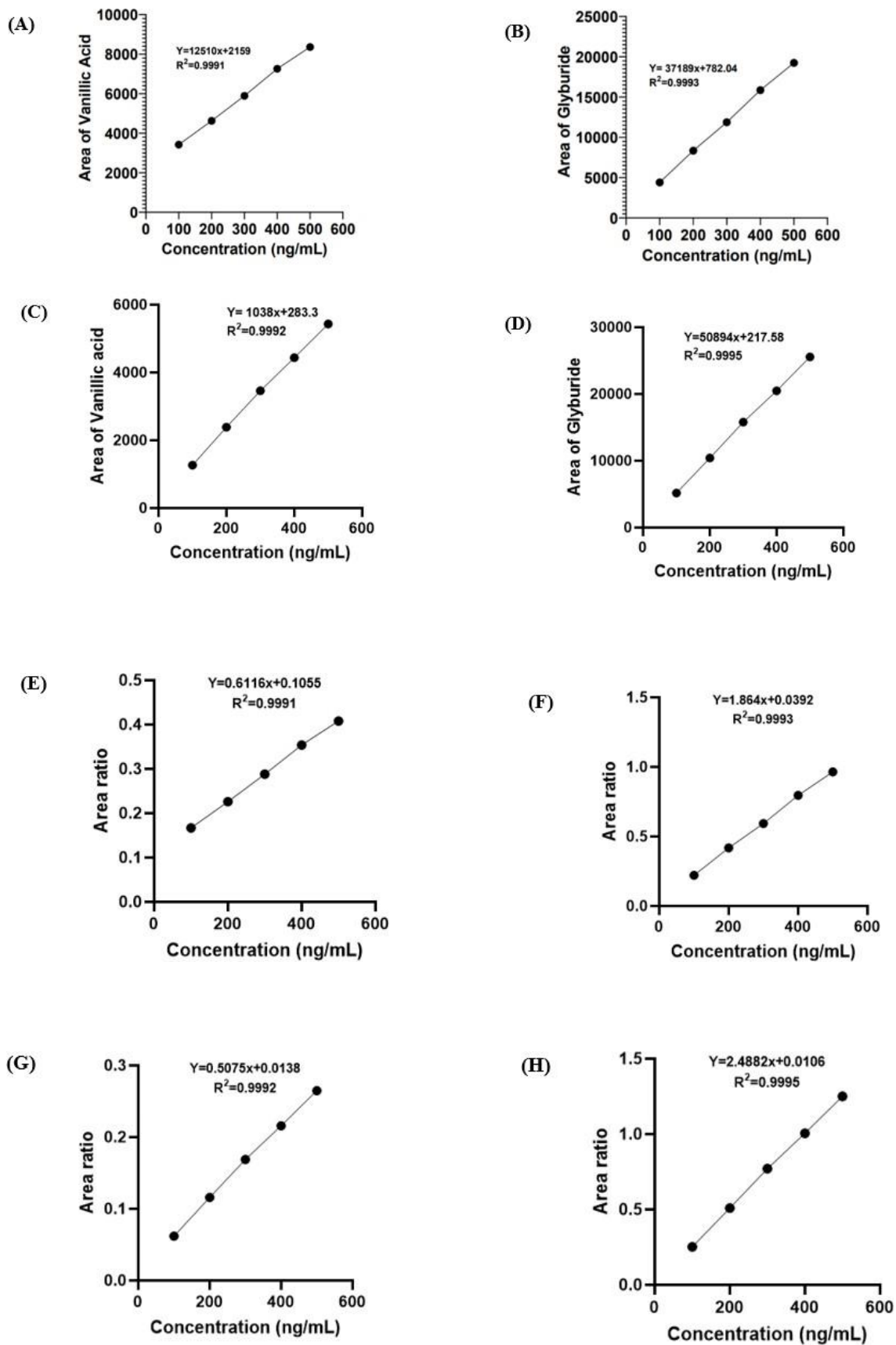


Fig 5.23: Calibration curve in plasma (A). VA, (B). Gly; Calibration curve in mobile phase (C). VA, (D). Gly; Area ratio of analyte/IS versus concentration in plasma (E). VA, (F). Gly; Area ratio of analyte/IS versus concentration in mobile phase (G). VA, (H). Gly

5.10.4 Accuracy studies

Accuracy was determined employing the percentage recovery method. Percentage recovery of both the drugs was determined from the prepared LQC, MQC and HQC solutions using *equation (23)*. The results revealed that the percentage recovery obtained for each sample were inside the acceptable boundaries (95%-105%) along with %RSD less than 2. This deemed established analytical method accurate under the experimental conditions. Results are presented in *Table 5.11*.

Table 5.11: Results of accuracy study for VA and Gly in plasma

Level	Concentration ($\mu\text{g/mL}$)	Drug Recovery ($\mu\text{g/mL}$)			Recovery in plasma (%)
		Mean	S.D	RSD (%)	
VA					
LQC	0.24	0.23	56.8	1.1	96.3
MQC	0.30	0.31	48.5	0.8	103.3
HQC	0.36	0.35	75.4	1.1	97.2
Gly					
LQC	0.24	0.25	165.9	1.6	105.0
MQC	0.30	0.30	205.1	1.6	100.0
HQC	0.36	0.36	250.2	1.7	100.0

5.10.5 Precision estimation of the developed method

Precision was measured by estimating the % RSD of the prepared HQC, MQC and LQC samples that were injected in six replicates at inter-analyst, intraday and inter-day precision. Under the experimental conditions, the % RSD was found to be lower than two, deeming the analytical method precise. The data is presented in *Table 5.12 (A, B and C)*.

5.10.6 LOQ and LOD

LOQ and LOD of the drugs (VA and Gly) were determined in plasma and in the mobile phase using *equation (24)* and *(25)*. LOD and LOQ of VA in plasma and in mobile phase were estimated to be 18, 55, 17 and 52 ng/mL correspondingly. While for Gly it was found to be 15, 47, 13 and 40 ng/mL correspondingly. Hence, a sensitive analytical method with the capability to detect and analyze the two drugs at low concentrations was developed.

Table 5.12A: Results of the intraday precision estimation for VA and Gly in plasma

Level	AUC 1 (cm ²)	AUC 2 (cm ²)	AUC 3 (cm ²)	AUC 4 (cm ²)	AUC 5 (cm ²)	AUC 6 (cm ²)	Mean (cm ²)	S.D.	RSD (%)
VA in plasma									
LQC	5212.9	5122.3	5056.8	5178.2	5187.1	5134.6	5148.6	56.2	1.0
MQC	6011.2	6067.3	6134.6	6101.3	6092.5	6045.2	6075.3	43.7	0.7
HQC	6634.2	6501.2	6499.8	6667.3	6623.4	6639.4	6594.2	74.0	1.1
Gly in plasma									
LQC	10211.3	10108.9	10367.5	10189.5	10453.9	10672.9	10333.9	190.0	1.8
MQC	12124.9	12471.3	12390.9	12534.1	12675.1	12815.1	12501.9	217.7	1.7
HQC	14122.1	14034.2	14371.3	14432.2	14128.3	14758.5	14307.7	246.3	1.7

Table 5.12B: Results of the interday precision estimation for VA and Gly in plasma

Level	Day	AUC 1 (cm ²)	AUC 2 (cm ²)	AUC 3 (cm ²)	AUC 4 (cm ²)	AUC 5 (cm ²)	AUC 6 (cm ²)	Mean (cm ²)	S.D.	RSD (%)
VA in plasma										
LQC	1	5218.2	5233.4	5165.3	5187.2	5167.2	5184.2	5192.5	27.6	0.5
	2	5123.1	5155.4	5167.4	5299.3	5245.4	5289.4	5213.3	74.5	1.4
	3	5271.3	5204.3	5219.3	5166.1	5134.2	5177.0	5195.3	47.6	0.9
MQC	1	6122.1	6135.6	6087.3	6092.2	6167.3	6189.9	6132.4	40.7	0.6
	2	6056.3	6178.2	6122.4	6101.4	6059.2	6154.3	6111.8	49.7	0.8
	3	6192.2	6205.6	6200.1	6288.3	6176.5	6113.5	6196	56.2	0.9
HQC	1	6623.4	6555.3	6584.5	6577.3	6685.3	6652.9	6613.1	49.6	0.7
	2	6532.4	6504.5	6657.3	6688.4	6671.3	6610.2	6610.6	76.5	1.1
	3	6488.4	6566.2	6622.5	6620.3	6511.5	6529.4	6556.3	56.4	0.8
Gly in plasma										
LQC	1	10211.3	10108.9	10367.5	10189.5	10453.9	10672.9	10333.9	190.0	1.8
	2	10342.4	11124.2	10253.5	10156.3	10378.3	10247.2	10200.3	117.7	1.1
	3	10288.2	10167.5	10021.4	10272.5	10143.7	10192.7	10181.0	97.0	0.9
MQC	1	12673.7	12989.9	12345.7	12623.2	12594.3	12926.6	12692.2	235.9	1.8
	2	12124.9	12471.3	12390.9	12534.1	12675.1	12815.1	12501.9	217.7	1.7
	3	12357.2	12162.5	12430.5	12163.6	12524.5	12003.6	12273.6	195.9	1.5
HQC	1	14026.5	14342.3	14084.3	13997.5	14283.6	14021.7	14125.9	148.7	1.0
	2	14233.6	14145.6	14262.4	14541.1	14039.5	14594.2	14319.4	209.3	1.4
	3	14122.1	14034.2	14371.3	14432.2	14128.3	14758.5	14307.7	246.3	1.7

Table 5.12C: Results for the Inter-analyst precision estimation for VA and Gly in plasma

Level	IA	AUC 1 (cm ²)	AUC 2 (cm ²)	AUC 3 (cm ²)	AUC 4 (cm ²)	AUC 5 (cm ²)	AUC 6 (cm ²)	Mean (cm ²)	S.D.	RSD (%)
VA in plasma										
LQC	IA1	5351.3	5204.3	5219.3	5126.1	5174.2	5177.0	5208.7	76.7	1.4
	IA2	5232.9	5162.3	5036.8	5168.2	5127.1	5164.6	5148.6	64.6	1.2
	IA3	5173.1	5105.4	5147.4	5219.3	5275.4	5219.4	5190.0	60.4	1.1
MQC	IA1	6122.1	6165.6	6027.3	6022.2	6137.3	6199.9	6112.4	72.9	1.1

	IA2	6010.2	6047.3	6234.6	6151.3	6142.5	6055.2	6106.8	83.8	1.3
	IA3	6192.2	6205.6	6200.1	6288.3	6176.5	6113.5	6196.0	56.2	0.9
HQC	IA1	6468.4	6546.2	6632.5	6670.3	6521.5	6429.4	6544.7	92.8	1.4
	IA2	6634.2	6521.2	6459.8	6627.3	6613.4	6579.4	6572.5	69.0	1.0
	IA3	6623.4	6555.3	6584.5	6577.3	6685.3	6652.9	6613.1	49.6	0.7
Gly in plasma										
LQC	IA1	10228.2	10117.5	10031.4	10572.5	10153.7	10172.7	10212.6	187.9	1.8
	IA2	10411.3	10208.9	10467.5	10689.5	10853.9	10972.9	10600.6	289.0	2.7
	IA3	10242.4	10024.2	10153.5	10006.3	10078.3	10147.2	10108.6	89.3	0.8
MQC	IA1	12324.9	12271.3	12190.9	12134.1	12375.1	12115.1	12235.2	105.3	0.8
	IA2	12024.9	12101.3	12020.9	12334.1	12475.1	12015.1	12161.9	195.7	1.6
	IA3	12657.2	12462.5	12630.5	12263.6	12624.5	12103.6	12456.9	228.2	1.8
HQC	IA1	14333.6	14245.6	14462.4	14641.1	14239.5	14194.2	14352.7	170.2	1.1
	IA2	14122.1	14034.2	14371.3	14432.2	14128.3	14758.5	14307.7	269.8	1.8
	IA3	14331.2	14552.2	14724.2	14023.3	14276.2	14221.5	14354.7	248.9	1.7

5.10.7 System suitability

Parameters indicating system suitability demonstrated good column efficiency and peak regularity under the test conditions used for this study. **Table 5.13** tabulates the results of the study.

5.10.8 Stability study

The stability of drugs in plasma at 3 levels that are, LQC, MQC and HQC in terms of freeze-thaw, short-term and long-term stability is presented in **Table 5.14 (A, B and C)** correspondingly. The results obtained indicated recovery of both the drugs inside the approved limits i.e., 95-105% with %RSD less than 2. This study confirmed that the drugs remained stable for the long period of time in the plasma matrix.

Table 5.13: The values depicting system suitability for drugs VA and Gly

Parameters	VA (Plasma)	Gly (Plasma)
HETP	22.9 µg/mL	75.2 µg/mL
Theoretical plate	6537.1	2992.7
Tailing factor	0.9	1.2

Table 5.14A: Short-term stability study

Actual Concentration of drug ($\mu\text{g mL}^{-1}$)	Area 1 (cm^2)	Area 2 (cm^2)	Area 3 (cm^2)	Mean (cm^2)	S.D.	%RSD	Amt drug recovered ($\mu\text{g/mL}$)	Recovery (%)
VA in plasma								
1 hour								
0.24 (LQC)	5120.0	5245.3	5201.6	5188.9	63.5	1.2	0.24	100.9
0.30 (MQC)	6122.3	6096.3	6108.3	6109.0	12.9	0.2	0.31	103.3
0.36 (HQC)	6560.4	6534.8	6411.4	6502.2	76.9	1.2	0.32	95
2 hour								
0.24 (LQC)	5222.2	5217.3	5191.3	5210.2	16.6	0.3	0.24	100.0
0.30 (MQC)	6034.7	6177.3	6097.8	6103.2	71.4	1.1	0.31	105.0
0.36 (HQC)	6605.6	6534.8	6675.3	6605.3	70.2	1.0	0.35	97.2
3 hour								
0.24 (LQC)	5255.7	5348.2	5228.6	5277.5	62.7	1.1	0.25	104.0
0.30 (MQC)	6112.6	6195.2	6002.9	6103.5	96.4	1.5	0.31	103.3
0.36 (HQC)	6467.3	6477.2	6389.7	6444.8	47.9	0.7	0.34	95.3
Gly in plasma								
1 hour								
0.24 (LQC)	10106.4	10362.5	10182.1	10217.0	131.5	1.2	0.25	105.0
0.30 (MQC)	12043.5	12173.8	12021.2	12079.5	82.4	0.6	0.30	100.0
0.36 (HQC)	14042.7	14264.5	14117.3	14141.5	112.8	0.7	0.35	99.7
2 hour								
0.24 (LQC)	10021.7	10222.3	10421.4	10221.8	199.8	1.9	0.25	105.7
0.30 (MQC)	12165.4	12108.9	12333	12202.4	116.5	0.9	0.30	100.0
0.36 (HQC)	14966.7	14865.3	14460.7	14764.2	267.7	1.8	0.37	102.7
3 hour								
0.24 (LQC)	10016.6	10237.2	10342.5	10198.7	166.3	1.6	0.25	105.5
0.30 (MQC)	12167.6	12282.1	12045.0	12164.9	118.5	0.9	0.30	100.0
0.36 (HQC)	14122.1	14365.8	14014.8	14167.5	179.8	1.2	0.35	99.9

Table 5.15B: Freeze thaw stability study

Actual Concentration of drug ($\mu\text{g/mL}$)	Area 1 (cm^2)	Area 2 (cm^2)	Area 3 (cm^2)	Mean	S.D.	RSD (%)	Amount of drug recovered in plasma sample ($\mu\text{g/mL}$)	Recovery (%)
VA in plasma								
Cycle 1								
0.24 (LQC)	5221	5289.5	5217.5	5242.6	40.5	0.7	0.24	102.7
0.30 (MQC)	6155.7	6180.3	6009.6	6115.2	92.2	1.5	0.31	105.4
0.36 (HQC)	6400.1	6455.3	6428.9	6428.1	27.6	0.4	0.34	94.7
Cycle 2								
0.24 (LQC)	5120.4	5188.4	5194.7	5167.8	41.1	0.7	0.24	100.2
0.30 (MQC)	6089.4	6016.7	6185.5	6097.2	84.6	1.3	0.31	104.9
0.36 (HQC)	6592.6	6518.7	6435.8	6515.7	78.4	1.2	0.34	96.7
Cycle 3								
0.24 (LQC)	5347.6	5302.7	5329.7	5326.6	22.6	0.4	0.25	105.5
0.30 (MQC)	6168.7	6117.6	6038.5	6108.2	65.5	1.0	0.31	105.2
0.36 (HQC)	6508.7	6547.3	6578.3	6544.7	34.8	0.5	0.35	97.3
Gly in plasma								
Cycle 1								
0.24 (LQC)	10024.5	10167.3	10278.7	10156.8	127.4	1.2	0.25	105.0
0.30 (MQC)	12156.4	12446.4	12764.2	12455.6	304.0	2.4	0.31	104.6
0.36 (HQC)	14163.2	14074.3	14026.8	14088.1	69.2	0.4	0.35	99.3
Cycle 2								
0.24 (LQC)	10188.6	10106.4	10267.6	10187.5	80.6	0.7	0.25	105.3
0.30 (MQC)	12243.7	12167.7	12067.3	12159.5	88.4	0.7	0.30	101.9
0.36 (HQC)	14034.6	14356.4	14067.6	14152.8	177.0	1.2	0.35	99.8
Cycle 3								
0.24 (LQC)	10123.7	10067.4	10176.8	10122.6	54.7	0.5	0.25	104.6

0.30 (MQC)	12474.7	12376.8	12076.5	12309.3	207.4	1.6	0.30	103.3
0.36 (HQC)	14364.5	14063.4	14176.8	14201.5	152.0	1.0	0.36	100.2

Table 5.16C: Long-term stability study

Actual Concentration of drug ($\mu\text{g/mL}$)	Area 1 (cm^2)	Area 2 (cm^2)	Area 3 (cm^2)	Mean	S.D.	RSD (%)	Amount of drug recovered in plasma sample ($\mu\text{g/mL}$)	Recovery (%)
VA in plasma								
Week 1								
0.24 (LQC)	5234.7	5278.5	5205.6	5239.6	36.6	0.7	0.24	102.6
0.30 (MQC)	6124.8	6156.7	6015.6	6099.0	73.9	1.2	0.31	104.9
0.36 (HQC)	6467.8	6464.4	6533.5	6488.5	38.9	0.6	0.34	96.1
Week 2								
0.24 (LQC)	5270.4	5223.6	5199.9	5231.3	35.8	0.6	0.24	102.3
0.30 (MQC)	6144.7	6108.9	6076.8	6110.1	33.9	0.5	0.31	105.2
0.36 (HQC)	6456.8	6487.9	6429.8	6458.1	29.0	0.4	0.34	95.4
Week 3								
0.24 (LQC)	5290.4	5212.4	5210.2	5237.6	45.6	0.8	0.24	102.5
0.30 (MQC)	6003.7	6119.4	6128.6	6083.9	69.6	1.1	0.31	104.5
0.36 (HQC)	6401.5	6427.7	6482.3	6437.1	41.2	0.6	0.34	94.9
Gly in plasma								
Week 1								
0.24 (LQC)	10115.3	10210.4	10008.0	10111.2	101.2	1.0	0.25	104.5
0.30 (MQC)	12167.3	12077.3	12440.0	12228.2	188.8	1.5	0.30	102.5
0.36 (HQC)	14156.9	14335.7	14021.9	14171.5	157.4	1.1	0.36	100.0
Week 2								
0.24 (LQC)	10013.8	10205.8	10286.3	10168.6	140.0	1.3	0.25	105.1
0.30 (MQC)	12044.2	12376.9	12009.9	12143.6	202.7	1.6	0.30	101.8
0.36 (HQC)	14365.3	14100.9	14323.5	14263.2	142.1	0.9	0.36	100.6

Week 3								
0.24 (LQC)	10122.8	10073.9	10366.3	10187.6	156.6	1.5	0.25	105.3
0.30 (MQC)	12431.5	12094.6	12162.8	12229.6	178.1	1.4	0.30	102.6
0.36 (HQC)	14354.8	14126.5	14358.4	14279.9	132.8	0.9	0.36	100.8

5.11 *In vivo studies*

The results are shown in **Table 5.17** and **Fig 5.24**. The results indicated that T_{max} of raw Gly was found to be 3h whereas it was 2h in the case of its physical mixture with VA. This indicated delayed absorption of raw Gly via the GIT into systemic circulation owing to its poor aqueous solubility. However, in a physical mixture with VA, Gly showed faster absorption which could be because of the polar hydroxyl groups of the VA contributing to augmenting its solubility. This result was in agreement with the *in vitro*-drug release study of Gly.

This has also led to the reduction of $t_{1/2}$ of Gly in the physical mixture by 1.0-folds than that of raw Gly. A significant difference was observed in their area under the curve (AUC) and C_{max} . The C_{max} of Gly in the physical mixture was found to be increased by 1.6-folds ($P<0.01$) than raw Gly. The loading of Gly in APMs did not affected any change in the T_{max} of Gly. However, the C_{max} and $AUC_{0-\infty}$ of Gly in GV-APMs were found to be increased by 1.5-fold ($P<0.01$) and 3.5-folds ($P<0.01$) than that of raw Gly. The $MRT_{(0-\infty)}$ of Gly in GV-APMs was increased by 5.2-folds ($P<0.01$) than raw Gly respectively.

In the case of VA, results indicated that maximum absorption of VA ($C_{max} = 88100$ ng/mL) was observed within 1h (T_{max}). Afterwards, rapid elimination of VA was observed in the next 2h, indicating its rapid elimination followed by poor oral bioavailability. This can be further understood by shorter $t_{1/2}$ (4.2 h) and mean residence time of (2.9 h). The $AUC_{0-\infty}$ of raw VA was found to be 113900 h*ng/mL. It is pertinent to add here that a longer half-life and residence time is required for a drug to have very good therapeutic efficacy and prolonged effect [274]. In the physical mixture, absorption of VA was observed within 2h (T_{max}), which indicated delayed absorption of VA that could be due to hydrophobicity of the Gly in the physical mixture. However, no significant change was observed in C_{max} of VA. The $AUC_{0-\infty}$ of VA in the physical mixture increased by 3.8-folds ($P<0.001$) than raw VA. Further, the $t_{1/2}$ of VA in the physical mixture was increased by 1.1-folds than raw VA, which indicated its longer residence in plasma. However, was not statistically significant. The loading of VA in APMs increased the $t_{1/2}$ and T_{max} of VA by 2.3-folds ($P<0.01$) and 5-folds ($P<0.05$) than the raw VA. However, no significant difference was observed in T_{max} of VA co-loaded in GV-APMs and VA-APMs. Significant in increase in the T_{max} of VA in GV-APMs was observed i.e., 4-folds ($P<0.05$) than VA in the physical mixture. The C_{max} of VA in APMs was increased by 1.0-fold than raw VA but was found

to be statistically insignificant. The $AUC_{0-\infty}$ of VA in APMs was increased by 7.7-folds ($P < 0.01$) than raw VA. Whereas in GV-APMs, $AUC_{0-\infty}$ and $MRT_{(0-\infty)}$ of VA were increased by 2.8-folds ($P < 0.01$) and 6.5-folds ($P < 0.01$) than VA in the physical mixture and raw VA respectively. The results of one-way ANOVA for the pharmacokinetic parameters among different treatment groups is presented in *Table 5.18 (A, B, C and D)*.

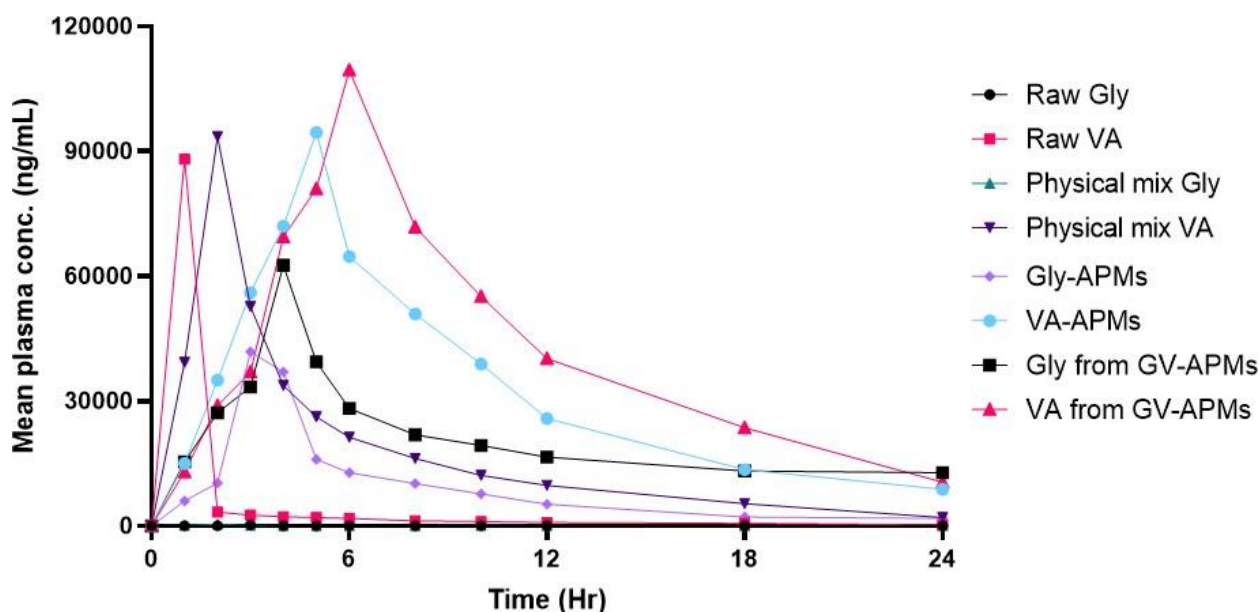


Fig 5.24: Pharmacokinetic data of raw drugs, their physical mixture, individual APMs and GV-APMs

Table 5.17: Pharmacokinetic data of raw drugs and their formulation

Pharmacokinetic parameter	Gly	VA	Physical mixture (Gly)	Physical mixture (VA)	Gly-APMs	VA-APMs	GV-APMs (Gly)	GV-APMs (VA)
T_{max} (h)	3.0	1.0	2.0	2.0	3.0	5.0	4.0	8.0
C_{max} (ng/mL)	240.0	88100.0	400.0	93400.0	41800.0	94500.0	62600.0	99500.0
$AUC_{(0-t)}$ (ng/mL*h)	560.0	11270.0	917.0	410000.0	204900.0	759750.0	486300.0	981250.0
$AUC_{(0-\infty)}$ (ng/mL*h)	568.2	113914.7	921.0	423000.0	221226.6	884931.4	774344.6	1225472.0
$t_{1/2}$ (h)	3.6	4.2	3.3	4.7	6.2	9.8	15.5	16.1
$MRT_{(0-\infty)}$ (h)	4.5	2.9	4.6	6.9	8.8	12.7	23.4	17.0

Table 5.18A: One-way ANOVA test for various pharmacokinetic parameters following treatments with raw Gly and Gly-APMs

Source of variation	SS	DF	MS	F	F _{crit}	P
AUC						
Between	40074834969	1	40074834969	2290.2	18.5	<0.001
Within	34996778	2	17498389			
Total	40109831747	3				
C_{max}						
Between	1650796900	1	1650796900	1874.0	18.5	<0.001
Within	1761709	2	880854.5			
Total	1652558609	3				
T_{max}						
Between	1650796900	1	1650796900	1874.0	18.5	<0.001
Within	1761709	2	880854.5			
Total	1652558609	3				
C_{max}/AUC						
Between	0.0546	1	0.0546	717.5	18.5	<0.001
Within	0.0001	2	7.61265E-05			
Total	0.0547	3				
MRT						
Between	17.2225	1	17.2225	58.8	18.5	<0.01
Within	0.585	2	0.2925			
Total	17.8075	3				

Table 5.18B: One-way ANOVA test for various pharmacokinetic parameters following treatments with raw VA and VA APMs

Source of variation	SS	DF	MS	F	F _{crit}	P
AUC						
Between	537009030481	1	537009030481	2035.3	18.5	<0.001
Within	527685857	2	263842928.5			
Total	537536716338	3				
C_{max}						
Between	66365462.2	1	66365462.25	3.4824	18.5	N.S
Within	38114424.5	2	19057212.25			
Total	104479886.75	3				
T_{max}						
Between	19.36	1	19.36	74.4615	18.5	<0.01
Within	0.52	2	0.26			
Total	19.88	3				
C_{max}/AUC						
Between	60.0382	1	60.03829	19481.9	18.5	N.S
Within	0.0061	2	0.0030			
Total	60.0444	3				
MRT						
Between	96.04	1	96.04	192.08	18.5	<0.05
Within	1	2	0.5			
Total	97.04	3				

Table 5.18C: One-way ANOVA test for various pharmacokinetic parameters following treatments with physical mix Gly and Gly in GV-APMs

Source of variation	SS	DF	MS	F	F _{crit}	P
AUC						
Between	2.02484E+11	1	2.02484E+11	161.4691	18.5	<0.01
Within	2508019730	2	1254009865			
Total	2.04992E+11	3				
C_{max}						
Between	3668300922.2	1	3668300922.2	1364.6	18.5	<0.001
Within	5375992.5	2	2687996.2			
Total	3673676914.7	3				
T_{max}						
Between	5.76	1	5.76	67.76471	18.5	<0.01
Within	0.17	2	0.085			
Total	5.93	3				
C_{max}/AUC						
Between	0.089467	1	0.089467	1748.672	18.51	<0.001
Within	0.000102	2	5.12E-05			
Total	0.089569	3				
MRT						
Between	329.4225	1	329.4225	331.9118388	18.51	<0.01
Within	1.985	2	0.9925			
Total	331.4075	3				

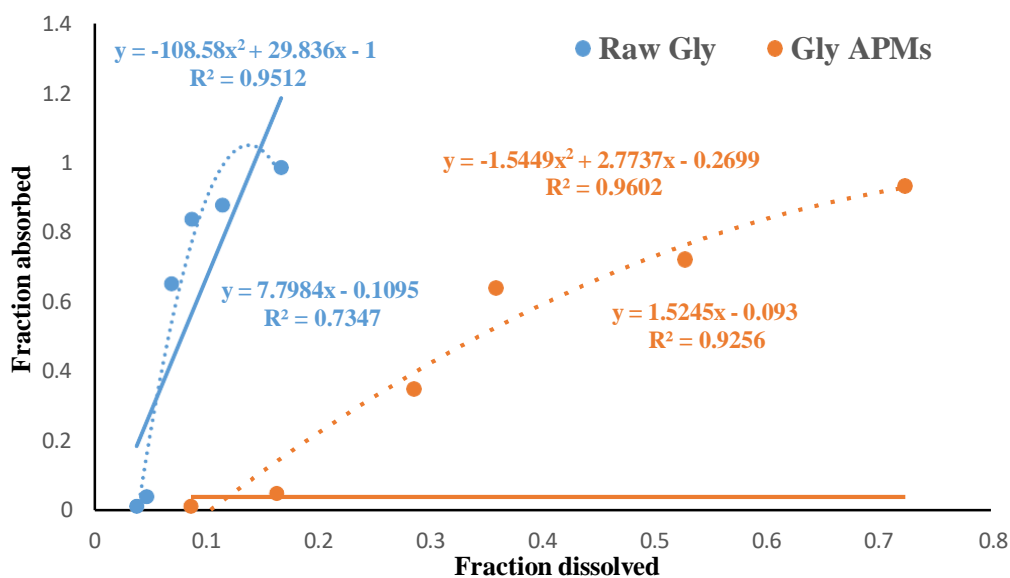
Table 5.18D: One-way ANOVA test for various pharmacokinetic parameters following treatments with physical mix VA and VA in GV-APMs

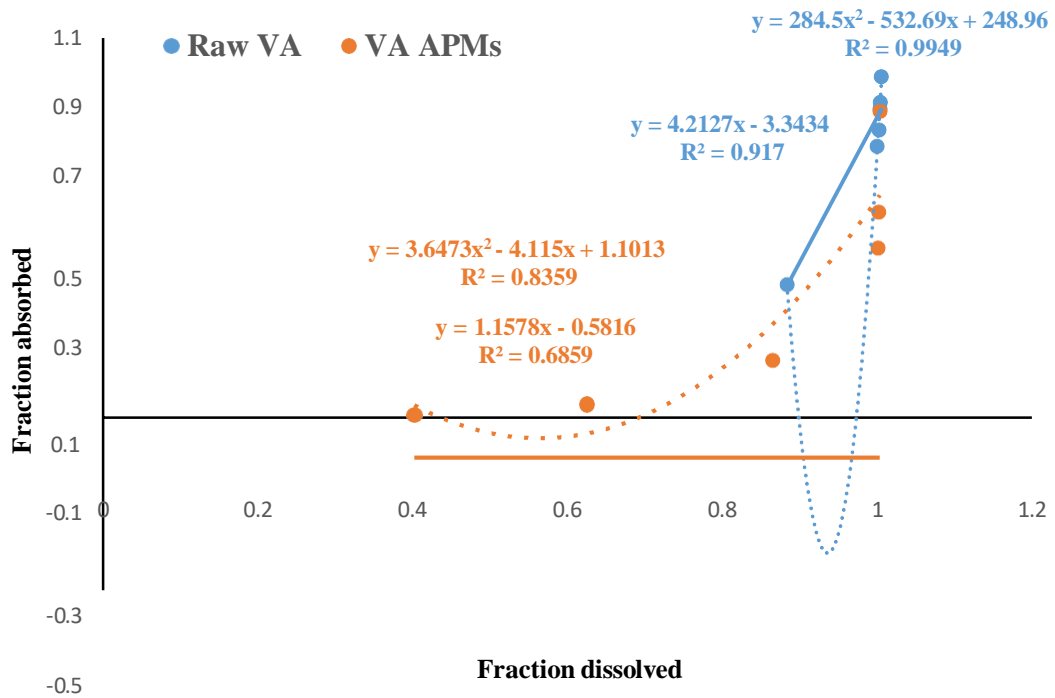
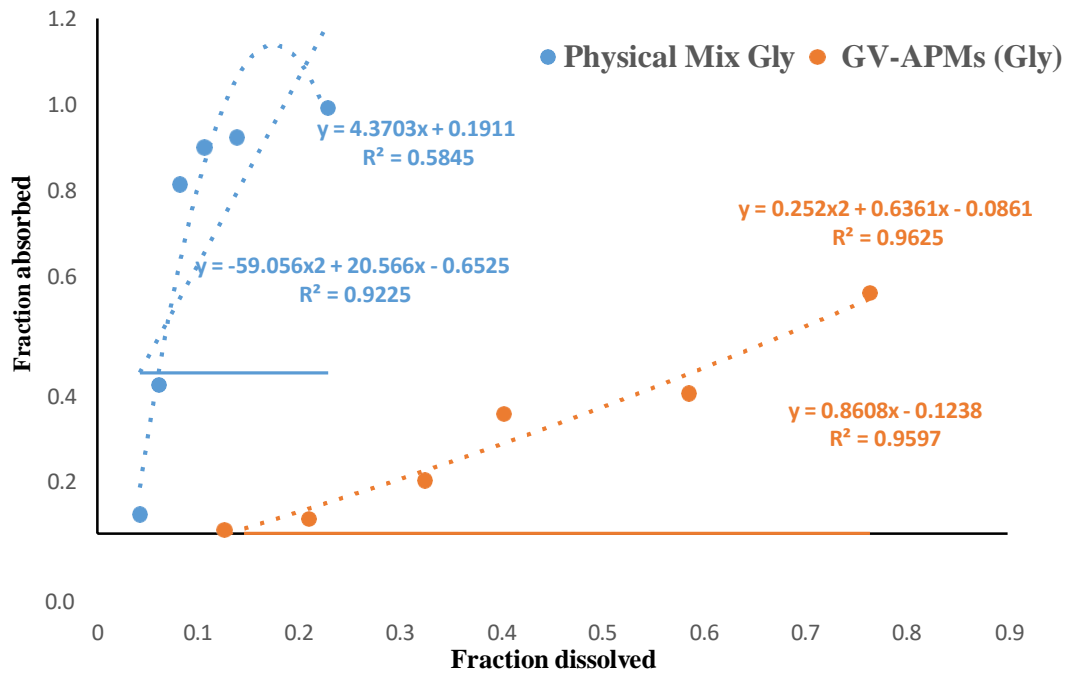
Source of variation	SS	DF	MS	F	F _{crit}	P
AUC						
Between	3.01E+11	1	3.01E+11	373.5206	18.5	<0.01
Within	1.61E+09	2	8.05E+08			
Total	3.02E+11	3				
C_{max}						
Between	23217942	1	23217942	1.492074	18.5	NS
Within	31121713	2	15560856			
Total	54339655	3				
T_{max}						
Between	26.5225	1	26.5225	71.20134	18.5	<0.01
Within	0.745	2	0.3725			
Total	27.2675	3				
C_{max}/AUC						
Between	0.015552	1	0.015552	2855.928	18.5	<0.001
Within	1.09E-05	2	5.45E-06			
Total	0.015563	3				
MRT						
Between	102.01	1	102.01	104.0918367	18.5	<0.01
Within	1.96	2	0.98			

Total	103.97	3
-------	--------	---

5.11.1 IVIVC

Both Gly and VA exhibit poor oral bioavailability and their co-loading in GV-APMs i.e., in the form of nanocombination therapy exhibited Level A association between *in vitro* dissolution and *in vivo* absorption. As per the Level A IVIVC, a high grade of association was formed amid proportion of drug dissolved and drug absorbed at their consecutive time-points. The Level A IVIVC profiles of drugs in the raw form, their physical mix and the nanoform as presented in **Fig 5.25 (A, B, C, and D)** indicate a higher grade of non-linear model fitting between the two parameters, viz., per cent drug dissolved and per cent drug absorbed for the raw Gly (R=0.9752), raw VA (R=0.9974), physical mix Gly (R=0.9604), physical mix VA (R=0.9471), Gly-APMs (R=0.9798), VA-APMs (R=0.9142), GV-APMs (Gly) (R=0.9796), and GV-APMs (VA) (R=0.9115) respectively. The quadratic model revealed superior data fitting that resulted in the development of curved IVIVC for the developed formulation(s). Superior fitting for the quadratic model in the case of developed GV-APMs can be attributed to improved and sustained drug release along with higher dissolution and bioavailability upon oral administration of GV-APMs respectively.





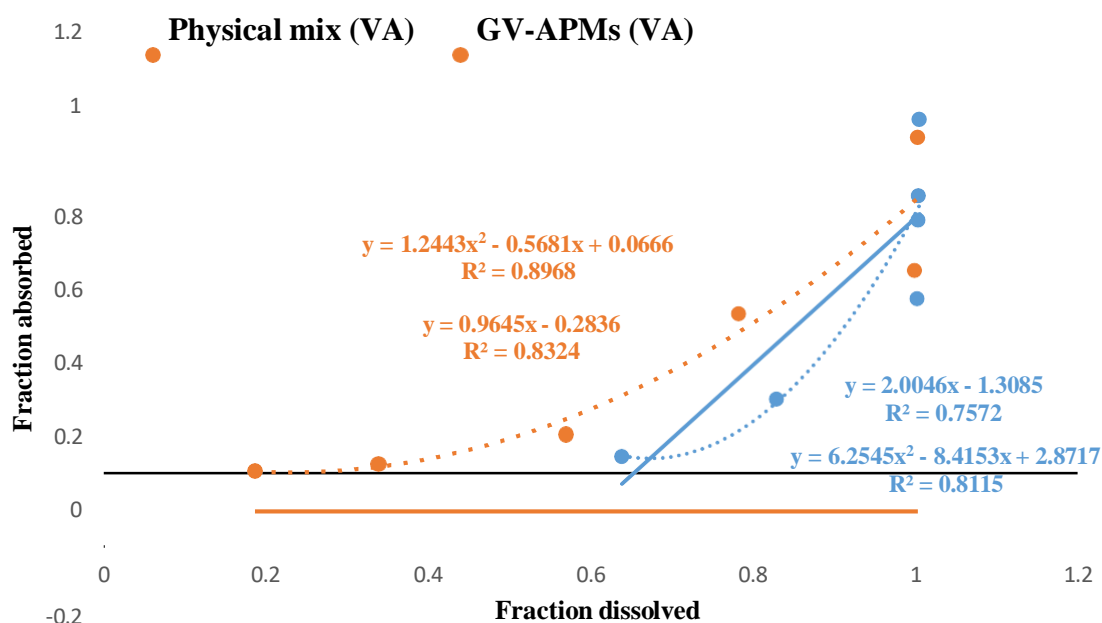


Fig 5.25: Level A IVIVC between (A) Raw Gly and Gly-APMs, (B) Raw VA and VA-APMs, (C) Physical mix (Gly) and GV-APMs (Gly), (D) Physical mix (VA) and GV-APMs (VA)

Therefore, the drug absorption was found to exhibit a non-linear relationship with the corresponding dissolution performance. The successful establishment of IVIVC relationships, revealed augmentation in the *in vitro* drug dissolution profile, which is an important variable in elucidating the corresponding enhancement in the biopharmaceutical performance of the developed optimized formulation(s). Superior fitting for the quadratic model in the case of optimized GV-APMs can be attributed to the improved and sustained drug release together with greater and faster absorption on oral administration of GV-APMs.

5.12 Pharmacodynamics study

5.12.1 OGTT

HFD administration in rats impairs hepatic glucose metabolism due to IR and reduced insulin secretion by the pancreas. This ultimately results in abnormal glucose tolerance in HFD fed-rats [357]. OGTT is basically used as a characteristic of metabolic phenotype and to determine the alteration in glucose metabolism. OGTT basically assesses the deposition of an orally administered glucose load over time by measuring the blood glucose levels [364]. The results of fluctuations in BGLs at different time-points post oral glucose administration pertaining to various groups is shown in **Table 5.19**. The results indicated more than 35 mg/dL BGLs in HFD fed-rats of G2 to G12 at the end of 1.5h.

This increase in BGLs at the end of 1.5h was at least +10 mg/dL in all the treatment groups as compared to rats of G1. The main purpose of this study was to check the duration taken by the rats to lowering down the glucose levels in order to maintain glucose homeostasis. Usually, the longer duration required by the body to bring glucose levels down represents the state of IR as a measure of low glucose tolerance. In case of G1, BGLs started lowering down after the end of 1h, indicating higher degree of glucose tolerance in control rats in response to oral glucose load. Further, in control rats, the secreted insulin under normal physiological functioning i.e., rats on NPD, was able to lower down the BGLs. This can be understood by the decrease in BGLs by 28 mg/dL in case of G1 rats between 1h to 4h. Whereas, in case of rats of G2 to G12, the rise in BGLs at the end of 1h was minimum of 24 mg/dL. Between 1h to 4h, negligible decrease in BGLs of rats of G2, G3, G6, G7, G8, G9 and G10 was observed, whereas, rats of G4, G5, G11 and G12 showed rise in BGLs. The overall results of treatments groups (G2-G12) indicated that their body was resistant to insulin owing to administration of HFD. Hence, was unable to maintain glucose homeostasis at normal level [357]. The patterns for changes in BGLs as per different time intervals of different groups are shown in **Fig 5.26** in which all the HFD fed rats showed significantly ($p < 0.001$) lower glucose tolerance in comparison to the control rats respectively.

Table 5.19: Blood glucose levels of different treatment groups after oral glucose load (Mean±SD, n=8)

Time (h)	G1 (mg/dL)	G2 (mg/dL)	G3 (mg/dL)	G4 (mg/dL)	G5 (mg/dL)	G6 (mg/dL)	G7 (mg/dL)	G8 (mg/dL)	G9 (mg/dL)	G10 (mg/dL)	G11 (mg/dL)	G12 (mg/dL)
0	116.3±10.9	126.1±15.2	124.3±9.4	120.9±14.4	122.0±10.5	120.0±11.8	127.8±11.8	124.8±10.5	123.7±14.8	121.7±11.3	124.6±9.9	125.2±5.5
1	143.5±2.1	172.5±3.5 ^γ	163.5±2.1 ^β	159.1±1.8 ^β	165.9±3.7 ^β	163.8±5.6 ^γ	160.7±2.6 ^β	159.1±4.1 ^γ	159.2±3.3 ^γ	158.5±4.1 ^γ	152.6±5.6 ^{ns}	162.5±5.3 ^γ
1.5	139.5±2.1	173.5±2.1	164.5±2.1	172.8±1.6	178.5±1.6	180.5±6.3	163.8±1.2	164.2±2.4	169.7±3.2	161.2±3.2	157.5±1.5	171.3±2.4
4	114.1±4.1	164.6±3.3 ^c	162.9±3.5 ^c	162.1±4.9 ^c	169.5±4.2 ^c	164.9±3.5 ^c	160.9±3.5 ^c	170.0±4.2 ^c	156.5±2.8 ^c	147.5±5.6 ^c	155.3±2.9 ^c	171.3±3.8 ^c
6	95.0±7.0	124.0±2.8 ^z	129.4±2.5 ^z	136.3±2.5 ^y	145.9±3.8 ^y	140.0±3.1 ^y	130.9±3.2 ^z	152.7±5.8 ^y	128.7±1.2 ^z	126.2±3.6 ^z	135.0±2.4 ^y	130.5±3.8 ^z

α, β, γ indicate p<0.001, p<0.01, p<0.05 with respect to control at 1h; and a, b, c, indicate p<0.001, p<0.01, p<0.05 with respect to control at 4h; x, y, z indicates p<0.001, p<0.01, p<0.05 with respect to control at 6h. Data are presented as mean±SD (8 rats in each groups) respectively.

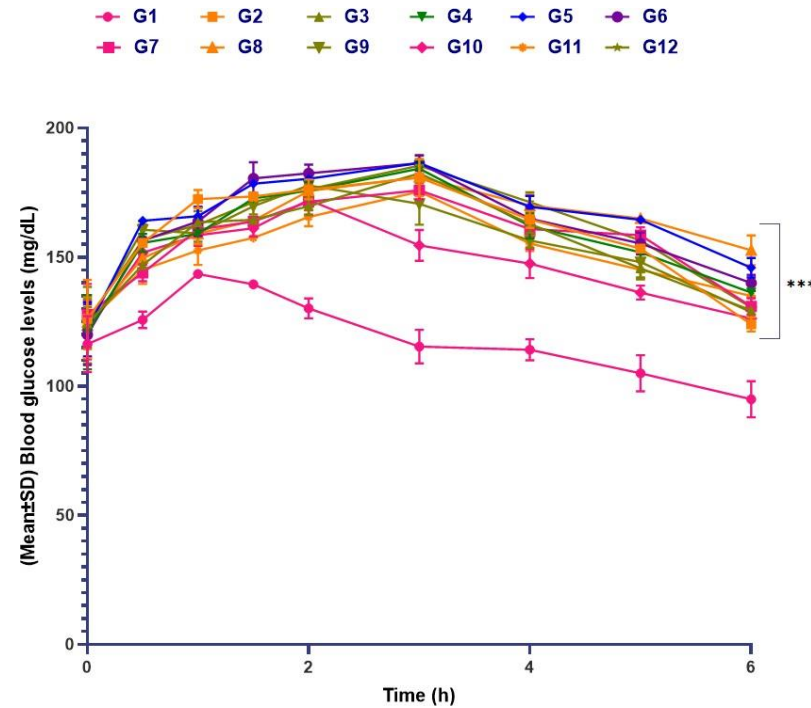


Fig 5.26: OGTT curve for different treatment groups; *** indicate statistically significant differences (p<0.001) with respect to control rats using two-way ANOVA, Data are presented as mean±SD (8 rats in each groups)

5.12.2 BGLs

In the present study a HFD and low dose of STZ were used to induce T2DM in rats. This model is suitable to resemble the T2DM as it replicates the natural history and metabolic characteristics of human T2DM. High lipid rich regimen consisting of huge caloric quantity supports obesity triggered glucose intolerance and IR rather than frank hyperglycaemia, which displays typical characteristics of T2DM. HFD administration primarily induces hepatic IR due to alteration in hepatic glucose metabolism followed by frank hyperglycaemia upon low dose of STZ administration in rats. Indeed, other induction models are also available such as alloxan-induced; however, is not widely preferred in terms toxicity aspect despite being less expensive than STZ [365]. In addition, there are surgical models and genetically modified or engineered diabetic/obese rodents that can be used for diabetes induction. However, the major drawbacks of such models such as invasiveness, caution during grafting, high cost, risk of early mortality due to severe diabetes makes them insignificant [366,367].

Except G1 the rats of all groups were fed with HFD for 15 days and their body weight, blood sugar levels, and lipid profile was measured in order to determine the influence of HFD administration on the aforementioned parameters. The results revealed that the rats from G2-G12 exhibited slight rise in the BGLs. This rise in BGLs was found significant in the range of 30 mg/dL to 52.2 mg/dL upon evaluation after 15th day (**Table 5.20**). This rise in BGLs indicated the appearance of IR in the body due to high fat diet consumption. This HFD regimen make our liver and other body parts fatty upon oral administration. Overall it causes gut dysbiosis and augmentation in the count of gram negative bacteria. These gram negative bacteria cause the release of lipopolysaccharides, which make the liver fatty and make the cells resistant to insulin, thus leading to hyperglycaemia. However, at this stage the rats cannot be considered as diabetic and the reversal in hepatic IR at this very point is quite obvious. Therefore, to induce frank hyperglycaemia in obese rats, STZ as a diabetogenic agent is injected that causes the complete appearance of signs and symptoms of T2DM.

Hence, as a continuation of study protocol, the obese rats of G2 to G12 were intraperitoneally administered with STZ 35 mg/kg on 16th day. To confirm the **complete hyperglycaemic state** (BGLs>200 mg/dL) in obese rats, the BGLs was monitored on 20th day [89]. All the obese rats of G2 to G12 on 20th day were found diabetic by showing BGLs<300 mg/dL with rise in the range of +150 mg/dL to +253 mg/dL respectively. Such results obtained, confirmed the complete diabetic state in the obese rats of each group.

The pharmacological screening of various test formulations was started from 21st day till the 48th day and the BGLs of all the rats were monitored on weekly basis (i.e., 27th, 34th, 41st and 48th day). A unique pattern of decrease in BGLs was observed for rats of different treatment groups based on their efficacy. The placebo treated group (G3) and experimental control (G2) group did not show any decrease in BGLs till the 48th day of the study protocol. However, the rats of G4 to G12 showed significant ($p < 0.001$) decrease in BGLs when the results of 20th day and 48th day were compared. The decrease in BGLs between rats of G4 to G12 after first week of treatment i.e., 27th day is shown below:

$$G12(-2.70\text{-folds}) > G11(-2.00\text{-folds}) > G10 (1.9\text{-folds}) > G8(-1.80\text{-folds}) > G9(-1.50\text{-folds}) > G6 (-1.30\text{-folds}) > G7(-1.20\text{-folds}) > G5(-1.15\text{-folds}) > G4(-1.11\text{-folds})$$

These results (Table 4) showed that the rapid response was observed in rats of G12 receiving co-loaded GV-APMs at higher dose followed by G11 and G10 respectively. There was non-significant difference in the reduction of BGLs in case of the rats of G8, G10 receiving low and high dose Gly-APMs and G11, receiving low dose of co-loaded GV-APMs. This showed the potential of APMs in enhancing the efficacy of Gly as compared to raw Gly. A significant difference in glucose lowering capacity ($p < 0.05$) of Gly-APMs (G8 and G10) was observed on 27th day itself as compared to the rats receiving its high dose G5. Similar observations were noted for the rats receiving VA-APMs alone at both the doses (G7 and G9) as compared to rats receiving raw VA at high dose (G4). This clearly indicated that developed APMs significantly enhanced the glucose lowering potential of both the therapeutics.

Gly is a well-known anti-diabetic drug used since decades, however, its poor aqueous solubility is still a challenge for the pharmaceutical industries. VA is an antioxidant that has shown good antidiabetic potential, but its rapid elimination from the body causes its failure to maintain glucose homeostasis. Both the biopharmaceutical issues of Gly and VA have been overcome by formulating APMs as this nanoarchitecture offers enhanced solubility and controlled drug release leading to sustained and enhanced oral bioavailability. Due to this fact, when both the drugs are loaded in APMs when administered alone, showed good anti-hyperglycaemic effect. This effect got further enhanced when both Gly and VA got co-loaded in APMs, due to their action on multiple pathways in body that cause elevation in BGLs. Interestingly, this effect was continued for the APMs formulation till the terminal day i.e. 48th day, wherein the BGLs for rats of G11 and G12 almost reached to normal (**Table 5.20 and Fig 5.27**).

Table 5.20: Effect of different treatment groups on BGLs upon weekly basis (Mean±SD, n=8)

Days	G1	G2	G3	G4	G5	G6	G7	G8	G9	G10	G11	G12
0 th	103.6±8.0	110.2±15.4	112.5±7.6	107.0±14.8	111.5±7.6	118.0±12.6	107.2±10.6	111.3±9.3	114.7±10.9	108.1±11.2	100.6±13.9	101.8±15.4
15 th	102.3±12.1	147.7±5.7 ^β	150.1±9.6 ^β	149.5±11.2 ^γ	148.7±15.4 ^γ	152.0±9.1 ^γ	153.7±14.0 ^γ	152.1±13.9 ^γ	145.5±85.0 ^γ	149.8±13.7 ^γ	151.6±15.9 ^γ	154±7.8 ^γ
		Rise in BGLs* by +37.5 mg/dL	Rise in BGLs* by +37.6 mg/dL	Rise in BGLs* by +42.5 mg/dL	Rise in BGLs* by +37.2 mg/dL	Rise in BGLs* by +34.0 mg/dL	Rise in BGLs* by +46.5 mg/dL	Rise in BGLs* by +40.8 mg/dL	Rise in BGLs* by +30.8 mg/dL	Rise in BGLs* by +41.7 mg/dL	Rise in BGLs* by +51.0 mg/dL	Rise in BGLs* by +52.2 mg/dL
20 th	101.5±10.2	400.7±28.6 ^a	389.0±36.5 ^a	336.5±70.0 ^a	334.2±30.6 ^a	331.0±85.5 ^a	310±93.6 ^a	387.3±106.3 ^a	362.8±15.0 ^a	370.3±96.2 ^a	344.6±92.3 ^a	395.3±89.4 ^a
		Rise in BGLs** by +253 mg/dL	Rise in BGLs** by +238.9 mg/dL	Rise in BGLs** by +187.0 mg/dL	Rise in BGLs** by +185.5 mg/dL	Rise in BGLs** by +179.0 mg/dL	Rise in BGLs** by +156.3 mg/dL	Rise in BGLs** by +235.2 mg/dL	Rise in BGLs** by +217.3 mg/dL	Rise in BGLs** by +220.5 mg/dL	Rise in BGLs** by +193.0 mg/dL	Rise in BGLs** by +241.3 mg/dL
27 th	101.4±9.8	393.3±63.2 ^a	380.5±64.9 ^a	301.1±19.9 ^z	290.2±29.3 ^x	251.0±23.5 ^x	241.7±37.2 ^{x, y}	210.5±25.7 ^{x, q}	232.1±30.1 ^{x, e}	186.7±17.8 ^{x, φ}	167.0±18.4 ^{x, p}	143.1±25.9 ^{x, p}
		Decline in BGLs [#] by - 7.4 mg/dL	Decline in BGLs [#] by - 8.5 mg/dL	Decline in BGLs [#] by - 35.4 mg/dL	Decline in BGLs [#] by - 44.0 mg/dL	Decline in BGLs [#] by - 80.0 mg/dL	Decline in BGLs [#] by - 68.3 mg/dL	Decline in BGLs [#] by - 176.8 mg/dL	Decline in BGLs [#] by - 130.7 mg/dL	Decline in BGLs [#] by - 183.6 mg/dL	Decline in BGLs [#] by - 177.6 mg/dL	Decline in BGLs [#] by - 252.2 mg/dL
48 th	97.8±13.2	375.2±44.6 ^a	360.2±88.0 ^a	258.0±15.3 ^x	184.7±8.0 ^x	157.0±9.8 ^x	152.4±23.4 ^{x, e}	142.1±13.2 ^{x, e}	139.6±13.6 ^{x, e}	133.9±24.4 ^{x, e}	116.2±14.8 ^{x, r}	109.4±24.3 ^{x, r}
		Decline in BGLs [#] by - 24.8 mg/dL	Decline in BGLs [#] by - 28.8 mg/dL	Decline in BGLs [#] by - 78.5 mg/dL	Decline in BGLs [#] by - 149.5 mg/dL	Decline in BGLs [#] by - 174.0 mg/dL	Decline in BGLs [#] by - 157.6 mg/dL	Decline in BGLs [#] by - 245.2 mg/dL	Decline in BGLs [#] by - 223.2 mg/dL	Decline in BGLs [#] by - 236.4 mg/dL	Decline in BGLs [#] by - 228.4 mg/dL	Decline in BGLs [#] by - 285.9 mg/dL

*Increase in BGLs in comparison to 0th day; ** Increase in BGLs in comparison to 15th day; # Decrease in BGLs in comparison to 20th day; α, β, γ, indicate p<0.001, p<0.01, and p<0.05 in comparison to 0th day; a, b, c indicates p<0.001, p<0.01, and p<0.05 in comparison to normal control (G1); x, y, z indicates p<0.001, p<0.01, and p<0.05 in comparison to experimental control (G2); φ, Ξ, q indicates p<0.001, p<0.01 and p<0.05 in comparison to raw Gly (G5); e, f, g indicate p<0.001, p<0.01, and p<0.05 in comparison to raw VA (G4); p, q, r indicates p<0.001, p<0.01 and p<0.05 in comparison to physical mixture.

5.12.3 Body weight

The intake of HFD causes obesity in the body followed by number of metabolic complications leading to cardiovascular diseases, hyperlipidaemia, gut dysbiosis, and IR [357,368]. Similar observations were noted in case of rats receiving HFD treatment (G2-G12) for 15 days. In all these rats, significant ($p < 0.05$) rise in body weight (body wt.) was observed (**Table 5.21**). More than 50 g enhancement in body wt. of all these rats was observed. In contrast to this, a significant drop in body wt. of obese rats was observed on 27th day of the treatment as compared to the body wt. noted on 15th day. This effect was due to the administration of STZ on 16th day that caused frank hyperglycaemia (BGLs > 200 mg/dL). Incidentally no significant decrease ($p > 0.05$) in body wt. was observed on 20th day as that of 15th day because the rise in BGLs did not show its impact on body metabolism by the 20th day. However, continuous high BGLs over a period of ten days (i.e., day 18 to day 28) led to the alteration in body metabolism causing drop in the body weight, which is a typical sign of T2DM [357]. It is important to note that the treatment of test and control formulations started from 20th day onwards. Hence, the change in body wt. noted on 27th day was also dependent on the efficacy of the treatment. The drop in the body wt. on 27th day in comparison to 15th day was found in the following order as given below.

$G2(-1.72\text{-folds}) > G3(-1.48\text{-folds}) > G4(-1.34\text{-folds}) > G6 = G5(-1.28\text{-folds}) = G7 > G9(-1.23\text{-folds}) > G10(-1.23\text{-folds}) > G8(-1.19\text{-folds}) > G11(-1.12\text{-folds}) = G12(-1.12\text{-folds})$

When the body wt. of rats was tested on 34th, 41st and 48th day, a gradual increase in their body wt. was observed as compared to their body weights noted on 27th day. The improvement in body wt. of rats was based on efficacy of treatment (**Table 5.21 and Fig 5.28**). The rise in body wt. of rats as compared to day 27th was in the following order as given below.

$G10(+1.16\text{-folds}) > G9(+1.14\text{-folds}) > G8(+1.12\text{-folds}) > G12 = G7 = G6(+1.11\text{-folds}) > G11(+1.08\text{-folds}) > G5(+1.07\text{-folds}) > G4(+1.02\text{-folds})$

It is very pertinent and interesting to note here that the rise in body wt. of G11 and G12 rats were less as that of their body wt. on 27th day as compared to other rats. This was due to the fact that the formulation was found highly efficacious as that of other treatments. This can be easily observed from the fact that the drop in their body wt. between 15th day and 27th day was just 35.6g (G11) and 25.0g (G12) respectively. Owing to these observations, it was noted that the rats treated with low as well as high doses of co-loaded GV-APMs was able to manage the BGLs as well as body wt. post administration of STZ and 28 days' treatment of test formulations i.e., GV-APMs.

Table 5.21: Effect of different treatment groups on body weight upon weekly basis (Mean±SD, n=8)

Days	G1	G2	G3	G4	G5	G6	G7	G8	G9	G10	G11	G12
0 th	250.0±0.0	256.6±0.5	250.0±0.0	250.0±0.0	253.3±0.3	250.0±0.0	249.7±0.6	253.0±0.2	251.0±0.1	252.0±0.2	252.0±0.2	257.0±0.5
15 th	250.0±0.0	321.8±27.5 ^a *Increase in body wt. by +65.2g	303.1±22.5 ^c *Increase in body wt. by +53.1g	316.8±23.2 ^a *Increase in body wt. by +66.8g	310.0±28.1 ^c *Increase in body wt. by +57.0g	317.5±24.7 ^c *Increase in body wt. by+67.5g	298.1±25.3 ^c *Increase in body wt. by +48.4g	304.0±18.6 ^a *Increase in body wt.by+51.0g	331.0±42.4 ^a *Increase in body wt. by+80.0g	319.3±25.1 ^c *Increase in body wt.by+67.3g	325.6±26.2 ^a *Increase in body wt. by +73.6g	318.7±14.0 ^c *Increase in body wt. by +61.7g
20 th	253.7±5.1	313.7±26.0 **Decrease in body wt. by- 8.1g	290.6±26.7 **Decrease in body wt. by-12.5g	301.0±23.7 **Decrease in body wt. by -15.8g	297.8±18.4 **Decrease in body wt. by-12.2g	302.5±42.7 **Decrease in body wt. by-15.3g	261.8±28.2 **Decrease in body wt. by-36.2g	286.0±25.3 **Decrease in body wt. by -18.0g	316.2±19.2 **Decrease in body wt. by-14.8g	305.3±19.7 **Decrease in body wt. by-14.0g	303.1±20.8 **Decrease in body wt. by -22.5g	294.3±19.5 **Decrease in body wt. by -24.4g
27 th	256.8±5.3	186.2±53.9 **Decrease in body wt. by - 135.6g	196.7±18.8 ^{ns} **Decrease in body wt. by -99.3g	235.0±13.0 ^z **Decrease in body wt. by -63.8g	241.5±10.6 ^x **Decrease in body wt. by -68.5g	246.2±31.1 ^x **Decrease in body wt. by -71.3g	232.5±17.5 ^z **Decrease in body wt. by -65.6g	254.3±13.9 ^x **Decrease in body wt. by -49.7g	267.5±13.0 ^x **Decrease in body wt. by -63.5g	259.3±7.2 ^x **Decrease in body wt. by -60.0g	290.0±18.5 ^x **Decrease in body wt. by -35.6g	283.7±6.9 ^x ** Decrease in body wt. by -35.0g
48 th	259.9±6.3	165.4±47.1 #Decrease in body wt. by - 20.6g	173.4±19.2 ^{ns} #Decrease in body wt. by -29.6g	242.7±11.4 ^x #Decrease in body wt. by -7.7g	258.5±7.5 ^x #Decrease in body wt. by -17.0g	273.5±22.6 ^x #Decrease in body wt. by -27.3g	259.5±7.9 ^x #Decrease in body wt. by -27.0g	286.1±4.0 ^x #Decrease in body wt. by -31.8g	305.9±12.7 ^x #Decrease in body wt. by -38.4g	301.4±6.1 ^x #Decrease in body wt. by -42.1g	315.9±13.5 ^x #Decrease in body wt. by -30.9g	315.5±16.3 ^z #Decrease in body wt. by -31.8g

*Increase in body wt. in comparison to 0th day; **Decrease in body wt. in comparison to 15th day; # Decrease in body wt. in comparison to 27th day; a, b, c indicates p<0.001, p<0.01, and p<0.05 in comparison to normal control (G1); x, y, z indicates p<0.001, p<0.01, and p<0.05 in comparison to experimental control (G2)

5.12.4 Lipid profile

In the present study HFD was administered orally for 15 days to rats of G2 to G12 with objective to develop obesity, fatty liver, and hyperlipidaemia for the induction of IR leading to T2DM. The lipid profile of all the rats were determined on 0th day and 15th day to assess the increase in the lipid-based biochemical parameters. The test was also performed on 48th day to check the effect of different treatments (except G2 and G3) on decrease in elevated levels of CHL, TGs, LDL, VLDL, CHL/HDL, and LDL/HDL ratio, and an increase in the declined levels of HDL respectively. The results are shown in **Table 5.22** and **Fig 5.29**. Further the results of LDL, VLDL, CHL/HDL, and LDL/HDL ratio were determined using *equation (19) to (22)*. On 15th day, all the lipid-based biochemical parameters related were found elevated in all the groups except G1 and the level of HDL was found declined, indicating the successful development of hyperlipidaemia (Ref). On 48th day, the results of lipid-based biochemical parameters were found to be ameliorated than that of the results obtained on 15th day, except for rats of G2 and G3 respectively. However, the efficacy of each treatment was different based on the nature of the drugs as well as in the formulation.

The results were found significantly ($p < 0.05$) improved in the case of rats receiving nanocombination of the both the drugs in APMs (G11 and G12) in a dose-dependent manner. This indicated that the developed APMs enhanced the therapeutic efficacy of both the drugs by overcoming the challenges associated with poor solubility and faster elimination. Similar observation was observed for APMs containing VA and Gly during the pharmacokinetic study, wherein both the drugs showed enhanced oral bioavailability as that of their raw form as well as their alone administrations respectively. Interestingly, on 48th day, the efficacy of raw VA and VA-APMs were found better in lowering the levels of CHL, TGs, LDL, VLDL, CHL/HDL, and LDL/HDL ratio and elevating the levels of HDL as compared to rats receiving treatment of raw Gly alone and in the form of APMs respectively. This could be attributed to the anti-obesity and anti-hyperlipidaemic activity of VA that works by stimulating AMPK α - and thermogenesis in obese rats, increases hepatic phosphorylated acetyl Co-A carboxylase protein expression, and by reducing the levels of circulating leptin hormone secreted by adipose tissues [14,357]. Previous studies on VA also indicated its anti-hyperlipidaemic potential by reducing serum leptin hormone having direct co-relation with lipid utilization by the body [357].

Whereas, the rats receiving Gly showed comparatively lesser effect in lowering lipid-based biochemical parameters as that of VA. This could be due to the fact that Gly is an anti-hyperglycaemic drug and have no direct action on attenuation of lipid/CHL levels. The slight attenuation observed in the rats receiving Gly could be due to better maintenance of BGLs that would have led to restriction in dyslipidaemia. The combination therapy of VA and Gly either in their raw form or in the form of APMs showed significantly better attenuation of elevated lipid levels due to lipid lowering properties of VA and reduction of BGLs by both the drugs (i.e. Gly and VA) respectively.

Table 5.22: Effect of different treatment groups on lipid parameters on different days (Mean±SD, n=8)

Days	G1	G2	G3	G4	G5	G6	G7	G8	G9	G10	G11	G12
CHL level												
0 th	63.90±0.68	64.70±0.18	64.50±0.24	64.40±0.53	66.00±0.38	65.10±0.24	64.40±0.37	64.30±0.28	64.40±0.38	64.80±0.38	64.30±0.50	64.80±0.49
15 th	62.50±2.45	155.60±2.03 _{a, a}	146.00±6.08 _{a, a}	155.40±3.84 _{a, a}	157.10±3.17 _{a, a}	146.20±0.93 _{a, a}	157.10±1.19 _{a, a}	144.20±1.84 _{a, a}	147.10±1.03 _{a, a}	144.10±1.32 _{a, a}	148.00±0.65 _{a, a}	144.10±1.67 ^{a, a}
	NA	*Increased by +2.40-folds	*Increased by +2.20-folds	*Increased by +2.40-folds	*Increased by +2.30-folds	*Increased by +2.20-folds	*Increased by +2.40-folds	*Increased by +2.20-folds	*Increased by +2.20-folds	*Increased by +2.20-folds	*Increased by +2.30-folds	*Increased by +2.20-folds
48 th	64.80±0.39	178.60±0.79	166.00±0.14	112.30±0.62 ^x	131.30±3.48 ^x	101.90±4.11 ^x	101.60±5.73 _{x, g}	124.30±1.16 _{x, g}	88.70±2.03 ^x _f	108.50±4.71 _{x, ¥}	84.30±0.86 ^x _r	70.50±2.38 ^{x, q}
	NA	**Increased by +1.14-folds	**Increased by +1.13-folds	##Decreased by -1.38-folds	##Decreased by -1.19-folds	##Decreased by -1.43-folds	##Decreased by -1.54-folds	##Decreased by -1.16-folds	##Decreased by -1.65-folds	##Decreased by -1.32-folds	##Decreased by -1.75-folds	##Decreased by -2.04-folds
TGs level												
0 th	53.10±2.01	57.80±0.90	62.70±1.20	63.70±0.53	63.10±0.35	62.50±1.30	62.70±0.40	62.80±0.90	62.70±0.35	62.70±0.38	58.40±0.29	57.70±0.59
15 th	62.50±1.29	133.10±4.40 _{γ, a}	132.30±6.08 _{a, a}	136.40±3.84 _{a, a}	147.70±1.15 _{a, a}	134.50±2.21 _{a, a}	133.70±1.82 _{a, a}	134.00±2.01 _{a, a}	135.20±1.44 _{a, a}	141.50±0.75 _{a, a}	144.20±3.89 _{a, a}	139.50±1.21 ^{a, a}
	NA	*Increased by +2.30-folds	*Increased by +2.10-folds	*Increased by +2.14-folds	*Increased by +2.34-folds	*Increased by +2.15-folds	*Increased by +2.13-folds	*Increased by +2.13-folds	*Increased by +2.15-folds	*Increased by +2.25-folds	*Increased by +2.46-folds	*Increased by +2.41-folds
48 th	58.90±0.56	166.70±0.56	155.70±3.96	106.50±0.39 ^x	128.70±3.46 ^x	95.20±10.04 ^x	98.87±1.55 ^x _g	112.10±2.44 _{x, g}	87.10±0.72 ^x _f	103.10±7.37 _{x, Φ}	78.40±4.66 ^x _r	61.30±5.32 ^{x, p}
	NA	**Increased by +1.2-folds	**Increased by +1.1-folds	##Decreased by -1.2-folds	##Decreased by -1.1-folds	##Decreased by -1.4-folds	##Decreased by -1.3-folds	##Decreased by -1.19-folds	##Decreased by -1.55-folds	##Decreased by -1.37-folds	##Decreased by -1.83-folds	##Decreased by -2.27-folds
HDL level												
0 th	53.80±0.83	53.70±0.47	53.30±0.80	51.40±0.70	55.00±0.90	58.00±0.18	61.40±0.64	62.90±0.37	51.40±0.90	56.30±0.90	59.70±0.18	58.70±0.67
15 th	54.00±3.51	19.20±5.92 ^γ _b	15.80±4.68 _{β, a}	15.50±2.02 ^{β, a}	13.50±5.09 ^{a, a}	12.60±0.73 ^{a, a}	13.80±1.98 ^{a, a}	14.80±3.71 ^{a, a}	14.30±1.11 ^{β, b}	15.00±0.74 ^{a, a}	13.70±0.63 ^{a, a}	13.30±1.45 ^{a, b}
	NA	#Decreased by -2.70-folds	#Decreased by -3.30-folds	#Decreased by -3.32-folds	#Decreased by -4.03-folds	#Decreased by -4.50-folds	#Decreased by -4.41-folds	#Decreased by -4.23-folds	#Decreased by -3.54-folds	#Decreased by -3.71-folds	#Decreased by -4.30-folds	#Decreased by -4.32-folds
48 th	55.30±0.41	10.70±4.98	11.20±5.15	26.90±2.68 ^γ	20.70±3.36 ^z	34.80±1.83 ^γ	38.20±2.66 ^{x, g}	29.00±1.60 ^γ _¥	43.80±3.81 ^{x, e}	32.50±4.07 ^γ _¥	48.60±1.84 ^{x, q}	55.40±6.28 ^{x, q}
	NA	##Decreased by -1.79-folds	##Decreased by -1.41-folds	**Increased by +1.73-folds	**Increased by +1.53-folds	**Increased by +2.76-folds	**Increased by +2.47-folds	**Increased by +1.95-folds	**Increased by +2.71-folds	**Increased by +2.16-folds	**Increased by +3.25-folds	**Increased by +4.09-folds
LDL level												
0 th	9.40±0.87	9.40±0.77	8.60±0.31	10.30±1.04	10.40±0.71	9.60±0.53	10.90±0.61	10.20±0.48	10.40±0.71	10.40±0.71	9.50±0.48	9.40±0.32

15 th	10.20±5.78	57.80±5.29 ^a	59.60±5.73 ^a	64.10±1.48 ^a	61.50±5.71 ^a	64.70±0.77 ^a	61.40±2.40 ^a	59.90±5.43 ^a	62.60±1.15 ^a	60.70±1.06 ^a	61.50±0.94 ^a	62.00±1.07 ^{a, a}
				*Increased by +6.19-folds	*Increased by +5.89-folds	*Increased by +6.69-folds	*Increased by +5.59-folds	*Increased by +5.87-folds	*Increased by +5.99-folds	*Increased by +5.80-folds	*Increased by +6.44-folds	*Increased by +6.55-folds
48 th	NA	NA	NA									
	10.10±0.69	55.50±5.62	58.30±5.14	38.50±4.17 ^x	53.20±6.04 ^z	32.90±2.40 ^x	34.70±3.65 ^{xg}	48.20±4.35 ^z _e	26.50±2.91 ^{xf}	41.10±2.29 ^x _¥	20.50±2.30 ^{xr}	13.70±4.07 ^{xq}
				##Decreased by -1.66- folds	##Decreased by -1.15- folds	##Decreased by -1.96- folds	##Decreased by -1.67- folds	##Decreased by -1.20- folds	##Decreased by -2.35- folds	##Decreased by -1.47- folds	##Decreased by -2.99- folds	##Decreased by - 4.49-folds
	NA	NA	NA									
VLDL level												
0 th	9.10±0.40	9.50±0.18	8.50±0.24	8.60±0.11	9.20±0.07	10.50±0.26	9.70±0.08	8.50±0.18	7.30±0.07	8.20±0.07	10.10±0.06	9.40±0.12
15 th	12.50±0.26	18.60±0.88 ^{a,b}	18.40±1.22 ^{β,c}	19.50±0.77 ^{β,c}	19.30±0.23 ^{β,b}	18.90±0.24 ^{a,b}	18.80±0.36 ^{a,b}	18.70±0.40 ^{a,b}	19.20±0.29 ^{a,b}	19.00±0.15 ^{β,b}	18.80±0.78 ^{β,b}	18.70±0.24 ^{a,b}
				*Increased by +2.26-folds	*Increased by +2.09-folds	*Increased by +1.79-folds	*Increased by +1.94-folds	*Increased by +2.18-folds	*Increased by +2.53-folds	*Increased by +2.27-folds	*Increased by +1.85-folds	*Increased by +1.97-folds
48 th	NA	NA	NA									
	11.50±0.11	19.30±0.79	18.70±0.08	15.00±2.00 ^y	17.30±0.69 ^z	12.00±0.31 ^z	11.00±0.49 ^{yg}	13.40±0.14 ^{ys} _e	10.40±1.47 ^{ys} _g	11.60±0.93 ^{ys} _¥	9.200±1.06 ^{yr}	7.20±0.78 ^{ysq}
				##Decreased by -1.32- folds	##Decreased by -1.11- folds	##Decreased by -1.56- folds	##Decreased by -1.70- folds	##Decreased by -1.39- folds	##Decreased by -1.84- folds	##Decreased by -1.63- folds	##Decreased by -2.04- folds	##Decreased by - 2.59-folds
	NA	NA	NA									
CHL/HDL ratio												
0 th	1.10±1.46	1.20±0.02	1.26±0.01	1.22±0.03	1.10±0.03	1.13±0.01	1.02±0.02	1.06±0.02	1.20±0.03	1.10±0.03	1.02±0.01	1.10±0.01
15 th	1.22±0.42	8.10±2.03 ^{β,b}	9.90±1.65 ^{a,a}	9.90±0.98 ^{a,b}	11.60±1.50 ^{a,a}	11.50±0.42 ^{a,a}	11.30±1.11 ^{a,a}	9.60±1.72 ^{β,b}	10.20±0.56 ^{β,b}	9.50±0.29 ^{β,b}	10.70±0.30 ^{a,a}	11.20±0.69 ^{β,b}
				*Increased by +7.97-folds	*Increased by +9.70-folds	*Increased by +10.31-folds	*Increased by +10.84-folds	*Increased by +9.48-folds	*Increased by +8.18-folds	*Increased by +8.34-folds	*Increased by +9.99-folds	*Increased by +9.77-folds
48 th	NA	NA	NA									
	1.31±0.02	15.32±0.61	14.70±0.17	4.10±0.06 ^x	6.30±0.19 ^x	3.90±0.04 ^x	2.90±0.08 ^{xg}	4.20±0.07 ^{x,e}	2.13±0.09 ^{xf}	3.30±0.07 ^{x,¥}	1.80±0.05 ^{xr}	1.18±0.14 ^{xr}
				##Decreased by -2.05- folds	##Decreased by -1.84- folds	##Decreased by -2.94- folds	##Decreased by -3.89- folds	##Decreased by -2.28- folds	##Decreased by -4.63- folds	##Decreased by -2.87- folds	##Decreased by -5.94- folds	##Decreased by - 8.91-folds
	NA	NA	NA									
LDL/HDL ratio												
0 th	0.17±0.02	0.17±0.02	0.16±0.01	0.20±0.03	0.18±0.02	0.16±0.01	0.17±0.02	0.16±0.01	0.20±0.02	0.18±0.02	0.15±0.01	0.16±0.01
15 th	0.18±0.35	3.01±1.59 ^{β,b}	3.75±1.37 ^{a,a}	4.11±0.78 ^{β,b}	4.56±1.21 ^{a,a}	5.13±0.34 ^{β,b}	4.44±0.09 ^{a,a}	4.03±1.40 ^{a,a}	4.35±0.43 ^{β,b}	4.04±0.23 ^{y,b}	4.47±0.23 ^{β,a}	4.63±0.53 ^{a,a}
	NA	*Increased by +17.10-folds	*Increased by +23.12-folds	*Increased by +20.47-folds	*Increased by +24.02-folds	*Increased by +30.78-folds	*Increased by +24.87-folds	*Increased by +24.88-folds	*Increased by +21.46-folds	*Increased by +21.77-folds	*Increased by +28.00-folds	*Increased by +28.82-folds
48 th	0.18±0.02	5.17±0.51	5.17±0.14	1.42±0.09 ^z	2.57±0.16 ^y	0.94±0.04 ^y	1.07±0.07 ^{ys, f}	1.71±0.15 ^{ys, e}	0.68±0.09 ^{ys, f}	1.26±0.06 ^{ys, ¥}	0.46±0.05 ^{ysq}	0.25±0.12 ^{ys, p}

NA	**Increased by +1.71- folds	**Increased by +1.37- folds	##Decreased by -2.88- folds	##Decreased by -1.77- folds	###Decreased by -5.44- folds	###Decreased by -4.15- folds	###Decreased by -2.34- folds	###Decreased by -6.37- folds	###Decreased by -3.19- folds	###Decreased by -9.73- folds	###Decreased by - 18.31-folds
----	-----------------------------------	-----------------------------------	-----------------------------------	-----------------------------------	------------------------------------	------------------------------------	------------------------------------	------------------------------------	------------------------------------	------------------------------------	----------------------------------

*Increase in the levels of CHL, TGs, LDL, VLDL, CHL/HDL and LDL/HDL ratio on 15th day in comparison to 0th day; **Increase in the levels of CHL, TGs, HDL, LDL/HDL ratio on 48th day in comparison to 15th day; #Decrease in the level of HDL on 15th day in comparison to 0th day; ##Decrease in the levels of CHL, TGs, HDL, LDL, VLDL, CHL/HDL, and LDL/HDL ratio on 48th day in comparison to 15th day respectively

α , β , γ , indicate $p < 0.001$, $p < 0.01$, and $p < 0.05$ in comparison to 0th day; a, b, c indicates $p < 0.001$, $p < 0.01$, and $p < 0.05$ in comparison to normal control (G1); x, y, z indicates $p < 0.001$, $p < 0.01$, and $p < 0.05$ in comparison to experimental control (G2); Φ , Ψ , ϱ indicates $p < 0.001$, $p < 0.01$ and $p < 0.05$ in comparison to raw Gly (G5); e, f, g indicates $p < 0.001$, $p < 0.01$, and $p < 0.05$ in comparison to raw VA (G4); p, q, r indicates $p < 0.001$, $p < 0.01$ and $p < 0.05$ in comparison to physical mixture (G6).

5.12.5 Hepatic and renal markers

Continuous administration of HFD causes hyperlipidaemia leading to fatty liver followed by alteration in liver metabolic enzymes. Certain studies reported the co-relation of hepatic IR with elevated SGPT, SGOT and ALP levels owing to HFD in obese/overweight population without frank hyperglycaemia [369]. Therefore, obesity is a main contributing factor of hepatic IR that amplifies the detrimental effects of IR on the liver functions [369].

In addition to this, hyperglycaemia being a major characteristic of T2DM is reported to cause serious complications in the diabetic patients if not controlled. Most prevalent one is the alterations in renal markers such as creatinine and urea due to the reduced functioning of kidneys filtering system in diabetics. With agreement to this, similar observations were observed in our study, after the complete induction of T2DM followed by HFD administration and low dose of STZ in the rats of each groups. However, in the treatment groups reduction in the hepatic and renal markers was found based upon the therapeutic efficacy of different treatments.

Similar to the results of lipid profile, on terminal day (48th day) of the study, the levels of SGPT, SGOT, ALP, creatinine and urea were found high in case of G2 and G3 rats and normal in case of rats of G4 to G12, as compared to rats of G2. However, a significant decrease ($p < 0.05$) in enzymes level was observed in case of rats receiving treatment of APMs of single drugs (VA-APMs and Gly-APMs) and their nanocombination (GV-APMs) i.e., from G7 to G12. The values of SGPT, SGOT and ALP for all the twelve groups and their fold decrease with respect to G2 are given in **Table 5.23**. In these cases, also the potential of VA in lowering the enzyme levels was found high as compared to Gly owing to the antioxidant, anti-obesity and anti-hyperglycaemic potential of VA as it can via multiple targets. However, Gly has shown its indirect action by maintaining glucose homeostasis in rats. The nanocombination therapy was found highly effective owing to the multiple health benefits of VA and Gly. Therefore, the decrease in the hepatic and renal markers by the different treatments was found in a following order as given below.

$$G1 > G12 > G11 > G9 > G6 > G7 > G10 > G4 > G8 > G5 > G2 = G3$$

Table 5.23: Effect of different treatments on hepatic/renal markers on 48th day (Mean±SD, n=8)

Hepatic/renal markers	G1	G2	G3	G4	G5	G6	G7	G8	G9	G10	G11	G12
SGPT	46.2±1.04	97.4±1.18	92.2±0.93 ^{ns}	66.5±0.11 ^x	78.3±0.57 ^x	58.1±1.67 ^x	62.4±3.21 ^{x, f}	69.8±2.88 ^{x, e}	56.7±3.06 ^{x, g}	63.1±2.13 ^{x, Φ}	47.2±1.46 ^{x, e}	40.5±0.48 ^{x, e}
	NA	NA	NA	##Decreased by -1.46-folds	##Decreased by -1.24-folds	##Decreased by -1.67-folds	##Decreased by -1.56-folds	##Decreased by -1.39-folds	##Decreased by -1.71-folds	##Decreased by -1.54-folds	##Decreased by -2.06-folds	##Decreased by -2.40-folds
SGOT	28.3±2.55	69.8±0.27	71.6±1.20 ^{ns}	47.0±1.37 ^x	61.0±0.23 ^z	40.0±1.22 ^x	40.3±2.02 ^{x, g}	51.1±0.87 ^{x, e}	37.1±3.44 ^{x, e}	46.2±1.85 ^{x, Φ}	36.6±1.93 ^{x, r}	30.1±4.22 ^{x, r}
	NA	NA	NA	##Decreased by -1.48-folds	##Decreased by -1.14-folds	##Decreased by -1.74-folds	##Decreased by -1.73-folds	##Decreased by -1.36-folds	##Decreased by -1.88-folds	##Decreased by -1.51-folds	##Decreased by -1.90-folds	##Decreased by -2.31-folds
ALP	42.8±1.71	97.9±1.36	94.6±0.78 ^{ns}	61.6±2.76 ^x	72.8±3.17 ^x	55.7±0.06 ^x	58.2±1.51 ^{x, g}	66.5±0.06 ^{x, e}	50.1±2.66 ^{x, f}	60.0±1.33 ^{x, e}	45.6±2.11 ^{x, r}	39.8±3.66 ^{x, r}
	NA	NA	NA	##Decreased by -1.58-folds	##Decreased by -1.34-folds	##Decreased by -1.75-folds	##Decreased by -1.68-folds	##Decreased by -1.47-folds	##Decreased by -1.95-folds	##Decreased by -1.63-folds	##Decreased by -2.14-folds	##Decreased by -2.45-folds
Creatinine	0.36±0.34	0.78±1.87	0.73±0.51 ^{ns}	0.58±0.23 ^z	0.67±1.88 ^y	0.49±0.82 ^x	0.52±0.03 ^y	0.59±0.51 ^{z, e}	0.45±2.20 ^z	0.56±2.07 ^{z, e}	0.41±1.12 ^{z, r}	0.31±0.02 ^{z, q}
	NA	NA	NA	##Decreased by -1.34-folds	##Decreased by -1.21-folds	##Decreased by -1.59-folds	##Decreased by -1.50-folds	##Decreased by -1.30-folds	##Decreased by -1.73-folds	##Decreased by -1.39-folds	##Decreased by -1.90-folds	##Decreased by -2.51-folds
Urea	24.62±2.02	62.40±0.67	65.80±0.32	47.52±1.71 ^z	53.30±1.02 ^z	40.86±0.71 ^x	42.64±1.31 ^x	46.78±0.83 ^{z, ¥}	36.52±2.16 ^x	41.36±3.65 ^{x, Φ}	32.27±1.28 ^{x, r}	26.17±0.19 ^{x, r}
	NA	NA	^{ns} NA	##Decreased by -1.31-folds	##Decreased by -1.17-folds	##Decreased by -1.52-folds	##Decreased by -1.46-folds	##Decreased by -1.33-folds	##Decreased by -1.70-folds	##Decreased by -1.50-folds	##Decreased by -1.93-folds	##Decreased by -2.38-folds

##Decrease in hepatic and renal markers with respect on G2; x, y, z indicates p<0.001, p<0.01, p<0.05 in comparison to G2; Φ, ¥, q indicates p<0.001, p<0.01 and p<0.05 in comparison to raw Gly (G5); e, f, g indicates p<0.001, p<0.01, and p<0.05 in comparison to raw VA (G4); p, q, r indicates p<0.001, p<0.01 and p<0.05 in comparison to G6.

5.12.6 Serum inflammatory markers

Inflammatory condition in diabetic rats is found to be in a positive co-relation with HFD consumption that is considered to be a contributing factor in the development of IR in rats [357]. In addition, the low dose of STZ used in this model is also a chief factor that causes oxidative stress-induced activation of inflammatory signalling in diabetic rats [370]. With agreement to this, the serum inflammatory markers viz. TNF- α and IL-6 were found to be elevated in the rats of experimental control group and placebo group i.e., G2 and G3. However, the administration of different treatment groups based on their efficacy and dose reduced the level of inflammatory markers in a following order as given below.

$$G1 > G12 > G11 > G10 > G9 > G8 > G7 > G6 > G5 > G4 > G2 = G3$$

Similar to the results of hepatic and renal markers on terminal day of the study, the levels of serum inflammatory markers were found normal in case of G1. Whereas in treatment groups i.e., from G4 to G12, a significant difference ($p < 0.05$) was observed in the levels of inflammatory markers in comparison to G2 respectively. However, a significant decrease in the cytokines levels (TNF- α and IL-6) was observed in case of rats receiving single drug loaded APMs (VA-APMs and Gly-APMs) and their nanocombination therapy (GV-APMs) i.e., from G7 to G12, respectively. The results obtained for each treatment groups in reducing the serum TNF- α and IL-6 levels along with their fold reduction in comparison to G2 is presented in **Table 5.24**. The results obtained indicated higher potential of VA in lowering serum cytokines levels than that of Gly that could be due to its natural antioxidant and anti-inflammatory activity i.e., by modulating nrf2/NF- κ B pathway [14]. In case of Gly, the reduction in serum cytokine levels with respect to G2 has been achieved due to its anti-hyperglycaemic activity. Therefore, the effect of nanocombination therapy at high dose i.e., G12 (GV-APMs) was found highly effective among all the different treatment groups owing to multiple health benefits of VA used in combination with Gly. In addition, the combination of both the drugs in nanoform provided higher absorption, higher mean residence time in the systemic circulations, and controlled-release property leading to higher oral bioavailability of both the drugs [371]. Overall, the administration of nanocombination therapy provided higher therapeutic efficacy than their individual APMs and raw drugs respectively. Hence indicated improved additive pharmacological interaction than their physical mix used.

Table 5.24: Effect of different treatments on serum inflammatory markers on 48th day (Mean±SD, n=8)

Groups	Mean ±SD (TNF-α)	Fold-decreased ^{##} (TNF-α)	Mean ±SD (IL-6)	Fold-decreased ^{##} (IL-6)
G1	6.8±0.3	NA	8.7±0.8	NA
G2	33.5±1.2	NA	44.6±2.6	NA
G3	32.4±0.4 ^{ns}	NA	46.3±0.3 ^{ns}	NA
G4	17.4±1.5 ^x	1.9	26.5±0.2 ^x	1.6
G5	25.3±0.1 ^x	1.3	32.6±0.5 ^x	1.3
G6	14.4±1.1 ^x	2.2	21.4±0.8 ^x	2.1
G7	15.3±0.1 ^{x, f}	1.1	20.2±1.4 ^{x, g}	1.3
G8	19.8±3.2 ^{x, q}	1.2	26.3±2.0 ^{x, q}	1.2
G9	14.6±0.4 ^{x, f}	0.9	15.8±1.0 ^{x, g}	1.3
G10	16.1±1.8 ^{x, Φ}	0.9	19.6±2.0 ^{x, q}	1.0
G11	11.4±1.6 ^{x, r}	1.7	12.0±2.1 ^{x, r}	2.1
G12	7.2±2.9 ^{x, p}	2.0	9.1±3.1 ^{x, r}	1.7

^{##}Decrease in TNF-α and IL-6 level with respect to G2; x, y, z indicates p<0.001, p<0.01, p<0.05 in comparison to G2; Φ, ¥, q indicates p<0.001, p<0.01 and p<0.05 in comparison to raw Gly (G5); e, f, g indicates p<0.001, p<0.01, and p<0.05 in comparison to raw VA (G4); p, q, r indicates p<0.001, p<0.01 and p<0.05 in comparison to physical mixture (G6).

5.12.7 Pancreatic oxidative stress

STZ being a cytotoxic agent causes degeneration of pancreatic β-cells leading to decreased insulin production i.e., frank hyperglycaemia followed by abnormal glucose homeostasis. Pancreatic β-cells are highly vulnerable towards oxidative stress due to their lower antioxidant capacity and higher metabolic activity [372]. Due to their vulnerability, STZ injection promotes generation of reactive oxygen species in pancreatic cells along with mitochondrial dysfunction that contributes in its cytotoxic effect. Hence, results in impairment of redox metabolism [373]. With this context, in the present study, reduction in the antioxidant enzymes i.e., CAT, GSH and elevated TBARS level was observed in experimental control group and placebo i.e., G2 and G3. Whereas, it was found normal in case of normal control group i.e., G1.

At the terminal day of the present study, significant difference (p<0.05) in CAT, GSH and TBARS levels was observed in all the treatment groups i.e., from G4 to G12. The results obtained in each treatment groups are presented in **Table 5.25**. The results clearly indicated higher antioxidant potential of the nanocombination therapy with respect to single drugs loaded in APMs, their raw form and their physical mixture, respectively. This increment in their antioxidant efficacy was attributed to the use of VA in combination with Gly in nanoform that overcome the challenge of rapid elimination of VA from plasma. As a result, provided enough time to the drug for interacting with the biological targets leading to enhanced

therapeutic efficacy than their raw forms respectively. The improvement in the CAT, GSH and TBARS level by the different treatment groups based on their efficacy and dose is shown in a following order as given below.

G1>G12>G11>G9>G10>G7>G6>G8>G4>G5>G2=G3

Table 5.25: Effect of different treatment groups on pancreatic oxidative markers on 48th day (Mean±SD, n=8)

Groups	Mean±SD (CAT)	Fold-increased** (CAT)	Mean±SD (GSH)	Fold-increased** (GSH)	Mean±SD (TBARS)	Fold-decreased### (TBARS)
G1	97.0±0.1	NA	80.0±1.0	NA	1.9±0.1	NA
G2	23.0±1.2	NA	16.0±2.4	NA	7.7±1.1	NA
G3	26.0±2.0	NA	20.0±1.5	NA	7.4±0.4	NA
G4	51.0±2.7 ^z	2.2	47.0±1.1 ^z	2.9	4.0±0.2 ^z	1.9
G5	45.0±1.8 ^z	1.9	35.0±1.6 ^z	2.1	5.6±1.5 ^z	1.3
G6	60.0±1.6 ^z	2.6	54.0±2.3 ^x	3.3	3.2±0.8 ^z	2.4
G7	63.0±2.3 ^{z, g}	2.7	58.0±2.0 ^{x, f}	3.6	3.0±1.2 ^{z, g}	2.5
G8	55.0±2.1 ^{z, e}	2.3	43.0±1.1 ^{z, ¥}	2.6	4.7±1.0 ^{z, e}	1.6
G9	71.0±1.4 ^{x, f}	3.0	65.0±2.9 ^{x, g}	4.0	2.7±0.4 ^{z, g}	2.8
G10	64.0±2.9 ^{z, Φ}	2.7	55.0±1.4 ^{x, e}	3.4	3.1±2.3 ^{z, e}	2.4
G11	89.0±1.5 ^{x, r}	3.8	68.0±1.0 ^{x, q}	4.2	1.7±2.2 ^{z, q}	4.3
G12	95.0±1.2 ^{x, r}	4.1	76.0±0.1 ^{x, r}	4.7	1.1±1.9 ^{z, r}	7.0

**Increase in CAT/GSH level with respect to G2; ##Decrease in level of TBARS with respect to G2; x, y, z indicates p<0.001, p<0.01, p<0.05 in comparison to G2; Φ, ¥, e indicates p<0.001, p<0.01 and p<0.05 in comparison to raw Gly (G5); e, f, g indicates p<0.001, p<0.01, and p<0.05 in comparison to raw VA (G4); p, q, r indicates p<0.001, p<0.01 and p<0.05 in comparison to physical mixture (G6).

5.13 Histopathology study

The results of histopathological study are presented in *Table 5.26*.

Table 5.26: Summary of histopathological changes in different treatment groups.

Groups	Pancreas	Liver
NC	Normal proliferating pancreatic islet that are closely packed with patent acini	No abnormalities observed in the liver in terms of histoarchitecture Hepatocytes were arranged in anatomizing cords radiating from the center to periphery
EC	Destructed and shrunken pancreatic islets along with vacuolar changes	Extensive cytoplasmic vacuolation in liver cells with cellular infiltrations around the central veins
Placebo	Destructed pancreatic islets in terms of size and number along with vacuolar enlargement	Severe vacuolar changes with cellular infiltrations between hepatocytes
Raw Gly	Partly recovered destructed pancreatic islets with reduced fat deposits	Mild congestion in the central veins with restoration of hepatocytes
Raw VA	Slightly recovered destructed pancreatic islet cells with higher reduction in fat deposits	Preservation of hepatocytes with minimal lipid droplets or cytoplasmic vacuoles
Gly-VA	Good recovery in destructed pancreatic islet cells with minimal fat deposits	Good congestion in the central veins with reduction in small lipid droplets
Gly-APMs (LD)	Good recovery in destructed pancreatic islet cells with lower fat deposits	Higher reduction in the multiple cytoplasmic vacuoles formed in hepatocytes
Gly-APMs (HD)	Excellent recovery in destructed pancreatic islet cells with very less fat deposits	Excellent shrinkage observed in the lipid droplets with few cellular infiltrations
VA-APMs (LD)	Good recovery in destructed pancreatic islet cells with lower fat deposits	Higher shrinkage in the central vacuole and multiple small cytoplasmic vacuolation in hepatocytes
VA-APMs (HD)	Excellent recovery in destructed pancreatic islet cells with good reduction in the number of fat vacuoles	Minimal fatty liver changes with higher congestion in central veins
GV-APMs (LD)	High density in the number of recovered destructed pancreatic islet cells with minimal fat deposits	Excellent restoration of the hepatocyte cytoplasm with fewer lipid droplets
GV-APMs (HD)	Excellent amelioration in the recovery of destructed pancreatic islet cells with no sign of fat deposits, vascular congestion and apoptosis	Excellent shrinkage in the size of lipid droplets with complete restoration of hepatic cells

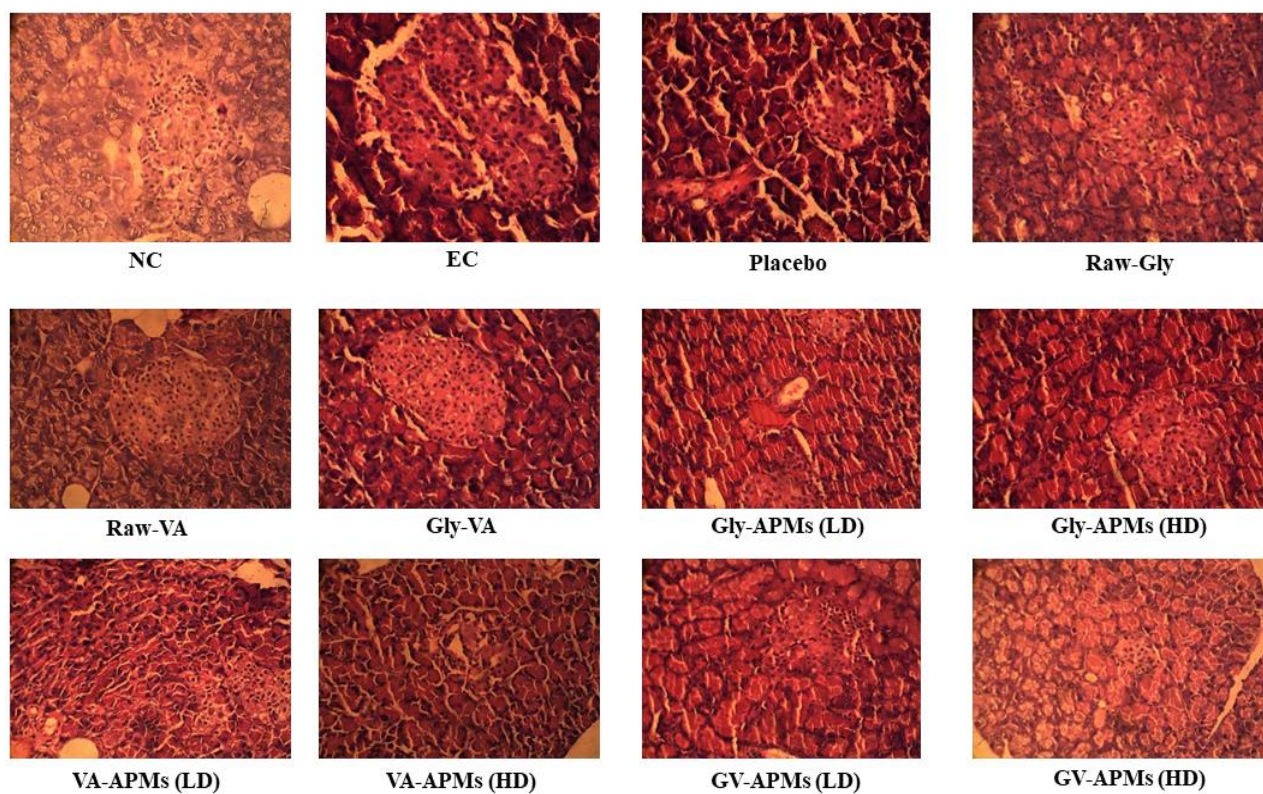


Fig 5.27: Histopathological images of pancreas for all treatment groups

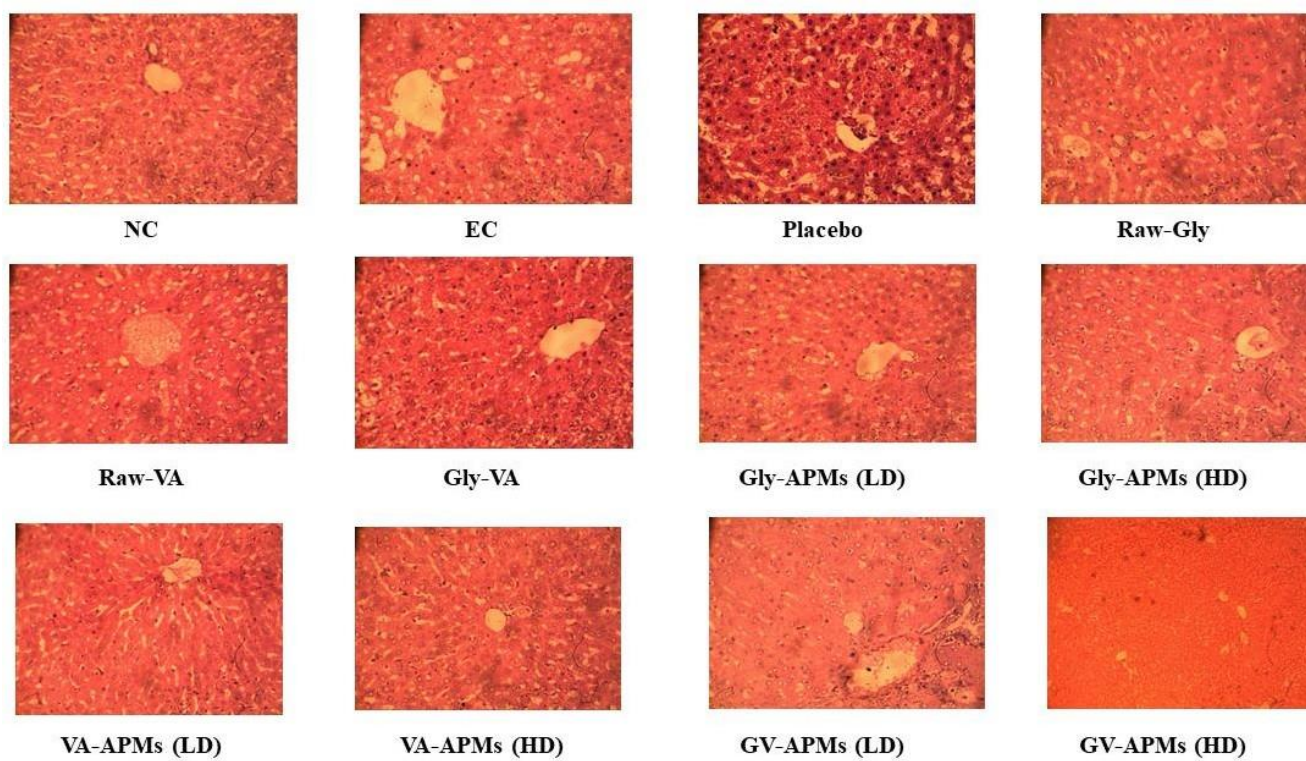


Fig 5.28: Histopathological images of liver for all treatment groups

Chapter 6
***Conclusion and
future perspective***

6.0 Conclusion and future perspective

The current study was designed with objective to overcome the common challenges associated with the anti-diabetic drug regimens including regimen complexity, secondary complications and dosing frequency. With such objectives, we used the combination of a natural product (VA) with a synthetic anti-diabetic drug (Gly) for the effective treatment of T2DM. The study was commenced with a hypothesis to provide synergistic and prolonged glycaemic control using VA in combination with Gly with potential to halt the side-effects and secondary CV complications associated with it. VA was selected based on its multiple therapeutic benefits such as anti-obesity, anti-hyperglycaemic, anti-inflammatory, anti-oxidant, anti-hyperlipidaemic etc., which has not been explored in combination with other anti-diabetic drugs till now. In addition, VA-APMs are also being reported for the first time for the treatment of T2DM either alone or, in combination with Gly.

To achieve the aforementioned objective, a nano-combination therapy containing VA and Gly was developed using APMs (GV-APMs) via LAP method by surfactant-copolymer (CTAB-mPEG-b-PCL) system. An attempt has been made to explore the use of mPEG-b-PCL copolymer based APMs with CTAB as a steric stabilizer for the entrapment of VA and Gly to enhance their oral bioavailability as well as efficacy to treat T2DM. The APMs were designed by applying BBD using drug to copolymer, drug to surfactant and solvent to antisolvent ratio as independent variables and particle size, EE, zeta potential and PDI as responses. This optimized composition was utilized to enhance the dissolution rate of the poorly water-soluble Gly and VA. The incorporation of CTAB along with the copolymer demonstrated to be effective nanocarriers as it provided good dispersion to the particles in the micellar system with smaller particle size and very good zeta potential. In addition to this, the APMs provided higher hydrophobicity to the micellar core, which resulted in higher drug entrapment and loading efficiency. The change in the concentration of the synthesized copolymer highly influenced the particle size of the APMs. Therefore, this indicated that formulation related parameters could be controlled by optimizing the process variables. This will help in the better understanding of the correlation between process variables and the physicochemical traits of the APMs.

The dissolution of lipophilic drug Gly was remarkably enhanced in a pH-dependent manner when loaded into the PCL core of the GV-APMs in comparison to raw Gly, a physical mixture with VA and Gly-APMs. This could be because of the influence of polar hydroxyl groups of the VA along with PEG corona in GV-APMs and greater hydrophobic interactions. Whereas the release of VA from GV-APMs was found to be more sustained than that of the raw VA, physical mixture and VA-APMs respectively. However, this effect was based on the hydrophobic interactions with CTAB/PCL, which provided a controlled release profile.

The co-loading of both the drugs in optimized APMs exhibited additive glucose-lowering activity ($p < 0.05$) than that of their raw forms, physical mixture and single drug loaded APMs respectively. In addition to this, exhibited lower cytotoxicity on Caco-2/HepG2 cells within the test concentration. Such increment in their glucose lowering effect was attributed to significant enhancement in their oral bioavailability upon loading into APMs i.e., 868% for Gly and 87% for VA with higher mean residence time in systemic circulations than their raw forms respectively. The developed APMs have shown significant improvement in oral bioavailability of VA and Gly either alone or in combination owing to sustained release profile, higher C_{max} , MRT and AUC as compared to their unprocessed forms. The enhancement in bioavailability of VA and Gly loaded in GV-APMs was 10.70- and 1362.80-folds as compared to raw form, and 2.89- and 840.7-folds than their physical mix respectively. In fact, a good correlation between in vitro release profile and pharmacokinetic profile was observed.

Further, due to the enhanced oral bioavailability, GV-APMs showed significant decrease in the levels of blood glucose, LDL, VLDL, TG, TC, SGOT, SGPT, ALP, urea, creatinine, IL-6 and TNF- α in HFD- low dose STZ induced rat model. Even the DM induced rats receiving combination therapy of GV-APMs at low as well high doses (G-11 and G12) have shown good recovery in the tissue architecture of liver and pancreas as compared to any other treatment groups receiving monotherapy of VA and Gly in their unprocessed form or, in the form of APMs, indicating the superiority of GV-APMs.

The developed herbal-synthetic drug combination therapy in nano form has been found successful in treating diabetes owing to multiple mechanistic pathways of VA and glucose lowering potential of Gly. These positive outcomes during preclinical studies provided a proof of concept to explore this formulation a pilot scale and conduct clinical studies for better assessment of therapeutic efficacy of GV-APMs. This study provides

future insights to check the effect of this combination therapy at molecular level as well as its efficacy in managing other diabetic complications owing to the multifaceted role of VA. Further, the developed combination can be used for its antidiabetic potential for the effective management of prolonged hyperglycemic condition at pre-clinical and clinical level in near future.

References

- [1] S. Alam, M.K. Hasan, S. Neaz, N. Hussain, M.F. Hossain, T. Rahman, Diabetes Mellitus: Insights from Epidemiology, Biochemistry, Risk Factors, Diagnosis, Complications and Comprehensive Management, *Diabetology*. 2 (2021) 36–50. <https://doi.org/10.3390/diabetology2020004>.
- [2] J. Upadhyay, S.A. Polyzos, N. Perakakis, B. Thakkar, S.A. Paschou, N. Katsiki, P. Underwood, K.H. Park, J. Seufert, E.S. Kang, E. Sternthal, A. Karagiannis, C.S. Mantzoros, Pharmacotherapy of type 2 diabetes: An update, *Metabolism*. 78 (2018) 13–42. <https://doi.org/10.1016/j.metabol.2017.08.010>.
- [3] M. Abdul, B. Khan, M.J. Hashim, J.K. King, R.D. Govender, H. Mustafa, J. Al Kaabi, Epidemiology of Type 2 Diabetes – Global Burden of Disease and Forecasted Trends, *J. Epidemiol. Glob. Health*. 10 (2020) 107–111.
- [4] D. Care, S.S. Suppl, 2. Classification and diagnosis of diabetes: Standards of medical care in diabetes-2021, *Diabetes Care*. 44 (2021) S15–S33. <https://doi.org/10.2337/dc21-S002>.
- [5] A. Chaudhury, C. Duvoor, V.S. Reddy Dendi, S. Kraleti, A. Chada, R. Ravilla, A. Marco, N.S. Shekhawat, M.T. Montales, K. Kuriakose, A. Sasapu, A. Beebe, N. Patil, C.K. Musham, G.P. Lohani, W. Mirza, Clinical Review of Antidiabetic Drugs: Implications for Type 2 Diabetes Mellitus Management, *Front. Endocrinol. (Lausanne)*. 8 (2017). <https://doi.org/10.3389/fendo.2017.00006>.
- [6] J.S. Patil, P.B. Patil, P. Sonawane, J.B. Naik, Design and development of sustained-release glyburide-loaded silica nanoparticles, *Bull. Mater. Sci*. 40 (2017) 263–270. <https://doi.org/10.1007/s12034-017-1369-1>.
- [7] H. Danafar, H. Jaberizadeh, S. Andalib, In vitro and in vivo delivery of gliclazide loaded mPEG-PCL micelles and its kinetic release and solubility study, *Artif. Cells, Nanomedicine Biotechnol*. 46 (2018) 1625–1636. <https://doi.org/10.1080/21691401.2017.1386191>.
- [8] A. Gedawy, J. Martinez, H. Al-Salami, C.R. Dass, Oral insulin delivery: existing barriers and current counter-strategies, *J. Pharm. Pharmacol*. 70 (2018) 197–213. <https://doi.org/10.1111/jphp.12852>.
- [9] S. Padhi, A.K. Nayak, A. Behera, Type II diabetes mellitus: a review on recent drug based therapeutics, *Biomed. Pharmacother*. 131 (2020) 110708. <https://doi.org/10.1016/j.biopha.2020.110708>.

- [10] G.R. Kokil, R.N. Veedu, G.A. Ramm, J.B. Prins, H.S. Parekh, Type 2 Diabetes Mellitus: Limitations of Conventional Therapies and Intervention with Nucleic Acid-Based Therapeutics, *Chem. Rev.* 115 (2015) 4719–4743.
<https://doi.org/10.1021/cr5002832>.
- [11] S. Chatterjee, K. Khunti, M.J. Davies, Type 2 diabetes, 2nd ed., Elsevier Inc., 2017. [https://doi.org/10.1016/S0140-6736\(17\)30058-2](https://doi.org/10.1016/S0140-6736(17)30058-2).
- [12] D. Sola, L. Rossi, G.P.C. Schianca, P. Maffioli, M. Bigliocca, R. Mella, F. Corlianò, G. Paolo Fra, E. Bartoli, G. Derosa, Sulfonylureas and their use in clinical practice, *Arch. Med. Sci.* 11 (2015) 840–848.
<https://doi.org/10.5114/aoms.2015.53304>.
- [13] A.J. Garber, D.S. Donovan, P. Dandona, S. Bruce, J.S. Park, Efficacy of glyburide/metformin tablets compared with initial monotherapy in type 2 diabetes, *J. Clin. Endocrinol. Metab.* 88 (2003) 3598–3604.
<https://doi.org/10.1210/jc.2002-021225>.
- [14] J. Kaur, M. Gulati, S.K. Singh, G. Kuppusamy, B. Kapoor, V. Mishra, S. Gupta, M.F. Arshad, O. Porwal, N.K. Jha, M.V.N.L. Chaitanya, D.K. Chellappan, G. Gupta, P.K. Gupta, K. Dua, R. Khursheed, A. Awasthi, L. Corrie, Discovering multifaceted role of vanillic acid beyond flavours: Nutraceutical and therapeutic potential, *Trends Food Sci. Technol.* 122 (2022) 187–200. <https://doi.org/10.1016/j.tifs.2022.02.023>.
- [15] F. Ul Amin, S.A. Shah, M.O. Kim, Vanillic acid attenuates A β 1-42-induced oxidative stress and cognitive impairment in mice, *Sci. Rep.* 7 (2017) 1–15.
<https://doi.org/10.1038/srep40753>.
- [16] J. Gong, S. Zhou, S. Yang, Vanillic acid suppresses HIF-1 α expression via inhibition of mTOR/p70S6K/4E-BP1 and Raf/MEK/ERK pathways in human colon cancer HCT116 cells, *Int. J. Mol. Sci.* 20 (2019) 1–18.
<https://doi.org/10.3390/ijms20030465>.
- [17] W.C. Chang, J.S.B. Wu, C.W. Chen, P.L. Kuo, H.M. Chien, Y.T. Wang, S.C. Shen, Protective effect of vanillic acid against hyperinsulinemia, hyperglycemia and hyperlipidemia via alleviating hepatic insulin resistance and inflammation in High-Fat Diet (HFD)-fed rats, *Nutrients.* 7 (2015) 9946–9959.
<https://doi.org/10.3390/nu7125514>.
- [18] Y. Jung, J. Park, H.L. Kim, J.E. Sim, D.H. Youn, J.W. Kang, S. Lim, M.Y. Jeong, W.M. Yang, S.G. Lee, K.S. Ahn, J.Y. Um, Vanillic acid attenuates

obesity via activation of the AMPK pathway and thermogenic factors in vivo and in vitro, *FASEB J.* 32 (2018) 1388–1402.

<https://doi.org/10.1096/fj.201700231RR>.

- [19] J. Kaur, V. Mishra, S.K. Singh, M. Gulati, B. Kapoor, D.K. Chellappan, G. Gupta, H. Dureja, K. Anand, K. Dua, G.L. Khatik, K. Gowthamarajan, Harnessing amphiphilic polymeric micelles for diagnostic and therapeutic applications: Breakthroughs and bottlenecks, *J. Control. Release.* 334 (2021) 64–95. <https://doi.org/10.1016/j.jconrel.2021.04.014>.
- [20] J. Kaur, M. Gulati, N.K. Jha, J. Disouza, V. Patravale, K. Dua, S.K. Singh, Recent advances in developing polymeric micelles for treating cancer: Breakthroughs and bottlenecks in their clinical translation, *Drug Discov. Today.* xxx (2022). <https://doi.org/10.1016/j.drudis.2022.02.005>.
- [21] J. Wang, X. Qian, J. Qian, Y. Xu, Micelle-induced versatile performance of amphiphilic intramolecular charge-transfer fluorescent molecular sensors, *Chem. - A Eur. J.* 13 (2007) 7543–7552. <https://doi.org/10.1002/chem.200700435>.
- [22] Biomedical applications of polymeric micelles of different drugs Jaskiran Kaur , Gopal Lal Khatik *, Navneet Khurana, (2019) 2019.
- [23] H. Danafar, H. Jaberizadeh, S. Andalib, In vitro and in vivo delivery of gliclazide loaded mPEG-PCL micelles and its kinetic release and solubility study, *Artif. Cells, Nanomedicine Biotechnol.* 46 (2018) 1625–1636. <https://doi.org/10.1080/21691401.2017.1386191>.
- [24] G. Zhang, X. Lin, S. Zhang, H. Xiu, C. Pan, W. Cui, A Protective Role of Glibenclamide in Inflammation-Associated Injury, *Mediators Inflamm.* 2017 (2017). <https://doi.org/10.1155/2017/3578702>.
- [25] K. Vinothiya, N. Ashokkumar, Modulatory effect of vanillic acid on antioxidant status in high fat diet-induced changes in diabetic hypertensive rats, *Biomed. Pharmacother.* 87 (2017) 640–652. <https://doi.org/10.1016/j.biopha.2016.12.134>.
- [26] M.C. Kim, S.J. Kim, D.S. Kim, Y.D. Jeon, S.J. Park, H.S. Lee, J.Y. Um, S.H. Hong, Vanillic acid inhibits inflammatory mediators by suppressing NF- κ B in lipopolysaccharide-stimulated mouse peritoneal macrophages, *Immunopharmacol. Immunotoxicol.* 33 (2011) 525–532. <https://doi.org/10.3109/08923973.2010.547500>.

- [27] P.K. Prabhakar, M. Doble, Effect of natural products on commercial oral antidiabetic drugs in enhancing 2-deoxyglucose uptake by 3T3-L1 adipocytes, *Ther. Adv. Endocrinol. Metab.* 2 (2011) 103–114. <https://doi.org/10.1177/2042018811411356>.
- [28] A.D. American Diabetes Association, 9. Pharmacologic approaches to glycemic treatment: Standards of medical care in diabetesd2019, *Diabetes Care.* 42 (2019) S90–S102. <https://doi.org/10.2337/dc19-S009>.
- [29] A.S. Al-Goblan, M.A. Al-Alfi, M.Z. Khan, Mechanism linking diabetes mellitus and obesity, *Diabetes, Metab. Syndr. Obes. Targets Ther.* 7 (2014) 587–591. <https://doi.org/10.2147/DMSO.S67400>.
- [30] M. Roden, Diabetes und adipositas, *Diabetologe.* 2 (2006) 203. <https://doi.org/10.1007/s11428-006-0056-4>.
- [31] R. June, Weight Loss Medications AADE Practice Advisory, *Am. Assoc. Diabetes Educ.* (2016). <https://doi.org/10.1001/jama.2016.6458.3>.
- [32] M.S.H. Akash, K. Rehman, S. Chen, Role of inflammatory mechanisms in pathogenesis of type 2 diabetes mellitus, *J. Cell. Biochem.* 114 (2013) 525–531. <https://doi.org/10.1002/jcb.24402>.
- [33] D.B. Zorov, M. Juhaszova, S.J. Sollott, Mitochondrial reactive oxygen species (ROS) and ROS-induced ROS release, *Physiol. Rev.* 94 (2014) 909–950. <https://doi.org/10.1152/physrev.00026.2013>.
- [34] F. Giacco, M. Brownlee, Oxidative stress and diabetic complications, *Circ. Res.* 107 (2010) 1058–1070. <https://doi.org/10.1161/CIRCRESAHA.110.223545>.
- [35] F. Folli, D. Corradi, P. Fanti, A. Davalli, A. Paez, A. Giaccari, C. Perego, G. Muscogiuri, The Role of Oxidative Stress in the Pathogenesis of Type 2 Diabetes Mellitus Micro- and Macrovascular Complications: Avenues for a Mechanistic-Based Therapeutic Approach, *Curr. Diabetes Rev.* 7 (2012) 313–324. <https://doi.org/10.2174/157339911797415585>.
- [36] C. Jiang, N. Yao, Q. Wang, J. Zhang, Y. Sun, N. Xiao, K. Liu, F. Huang, S. Fang, X. Shang, B. Liu, Y. Ni, Z. Yin, J. Zhang, *Cyclocarya paliurus* extract modulates adipokine expression and improves insulin sensitivity by inhibition of inflammation in mice, *J. Ethnopharmacol.* 153 (2014) 344–351. <https://doi.org/10.1016/j.jep.2014.02.003>.
- [37] M.S.H. Akash, K. Rehman, A. Liaqat, Tumor Necrosis Factor-Alpha: Role in

Development of Insulin Resistance and Pathogenesis of Type 2 Diabetes Mellitus, *J. Cell. Biochem.* 119 (2018) 105–110.

<https://doi.org/10.1002/jcb.26174>.

- [38] K. Rehman, M.S.H. Akash, A. Liaqat, S. Kamal, M.I. Qadir, A. Rasul, Role of interleukin-6 in development of insulin resistance and type 2 diabetes mellitus, *Crit. Rev. Eukaryot. Gene Expr.* 27 (2017) 229–236.
<https://doi.org/10.1615/CritRevEukaryotGeneExpr.2017019712>.
- [39] T. Tomita, Islet amyloid polypeptide in pancreatic islets from type 2 diabetic subjects, *Islets*. 4 (2012) 223–232. <https://doi.org/10.4161/isl.20477>.
- [40] J.W.M. Höppener, C.J.M. Lips, Role of islet amyloid in type 2 diabetes mellitus, *Int. J. Biochem. Cell Biol.* 38 (2006) 726–736.
<https://doi.org/10.1016/j.biocel.2005.12.009>.
- [41] E.T.A.S. Jaikaran, A. Clark, Islet amyloid and type 2 diabetes: From molecular misfolding to islet pathophysiology, *Biochim. Biophys. Acta - Mol. Basis Dis.* 1537 (2001) 179–203. [https://doi.org/10.1016/S0925-4439\(01\)00078-3](https://doi.org/10.1016/S0925-4439(01)00078-3).
- [42] Z. Sepehri, Z. Kiani, A.A. Nasiri, F. Kohan, Toll-like receptor 2 and type 2 diabetes, *Cell. Mol. Biol. Lett.* 21 (2016) 1–9. <https://doi.org/10.1186/s11658-016-0002-4>.
- [43] T.M. Belete, A recent achievement in the discovery and development of novel targets for the treatment of type-2 diabetes mellitus, *J. Exp. Pharmacol.* 12 (2020) 1–15. <https://doi.org/10.2147/JEP.S226113>.
- [44] S. Leonard, G.K. Kinsella, E. Benetti, J.B.C. Findlay, Regulating the effects of GPR21, a novel target for type 2 diabetes, *Sci. Rep.* 6 (2016).
<https://doi.org/10.1038/srep27002>.
- [45] S. Banu, A. Bhowmick, Therapeutic Targets of Type 2 Diabetes: an Overview, *MOJ Drug Des. Dev. Ther.* 1 (2017) 2–7.
<https://doi.org/10.15406/mojddt.2017.01.00011>.
- [46] P. Shende, C. Patel, siRNA: an alternative treatment for diabetes and associated conditions, *J. Drug Target.* 27 (2019) 174–182.
<https://doi.org/10.1080/1061186X.2018.1476518>.
- [47] S. Huang, G. Chen, J. Sun, Y. Chen, N. Wang, Y. Dong, E. Shen, Z. Hu, W. Gong, L. Jin, W. Cong, Histone deacetylase 3 inhibition alleviates type 2 diabetes mellitus-induced endothelial dysfunction via Nrf2, *Cell Commun. Signal.* 19 (2021) 1–16. <https://doi.org/10.1186/s12964-020-00681-z>.

- [48] L. Wu, J. Sun, L. Liu, X. Du, Y. Liu, X. Yan, E. Kombo Osoro, F. Zhang, L. Feng, D. Liang, Y. Li, Q. Chen, S. Sun, L. Zhang, X. Lan, D. Li, S. Lu, Anti-toll-like receptor 2 antibody ameliorates hepatic injury, inflammation, fibrosis and steatosis in obesity-related metabolic disorder rats via regulating MAPK and NF- κ B pathways, *Int. Immunopharmacol.* 82 (2020) 106368. <https://doi.org/10.1016/j.intimp.2020.106368>.
- [49] M. Alibashe-Ahmed, E. Brioudes, W. Reith, D. Bosco, T. Berney, Toll-like receptor 4 inhibition prevents autoimmune diabetes in NOD mice, *Sci. Rep.* 9 (2019) 1–8. <https://doi.org/10.1038/s41598-019-55521-z>.
- [50] Y. Duan, Q. Luo, Y. Wang, Y. Ma, F. Chen, X. Zhu, J. Shi, Adipose mesenchymal stem cell-derived extracellular vesicles containing microRNA-26a-5p target TLR4 and protect against diabetic nephropathy, *J. Biol. Chem.* 295 (2020) 12868–12884. <https://doi.org/10.1074/jbc.ra120.012522>.
- [51] J.H. Pettus, D. D'Alessio, J.P. Frias, E.G. Vajda, J.D. Pipkin, J. Rosenstock, G. Williamson, M.A. Zangmeister, L. Zhi, K.B. Marschke, Efficacy and safety of the glucagon receptor antagonist RVT-1502 in type 2 diabetes uncontrolled on metformin monotherapy: A 12-week dose-ranging study, *Diabetes Care.* 43 (2020) 161–168. <https://doi.org/10.2337/dc19-1328>.
- [52] N. Tsuda, A. Kawaji, T. Sato, M. Takagi, C. Higashi, Y. Kato, K. Ogawa, H. Naba, M. Ohkouchi, M. Nakamura, Y. Hosaka, J. Sakaki, A novel free fatty acid receptor 1 (GPR40/FFAR1) agonist, MR1704, enhances glucose-dependent insulin secretion and improves glucose homeostasis in rats, *Pharmacol. Res. Perspect.* 5 (2017) 1–12. <https://doi.org/10.1002/prp2.340>.
- [53] H. Yang, M. Wang, Y. Huang, Q. Qiao, C. Zhao, M. Zhao, In vitro and in vivo evaluation of a novel mitomycin nanomicelle delivery system, *RSC Adv.* 9 (2019) 14708–14717. <https://doi.org/10.1039/c9ra02660f>.
- [54] G. Lori, L. Cecchi, N. Mulinacci, F. Melani, A. Caselli, P. Cirri, L. Pazzagli, S. Luti, L. Mazzoli, P. Paoli, Honey extracts inhibit PTP1B, upregulate insulin receptor expression, and enhance glucose uptake in human HepG2 cells, *Biomed. Pharmacother.* 113 (2019) 108752. <https://doi.org/10.1016/j.biopha.2019.108752>.
- [55] X. Li, C. Zhang, Q. Zheng, X. Shi, ROS-responsive targeting micelles for optical imaging-guided chemo-phototherapy of cancer, *Colloids Surfaces B Biointerfaces.* 179 (2019) 218–225.

<https://doi.org/10.1016/j.colsurfb.2019.04.005>.

- [56] R.F. Rocha, T. Rodrigues, A.C.O. Menegatti, G.J.L. Bernardes, H. Terenzi, The antidiabetic drug lobeglitazone has the potential to inhibit PTP1B activity, *Bioorg. Chem.* 100 (2020) 103927. <https://doi.org/10.1016/j.bioorg.2020.103927>.
- [57] M. Riopel, J.S. Moon, G.K. Bandyopadhyay, S. You, K. Lam, X. Liu, T. Kisseleva, D. Brenner, Y.S. Lee, Inhibition of prolyl hydroxylases increases hepatic insulin and decreases glucagon sensitivity by an HIF-2 α -dependent mechanism, *Mol. Metab.* 41 (2020) 101039. <https://doi.org/10.1016/j.molmet.2020.101039>.
- [58] M. Sugahara, S. Tanaka, T. Tanaka, H. Saito, Y. Ishimoto, T. Wakashima, M. Ueda, K. Fukui, A. Shimizu, R. Inagi, T. Yamauchi, T. Kadowaki, M. Nangaku, Prolyl hydroxylase domain inhibitor protects against metabolic disorders and associated kidney disease in obese type 2 diabetic mice, *J. Am. Soc. Nephrol.* 31 (2020) 560–577. <https://doi.org/10.1681/ASN.2019060582>.
- [59] L. Ren, P. Zhan, Q. Wang, C. Wang, Y. Liu, Z. Yu, S. Zhang, Curcumin upregulates the Nrf2 system by repressing inflammatory signaling-mediated Keap1 expression in insulin-resistant conditions, *Biochem. Biophys. Res. Commun.* 514 (2019) 691–698. <https://doi.org/10.1016/j.bbrc.2019.05.010>.
- [60] H. Yao, N. Zhang, W. Zhang, J. Li, H. Hua, Y. Li, Discovery of polyposidide as a Keap1-dependent Nrf2 activator attenuating oxidative stress and accumulation of extracellular matrix in glomerular mesangial cells under high glucose, *Bioorganic Med. Chem.* 28 (2020) 115833. <https://doi.org/10.1016/j.bmc.2020.115833>.
- [61] Q. Zhao, F. Zhang, Z. Yu, S. Guo, N. Liu, Y. Jiang, E.H. Lo, Y. Xu, X. Wang, HDAC3 inhibition prevents blood-brain barrier permeability through Nrf2 activation in type 2 diabetes male mice, *J. Neuroinflammation.* 16 (2019) 1–15. <https://doi.org/10.1186/s12974-019-1495-3>.
- [62] T. Kawasaki, T. Kawai, Toll-like receptor signaling pathways, *Front. Immunol.* 5 (2014) 1–9. <https://doi.org/10.3389/fimmu.2014.00461>.
- [63] D.D. Sears, J.J. Kim, TLR4 and insulin resistance, *Gastroenterol. Res. Pract.* 2010 (2010). <https://doi.org/10.1155/2010/212563>.
- [64] L.H. Kuo, P.J. Tsai, M.J. Jiang, Y.L. Chuang, L. Yu, K.T.A. Lai, Y.S. Tsai, Toll-like receptor 2 deficiency improves insulin sensitivity and hepatic insulin

- signalling in the mouse, *Diabetologia*. 54 (2011) 168–179.
<https://doi.org/10.1007/s00125-010-1931-5>.
- [65] H. Liang, H. Wang, L. Luo, S. Fan, L. Zhou, Z. Liu, S. Yao, X. Zhang, K. Zhong, H. Zhao, Z. Zha, Toll-like receptor 4 promotes high glucose-induced catabolic and inflammatory responses in chondrocytes in an NF- κ B-dependent manner, *Life Sci*. 228 (2019) 258–265.
<https://doi.org/10.1016/j.lfs.2019.04.011>.
- [66] S.M. Reyna, S. Ghosh, P. Tantiwong, C.S.R.M. Meka, P. Eagan, C.P. Jenkinson, E. Cersosimo, R.A. Defronzo, D.K. Coletta, A. Sriwijitkamol, N. Musi, Elevated toll-like receptor 4 expression and signaling in muscle from insulin-resistant subjects, *Diabetes*. 57 (2008) 2595–2602.
<https://doi.org/10.2337/db08-0038>.
- [67] M.R. Dasu, S. Devaraj, S. Park, I. Jialal, Increased Toll-Like Receptor (TLR) activation and TLR ligands in recently diagnosed type 2 diabetic subjects, *Diabetes Care*. 33 (2010) 861–868. <https://doi.org/10.2337/dc09-1799>.
- [68] L. Janah, S. Kjeldsen, K.D. Galsgaard, M. Winther-Sørensen, E. Stojanovska, J. Pedersen, F.K. Knop, J.J. Holst, N.J.W. Albrechtsen, Glucagon receptor signaling and glucagon resistance, *Int. J. Mol. Sci*. 20 (2019).
<https://doi.org/10.3390/ijms20133314>.
- [69] S.L. Conarello, G. Jiang, J. Mu, Z. Li, J. Woods, E. Zycband, J. Ronan, F. Liu, R.S. Roy, L. Zhu, M.J. Charron, B.B. Zhang, Glucagon receptor knockout mice are resistant to diet-induced obesity and streptozotocin-mediated beta cell loss and hyperglycaemia, *Diabetologia*. 50 (2007) 142–150.
<https://doi.org/10.1007/s00125-006-0481-3>.
- [70] R.W. Gelling, P.M. Vuguin, Q. Du Xiu, L. Cui, J. Rømer, R.A. Pederson, M. Leiser, H. Sørensen, J.J. Holst, C. Fledelius, P.B. Johansen, N. Fleischer, C.H.S. McIntosh, E. Nishimura, M.J. Charron, Pancreatic β -cell overexpression of the glucagon receptor gene results in enhanced β -cell function and mass, *Am. J. Physiol. - Endocrinol. Metab*. 297 (2009).
<https://doi.org/10.1152/ajpendo.00082.2009>.
- [71] O. Osborn, D.Y. Oh, J. McNelis, M. Sanchez-Alavez, S. Talukdar, M. Lu, P.P. Li, L. Thiede, H. Morinaga, J.J. Kim, J. Heinrichsdorff, S. Nalbandian, J.M. Ofrecio, M. Scadeng, S. Schenk, J. Hadcock, T. Bartfai, J.M. Olefsky, G protein-coupled receptor 21 deletion improves insulin sensitivity in diet-

- induced obese mice, *J. Clin. Invest.* 122 (2012) 2444–2453.
<https://doi.org/10.1172/JCI61953>.
- [72] J. Gardner, S. Wu, L. Ling, J. Danao, Y. Li, W.C. Yeh, H. Tian, H. Baribault, G-protein-coupled receptor GPR21 knockout mice display improved glucose tolerance and increased insulin response, *Biochem. Biophys. Res. Commun.* 418 (2012) 1–5. <https://doi.org/10.1016/j.bbrc.2011.11.117>.
- [73] C. Eleazu, A. Charles, K. Eleazu, N. Achi, Free fatty acid receptor 1 as a novel therapeutic target for type 2 diabetes mellitus-current status, *Chem. Biol. Interact.* 289 (2018) 32–39. <https://doi.org/10.1016/j.cbi.2018.04.026>.
- [74] K.R. Watterson, B.D. Hudson, T. Ulven, G. Milligan, Treatment of type 2 diabetes by free fatty acid receptor agonists, *Front. Endocrinol. (Lausanne)*. 5 (2014) 1–9. <https://doi.org/10.3389/fendo.2014.00137>.
- [75] C.F. Burant, Activation of GPR40 as a therapeutic target for the treatment of type 2 diabetes, *Diabetes Care*. 36 (2013) 175–179.
<https://doi.org/10.2337/dcS13-2037>.
- [76] P. Steneberg, N. Rubins, R. Bartoov-Shifman, M.D. Walker, H. Edlund, The FFA receptor GPR40 links hyperinsulinemia, hepatic steatosis, and impaired glucose homeostasis in mouse, *Cell Metab.* 1 (2005) 245–258.
<https://doi.org/10.1016/j.cmet.2005.03.007>.
- [77] K. Nagasumi, R. Esaki, K. Iwachidow, Y. Yasuhara, K. Ogi, H. Tanaka, M. Nakata, T. Yano, K. Shimakawa, S. Taketomi, K. Takeuchi, H. Odaka, Y. Kaisho, Overexpression of GPR40 in pancreatic β -cells augments glucose-stimulated insulin secretion and improves glucose tolerance in normal and diabetic mice, *Diabetes*. 58 (2009) 1067–1076. <https://doi.org/10.2337/db08-1233>.
- [78] C. Ramachandran, B. Kennedy, Protein Tyrosine Phosphatase 1B: A Novel Target for Type 2 Diabetes and Obesity, *Curr. Top. Med. Chem.* 3 (2005) 749–757. <https://doi.org/10.2174/1568026033452276>.
- [79] M.I. and R.P.M. Tanvi A Deshpande, PTP1B Inhibitors as Potential Target for Type II Diabetes, *Curr. Res. Diabetes Obes. J.* 14 (2020) 1–13.
<https://doi.org/10.19080/crdoj.2020.14.555876>.
- [80] B.J. Goldstein, Protein-tyrosine phosphatase 1B (PTP1B): a novel therapeutic target for type 2 diabetes mellitus, obesity and related states of insulin resistance., *Curr. Drug Targets. Immune. Endocr. Metabol. Disord.* 1 (2001)

265–275. <https://doi.org/10.2174/1568008013341163>.

- [81] A. Zimna, M. Kurpisz, Hypoxia-Inducible factor-1 in physiological and pathophysiological angiogenesis: Applications and therapies, *Biomed Res. Int.* 2015 (2015) 1–13. <https://doi.org/10.1155/2015/549412>.
- [82] P.S. Rabbani, M.A. Soares, S.G. Hameedi, R.L. Kadle, A. Mubasher, M. Kowzun, D.J. Ceradini, Dysregulation of Nrf2/Keap1 redox pathway in diabetes affects multipotency of stromal cells, *Diabetes*. 68 (2019) 141–155. <https://doi.org/10.2337/db18-0232>.
- [83] A. Uruno, Y. Furusawa, Y. Yagishita, T. Fukutomi, H. Muramatsu, T. Negishi, A. Sugawara, T.W. Kensler, M. Yamamoto, The Keap1-Nrf2 System Prevents Onset of Diabetes Mellitus, *Mol. Cell. Biol.* 33 (2013) 2996–3010. <https://doi.org/10.1128/mcb.00225-13>.
- [84] C. Sathishkumar, P. Prabu, M. Balakumar, R. Lenin, D. Prabhu, R.M. Anjana, V. Mohan, M. Balasubramanyam, Augmentation of histone deacetylase 3 (HDAC3) epigenetic signature at the interface of proinflammation and insulin resistance in patients with type 2 diabetes, *Clin. Epigenetics*. 8 (2016) 1–12. <https://doi.org/10.1186/s13148-016-0293-3>.
- [85] Y. Fu, Y. Wang, X. Gao, H. Li, Y. Yuan, Dynamic Expression of HDAC3 in db/db Mouse RGCs and Its Relationship with Apoptosis and Autophagy, *J. Diabetes Res.* 2020 (2020). <https://doi.org/10.1155/2020/6086780>.
- [86] B. Lorenzati, C. Zucco, S. Miglietta, F. Lamberti, G. Bruno, Oral hypoglycemic drugs: Pathophysiological basis of their mechanism of action, *Pharmaceuticals*. 3 (2010) 3005–3020. <https://doi.org/10.3390/ph3093005>.
- [87] A.J. Nathan, A. Scobell, *How China sees America*, 2012. <https://doi.org/10.1017/CBO9781107415324.004>.
- [88] P.M. Thulé, G. Umpierrez, Sulfonylureas: A new look at old therapy topical collection on pharmacologic treatment of type 2 diabetes, *Curr. Diab. Rep.* 14 (2014). <https://doi.org/10.1007/s11892-014-0473-5>.
- [89] S. Kalra, A.H. Aamir, A. Raza, A.K. Das, A.K.A. Khan, D. Shrestha, M.F. Qureshi, M. Fariduddin, M.F. Pathan, F. Jawad, J. Bhattarai, N. Tandon, N. Somasundaram, P. Katulanda, R. Sahay, S. Dhungel, S. Bajaj, S. Chowdhury, S. Ghosh, S. V. Madhu, T. Ahmed, U. Bulughapitiya, Place of sulfonylureas in the management of type 2 diabetes mellitus in South Asia: A consensus statement, *Indian J. Endocrinol. Metab.* 19 (2015) 577–596.

<https://doi.org/10.4103/2230-8210.163171>.

- [90] B.J. Kocsis, L.M. Scher, *Pharmacotherapy*, 2015.
<https://doi.org/10.32388/swc66c>.
- [91] J.M. Pappachan, C.J. Fernandez, E.C. Chacko, Diabesity and antidiabetic drugs, *Mol. Aspects Med.* 66 (2019) 3–12.
<https://doi.org/10.1016/j.mam.2018.10.004>.
- [92] W. Klein-Schwartz, G.L. Stassinis, G.K. Isbister, Treatment of sulfonylurea and insulin overdose, *Br. J. Clin. Pharmacol.* 81 (2016) 496–504.
<https://doi.org/10.1111/bcp.12822>.
- [93] J.R. White, A Brief History of the Development of Chain, *Diabetes Spectr.* 27 (2005) 1–16. <https://doi.org/10.1201/9781420027341.ch1>.
- [94] J.S. Grant, L.J. Graven, Progressing from Metformin to Sulfonylureas or Meglitinides, *Work. Heal. Saf.* 64 (2016) 433–439.
<https://doi.org/10.1177/2165079916644263>.
- [95] R. Guardado-Mendoza, A. Prioletta, L.M. Jiménez-Ceja, A. Sosale, F. Folli, The role of nateglinide and repaglinide, derivatives of meglitinide, in the treatment of type 2 diabetes mellitus, *Arch. Med. Sci.* 9 (2013) 936–943.
<https://doi.org/10.5114/aoms.2013.34991>.
- [96] J. Rosenstock, D.R. Hassman, R.D. Madder, S.A. Brazinsky, J. Farrell, N. Khutoryansky, P.M. Hale, Repaglinide versus nateglinide monotherapy: A randomized, multicenter study, *Diabetes Care.* 27 (2004) 1265–1270.
<https://doi.org/10.2337/diacare.27.6.1265>.
- [97] M.A. Hossain, R. Pervin, *Current Antidiabetic Drugs*, Second Edi, Elsevier Inc., 2018. <https://doi.org/10.1016/b978-0-12-812019-4.00034-9>.
- [98] H. R.S, I. S.E, Metformin: New Understandings, New Uses, *Drugs.* 63 (2003) 1879.
- [99] G. Charpentier, Oral combination therapy for type 2 diabetes, *Diabetes. Metab. Res. Rev.* 18 (2002) 70–76. <https://doi.org/10.1002/dmrr.278>.
- [100] Yki-Jarvinen H, Drug Therapy: Thiazolidinediones, *N Engl J Med.* 351 (2004) 1106–1118.
- [101] J.A. Dormandy, B. Charbonnel, D.J.A. Eckland, E. Erdmann, M. Massi-Benedetti, I.K. Moules, A.M. Skene, M.H. Tan, P.J. Lefèbvre, G.D. Murray, E. Standl, R.G. Wilcox, L. Wilhelmsen, J. Betteridge, K. Birkeland, A. Golay, R.J. Heine, L. Korányi, M. Laakso, M. Mokáň, A. Norkus, V. Pirags, T. Podar,

- A. Scheen, W. Scherbaum, G. Scherthaner, O. Schmitz, J. Škrha, U. Smith, J. Tatoň, Secondary prevention of macrovascular events in patients with type 2 diabetes in the PROactive Study (PROspective pioglitAzone Clinical Trial in macroVascular Events): A randomised controlled trial, *Lancet*. 366 (2005) 1279–1289. [https://doi.org/10.1016/S0140-6736\(05\)67528-9](https://doi.org/10.1016/S0140-6736(05)67528-9).
- [102] K.D. Ko, K.K. Kim, K.R. Lee, Does Weight Gain Associated with Thiazolidinedione Use Negatively Affect Cardiometabolic Health?, *J. Obes. Metab. Syndr.* 26 (2017) 102–106. <https://doi.org/10.7570/jomes.2017.26.2.102>.
- [103] J. Wilding, Thiazolidinediones, insulin resistance and obesity: Finding a balance, *Int. J. Clin. Pract.* 60 (2006) 1272–1280. <https://doi.org/10.1111/j.1742-1241.2006.01128.x>.
- [104] J.W.F. Elte, J.F. Blicklé, Thiazolidinediones for the treatment of type 2 diabetes, *Eur. J. Intern. Med.* 18 (2007) 18–25. <https://doi.org/10.1016/j.ejim.2006.09.007>.
- [105] D. Hinnen, Glucagon-like peptide 1 receptor agonists for type 2 diabetes, *Diabetes Spectr.* 30 (2017) 202–210. <https://doi.org/10.2337/ds16-0026>.
- [106] L. Yammine, T.R. Kosten, M. Pimenova, J.M. Schmitz, Cigarette smoking, type 2 diabetes mellitus, and glucagon-like peptide-1 receptor agonists as a potential treatment for smokers with diabetes: An integrative review, *Diabetes Res. Clin. Pract.* 149 (2019) 78–88. <https://doi.org/10.1016/j.diabres.2019.01.033>.
- [107] A.R. Meloni, M.B. Deyoung, C. Lowe, D.G. Parkes, GLP-1 receptor activated insulin secretion from pancreatic β -cells: Mechanism and glucose dependence, *Diabetes, Obes. Metab.* 15 (2013) 15–27. <https://doi.org/10.1111/j.1463-1326.2012.01663.x>.
- [108] Essentials of Medical Pharmacology, 7th Edition.pdf - Filecad, (n.d.). <https://www.filecad.com/1jlx> (accessed May 7, 2017).
- [109] H. Soni, Peptide-based GLP-1/glucagon co-agonists: A double-edged sword to combat diabetes, *Med. Hypotheses.* 95 (2016) 5–9. <https://doi.org/10.1016/j.mehy.2016.08.005>.
- [110] C.F. Deacon, Corrigendum: Physiology and pharmacology of DPP-4 in glucose homeostasis and the treatment of type 2 diabetes (*Frontiers in Endocrinology* (2019) 10:80 DOI: 10.3389/fendo.2019.00080), *Front. Endocrinol.* (Lausanne).

- 10 (2019). <https://doi.org/10.3389/fendo.2019.00275>.
- [111] D. Dicker, DPP-4 Inhibitors: Impact on glycemic control and cardiovascular risk factors, *Diabetes Care*. 34 (2011) 276–278. <https://doi.org/10.2337/dc11-s229>.
- [112] R. Pathak, M.B. Bridgeman, Dipeptidyl peptidase-4 (DPP-4) inhibitors in the management of diabetes, *P T*. 35 (2010) 509–513.
<http://www.ncbi.nlm.nih.gov/pubmed/20975810> (accessed August 30, 2019).
- [113] N.A. Thornberry, B. Gallwitz, Mechanism of action of inhibitors of dipeptidyl-peptidase-4 (DPP-4), *Best Pract. Res. Clin. Endocrinol. Metab.* 23 (2009) 479–486. <https://doi.org/10.1016/j.beem.2009.03.004>.
- [114] R.E. Amori, J. Lau, A.G. Pittas, Efficacy and safety of incretin therapy in type 2 diabetes: Systematic review and meta-analysis, *J. Am. Med. Assoc.* 298 (2007) 194–206. <https://doi.org/10.1001/jama.298.2.194>.
- [115] Diabetes.co.uk, DPP-4 Inhibitors (Gliptins) - Drugs, Suitability, Benefits & Side Effects, (n.d.). <https://www.diabetes.co.uk/diabetes-medication/dpp-4-inhibitors.html> (accessed August 1, 2019).
- [116] Z. Yin, W. Zhang, F. Feng, Y. Zhang, W. Kang, α -Glucosidase inhibitors isolated from medicinal plants, *Food Sci. Hum. Wellness*. 3 (2014) 136–174. <https://doi.org/10.1016/j.fshw.2014.11.003>.
- [117] D. Precose, NDA 20-482/S-023 Page 3, (n.d.) 3–14.
- [118] G. Derosa, P. Maffioli, α -Glucosidase inhibitors and their use in clinical practice, *Arch. Med. Sci.* 8 (2012) 899–906.
<https://doi.org/10.5114/aoms.2012.31621>.
- [119] A.J. Krentz, *Evolution of Glucose-Lowering Drugs for Type 2 Diabetes*, Second Edi, Elsevier Inc., 2018. <https://doi.org/10.1016/b978-0-12-812019-4.00033-7>.
- [120] Sodium-glucose Cotransporter-2 (SGLT2) Inhibitors | FDA, (n.d.).
<https://www.fda.gov/drugs/postmarket-drug-safety-information-patients-and-providers/sodium-glucose-cotransporter-2-sgl2-inhibitors> (accessed August 1, 2019).
- [121] FDA, FDA warns about rare occurrences of a serious infection of the genital area with SGLT2 inhibitors for diabetes, FDA, *Saf. Announc.* (2018) 1–6.
<https://www.fda.gov/media/115602/download> (accessed August 1, 2019).
- [122] D.S. Hsia, O. Grove, W.T. Cefalu, An update on sodium-glucose co-

transporter-2 inhibitors for the treatment of diabetes mellitus, *Curr. Opin. Endocrinol. Diabetes Obes.* 24 (2017) 73–79.
<https://doi.org/10.1097/MED.0000000000000311>.

- [123] A.M. Zurek, R. Yendapally, E.M. Urteaga, A review of the efficacy and safety of sodium- Glucose cotransporter 2 inhibitors: A focus on diabetic ketoacidosis, *Diabetes Spectr.* 30 (2017) 137–142.
<https://doi.org/10.2337/ds16-0030>.
- [124] A. Schork, J. Saynisch, A. Vosseler, B.A. Jaghutriz, N. Heyne, A. Peter, H.U. Häring, N. Stefan, A. Fritsche, F. Artunc, Effect of SGLT2 inhibitors on body composition, fluid status and renin-angiotensin-aldosterone system in type 2 diabetes: a prospective study using bioimpedance spectroscopy, *Cardiovasc. Diabetol.* 18 (2019) 1–12. <https://doi.org/10.1186/s12933-019-0852-y>.
- [125] J. Kaur, P. Famta, N. Khurana, M. Vyas, G.L. Khatik, Pharmacotherapy of Type 2 Diabetes, *Obes. Diabetes.* (2020) 679–694. https://doi.org/10.1007/978-3-030-53370-0_50.
- [126] A Single Dose, Tolerance and Pharmacokinetic Study in Obese or Overweight Type 2 Diabetic Volunteers - Full Text View - [ClinicalTrials.gov](https://clinicaltrials.gov), (n.d.).
<https://clinicaltrials.gov/ct2/show/NCT00606112?term=DRUGS+in+phase+1&cond=Obesity%3B+Endocrine&cntry=US&draw=2> (accessed August 8, 2019).
- [127] NCT03745937, A Study to Evaluate the Safety and Tolerability of MEDI0382 in Overweight and Obese Subjects With Type 2 Diabetes Mellitus, <https://Clinicaltrials.Gov/Show/NCT03745937>. (2018).
<https://www.cochranelibrary.com/central/doi/10.1002/central/CN-01918410/full> (accessed August 8, 2019).
- [128] Nct, A Study to Assess the Safety and Efficacy of SAR425899 in Patients With Type 2 Diabetes Mellitus, <https://Clinicaltrials.Gov/Show/NCT02973321>. (2016). <https://www.cochranelibrary.com/central/doi/10.1002/central/CN-01594209/full> (accessed August 8, 2019).
- [129] Phase II Safety and Efficacy Study of Oral ORMD-0801 in Patients With Type 2 Diabetes Mellitus - Full Text View - [ClinicalTrials.gov](https://clinicaltrials.gov), (n.d.).
<https://clinicaltrials.gov/ct2/show/NCT02496000?term=Oramed&cond=Diabetes+Mellitus&draw=1&rank=7> (accessed August 30, 2019).
- [130] B. Zambrowicz, J. Freiman, P.M. Brown, K.S. Frazier, A. Turnage, J. Bronner, D. Ruff, M. Shadoan, P. Banks, F. Mseeh, D.B. Rawlins, N.C. Goodwin, R.

- Mabon, B.A. Harrison, A. Wilson, A. Sands, D.R. Powell, LX4211, a dual SGLT1/SGLT2 inhibitor, improved glycemic control in patients with type 2 diabetes in a Randomized, placebo-controlled trial, *Clin. Pharmacol. Ther.* 92 (2012) 158–169. <https://doi.org/10.1038/clpt.2012.58>.
- [131] G.B. Bolli, M.C. Riddle, R.M. Bergenstal, M. Ziemien, K. Sestakauskas, H. Goyeau, P.D. Home, New insulin glargine 300 U/ml compared with glargine 100 U/ml in insulin-naïve people with type 2 diabetes on oral glucose-lowering drugs: A randomized controlled trial (EDITION 3), *Diabetes, Obes. Metab.* 17 (2015) 386–394. <https://doi.org/10.1111/dom.12438>.
- [132] I.B. Halberg, K. Lyby, K. Wassermann, T. Heise, E. Zijlstra, L. Plum-Mörschel, Efficacy and safety of oral basal insulin versus subcutaneous insulin glargine in type 2 diabetes: a randomised, double-blind, phase 2 trial, *Lancet Diabetes Endocrinol.* 7 (2019) 179–188. [https://doi.org/10.1016/S2213-8587\(18\)30372-3](https://doi.org/10.1016/S2213-8587(18)30372-3).
- [133] T. M., FDA Approves Inhaled Insulin Afrezza for Diabetes. *Medscape, Med. News.* (2014). <https://www.medscape.com/viewarticle/827539> (accessed August 30, 2019).
- [134] FDA approves first treatment for severe hypoglycemia that can be administered without an injection, *Case Med. Res.* (2019). <https://doi.org/10.31525/cm-1876a33>.
- [135] Z.T. Bloomgarden, R. Dodis, C.M. Viscoli, E.S. Holmboe, S.E. Inzucchi, Lower baseline glycemia reduces apparent oral agent glucose-lowering efficacy: A meta-regression analysis, *Diabetes Care.* 29 (2006) 2137–2139. <https://doi.org/10.2337/dc06-1120>.
- [136] D. Care, S.S. Suppl, 8. Obesity management for the treatment of type 2 diabetes: Standards of medical care in diabetesd2019, *Diabetes Care.* 42 (2019) S81–S89. <https://doi.org/10.2337/dc19-S008>.
- [137] S. Kalepu, M. Manthina, V. Padavala, Oral lipid-based drug delivery systems – an overview, *Acta Pharm. Sin. B.* 3 (2013) 361–372. <https://doi.org/10.1016/j.apsb.2013.10.001>.
- [138] KATJA ^ERP NJAK1 ALENKA ZVONAR2 MIRJANA GA[PERLIN2* FRANC VRE^ER1, Lipid-based systems as a promising approach for enhancing the bioavailability of poorly water-soluble drugs, *Acta Pharm.* 63 (2013) 427–445.

- [139] J. Hanato, K. Kuriyama, T. Mizumoto, K. Debari, J. Hatanaka, S. Onoue, S. Yamada, Liposomal formulations of glucagon-like peptide-1: Improved bioavailability and anti-diabetic effect, *Int. J. Pharm.* 382 (2009) 111–116. <https://doi.org/10.1016/j.ijpharm.2009.08.013>.
- [140] B. Kumar, G. Jeyabalan, Development of Anti-diabetic Niosomes Formulation Containing Metformin and Gliclazide, *Indian J. Pharm. Biol. Res.* 5 (2017) 24–28.
- [141] H.A. Ebrahimi, Y. Javadzadeh, M. Hamidi, M.B. Jalali, Repaglinide-loaded solid lipid nanoparticles: Effect of using different surfactants/stabilizers on physicochemical properties of nanoparticles, *DARU, J. Pharm. Sci.* 23 (2015) 1–11. <https://doi.org/10.1186/s40199-015-0128-3>.
- [142] C.Y. Wong, H. Al-Salami, C.R. Dass, Recent advancements in oral administration of insulin-loaded liposomal drug delivery systems for diabetes mellitus, *Int. J. Pharm.* 549 (2018) 201–217. <https://doi.org/10.1016/j.ijpharm.2018.07.041>.
- [143] J.R. Yazdi, M. Tafaghodi, K. Sadri, M. Mashreghi, A.R. Nikpoor, S. Nikoofal-Sahlabadi, J. Chamani, R. Vakili, S.A. Moosavian, M.R. Jaafari, Folate targeted PEGylated liposomes for the oral delivery of insulin: In vitro and in vivo studies, *Colloids Surfaces B Biointerfaces.* 194 (2020) 111203. <https://doi.org/10.1016/j.colsurfb.2020.111203>.
- [144] M. Niu, Y. Lu, L. Hovgaard, P. Guan, Y. Tan, R. Lian, J. Qi, W. Wu, Hypoglycemic activity and oral bioavailability of insulin-loaded liposomes containing bile salts in rats: The effect of cholate type, particle size and administered dose, *Eur. J. Pharm. Biopharm.* 81 (2012) 265–272. <https://doi.org/10.1016/j.ejpb.2012.02.009>.
- [145] A.K. Agrawal, H. Harde, K. Thanki, S. Jain, Improved stability and antidiabetic potential of insulin containing folic acid functionalized polymer stabilized multilayered liposomes following oral administration, *Biomacromolecules.* 15 (2014) 350–360. <https://doi.org/10.1021/bm401580k>.
- [146] X. Zhang, J. Qi, Y. Lu, X. Hu, W. He, W. Wu, Enhanced hypoglycemic effect of biotin-modified liposomes loading insulin: effect of formulation variables, intracellular trafficking, and cytotoxicity, *Nanoscale Res. Lett.* 9 (2014) 1–10. <https://doi.org/10.1186/1556-276X-9-185>.
- [147] M. Barani, M. Mirzaei, M. Torkzadeh-Mahani, M. Adeli-sardou, Evaluation of

- Carum-loaded Niosomes on Breast Cancer Cells: Physicochemical Properties, In Vitro Cytotoxicity, Flow Cytometric, DNA Fragmentation and Cell Migration Assay, *Sci. Rep.* 9 (2019) 1–10. <https://doi.org/10.1038/s41598-019-43755-w>.
- [148] M. Gharbavi, J. Amani, H. Kheiri-Manjili, H. Danafar, A. Sharafi, Niosome: A Promising Nanocarrier for Natural Drug Delivery through Blood-Brain Barrier, *Adv. Pharmacol. Sci.* 2018 (2018). <https://doi.org/10.1155/2018/6847971>.
- [149] R. Khan, R. Irchhaiya, Niosomes: a potential tool for novel drug delivery, *J. Pharm. Investig.* 46 (2016) 195–204. <https://doi.org/10.1007/s40005-016-0249-9>.
- [150] A. Sankhyan, P.K. Pawar, Metformin loaded non-ionic surfactant vesicles: Optimization of formulation, effect of process variables and characterization, *DARU, J. Pharm. Sci.* 21 (2013) 1. <https://doi.org/10.1186/2008-2231-21-7>.
- [151] A.M. Mohsen, M.M. AbouSamra, S.A. ElShebiney, Enhanced oral bioavailability and sustained delivery of glimepiride via niosomal encapsulation: in-vitro characterization and in-vivo evaluation, *Drug Dev. Ind. Pharm.* 43 (2017) 1254–1264. <https://doi.org/10.1080/03639045.2017.1310224>.
- [152] R. Arshad, T.A. Tabish, M.H. Kiani, I.M. Ibrahim, G. Shahnaz, A. Rahdar, M. Kang, S. Pandey, A hyaluronic acid functionalized self-nano-emulsifying drug delivery system (Snedds) for enhancement in ciprofloxacin targeted delivery against intracellular infection, *Nanomaterials.* 11 (2021). <https://doi.org/10.3390/nano11051086>.
- [153] M. Nadiyah, M. Izham, Y. Hussin, M. Nazirul, M. Aziz, S.K. Yeap, H.S. Rahman, M. Ja, Preparation and Characterization of Self Nano-Emulsifying Drug Delivery System Loaded with Citraland Its Antiproliferative Effect on Colorectal Cells in Vitro, *Nanomaterials.* 9 (2019) 1–18.
- [154] R. Mukhopadhyay, J. Kazi, M.C. Debnath, Synthesis and characterization of copper nanoparticles stabilized with *Quisqualis indica* extract: Evaluation of its cytotoxicity and apoptosis in B16F10 melanoma cells, *Biomed. Pharmacother.* 97 (2018) 1373–1385. <https://doi.org/10.1016/j.biopha.2017.10.167>.
- [155] M. Rashid, T.U. Wani, N. Mishra, H.S. Sofi, F.A. Sheikh, Development and Characterization of Drug-Loaded Self-Solidnano-Emulsified Drug Delivery System for Treatment of Diabetes, *Mater. Sci. Res. India.* 15 (2018) 01–11.

<https://doi.org/10.13005/msri/150101>.

- [156] Ameenuzzafar, I. El-Bagory, N.K. Alruwaili, M.H. Elkomy, J. Ahmad, M. Afzal, N. Ahmad, M. Elmowafy, K.S. Alharbi, Md Shoaib Alam, Development of novel dapagliflozin loaded solid self-nanoemulsifying oral delivery system: Physicochemical characterization and in vivo antidiabetic activity, *J. Drug Deliv. Sci. Technol.* 54 (2019) 101279. <https://doi.org/10.1016/j.jddst.2019.101279>.
- [157] M. Kazi, A. Alqahtani, A. Ahmad, O.M. Noman, M.S. Aldughaim, A.S. Alqahtani, F.K. Alanazi, Development and optimization of sitagliptin and dapagliflozin loaded oral self-nanoemulsifying formulation against type 2 diabetes mellitus, *Drug Deliv.* 28 (2021) 100–114. <https://doi.org/10.1080/10717544.2020.1859001>.
- [158] J.R. Campos, P. Severino, A. Santini, A.M. Silva, R. Shegokar, S.B. Souto, E.B. Souto, Solid lipid nanoparticles (SLN): Prediction of toxicity, metabolism, fate and physicochemical properties. prediction of toxicity, metabolism, fate and physicochemical properties., Elsevier, 2020. <https://doi.org/10.1016/B978-0-12-817778-5.00001-4>.
- [159] J.S. Baek, S.C. Shin, C.W. Cho, Effect of lipid on physicochemical properties of solid lipid nanoparticle of paclitaxel, *J. Pharm. Investig.* 42 (2012) 279–283. <https://doi.org/10.1007/s40005-012-0038-z>.
- [160] C.H. Lin, C.H. Chen, Z.C. Lin, J.Y. Fang, Recent advances in oral delivery of drugs and bioactive natural products using solid lipid nanoparticles as the carriers, *J. Food Drug Anal.* 25 (2017) 219–234. <https://doi.org/10.1016/j.jfda.2017.02.001>.
- [161] S.S.D. MANOJ K. RAWAT, ACHINT JAIN, InVivoand Cytotoxicity Evaluation of Repaglinide-Loaded Binary Solid Lipid Nanoparticles After Oral Administration to Rats, *J. Pharm. Sci.* 101 (2012) 2271–2280. <https://doi.org/10.1002/jps>.
- [162] J. Kaur, M. Gulati, F. Zacconi, H. Dureja, R. Loebenberg, M.S. Ansari, O. AlOmeir, A. Alam, D.K. Chellappan, G. Gupta, N.K. Jha, T. de J.A. Pinto, A. Morris, Y.E. Choonara, J. Adams, K. Dua, S.K. Singh, Biomedical Applications of polymeric micelles in the treatment of diabetes mellitus: Current success and future approaches, *Expert Opin. Drug Deliv.* 00 (2022) 1–23. <https://doi.org/10.1080/17425247.2022.2087629>.

- [163] Title: Recent advances in developing polymeric micelles for treating cancer: Breakthrough and bottlenecks in their clinical translation List of authors Jaskiran Kaur, (2007).
- [164] A.A. Kassem, S.H. Abd El-Alim, M. Basha, A. Salama, Phospholipid complex enriched micelles: A novel drug delivery approach for promoting the antidiabetic effect of repaglinide, *Eur. J. Pharm. Sci.* 99 (2017) 75–84. <https://doi.org/10.1016/j.ejps.2016.12.005>.
- [165] W.Y. Hu, Z.M. Wu, Q.Q. Yang, Y.J. Liu, J. Li, C.Y. Zhang, Smart pH-responsive polymeric micelles for programmed oral delivery of insulin, *Colloids Surfaces B Biointerfaces.* 183 (2019) 110443. <https://doi.org/10.1016/j.colsurfb.2019.110443>.
- [166] F. Bahman, S. Taurin, D. Altayeb, S. Taha, M. Bakhiet, K. Greish, Oral insulin delivery using poly (Styrene co-Maleic acid) micelles in a diabetic mouse model, *Pharmaceutics.* 12 (2020) 1–17. <https://doi.org/10.3390/pharmaceutics12111026>.
- [167] 2 Aleksandra Zielińska 1, B.P. 1, Filipa Carreiró 1, Ana M. Oliveira 1, Andreia Neves 1, D.N.V. 3, A.D. 4, P.E. 5, Massimo Lucarini 4, 7 Amélia M. Silva 6, 9, Antonello Santini 8,* and Eliana B. Souto 1, Polymeric Nanoparticles: Production, Characterization, Toxicology and Ecotoxicology, *Molecules.* 25 (2020) 3731.
- [168] and O.C.F. Eric M. Pridgen1,*, Frank Alexis2, Polymeric Nanoparticle Technologies for Oral Drug Delivery, *Clin Gastroenterol Hepatol.* 23 (2014) 1–7. <https://doi.org/10.1016/j.cgh.2014.06.018>.Polymeric.
- [169] B. Begines, T. Ortiz, M. Pérez-Aranda, G. Martínez, M. Merinero, F. Argüelles-Arias, A. Alcudia, Polymeric nanoparticles for drug delivery: Recent developments and future prospects, *Nanomaterials.* 10 (2020) 1–41. <https://doi.org/10.3390/nano10071403>.
- [170] M. Gagat, W. Zielińska, A. Grzanka, Cell-penetrating peptides and their utility in genome function modifications (Review), *Int. J. Mol. Med.* 40 (2017) 1615–1623. <https://doi.org/10.3892/ijmm.2017.3172>.
- [171] F. Araújo, N. Shrestha, M.J. Gomes, B. Herranz-Blanco, D. Liu, J.J. Hirvonen, P.L. Granja, H.A. Santos, B. Sarmiento, In vivo dual-delivery of glucagon like peptide-1 (GLP-1) and dipeptidyl peptidase-4 (DPP4) inhibitor through composites prepared by microfluidics for diabetes therapy, *Nanoscale.* 8 (2016)

10706–10713. <https://doi.org/10.1039/c6nr00294c>.

- [172] N. Shrestha, F. Araújo, M.A. Shahbazi, E. Mäkilä, M.J. Gomes, M. Airavaara, E.I. Kauppinen, J. Raula, J. Salonen, J. Hirvonen, B. Sarmiento, H.A. Santos, Oral hypoglycaemic effect of GLP-1 and DPP4 inhibitor based nanocomposites in a diabetic animal model, *J. Control. Release.* 232 (2016) 113–119. <https://doi.org/10.1016/j.jconrel.2016.04.024>.
- [173] V.B. Junyaprasert, B. Morakul, Nanocrystals for enhancement of oral bioavailability of poorly water-soluble drugs, *Asian J. Pharm. Sci.* 10 (2015) 13–23. <https://doi.org/10.1016/j.ajps.2014.08.005>.
- [174] Z. Chen, W. Wu, Y. Lu, What is the future for nanocrystal-based drug-delivery systems?, *Ther. Deliv.* 11 (2020) 225–229. <https://doi.org/10.4155/tde-2020-0016>.
- [175] T. Liu, X. Yu, H. Yin, J.P. Möschwitzer, Advanced modification of drug nanocrystals by using novel fabrication and downstream approaches for tailor-made drug delivery, *Drug Deliv.* 26 (2019) 1092–1103. <https://doi.org/10.1080/10717544.2019.1682721>.
- [176] W.S. Abo-Elseoud, M.L. Hassan, M.W. Sabaa, M. Basha, E.A. Hassan, S.M. Fadel, Chitosan nanoparticles/cellulose nanocrystals nanocomposites as a carrier system for the controlled release of repaglinide, *Int. J. Biol. Macromol.* 111 (2018) 604–613. <https://doi.org/10.1016/j.ijbiomac.2018.01.044>.
- [177] M. Labieniec-Watala, T. Przygodzki, K. Sebekova, C. Watala, Can metabolic impairments in experimental diabetes be cured with poly(amido)amine (PAMAM) G4 dendrimers? - In the search for minimizing of the adverse effects of PAMAM administration, *Int. J. Pharm.* 464 (2014) 152–167. <https://doi.org/10.1016/j.ijpharm.2014.01.011>.
- [178] Y. V. Simos, K. Spyrou, M. Patila, N. Karouta, H. Stamatis, D. Gournis, E. Dounousi, D. Peschos, Trends of nanotechnology in type 2 diabetes mellitus treatment, *Asian J. Pharm. Sci.* 16 (2021) 62–76. <https://doi.org/10.1016/j.ajps.2020.05.001>.
- [179] Y. Kumari, G. Kaur, R. Kumar, S.K. Singh, M. Gulati, R. Khursheed, A. Clarisse, K. Gowthamarajan, V.V.S.N.R. Karri, R. Mahalingam, D. Ghosh, A. Awasthi, R. Kumar, A.K. Yadav, B. Kapoor, P.K. Singh, K. Dua, O. Porwal, Gold nanoparticles: New routes across old boundaries, *Adv. Colloid Interface Sci.* 274 (2019) 102037. <https://doi.org/10.1016/j.cis.2019.102037>.

- [180] S. Fayyaz, D. Ahmed, S. Khalid, S.N. Khan, M.R. Shah, M.I. Choudhary, Synthesis of vildagliptin conjugated metal nanoparticles for type II diabetes control: Targeting the DPP-IV enzyme, *New J. Chem.* 44 (2020) 20853–20860. <https://doi.org/10.1039/d0nj04202a>.
- [181] M. Pérez-Ortiz, C. Zapata-Urzúa, G.A. Acosta, A. Álvarez-Lueje, F. Albericio, M.J. Kogan, Gold nanoparticles as an efficient drug delivery system for GLP-1 peptides, *Colloids Surfaces B Biointerfaces.* 158 (2017) 25–32. <https://doi.org/10.1016/j.colsurfb.2017.06.015>.
- [182] S. Mignani, X. Shi, A. Karpus, J.P. Majoral, Non-invasive intranasal administration route directly to the brain using dendrimer nanoplatforms: An opportunity to develop new CNS drugs, *Eur. J. Med. Chem.* 209 (2021) 112905. <https://doi.org/10.1016/j.ejmech.2020.112905>.
- [183] S.S. Kesharwani, S. Kaur, H. Tummala, A.T. Sangamwar, Multifunctional approaches utilizing polymeric micelles to circumvent multidrug resistant tumors, *Colloids Surfaces B Biointerfaces.* 173 (2019) 581–590. <https://doi.org/10.1016/j.colsurfb.2018.10.022>.
- [184] and S.W.K. Pyung-Hwan Kim¹, Minhyung Lee², Kihoon Nam¹, Enhanced Incretin Effects of Exendin-4 Expressing Chimeric Plasmid Based On Two-Step Transcription Amplification System with Dendritic Bioreducible Polymer for the Treatment of Type 2 Diabetes, *J Gene Ther.* 83 (2013) 7–15. <https://doi.org/10.1016/j.earlhumdev.2006.05.022>.
- [185] M. Manconi, A. Náchér, V. Merino, M. Merino-Sanjuan, M.L. Manca, C. Mura, S. Mura, A.M. Fadda, O. Diez-Sales, Improving oral bioavailability and pharmacokinetics of liposomal metformin by glycerolphosphate-chitosan microcomplexation, *AAPS PharmSciTech.* 14 (2013) 485–496. <https://doi.org/10.1208/s12249-013-9926-4>.
- [186] A.A. Hasan, H. Madkor, S. Wageh, Formulation and evaluation of metformin hydrochloride-loaded niosomes as controlled release drug delivery system, *Drug Deliv.* 20 (2013) 120–126. <https://doi.org/10.3109/10717544.2013.779332>.
- [187] J. Rathi, S. Tamizharasi, A. Dubey, V. Rathi, Development and characterization of niosomal drug delivery of gliclazide, *J. Young Pharm.* 1 (2009) 205. <https://doi.org/10.4103/0975-1483.57065>.
- [188] A.B. Mohd, K. Sanka, S. Bandi, P. V. Diwan, N. Shastri, Solid self-

- nanoemulsifying drug delivery system (S-SNEDDS) for oral delivery of glimepiride: Development and antidiabetic activity in albino rabbits, *Drug Deliv.* 22 (2015) 499–508. <https://doi.org/10.3109/10717544.2013.879753>.
- [189] H. Liu, K. Shang, W. Liu, D. Leng, R. Li, Y. Kong, T. Zhang, Improved oral bioavailability of glyburide by a self-nanoemulsifying drug delivery system, *J. Microencapsul.* 31 (2014) 277–283. <https://doi.org/10.3109/02652048.2013.843598>.
- [190] S. Shaveta, J. Singh, M. Afzal, R. Kaur, S.S. Imam, N.K. Alruwaili, K.S. Alharbi, N.H. Alotaibi, M.S. Alshammari, I. Kazmi, M. Yasir, A. Goyel, Ameenuzzafar, Development of solid lipid nanoparticle as carrier of pioglitazone for amplification of oral efficacy: Formulation design optimization, in-vitro characterization and in-vivo biological evaluation, *J. Drug Deliv. Sci. Technol.* 57 (2020) 101674. <https://doi.org/10.1016/j.jddst.2020.101674>.
- [191] L.M.D. Gonçalves, F. Maestrelli, L.C. Mannelli, C. Ghelardini, A.J. Almeida, P. Mura, Development of solid lipid nanoparticles as carriers for improving oral bioavailability of glibenclamide, *Eur. J. Pharm. Biopharm.* 102 (2016) 41–50. <https://doi.org/10.1016/j.ejpb.2016.02.012>.
- [192] L. Ye, Y. Zhang, B. Yang, X. Zhou, J. Li, Z. Qin, D. Dong, Y. Cui, F. Yao, Zwitterionic-Modified Starch-Based Stealth Micelles for Prolonging Circulation Time and Reducing Macrophage Response, *ACS Appl. Mater. Interfaces.* 8 (2016) 4385–4398. <https://doi.org/10.1021/acsami.5b10811>.
- [193] G. Wu, C. Li, X. Liu, J. Lv, Y. Ding, Y. Liu, Y. Liu, F. Huang, L. Shi, Y. An, R. Ma, Glucose-responsive complex micelles for self-regulated delivery of insulin with effective protection of insulin and enhanced hypoglycemic activity in vivo, *Colloids Surfaces B Biointerfaces.* 180 (2019) 376–383. <https://doi.org/10.1016/j.colsurfb.2019.05.003>.
- [194] Z. Zeng, D. Qi, L. Yang, J. Liu, Y. Tang, H. Chen, X. Feng, Stimuli-responsive self-assembled dendrimers for oral protein delivery, *J. Control. Release.* 315 (2019) 206–213. <https://doi.org/10.1016/j.jconrel.2019.10.049>.
- [195] S.K. Chinnaiyan, D. Karthikeyan, V.R. Gadela, Development and Characterization of Metformin Loaded Pectin Nanoparticles for T2 Diabetes Mellitus, *Pharm. Nanotechnol.* 6 (2018) 253–263. <https://doi.org/10.2174/2211738507666181221142406>.

- [196] C.P. Dora, S.K. Singh, S. Kumar, A.K. Datusalia, A. Deep, Development and characterization of nanoparticles of glibenclamide by solvent displacement method, *Acta Pol. Pharm. - Drug Res.* 67 (2010) 283–290.
- [197] H.S.M. Ali, A.F. Hanafy, A. Alqurshi, Engineering of solidified glyburide nanocrystals for tablet formulation via loading of carriers: downstream processing, characterization, and bioavailability, *Int. J. Nanomedicine.* 14 (2019) 1893–1906. <https://doi.org/10.2147/IJN.S194734>.
- [198] B. Du, G. Shen, D. Wang, L. Pang, Z. Chen, Z. Liu, Development and characterization of glimepiride nanocrystal formulation and evaluation of its pharmacokinetic in rats, *Drug Deliv.* 20 (2013) 25–33. <https://doi.org/10.3109/10717544.2012.742939>.
- [199] B.P. Panda, R. Krishnamoorthy, S.K. Bhattamisra, N.K.H. Shivashkaregowda, L. Bin Seng, S. Patnaik, Fabrication of Second Generation Smarter PLGA Based Nanocrystal Carriers for Improvement of Drug Delivery and Therapeutic Efficacy of Gliclazide in Type-2 Diabetes Rat Model, *Sci. Rep.* 9 (2019) 1–15. <https://doi.org/10.1038/s41598-019-53996-4>.
- [200] P. Mukhopadhyay, K. Sarkar, S. Bhattacharya, R. Mishra, P.P. Kundu, Efficient oral insulin delivery by dendronized chitosan: In vitro and in vivo studies, *RSC Adv.* 4 (2014) 43890–43902. <https://doi.org/10.1039/c4ra07511k>.
- [201] H.J. Cho, J. Oh, M.K. Choo, J.I. Ha, Y. Park, H.J. Maeng, Chondroitin sulfate-capped gold nanoparticles for the oral delivery of insulin, *Int. J. Biol. Macromol.* 63 (2014) 15–20. <https://doi.org/10.1016/j.ijbiomac.2013.10.026>.
- [202] K.T. Savjani, A.K. Gajjar, J.K. Savjani, Drug Solubility: Importance and Enhancement Techniques, *ISRN Pharm.* 2012 (2012) 1–10. <https://doi.org/10.5402/2012/195727>.
- [203] M. Cirri, F. Maestrelli, G. Corti, P. Mura, M. Valleri, Fast-dissolving tablets of glyburide based on ternary solid dispersions with PEG 6000 and surfactants, *Drug Deliv.* 14 (2007) 247–255. <https://doi.org/10.1080/10717540601067802>.
- [204] Y.G. Bachhav, V.B. Patravale, SMEDDS of glyburide: Formulation, in vitro evaluation, and stability studies, *AAPS PharmSciTech.* 10 (2009) 482–487. <https://doi.org/10.1208/s12249-009-9234-1>.
- [205] J.S. Patil, P.B. Patil, P. Sonawane, J.B. Naik, Design and development of sustained-release glyburide-loaded silica nanoparticles, *Bull. Mater. Sci.* 40 (2017) 263–270. <https://doi.org/10.1007/s12034-017-1369-1>.

- [206] S. Mukherjee, S. Maity, B. Ghosh, T. Chakraborty, A. Mondal, A. Bishayee, Assessment of the antidiabetic potentiality of glyburide loaded glyceryl monostearate solid lipid nanoparticles, *J. Drug Deliv. Sci. Technol.* 55 (2020) 101451. <https://doi.org/10.1016/j.jddst.2019.101451>.
- [207] C. Zhao, Y. Jia, F. Lu, Angelica Stem: A potential low-cost source of bioactive phthalides and phytosterols, *Molecules.* 23 (2018). <https://doi.org/10.3390/molecules23123065>.
- [208] H.J. Jeong, S.Y. Nam, H.Y. Kim, M.H. Jin, M.H. Kim, S.S. Roh, H.M. Kim, Anti-allergic inflammatory effect of vanillic acid through regulating thymic stromal lymphopoietin secretion from activated mast cells, *Nat. Prod. Res.* 32 (2018) 2945–2949. <https://doi.org/10.1080/14786419.2017.1389938>.
- [209] S. Kiokias, C. Proestos, V. Oreopoulou, Phenolic acids of plant origin—a review on their antioxidant activity in vitro (O/W emulsion systems) along with their in vivo health biochemical properties, *Foods.* 9 (2020). <https://doi.org/10.3390/foods9040534>.
- [210] G. Ebinger, R. Verheyden, On the occurrence of vanillic acid in human brain and cerebrospinal fluid, *J. Neurol.* 212 (1976) 133–138. <https://doi.org/10.1007/BF00329156>.
- [211] N. Sharma, N. Tiwari, M. Vyas, N. Khurana, A. Muthuraman, P. Utreja, An overview of therapeutic effects of vanillic acid, *Plant Arch.* 20 (2020) 3053–3059.
- [212] Y.S. Park, H. Leontowicz, M. Leontowicz, J. Namiesnik, M. Suhaj, M. Cvikrová, O. Martincová, M. Weisz, S. Gorinstein, Comparison of the contents of bioactive compounds and the level of antioxidant activity in different kiwifruit cultivars, *J. Food Compos. Anal.* 24 (2011) 963–970. <https://doi.org/10.1016/j.jfca.2010.08.010>.
- [213] K. V. Shastri, V. Bhatia, P.R.P. Chapekar, V.N. Chapekar, *Actinidia Deliciosa* : a Review, *Int. J. Pharm. Sci. Res.* 3 (2012) 3543–3549. www.ijpsr.com.
- [214] H.W. Huang, A.R. Ferguson, *Actinidia* in China: Natural diversity, phylogeographical evolution, interspecific gene flow and kiwifruit cultivar improvement, *Acta Hort.* 753 (2007) 31–40. <https://doi.org/10.17660/ActaHortic.2007.753.1>.
- [215] A. Kakumani, H.R. Kethu, N. Boggula, R.R. Sankepally, B.G. Ranga, M.P. Reddy, V. Bakshi, N. Boggula, Ethnopharmacological importance of *Actinidia*

deliciosa: A literature based review, *Int. J. Res. Pharm. Pharm. Sci.* 5 (2020) 30–37.

http://webcache.googleusercontent.com/search?q=cache:FH7hTsH_CNEJ:www.pharmacyjournal.in/download/336/5-2-18-579.pdf+&cd=2&hl=en&ct=clnk&gl=in.

- [216] Y.E. Kim, C.H. Cho, H. Kang, H.J. Heo, Y.S. Cho, D.O. Kim, Kiwifruit of *Actinidia eriantha* cv. Bidan has in vitro antioxidative, anti-inflammatory and immunomodulatory effects on macrophages and splenocytes isolated from male BALB/c mice, *Food Sci. Biotechnol.* 27 (2018) 1503–1511. <https://doi.org/10.1007/s10068-018-0321-5>.
- [217] I. Lee, S. Im, C.R. Jin, H.J. Heo, Y.S. Cho, M.Y. Baik, D.O. Kim, Effect of maturity stage at harvest on antioxidant capacity and total phenolics in kiwifruits (*Actinidia* spp.) grown in Korea, *Hortic. Environ. Biotechnol.* 56 (2015) 841–848. <https://doi.org/10.1007/s13580-015-1085-y>.
- [218] S. Lee, S.K. Rasmussen, 10.1023%2FA-1003919416122.pdf, (2000) 87–91.
- [219] M.Y. Ali, S.H. Seong, S. Jannat, H.A. Jung, J.S. Choi, Ethnobotany, phytochemistry, and pharmacology of *angelica decursiva* fr. Et sav., *Nat. Prod. Sci.* 25 (2019) 181–199. <https://doi.org/10.20307/nps.2019.25.3.181>.
- [220] D. Zhao, M.N. Islam, B.R. Ahn, H.A. Jung, B.W. Kim, J.S. Choi, In vitro antioxidant and anti-inflammatory activities of *Angelica decursiva*, *Arch. Pharm. Res.* 35 (2012) 179–192. <https://doi.org/10.1007/s12272-012-0120-0>.
- [221] P. Sitarek, E. Skąła, H. Wysokińska, M. Wielanek, J. Szemraj, M. Toma, T. liwiński, The effect of *leonurus sibiricus* plant extracts on stimulating repair and protective activity against oxidative DNA damage in CHO cells and content of phenolic compounds, *Oxid. Med. Cell. Longev.* 2016 (2016). <https://doi.org/10.1155/2016/5738193>.
- [222] A. Dad, I. Ali, N. Engel, M. Atif, H. Hussain, V.U. Ahmad, P. Langer, I.R. Green, The Phytochemical Investigation and Biological Activities of *Berberis Orthobotrys*, *Int. J. Phytomedicine.* 9 (2017). <https://doi.org/10.5138/09750185.1899>.
- [223] B. Salehi, Z.A. Zakaria, R. Gyawali, S.A. Ibrahim, J. Rajkovic, Z.K. Shinwari, T. Khan, J. Sharifi-Rad, A. Ozleyen, E. Turkdonmez, M. Valussi, T.B. Tumer, L.M. Fidalgo, M. Martorell, W.N. Setzer, Piper species: A comprehensive review on their phytochemistry, biological activities and applications, 2019.

<https://doi.org/10.3390/molecules24071364>.

- [224] Alamgeer, M. Tarar, U.H. Hasan, M. Saleem, Evaluation of anticoagulant and thrombolytic activity of *Berberis orthobotrys* in animal model, *Bangladesh J. Pharmacol.* 13 (2018) 196–202. <https://doi.org/10.3329/bjp.v13i2.36201>.
- [225] N. Giacomelli, Y. Yongping, F. Huber, A. Ankli, C. Weckerle, *Angelica sinensis* (Oliv.) Diels: Influence of Value Chain on Quality Criteria and Marker Compounds Ferulic Acid and Z-Ligustilide, *Medicines*. 4 (2017) 14. <https://doi.org/10.3390/medicines4010014>.
- [226] M. Mitić, S. Janković, P. Mašković, B. Arsić, J. Mitić, J. Ickovski, Kinetic models of the extraction of vanillic acid from pumpkin seeds, *Open Chem.* 18 (2020) 22–30. <https://doi.org/10.1515/chem-2020-0001>.
- [227] V. Krimer-Malešević, Pumpkin Seeds, Nuts Seeds Heal. *Dis. Prev.* (2020) 533–542. <https://doi.org/10.1016/b978-0-12-818553-7.00037-1>.
- [228] Y. Lee, C.O. Hong, M.H. Nam, J.H. Kim, Y. Ma, Y.B. Kim, K.W. Lee, Antioxidant and glycation inhibitory activities of gold kiwifruit, *Actinidia chinensis*, *J. Appl. Biol. Chem.* 54 (2011) 460–467. <https://doi.org/10.3839/jksabc.2011.071>.
- [229] P. Sitarek, E. Skąła, H. Wysokińska, M. Wielanek, J. Szemraj, M. Toma, T. liwiński, The effect of *Leonurus sibiricus* plant extracts on stimulating repair and protective activity against oxidative DNA damage in CHO cells and content of phenolic compounds, *Oxid. Med. Cell. Longev.* 2016 (2016). <https://doi.org/10.1155/2016/5738193>.
- [230] Y. Feng, A.R. Carroll, R. Addepalli, G.A. Fechner, V.M. Avery, R.J. Quinn, Vanillic acid derivatives from the green algae *Cladophora socialis* as potent protein tyrosine phosphatase 1B inhibitors, *J. Nat. Prod.* 70 (2007) 1790–1792. <https://doi.org/10.1021/np070225o>.
- [231] X. Han, J. Guo, Y. You, M. Yin, J. Liang, C. Ren, J. Zhan, W. Huang, Vanillic acid activates thermogenesis in brown and white adipose tissue, *Food Funct.* 9 (2018) 4366–4375. <https://doi.org/10.1039/c8fo00978c>.
- [232] V.P. Mahendra, D.J. Haware, R. Kumar, cAMP-PKA dependent ERK1/2 activation is necessary for vanillic acid potentiated glucose-stimulated insulin secretion in pancreatic β -cells, *J. Funct. Foods.* 56 (2019) 110–118. <https://doi.org/10.1016/j.jff.2019.02.047>.
- [233] G. Ji, R. Sun, H. Hu, F. Xu, X. Yu, V. Priya Veeraghavan, S. Krishna

- Mohan, X. Chi, Vanillic acid ameliorates hyperglycemia-induced oxidative stress and inflammation in streptozotocin-induced diabetic rats, *J. King Saud Univ. - Sci.* 32 (2020) 2905–2911. <https://doi.org/10.1016/j.jksus.2020.04.010>.
- [234] S. Pawar, S. Khairnar, V. Patil, R. Bhambar, Effect of vanillic acid on nerve conduction velocity in chronic constriction injury model of neuropathy, *Indian J. Pharm. Educ. Res.* 54 (2020) 108–113. <https://doi.org/10.5530/ijper.54.1.13>.
- [235] A.C. Mirza, S.S. Panchal, Safety assessment of vanillic acid: Subacute oral toxicity studies in wistar rats, 2020. <https://doi.org/10.4274/tjps.galenos.2019.92678>.
- [236] M.G. Erdem, N. Cinkilic, O. Vatan, D. Yilmaz, D. Bagdas, R. Bilaloglu, Genotoxic and anti-genotoxic effects of vanillic acid against mitomycin c-induced genomic damage in human lymphocytes in vitro, *Asian Pacific J. Cancer Prev.* 13 (2012) 4993–4998. <https://doi.org/10.7314/APJCP.2012.13.10.4993>.
- [237] I. V. Almeida, F.M.L. Cavalcante, V.E.P. Vicentini, Different responses of vanillic acid, a phenolic compound, in HTC cells: Cytotoxicity, antiproliferative activity, and protection from DNA-induced damage, *Genet. Mol. Res.* 15 (2016) 1–12. <https://doi.org/10.4238/gmr15049388>.
- [238] G. Taner, D. Özkan Vardar, S. Aydin, Z. Aytaç, A. Başaran, N. Başaran, Use of in vitro assays to assess the potential cytotoxic, genotoxic and antigenotoxic effects of vanillic and cinnamic acid, *Drug Chem. Toxicol.* 40 (2017) 183–190. <https://doi.org/10.1080/01480545.2016.1190740>.
- [239] R. Ullah, M. Ikram, T.J. Park, R. Ahmad, K. Saeed, S.I. Alam, I.U. Rehman, A. Khan, I. Khan, M.G. Jo, M.O. Kim, Vanillic acid, a bioactive phenolic compound, counteracts lps-induced neurotoxicity by regulating c-jun n-terminal kinase in mouse brain, *Int. J. Mol. Sci.* 22 (2021) 1–21. <https://doi.org/10.3390/ijms22010361>.
- [240] D. Lombardo, M.A. Kiselev, S. Magazù, P. Calandra, Amphiphiles self-assembly: Basic concepts and future perspectives of supramolecular approaches, *Adv. Condens. Matter Phys.* 2015 (2015). <https://doi.org/10.1155/2015/151683>.
- [241] K. Letchford, H. Burt, A review of the formation and classification of amphiphilic block copolymer nanoparticulate structures: micelles, nanospheres, nanocapsules and polymersomes, *Eur. J. Pharm. Biopharm.* 65 (2007) 259–

269. <https://doi.org/10.1016/j.ejpb.2006.11.009>.
- [242] H. Feng, X. Lu, W. Wang, N.G. Kang, J.W. Mays, Block copolymers: Synthesis, self-assembly, and applications, *Polymers (Basel)*. 9 (2017). <https://doi.org/10.3390/polym9100494>.
- [243] V. Agrahari, V. Agrahari, Advances and applications of block-copolymer-based nanoformulations, *Drug Discov. Today*. 23 (2018) 1139–1151. <https://doi.org/10.1016/j.drudis.2018.03.004>.
- [244] W.A. Braunecker, K. Matyjaszewski, Controlled/living radical polymerization: Features, developments, and perspectives, *Prog. Polym. Sci.* 32 (2007) 93–146. <https://doi.org/10.1016/j.progpolymsci.2006.11.002>.
- [245] G. Riess, Polymer Micelles: Amphiphilic Block and Graft Copolymers as Polymeric Surfactants, *Handb. Ind. Water Soluble Polym.* (2007) 174–238. <https://doi.org/10.1002/9780470988701.ch7>.
- [246] R.B. Grubbs, Nitroxide-mediated radical polymerization: Limitations and versatility, *Polym. Rev.* 51 (2011) 104–137. <https://doi.org/10.1080/15583724.2011.566405>.
- [247] M. Destarac, On the critical role of RAFT agent design in reversible addition-fragmentation chain transfer (RAFT) polymerization, *Polym. Rev.* 51 (2011) 163–187. <https://doi.org/10.1080/15583724.2011.568130>.
- [248] D.J. Keddie, A guide to the synthesis of block copolymers using reversible-addition fragmentation chain transfer (RAFT) polymerization, *Chem. Soc. Rev.* 43 (2014) 496–505. <https://doi.org/10.1039/c3cs60290g>.
- [249] S.Y. Avsar, M. Kyropoulou, S. Di Leone, C.A. Schoenenberger, W.P. Meier, C.G. Palivan, Biomolecules turn self-assembling amphiphilic block co-polymer platforms into biomimetic interfaces, *Front. Chem.* 7 (2019) 1–29. <https://doi.org/10.3389/fchem.2018.00645>.
- [250] K. Matyjaszewski, J. Spanswick, Controlled/living radical polymerization, *Mater. Today*. 8 (2005) 26–33. [https://doi.org/10.1016/S1369-7021\(05\)00745-5](https://doi.org/10.1016/S1369-7021(05)00745-5).
- [251] V. Yadav, N. Hashmi, W. Ding, T.H. Li, M.K. Mahanthappa, J.C. Conrad, M.L. Robertson, Dispersity control in atom transfer radical polymerizations through addition of phenylhydrazine, *Polym. Chem.* 9 (2018) 4332–4342. <https://doi.org/10.1039/c8py00033f>.
- [252] D. Braun, Origins and development of initiation of free radical polymerization

- processes, *Int. J. Polym. Sci.* 2009 (2009).
<https://doi.org/10.1155/2009/893234>.
- [253] G. Gody, P.B. Zetterlund, S. Perrier, S. Harrisson, The limits of precision monomer placement in chain growth polymerization, *Nat. Commun.* 7 (2016) 1–8. <https://doi.org/10.1038/ncomms10514>.
- [254] C. Hagiopol, C. Llc, Copolymers \$ Binary Copolymerization, *Mater. Sci. Mater. Eng.* (2016) 1–5. <https://doi.org/10.1016/B978-0-12-803581-8.01126-7>.
- [255] A. Solmaz, Amphiphilic Block Copolymer Micelles for Drug Delivery Vehicles, *Fac. Math. Nat. Sci.* (2010) 1–26.
- [256] V.K. Mourya, N. Inamdar, R.B. Nawale, S.S. Kulthe, Polymeric micelles: General considerations and their applications, *Indian J. Pharm. Educ. Res.* 45 (2011) 128–138.
- [257] X. Liu, Y. Chen, X. Chen, J. Su, C. Huang, Enhanced efficacy of baicalin-loaded TPGS polymeric micelles against periodontitis, *Mater. Sci. Eng. C.* 101 (2019) 387–395. <https://doi.org/10.1016/j.msec.2019.03.103>.
- [258] M.L. Adams, A. Lavasanifar, G.S. Kwon, Amphiphilic block copolymers for drug delivery, *J. Pharm. Sci.* 92 (2003) 1343–1355.
<https://doi.org/10.1002/jps.10397>.
- [259] U. Sheth, S. Tiwari, A. Bahadur, Preparation and characterization of anti-tubercular drugs encapsulated in polymer micelles, *J. Drug Deliv. Sci. Technol.* 48 (2018) 422–428. <https://doi.org/10.1016/j.jddst.2018.10.021>.
- [260] Z. Sezgin, N. Yüksel, T. Baykara, Preparation and characterization of polymeric micelles for solubilization of poorly soluble anticancer drugs, *Eur. J. Pharm. Biopharm.* 64 (2006) 261–268.
<https://doi.org/10.1016/j.ejpb.2006.06.003>.
- [261] H.C. Shin, A.W.G. Alani, D.A. Rao, N.C. Rockich, G.S. Kwon, Multi-drug loaded polymeric micelles for simultaneous delivery of poorly soluble anticancer drugs, *J. Control. Release.* 140 (2009) 294–300.
<https://doi.org/10.1016/j.jconrel.2009.04.024>.
- [262] R. Trivedi, U.B. Kompella, Nanomicellar formulations for sustained drug delivery: Strategies and underlying principles, *Nanomedicine.* 5 (2010) 485–505. <https://doi.org/10.2217/nnm.10.10>.
- [263] N. Nishiyama, K. Kataoka, Current state, achievements, and future prospects of polymeric micelles as nanocarriers for drug and gene delivery, *Pharmacol.*

- Ther. 112 (2006) 630–648. <https://doi.org/10.1016/j.pharmthera.2006.05.006>.
- [264] H. Cabral, K. Kataoka, Progress of drug-loaded polymeric micelles into clinical studies, *J. Control. Release.* 190 (2014) 465–476. <https://doi.org/10.1016/j.jconrel.2014.06.042>.
- [265] X. Guo, Z. Zhao, D. Chen, M. Qiao, F. Wan, D. Cun, Y. Sun, M. Yang, Co-delivery of resveratrol and docetaxel via polymeric micelles to improve the treatment of drug-resistant tumors, *Asian J. Pharm. Sci.* 14 (2019) 78–85. <https://doi.org/10.1016/j.ajps.2018.03.002>.
- [266] G. Sun, J. Liu, X. Wang, M. Li, X. Cui, L. Zhang, D. Wu, P. Tang, Fabrication of dual-sensitive poly(β -hydroxyl amine) micelles for controlled drug delivery, *Eur. Polym. J.* 114 (2019) 338–345. <https://doi.org/10.1016/j.eurpolymj.2019.02.048>.
- [267] S.B. La, T. Okano, K. Kataoka, Preparation and Characterization of the Micelle-Forming Polymeric Drug Indomethacin-Incorporated Poly(ethylene oxide)–Poly(-benzyl), *J. Pharm. Sci.* 85 (1996) 85–90.
- [268] Y. Yamamoto, K. Yasugi, A. Harada, Y. Nagasaki, K. Kataoka, Temperature-related change in the properties relevant to drug delivery of poly(ethylene glycol)-poly(D,L-lactide) block copolymer micelles in aqueous milieu, *J. Control. Release.* 82 (2002) 359–371. [https://doi.org/10.1016/S0168-3659\(02\)00147-5](https://doi.org/10.1016/S0168-3659(02)00147-5).
- [269] C. Li, C.C. Tho, D. Galaktionova, X. Chen, P. Král, U. Mirsaidov, Dynamics of amphiphilic block copolymers in an aqueous solution: Direct imaging of micelle formation and nanoparticle encapsulation, *Nanoscale.* 11 (2019) 2299–2305. <https://doi.org/10.1039/c8nr08922a>.
- [270] Y.H.A. Hussein, M. Youssry, Polymeric micelles of biodegradable diblock copolymers: Enhanced encapsulation of hydrophobic drugs, *Materials (Basel).* 11 (2018). <https://doi.org/10.3390/ma11050688>.
- [271] T. Chida, Y. Miura, H. Cabral, T. Nomoto, K. Kataoka, N. Nishiyama, Epirubicin-loaded polymeric micelles effectively treat axillary lymph nodes metastasis of breast cancer through selective accumulation and pH-triggered drug release, *J. Control. Release.* 292 (2018) 130–140. <https://doi.org/10.1016/j.jconrel.2018.10.035>.
- [272] A.S. Deshmukh, P.N. Chauhan, M.N. Noolvi, K. Chaturvedi, K. Ganguly, S.S. Shukla, M.N. Nadagouda, T.M. Aminabhavi, Polymeric micelles: Basic

- research to clinical practice, *Int. J. Pharm.* 532 (2017) 249–268.
<https://doi.org/10.1016/j.ijpharm.2017.09.005>.
- [273] M. Oak, R. Mandke, J. Singh, Smart polymers for peptide and protein parenteral sustained delivery, *Drug Discov. Today Technol.* 9 (2012) e131–e140. <https://doi.org/10.1016/j.ddtec.2012.05.001>.
- [274] W. Xu, P. Ling, T. Zhang, Polymeric Micelles, a Promising Drug Delivery System to Enhance Bioavailability of Poorly Water-Soluble Drugs, *J. Drug Deliv.* 2013 (2013) 1–15. <https://doi.org/10.1155/2013/340315>.
- [275] D. Hwang, J.D. Ramsey, A. V. Kabanov, Polymeric micelles for the delivery of poorly soluble drugs: From nanoformulation to clinical approval, *Adv. Drug Deliv. Rev.* 156 (2020) 80–118. <https://doi.org/10.1016/j.addr.2020.09.009>.
- [276] G. Gaucher, P. Satturwar, M.C. Jones, A. Furtos, J.C. Leroux, Polymeric micelles for oral drug delivery, *Eur. J. Pharm. Biopharm.* 76 (2010) 147–158. <https://doi.org/10.1016/j.ejpb.2010.06.007>.
- [277] L. Dian, E. Yu, X. Chen, X. Wen, Z. Zhang, L. Qin, Q. Wang, G. Li, C. Wu, Enhancing oral bioavailability of quercetin using novel soluplus polymeric micelles, *Nanoscale Res. Lett.* 9 (2014) 1–11. <https://doi.org/10.1186/1556-276X-9-684>.
- [278] T. Zhang, J. Luo, Y. Fu, H. Li, R. Ding, T. Gong, Z. Zhang, Novel oral administrated paclitaxel micelles with enhanced bioavailability and antitumor efficacy for resistant breast cancer, *Colloids Surfaces B Biointerfaces.* 150 (2017) 89–97. <https://doi.org/10.1016/j.colsurfb.2016.11.024>.
- [279] M.S. Alai, W.J. Lin, S.S. Pingale, Application of polymeric nanoparticles and micelles in insulin oral delivery, *J. Food Drug Anal.* 23 (2015) 351–358. <https://doi.org/10.1016/j.jfda.2015.01.007>.
- [280] A. Salimi, B.S. Makhmal Zadeh, M. Kazemi, Preparation and optimization of polymeric micelles as an oral drug delivery system for deferoxamine mesylate: In vitro and ex vivo studies, *Res. Pharm. Sci.* 14 (2019) 293–307. <https://doi.org/10.4103/1735-5362.263554>.
- [281] H. Deng, J. Liu, X. Zhao, Y. Zhang, J. Liu, S. Xu, L. Deng, A. Dong, J. Zhang, PEG-b-PCL copolymer micelles with the ability of pH-controlled negative-to-positive charge reversal for intracellular delivery of doxorubicin, *Biomacromolecules.* 15 (2014) 4281–4292. <https://doi.org/10.1021/bm501290t>.
- [282] T. Yin, X. Liu, J. Wang, Y. An, Z. Zhang, L. Shi, Thermosensitive mixed shell

polymeric micelles decorated with gold nanoparticles at the outmost surface: Tunable surface plasmon resonance and enhanced catalytic properties with excellent colloidal stability, *RSC Adv.* 5 (2015) 47458–47465.

<https://doi.org/10.1039/c5ra06021d>.

- [283] S. Bas, M.D. Soucek, Synthesis, characterization and properties of amphiphilic block copolymers of 2-hydroxyethyl methacrylate and polydimethylsiloxane prepared by atom transfer radical polymerization, *Polym. J.* 44 (2012) 1087–1097. <https://doi.org/10.1038/pj.2012.86>.
- [284] M. Bagheri, J. Bresseleers, A. Varela-Moreira, O. Sandre, S.A. Meeuwissen, R.M. Schiffelers, J.M. Metselaar, C.F. Van Nostrum, J.C.M. Van Hest, W.E. Hennink, Effect of Formulation and Processing Parameters on the Size of mPEG- b-p(HPMA-Bz) Polymeric Micelles, *Langmuir.* 34 (2018) 15495–15506. <https://doi.org/10.1021/acs.langmuir.8b03576>.
- [285] W. Li, M. Nakayama, J. Akimoto, T. Okano, Effect of block compositions of amphiphilic block copolymers on the physicochemical properties of polymeric micelles, *Polymer (Guildf).* 52 (2011) 3783–3790. <https://doi.org/10.1016/j.polymer.2011.06.026>.
- [286] L. Glavas, P. Olsén, K. Odelius, A.C. Albertsson, Achieving micelle control through core crystallinity, *Biomacromolecules.* 14 (2013) 4150–4156. <https://doi.org/10.1021/bm401312j>.
- [287] C. de O. Rangel-Yagui, A. Pessoa, L.C. Tavares, Micellar solubilization of drugs, *J. Pharm. Pharm. Sci.* 8 (2005) 147–163.
- [288] S.S. Kulthe, Y.M. Choudhari, N.N. Inamdar, V. Mourya, Polymeric micelles: Authoritative aspects for drug delivery, *Des. Monomers Polym.* 15 (2012) 465–521. <https://doi.org/10.1080/1385772X.2012.688328>.
- [289] N. Saadah, M. Yusof, M. Ashokkumar, *Handbook of Ultrasonics and Sonochemistry*, 2016. <https://doi.org/10.1007/978-981-287-470-2>.
- [290] H.M. Aliabadi, A. Lavasanifar, Polymeric micelles for drug delivery, *Expert Opin. Drug Deliv.* 3 (2006) 139–162. <https://doi.org/10.1517/17425247.3.1.139>.
- [291] S.M.N. Simões, A.R. Figueiras, F. Veiga, A. Concheiro, C. Alvarez-Lorenzo, Polymeric micelles for oral drug administration enabling locoregional and systemic treatments, *Expert Opin. Drug Deliv.* 12 (2015) 297–318. <https://doi.org/10.1517/17425247.2015.960841>.

- [292] K. Knop, G.M. Pavlov, T. Rudolph, K. Martin, D. Pretzel, B.O. Jahn, D.H. Scharf, A.A. Brakhage, V. Makarov, U. Möllmann, F.H. Schacher, U.S. Schubert, Amphiphilic star-shaped block copolymers as unimolecular drug delivery systems: Investigations using a novel fungicide, *Soft Matter*. 9 (2013) 715–726. <https://doi.org/10.1039/c2sm26509e>.
- [293] B.J. Ree, J. Lee, Y. Satoh, K. Kwon, T. Isono, T. Satoh, M. Ree, A comparative study of dynamic light and X-ray scatterings on micelles of topological polymer amphiphiles, *Polymers (Basel)*. 10 (2018). <https://doi.org/10.3390/polym10121347>.
- [294] J. Cvejić, M. Poša, A. Sebenji, M. Atanacković, Comparison of solubilization capacity of resveratrol in sodium 3 α ,12 α -dihydroxy-7-oxo-5 β -cholanoate and sodium dodecyl sulfate, *Sci. World J.* 2014 (2014) 1–8. <https://doi.org/10.1155/2014/265953>.
- [295] J.E. Park, S.E. Chun, D. Reichel, J.S. Min, S.C. Lee, S. Han, G. Ryoo, Y. Oh, S.H. Park, H.M. Ryu, K.B. Kim, H.Y. Lee, S.K. Bae, Y. Bae, W. Lee, Polymer micelle formulation for the proteasome inhibitor drug carfilzomib: Anticancer efficacy and pharmacokinetic studies in mice, *PLoS One*. 12 (2017) 1–12. <https://doi.org/10.1371/journal.pone.0173247>.
- [296] Y. Wan, Z. Gan, Z. Li, Effects of the surface charge on the stability of PEG-b-PCL micelles: Simulation of the interactions between charged micelles and plasma components, *Polym. Chem.* 5 (2014) 1720–1727. <https://doi.org/10.1039/c3py01281f>.
- [297] Y. Ahn, Y. Jun, Measurement of pain-like response to various NICU stimulants for high-risk infants, *Early Hum. Dev.* 83 (2007) 255–262. <https://doi.org/10.1016/j.earlhumdev.2006.05.022>.
- [298] C. Allen, D. Maysinger, A. Eisenberg, 1-s2.0-S0927776599000582-main.pdf, *Colloids Surfaces B Biointerfaces*. 16 (1999) 3–27.
- [299] A. Richter, C. Olbrich, M. Krause, T. Kissel, Solubilization of Sagopilone, a poorly water-soluble anticancer drug, using polymeric micelles for parenteral delivery, *Int. J. Pharm.* 389 (2010) 244–253. <https://doi.org/10.1016/j.ijpharm.2010.01.032>.
- [300] N. Larson, H. Ghandehari, Polymeric conjugates for drug delivery, *Chem. Mater.* 24 (2012) 840–853. <https://doi.org/10.1021/cm2031569>.
- [301] H. Ringsdorf, *Structure and Properties of Pharmacologically Active Polymers.*,

- J Polym Sci Polym Symp. 153 (1975) 135–153.
<https://doi.org/10.1002/polc.5070510111>.
- [302] M. Yokoyama, Polymeric micelles as a new drug carrier system and their required considerations for clinical trials, *Expert Opin. Drug Deliv.* 7 (2010) 145–158. <https://doi.org/10.1517/17425240903436479>.
- [303] V.P. Torchilin, PEG-based micelles as carriers of contrast agents for different imaging modalities, *Adv. Drug Deliv. Rev.* 54 (2002) 235–252.
[https://doi.org/10.1016/S0169-409X\(02\)00019-4](https://doi.org/10.1016/S0169-409X(02)00019-4).
- [304] K. Cholkar, A. Patel, A. Dutt Vadlapudi, A. K. Mitra, Novel Nanomicellar Formulation Approaches for Anterior and Posterior Segment Ocular Drug Delivery, *Recent Patents Nanomedicine*. 2 (2012) 82–95.
<https://doi.org/10.2174/1877912311202020082>.
- [305] A. Mandal, R. Bisht, I.D. Rupenthal, A.K. Mitra, K. City, B. Ocular, T. Unit, N. Zealand, N. Eye, N. Zealand, HHS Public Access, (2018) 96–116.
<https://doi.org/10.1016/j.jconrel.2017.01.012.Polymeric>.
- [306] E. V. Batrakova, T.K. Bronich, J.A. Vetro, A. V. Kabanov, Polymer micelles as drug carriers, *Nanoparticulates as Drug Carriers*. (2006) 57–93.
https://doi.org/10.1142/9781860949074_0005.
- [307] V.P. Torchilin, Structure and design of polymeric surfactant-based drug delivery systems, *J. Control. Release*. 73 (2001) 137–172.
[https://doi.org/10.1016/S0168-3659\(01\)00299-1](https://doi.org/10.1016/S0168-3659(01)00299-1).
- [308] Y.H. Feng, X.P. Zhang, J.Y. Li, X.D. Guo, How is a micelle formed from amphiphilic polymers in a dialysis process: Insight from mesoscopic studies, *Chem. Phys. Lett.* 754 (2020) 137711.
<https://doi.org/10.1016/j.cplett.2020.137711>.
- [309] J. Liu, F. Zeng, C. Allen, Influence of serum protein on polycarbonate-based copolymer micelles as a delivery system for a hydrophobic anti-cancer agent, *J. Control. Release*. 103 (2005) 481–497.
<https://doi.org/10.1016/j.jconrel.2004.12.013>.
- [310] X. Ai, L. Zhong, H. Niu, Z. He, Thin-film hydration preparation method and stability test of DOX-loaded disulfide-linked polyethylene glycol 5000-lysine-di-tocopherol succinate nanomicelles, *Asian J. Pharm. Sci.* 9 (2014) 244–250.
<https://doi.org/10.1016/j.ajps.2014.06.006>.
- [311] M. Almeida, M. Magalhães, F. Veiga, A. Figueiras, Poloxamers, poloxamines

- and polymeric micelles: Definition, structure and therapeutic applications in cancer, *J. Polym. Res.* 25 (2018). <https://doi.org/10.1007/s10965-017-1426-x>.
- [312] K. Esparza, H. Onyuksel, Development of co-solvent freeze-drying method for the encapsulation of water-insoluble thiostrepton in sterically stabilized micelles, *Int. J. Pharm.* 556 (2019) 21–29. <https://doi.org/10.1016/j.ijpharm.2018.12.001>.
- [313] H. Chen, C. Khemtong, X. Yang, X. Chang, J. Gao, Nanonization strategies for poorly water-soluble drugs, *Drug Discov. Today.* 16 (2011) 354–360. <https://doi.org/10.1016/j.drudis.2010.02.009>.
- [314] Z. Karami, S. Sadighian, K. Rostamizadeh, S.H. Hosseini, S. Rezaee, M. Hamidi, Magnetic brain targeting of naproxen-loaded polymeric micelles: pharmacokinetics and biodistribution study, *Mater. Sci. Eng. C.* 100 (2019) 771–780. <https://doi.org/10.1016/j.msec.2019.03.004>.
- [315] L. Marinelli, I. Cacciatore, E. Fornasari, C. Gasbarri, G. Angelini, A. Marrazzo, A. Pandolfi, D. Mandatori, Y. Shi, C.F. Van Nostrum, W.E. Hennink, A. Di Stefano, Preparation and characterization of polymeric micelles loaded with a potential anticancer prodrug, *J. Drug Deliv. Sci. Technol.* 35 (2016) 24–29. <https://doi.org/10.1016/j.jddst.2016.06.006>.
- [316] D. Neradovic, O. Soga, C.F. Van Nostrum, W.E. Hennink, The effect of the processing and formulation parameters on the size of nanoparticles based on block copolymers of poly(ethylene glycol) and poly(N-isopropylacrylamide) with and without hydrolytically sensitive groups, *Biomaterials.* 25 (2004) 2409–2418. <https://doi.org/10.1016/j.biomaterials.2003.09.024>.
- [317] S. Biswas, P. Kumari, P.M. Lakhani, B. Ghosh, Recent advances in polymeric micelles for anti-cancer drug delivery, Elsevier B.V., 2016. <https://doi.org/10.1016/j.ejps.2015.12.031>.
- [318] B. Ghosh, S. Biswas, Polymeric micelles in cancer therapy: State of the art, *J. Control. Release.* 332 (2021) 127–147. <https://doi.org/10.1016/j.jconrel.2021.02.016>.
- [319] I. Romera, A. Cebrián-Cuenca, F. Álvarez-Guisasola, F. Gomez-Peralta, J. Reviriego, A Review of Practical Issues on the Use of Glucagon-Like Peptide-1 Receptor Agonists for the Management of Type 2 Diabetes, *Diabetes Ther.* 10 (2019) 5–19. <https://doi.org/10.1007/s13300-018-0535-9>.
- [320] S. Senapati, A.K. Mahanta, S. Kumar, P. Maiti, Controlled drug delivery

- vehicles for cancer treatment and their performance, *Signal Transduct. Target. Ther.* 3 (2018) 1–19. <https://doi.org/10.1038/s41392-017-0004-3>.
- [321] I. Dasgupta, A. Chatterjee, Recent advances in miRNA delivery systems, *Methods Protoc.* 4 (2021) 1–18. <https://doi.org/10.3390/mps4010010>.
- [322] Y. Bae, N. Nishiyama, S. Fukushima, H. Koyama, M. Yasuhiro, K. Kataoka, Preparation and biological characterization of polymeric micelle drug carriers with intracellular pH-triggered drug release property: Tumor permeability, controlled subcellular drug distribution, and enhanced in vivo antitumor efficacy, *Bioconjug. Chem.* 16 (2005) 122–130. <https://doi.org/10.1021/bc0498166>.
- [323] Y. Liu, W. Wang, J. Yang, C. Zhou, J. Sun, pH-sensitive polymeric micelles triggered drug release for extracellular and intracellular drug targeting delivery, *Asian J. Pharm. Sci.* 8 (2013) 159–167. <https://doi.org/10.1016/j.ajps.2013.07.021>.
- [324] X. Han, Y. Lu, J. Xie, E. Zhang, H. Zhu, H. Du, K. Wang, B. Song, C. Yang, Y. Shi, Z. Cao, Zwitterionic micelles efficiently deliver oral insulin without opening tight junctions, *Nat. Nanotechnol.* 15 (2020) 605–614. <https://doi.org/10.1038/s41565-020-0693-6>.
- [325] M. Lopes, S. Simões, F. Veiga, R. Seça, A. Ribeiro, Why most oral insulin formulations do not reach clinical trials, *Ther. Deliv.* 6 (2015) 973–987. <https://doi.org/10.4155/TDE.15.47>.
- [326] P. Fonte, F. Araújo, S. Reis, B. Sarmiento, Oral insulin delivery: How far are we?, *J. Diabetes Sci. Technol.* 7 (2013) 520–531. <https://doi.org/10.1177/193229681300700228>.
- [327] N.A.N. Hanafy, M. El-Kemary, S. Leporatti, Micelles structure development as a strategy to improve smart cancer therapy, *Cancers (Basel)*. 10 (2018) 1–14. <https://doi.org/10.3390/cancers10070238>.
- [328] J. Hu, S. Miura, K. Na, Y.H. Bae, PH-responsive and charge shielded cationic micelle of poly(l-histidine)- block-short branched PEI for acidic cancer treatment, *J. Control. Release.* 172 (2013) 69–76. <https://doi.org/10.1016/j.jconrel.2013.08.007>.
- [329] J. Yang, G. Zhang, X. Zhang, H. Shen, J. Yang, Smarter glucose-sensitivity of polymeric micelles formed from phenylborate ester-co-pyrenylboronic ester for insulin delivery at physiological pH, *RSC Adv.* 4 (2014) 49964–49973.

<https://doi.org/10.1039/c4ra08593k>.

- [330] P.E. Bunney, A.N. Zink, A.A. Holm, C.J. Billington, C.M. Kotz, Orexin activation counteracts decreases in nonexercise activity thermogenesis (NEAT) caused by high-fat diet, *Physiol. Behav.* 176 (2017) 139–148.
<https://doi.org/10.1016/j.physbeh.2017.03.040>.
- [331] N. Wen, S. Lü, C. Gao, X. Xu, X. Bai, C. Wu, P. Ning, M. Liu, Glucose-responsive zwitterionic dialdehyde starch-based micelles with potential anti-phagocytic behavior for insulin delivery, *Chem. Eng. J.* 335 (2018) 52–62.
<https://doi.org/10.1016/j.cej.2017.10.096>.
- [332] G. Liu, R. Ma, J. Ren, Z. Li, H. Zhang, Z. Zhang, Y. An, L. Shi, A glucose-responsive complex polymeric micelle enabling repeated on-off release and insulin protection, *Soft Matter*. 9 (2013) 1636–1644.
<https://doi.org/10.1039/c2sm26690c>.
- [333] T. Tong, Q. Lou, M. Zhao, L. Mou, Development of cationic polymer-based nanoplatforM for insulin delivery and diabetes treatment, *Mater. Express*. 10 (2020) 374–383. <https://doi.org/10.1166/mex.2020.1649>.
- [334] L. Zhao, J. Ding, C. Xiao, P. He, Z. Tang, X. Pang, X. Zhuang, X. Chen, Glucose-sensitive polypeptide micelles for self-regulated insulin release at physiological pH, *J. Mater. Chem.* 22 (2012) 12319–12328.
<https://doi.org/10.1039/c2jm31040f>.
- [335] C.C.L. Quianzon, I.E. Cheikh, History of current non-insulin medications for diabetes mellitus, *J. Community Hosp. Intern. Med. Perspect.* 2 (2012) 19081.
<https://doi.org/10.3402/jchimp.v2i3.19081>.
- [336] C.E. Leonard, S. Hennessy, X. Han, D.S. Siscovick, J.H. Flory, R. Deo, Pro- and anti-arrhythmic actions of sulfonylureas: mechanistic and clinical evidence, *Trends Endocrinol Metab.* 28 (2018) 561–586.
<https://doi.org/10.1016/j.tem.2017.04.003>.
- [337] M. Tabbakhian, F. Hasanzadeh, N. Tavakoli, Z. Jamshidian, Dissolution enhancement of glibenclamide by solid dispersion: Solvent evaporation versus a supercritical fluid-based solvent -antisolvent technique, *Res. Pharm. Sci.* 9 (2014) 337–350.
- [338] H. Mandil, A.A. Sakur, S. Alulu, Differential pulse polarographic analysis of glyburide in pure form and pharmaceutical formulations, *Asian J. Chem.* 24 (2012) 2980–2984.

- [339] A.L. Glover, S.M. Nikles, J.A. Nikles, C.S. Brazel, D.E. Nikles, Polymer micelles with crystalline cores for thermally triggered release, *Langmuir*. 28 (2012) 10653–10660. <https://doi.org/10.1021/la300895c>.
- [340] A.A. Thorat, S. V. Dalvi, Liquid antisolvent precipitation and stabilization of nanoparticles of poorly water soluble drugs in aqueous suspensions: Recent developments and future perspective, *Chem. Eng. J.* 181–182 (2012) 1–34. <https://doi.org/10.1016/j.cej.2011.12.044>.
- [341] R. Kumar, R. Khursheed, R. Kumar, A. Awasthi, N. Sharma, S. Khurana, B. Kapoor, N. Khurana, S.K. Singh, K. Gowthamarajan, A. Wadhvani, Self-nanoemulsifying drug delivery system of fisetin: Formulation, optimization, characterization and cytotoxicity assessment, *J. Drug Deliv. Sci. Technol.* 54 (2019). <https://doi.org/10.1016/j.jddst.2019.101252>.
- [342] C.F. Mandenius, A. Brundin, Bioprocess optimization using design-of-experiments methodology, *Biotechnol. Prog.* 24 (2008) 1191–1203. <https://doi.org/10.1002/btpr.67>.
- [343] L.X. Yu, G. Amidon, M.A. Khan, S.W. Hoag, J. Polli, G.K. Raju, J. Woodcock, Understanding pharmaceutical quality by design, *AAPS J.* 16 (2014) 771–783. <https://doi.org/10.1208/s12248-014-9598-3>.
- [344] A. Czyski, J. Sznura, The application of Box-Behnken-Design in the optimization of HPLC separation of fluoroquinolones, *Sci. Rep.* 9 (2019) 1–10. <https://doi.org/10.1038/s41598-019-55761-z>.
- [345] T.F. Zhang, J.F. Yang, D.K.J. Lin, Small Box-Behnken design, *Stat. Probab. Lett.* 81 (2011) 1027–1033. <https://doi.org/10.1016/j.spl.2011.02.024>.
- [346] N. Thotakura, M. Dadarwal, R. Kumar, B. Singh, G. Sharma, P. Kumar, O.P. Katare, K. Raza, Chitosan-palmitic acid based polymeric micelles as promising carrier for circumventing pharmacokinetic and drug delivery concerns of tamoxifen, *Int. J. Biol. Macromol.* 102 (2017) 1220–1225. <https://doi.org/10.1016/j.ijbiomac.2017.05.016>.
- [347] H. Danafar, S. Davaran, K. Rostamizadeh, H. Valizadeh, M. Hamidi, Biodegradable m-PEG/PCL core-shell micelles: Preparation and characterization as a sustained release formulation for curcumin, *Adv. Pharm. Bull.* 4 (2014) 501–510. <https://doi.org/10.5681/apb.2014.074>.
- [348] Q. Huang, L. Chen, H. Teng, H. Song, X. Wu, M. Xu, Phenolic compounds ameliorate the glucose uptake in HepG2 cells' insulin resistance via activating

- AMPK: Anti-diabetic effect of phenolic compounds in HepG2 cells, *J. Funct. Foods*. 19 (2015) 487–494. <https://doi.org/10.1016/j.jff.2015.09.020>.
- [349] V. Vichai, K. Kirtikara, Sulforhodamine B colorimetric assay for cytotoxicity screening, *Nat. Protoc.* 1 (2006) 1112–1116. <https://doi.org/10.1038/nprot.2006.179>.
- [350] V.K. Reddy, N. Swamy, R. Rathod, P. Sengupta, A Bioanalytical Method for Eliglustat Quantification in Rat Plasma, *J. Chromatogr. Sci.* 57 (2019) 600–605. <https://doi.org/10.1093/chromsci/bmz033>.
- [351] M. Barfield, R. Wheller, Use of dried plasma spots in the determination of pharmacokinetics in clinical studies: Validation of a quantitative bioanalytical method, *Anal. Chem.* 83 (2011) 118–124. <https://doi.org/10.1021/ac102003t>.
- [352] W. Nowatzke, E. Woolf, Best practices during bioanalytical method validation for the characterization of assay reagents and the evaluation of analyte stability in assay standards, quality controls, and study samples, *AAPS J.* 9 (2007) 117–122. <https://doi.org/10.1208/aapsj0902013>.
- [353] M. Manikandan, K. Kannan, Study on in vivo release and in vivo absorption of Camptothecin-loaded polymeric nanoparticles: Level a in vitro-in vivo correlation, *Asian J. Pharm. Clin. Res.* 9 (2016).
- [354] A. Jain, R. Kaur, S. Beg, V. Kushwah, S. Jain, B. Singh, Novel cationic supersaturable nanomicellar systems of raloxifene hydrochloride with enhanced biopharmaceutical attributes, *Drug Deliv. Transl. Res.* 8 (2018) 670–692. <https://doi.org/10.1007/s13346-018-0514-8>.
- [355] K. Srinivasan, B. Viswanad, L. Asrat, C.L. Kaul, P. Ramarao, Combination of high-fat diet-fed and low-dose streptozotocin-treated rat: A model for type 2 diabetes and pharmacological screening, *Pharmacol. Res.* 52 (2005) 313–320. <https://doi.org/10.1016/j.phrs.2005.05.004>.
- [356] F. Wang, W. Dai, Y. Wang, M. Shen, K. Chen, P. Cheng, Y. Zhang, C. Wang, J. Li, Y. Zheng, J. Lu, J. Yang, R. Zhu, H. Zhang, Y. Zhou, L. Xu, C. Guo, The synergistic in vitro and in vivo antitumor effect of combination therapy with salinomycin and 5-fluorouracil against hepatocellular carcinoma, *PLoS One*. 9 (2014) e97414. <https://doi.org/10.1371/journal.pone.0097414>.
- [357] W.C. Chang, J.S.B. Wu, C.W. Chen, P.L. Kuo, H.M. Chien, Y.T. Wang, S.C. Shen, Protective effect of vanillic acid against hyperinsulinemia, hyperglycemia and hyperlipidemia via alleviating hepatic insulin resistance and

- inflammation in High-Fat Diet (HFD)-fed rats, *Nutrients*. 7 (2015) 9946–9959. <https://doi.org/10.3390/nu7125514>.
- [358] S.E. Borst, C.F. Conover, High-fat diet induces increased tissue expression of TNF- α , *Life Sci*. 77 (2005) 2156–2165. <https://doi.org/10.1016/j.lfs.2005.03.021>.
- [359] R. Kumar, R. Kumar, N. Khurana, S.K. Singh, S. Khurana, S. Verma, N. Sharma, B. Kapoor, M. Vyas, R. Khursheed, A. Awasthi, J. Kaur, L. Corrie, Enhanced oral bioavailability and neuroprotective effect of fisetin through its SNEDDS against rotenone-induced Parkinson's disease rat model, *Food Chem. Toxicol*. 144 (2020) 111590. <https://doi.org/10.1016/j.fct.2020.111590>.
- [360] B. Isomaa, J. Reuter, B.M. Djupsund, The subacute and chronic toxicity of cetyltrimethylammonium bromide (CTAB), a cationic surfactant, in the rat, *Arch. Toxicol*. 35 (1976) 91–96. <https://doi.org/10.1007/BF00372762>.
- [361] S. Mourdikoudis, R.M. Pallares, N.T.K. Thanh, Characterization techniques for nanoparticles: Comparison and complementarity upon studying nanoparticle properties, *Nanoscale*. 10 (2018) 12871–12934. <https://doi.org/10.1039/c8nr02278j>.
- [362] S.B. Rice, C. Chan, S.C. Brown, P. Eschbach, L. Han, D.S. Ensor, A.B. Stefaniak, J. Bonevich, A.E. Vladár, A.R.H. Walker, J. Zheng, C. Starnes, A. Stromberg, J. Ye, E.A. Grulke, Particle size distributions by transmission electron microscopy: An interlaboratory comparison case study, *Metrologia*. 50 (2013) 663–678. <https://doi.org/10.1088/0026-1394/50/6/663>.
- [363] P. Nimtrakul, D.B. Williams, W. Tiyaboonchai, C.A. Prestidge, Copolymeric micelles overcome the oral delivery challenges of amphotericin B, *Pharmaceuticals*. 13 (2020) 1–14. <https://doi.org/10.3390/ph13060121>.
- [364] C. Nagy, E. Einwallner, Study of in vivo glucose metabolism in high-fat diet-fed mice using oral glucose tolerance test (OGTT) and insulin tolerance test (ITT), *J. Vis. Exp.* 2018 (2018) 1–12. <https://doi.org/10.3791/56672>.
- [365] O.M. Ighodaro, A.M. Adeosun, O.A. Akinloye, Alloxan-induced diabetes, a common model for evaluating the glycemic-control potential of therapeutic compounds and plants extracts in experimental studies, *Med*. 53 (2017) 365–374. <https://doi.org/10.1016/j.medic.2018.02.001>.
- [366] C.P.D. Kottaisamy, D.S. Raj, V. Prasanth Kumar, U. Sankaran, Experimental animal models for diabetes and its related complications—a review, *Lab*.

- Anim. Res. 37 (2021) 1–14. <https://doi.org/10.1186/s42826-021-00101-4>.
- [367] A.J.F. King, The use of animal models in diabetes research, *Br. J. Pharmacol.* 166 (2012) 877–894. <https://doi.org/10.1111/j.1476-5381.2012.01911.x>.
- [368] Y. Xiong, L. Shen, K.J. Liu, P. Tso, Y. Xiong, G. Wang, S.C. Woods, M. Liu, Antiobesity and antihyperglycemic effects of ginsenoside Rb1 in rats, *Diabetes.* 59 (2010) 2505–2512. <https://doi.org/10.2337/db10-0315>.
- [369] C. Liu, M. Shao, L. Lu, C. Zhao, L. Qiu, Z. Liu, Obesity, insulin resistance and their interaction on liver enzymes, *PLoS One.* 16 (2021) 1–9. <https://doi.org/10.1371/journal.pone.0249299>.
- [370] S. Samarghandian, A. Borji, T. Farkhondeh, Attenuation of Oxidative Stress and Inflammation by *Portulaca oleracea* in Streptozotocin-Induced Diabetic Rats, *J. Evidence-Based Complement. Altern. Med.* 22 (2017) 562–566. <https://doi.org/10.1177/2156587217692491>.
- [371] J. Kaur, M. Gulati, P. Famta, L. Corrie, A. Awasthi, S. Saini, G.L. Khatik, V.G. Bettada, S. V Madhunapantula, K. Raj, G. Gupta, D. Kumar, M.F. Arshad, J. Adams, K. Gowthamarajan, K. Dua, P.M. Hansbro, K. Singh, Polymeric micelles loaded with glyburide and vanillic acid : I . Formulation development , in-vitro characterization and bioavailability studies, *Int. J. Pharm.* 624 (2022) 121987. <https://doi.org/10.1016/j.ijpharm.2022.121987>.
- [372] N. Wang, J. Zhang, M. Qin, W. Yi, S. Yu, Y. Chen, J. Guan, R. Zhang, Amelioration of streptozotocin-induced pancreatic β cell damage by morin: Involvement of the AMPK-FOXO3-catalase signaling pathway, *Int. J. Mol. Med.* 41 (2018) 1409–1418. <https://doi.org/10.3892/ijmm.2017.3357>.
- [373] A.M.T.A. Nahdi, A. John, H. Raza, Elucidation of Molecular Mechanisms of Streptozotocin-Induced Oxidative Stress, Apoptosis, and Mitochondrial Dysfunction in Rin-5F Pancreatic β -Cells, *Oxid. Med. Cell. Longev.* 2017 (2017). <https://doi.org/10.1155/2017/7054272>.

List of publications

- **Jaskiran Kaur**, Monica Gulati, Kumar Singh, Gowthamarajan Kuppusamy, Bhupinder Kapoor, Vijay Mishra, Saurabh Gupta, Mohammed F Arshad, Omji Porwal, Niraj Kumar Jha, VNL Chaitanya, Dinesh Kumar Chellappan, Gaurav Gupta, Piyush Kumar Gupta, Kamal Dua, Ankit Awsathi, Leander Corrie. Discovering multifaceted role of vanillic acid beyond flavours: Nutraceutical and therapeutic potential. Trends in Food Science and Technology, **2022**, 187-200 (**Impact factor: 16.0**)
- **Jaskiran Kaur**, Vijay Mishra, Sachin Kumar Singh*, Monica Gulati, Bhupinder Kapoor, Dinesh Kumar Chellappan, Gaurav Gupta, Harish Dureja, Krishnan Anand, Kamal Dua, Gopal L. Khatik, Kuppusamy Gowthamarajan, Harnessing amphiphilic polymeric micelles for diagnostic and therapeutic applications: Breakthroughs and bottlenecks, Journal of Controlled Release, 334 (**2021**), 64-95 (**Impact factor: 9.2**)
- **Kaur, J.**, Gulati, M., Zacconi, F., Dureja, H., Loebenberg, R., Ansari, M.S., AlOmeir, O., Alam, A., Chellappan, D.K., Gupta, G., Jha, N.K., Pinto, T. de J.A., Morris, A., Choonara, Y.E., Adams, J., Dua, K., Singh, S.K., **2022**. Biomedical Applications of polymeric micelles in the treatment of diabetes mellitus: Current success and future approaches. Expert Opin. Drug Deliv. 00, 1–23. (**Impact factor 8.3**).
- **Jaskiran Kaur**, Monica Gulati, Niraj Kumar Jha, John Disouza, Vandana Patravale, Kamal Dua, Sachin Kumar Singh. Recent advances in developing polymeric micelles for treating cancer: Breakthroughs and bottlenecks in their clinical translation. Drug Discovery Today, **2022**. (**Impact factor: 8.3**)
- **Jaskiran Kaur**, Monica Gulati, Bhupinder Kapoor, Niraj Kumar Jha, Piyush Kumar Gupta, Gaurav Gupta, Dinesh Kumar Chellappan, Hari Prasad Devkota, Parteek Prasher, Kamal Dua, Sachin Kumar Singh, Advances in designing of polymeric micelles for biomedical application in brain related diseases. Chemico-biological interactions, **2022** (**Impact factor: 5.1**)
- **Jaskiran Kaur**, Paras Famta, Mani Famta, Meenu Mehta, Saurabh Satija, Neha Sharma, Manish Vyas, Gopal Lal Khatik, Dinesh Kumar Chellappan, Kamal Dua, Navneet Khurana*, Potential Anti-epileptic Phytoconstituents: An Updated Review, Journal of Ethnopharmacology, 268 (**2021**), 113565 (**Impact factor: 3.8**)
- **Jaskiran Kaur**, Monica Gulati, K. Gowthamarajan, Sukriti Vishwas, Dinesh Kumar Chellappan, Gaurav Gupta, Kamal Dua, Narendra Kumar Pandey, Bimlesh Kumar, Sachin Kumar Singh*, Combination therapy of vanillic acid and oxaliplatin co-loaded in polysaccharide based functionalized polymeric micelles could offer effective treatment for

colon cancer: A hypothesis, *Medical Hypothesis*, **2021**, 110679. (**Impact factor: 1.5**)

- **Jaskiran Kaur**, Paras Famta, Navneet Khurana, Manish Vyas, and Gopal L. Khatik*, Biomedical applications of 4-hydroxycoumarin as a fungal metabolite and its derivatives, in: V. Gupta (Eds.), *New and Future Developments in Microbial Biotechnology and Bioengineering*, Elsevier., United States of America, **2020**, pp. 209-218 (**book chapter**).
 - **Jaskiran Kaur**, Paras Famta, Navneet Khurana, Manish Vyas, and Gopal L. Khatik*, Pharmacotherapy of type 2 diabetes, in: J. Faintuch, Salomao (Eds.), *Obesity and diabetes scientific advances and best practices*, Springer, **2020**, pp. 679-694 (**book chapter**).
- [1] S. Alam, M.K. Hasan, S. Neaz, N. Hussain, M.F. Hossain, T. Rahman, *Diabetes Mellitus: Insights from Epidemiology, Biochemistry, Risk Factors, Diagnosis, Complications and Comprehensive Management*, *Diabetology*. 2 (2021) 36–50. <https://doi.org/10.3390/diabetology2020004>.
- [2] R. Khursheed, S.K. Singh, S. Wadhwa, M. Gulati, B. Kapoor, S.K. Jain, K. Gowthamarajan, F. Zacconi, D.K. Chellappan, G. Gupta, N.K. Jha, P.K. Gupta, K. Dua, Development of mushroom polysaccharide and probiotics based solid self-nanoemulsifying drug delivery system loaded with curcumin and quercetin to improve their dissolution rate and permeability: State of the art, *Int. J. Biol. Macromol.* 189 (2021) 744–757. <https://doi.org/10.1016/j.ijbiomac.2021.08.170>.
- [3] S. Ramachandran, A. Rajasekaran, N. Adhirajan, *In Vivo and In Vitro Antidiabetic Activity of Terminalia paniculata Bark: An Evaluation of Possible Phytoconstituents and Mechanisms for Blood Glucose Control in Diabetes*, *ISRN Pharmacol.* 2013 (2013) 1–10. <https://doi.org/10.1155/2013/484675>.
- **Jaskiran Kaur**, Monica Gulati, Narendra Kumar Pandey, Bimlesh Kumar, Saurabh Singh, Sachin Kumar Singh, Validated Reverse Phase-High-Performance Liquid Chromatography Method for Simultaneous Determination of Vanillic acid and Glyburide in amphiphilic polymeric micelles, **2022**, *Nanoscience and nanotechnology-Asia*, (**Accepted and in press**)

Annexures



L OVELY
P ROFESSIONAL
U NIVERSITY

Centre for
Research Degree Programmes

LPU/CRDP/PHD/EC/20201226/001191

Dated: 16 Jul 2021

Jaskiran
Registration Number: 41700206
Programme Name: Doctor of Philosophy (Pharmacology)

Subject: Letter of Candidacy for Ph.D.

Dear Candidate,

We are very pleased to inform you that the Department Doctoral Board has approved your candidacy for the Ph.D. Programme on 21 Sep 2018 by accepting your research proposal entitled: "Development and optimization of polyethylene glycol methyl ether-polycaprolactone based glyburide and vanillic acid co-loaded amphiphilic polymeric micelles for the management of type-2 diabetes mellitus" under the supervision of Dr. Sachin Kumar Singh.

As a Ph.D. candidate you are required to abide by the conditions, rules and regulations laid down for Ph.D. Programme of the University, and amendments, if any, made from time to time.

We wish you the very best!!

In case you have any query related to your programme, please contact Centre of Research Degree Programmes.

Head

Centre for Research Degree Programmes

Note:-This is a computer generated certificate and no signature is required. Please use the reference number generated on this certificate for future conversations.

CENTRAL ANIMAL HOUSE FACILITY (CAHF)
Lovely Institute of Technology (Pharmacy), Lovely Professional University
Ludhiana- Jalandhar G.T. Road, Phagwara (Punjab), 144411
Registration Number -954/PO/ReRcBiBt/S/06/CPCSEA

CERTIFICATE

This is to certify that the project titled "*Development and optimization of polyethylene glycol methyl ether-polycaprolactone based glyburide and vanillic acid co-loaded amphiphilic polymeric micelles for the management of type-2 diabetes mellitus*" has been approved by the IAEC.

Name of Principal Investigator: Dr. Sachin Kumar Singh

IAEC approval number: LPU/IAEC/2021/78

Date of Approval: 30th January 2021

Animals approved: Sprague Dawley rats, Male: 94

Remarks if any: - NA


Dr. Monica Gulati

Biological Scientist,
Chairperson IAEC


Dr. Navneet Khurana

Scientist from different discipline


Dr. Bimlesh Kumar

Scientist In-Charge of Animal House,
Member Secretary IAEC



Contents lists available at ScienceDirect

Journal of Controlled Release

journal homepage: www.elsevier.com/locate/jconrel



Review article

Harnessing amphiphilic polymeric micelles for diagnostic and therapeutic applications: Breakthroughs and bottlenecks

Jaskiran Kaur^a, Vijay Mishra^a, Sachin Kumar Singh^{a,*}, Monica Gulati^a, Bhupinder Kapoor^a, Dinesh Kumar Chellappan^b, Gaurav Gupta^c, Harish Dureja^d, Krishnan Anand^e, Kamal Dua^f, Gopal L. Khatik^g, Kuppusamy Gowthamarajan^{h,i}

^a School of Pharmaceutical sciences, Lovely Professional University, Jalandhar-Delhi G.T Road, Phagwara, Punjab, India

^b School of Pharmacy, International Medical University, Bukit Jalil, Kuala Lumpur, Malaysia

^c School of Pharmacy, Suresh Gyan Vihar University, Jagatpura Mahal Road, Jaipur, India

^d Department of Pharmaceutical Sciences, Maharshi Dayanand University, Rohtak, Haryana, India

^e Department of Chemical Pathology, School of Pathology, Faculty of Health Sciences and National Health Laboratory Service, University of the Free State, Bloemfontein, South Africa

^f Discipline of Pharmacy, Graduate School of Health, University of Technology Sydney, Ultimo, NSW 2007, Australia

^g National Institute of Pharmaceutical Education and Research, Bijnor-Sisendi road, Sarojini Nagar, Lucknow, Uttar Pradesh 226301, India

^h Department of Pharmaceutics, JSS College of Pharmacy, JSS Academy of Higher Education & Research, Ooty, Nilgiris, Tamil Nadu, India

ⁱ Centre of Excellence in Nanoscience & Technology, JSS College of Pharmacy, JSS Academy of Higher Education & Research, Ooty, Nilgiris, Tamil Nadu, India.



ARTICLE INFO

Keywords:
Amphiphilic polymeric micelles
Block copolymer
Drug delivery
Theranostics
Cancer

ABSTRACT

Amphiphilic block copolymers are widely utilized in the design of formulations owing to their unique physicochemical properties, flexible structures and functional chemistry. Amphiphilic polymeric micelles (APMs) formed from such copolymers have gained attention of the drug delivery scientists in past few decades for enhancing the bioavailability of lipophilic drugs, molecular targeting, sustained release, stimuli-responsive properties, enhanced therapeutic efficacy and reducing drug associated toxicity. Their properties including ease of surface modification, high surface area, small size, and enhanced permeation as well as retention (EPR) effect are mainly responsible for their utilization in the diagnosis and therapy of various diseases. However, some of the challenges associated with their use are premature drug release, low drug loading capacity, scale-up issues and their poor stability that need to be addressed for their wider clinical utility and commercialization. This review describes comprehensively their physicochemical properties, various methods of preparation, limitations followed by approaches employed for the development of optimized APMs, the impact of each preparation technique on the physicochemical properties of the resulting APMs as well as various biomedical applications of APMs. Based on the current scenario of their use in treatment and diagnosis of diseases, the directions in which future studies need to be carried out to explore their full potential are also discussed.



Recent advances in developing polymeric micelles for treating cancer: Breakthroughs and bottlenecks in their clinical translation

Jaskiran Kaur^a, Monica Gulati^a, Niraj Kumar Jha^b, John Disouza^c,
Vandana Patravale^d, Kamal Dua^{e,f}, Sachin Kumar Singh^{a,*}

^aSchool of Pharmaceutical Sciences, Lovely Professional University, Jalandhar-Delhi G.T Road, Phagwara 144411, Punjab, India

^bDepartment of Biotechnology, School of Engineering & Technology (SET), Sharda University, Greater Noida, 201310 Uttar Pradesh, India

^cTatyasaheb Kore College of Pharmacy, Warananagar, Panhala, Kolhapur, Maharashtra 416113, India

^dDepartment of Pharmaceutical Sciences and Technology, Institute of Chemical Technology, Matunga, Mumbai, Maharashtra 400019, India

^eDiscipline of Pharmacy, Graduate School of Health, University of Technology Sydney, NSW 2007, Australia

^fFaculty of Health, Australian Research Centre in Complementary and Integrative Medicine, University of Technology Sydney, Ultimo, NSW 2007, Australia

Polymeric micelles (PMs) have been explored pre-clinically for the delivery of chemotherapeutics to treat cancer. Their unique features, such as easy surface functionalization, stimuli-responsiveness, good stability, ability to modify drug release, enhanced permeation and retention effect, and potential to encapsulate more than one type of therapeutic molecules at a time, make them unique carriers for the targeted delivery or for enhancing the bioavailability of chemotherapeutics. PMs can also be used as theranostic nanocarriers for the mapping of drug therapy along with tumor imaging in patients with cancer. This review focuses on the limitations of existing treatment strategies and on innovative approaches employed for the functionalization of PMs for targeting cancer cells. In addition, the bottlenecks associated with the translation of PMs from the laboratory to clinics are also discussed.

Keywords: Cancer; Polymeric micelles; Site-specificity; Theranostic; Clinical applications



Contents lists available at ScienceDirect

Trends in Food Science & Technology

journal homepage: www.elsevier.com/locate/tifs

Discovering multifaceted role of vanillic acid beyond flavours: Nutraceutical and therapeutic potential

Jaskiran Kaur^a, Monica Gulati^a, Sachin Kumar Singh^{a,*}, Gowthamarajan Kuppasamy^{b,c}, Bhupinder Kapoor^a, Vijay Mishra^a, Saurabh Gupta^d, Mohammed F. Arshad^e, Omji Porwal^f, Niraj Kumar Jha^g, M.V.N.L. Chaitanya^d, Dinesh Kumar Chellappan^h, Gaurav Gupta^{i,m}, Piyush Kumar Gupta^j, Kamal Dua^{k,l}, Rubiya Khursheed^a, Ankit Awasthi^a, Leander Corrie^a

^a School of Pharmaceutical Sciences, Lovely Professional University, Punjab, India

^b Department of Pharmaceutics, JSS College of Pharmacy, JSS Academy of Higher Education & Research, Ooty, Nilgiris, Tamil Nadu, India

^c Centre of Excellence in Nanoscience & Technology, JSS College of Pharmacy, JSS Academy of Higher Education & Research, Ooty, Nilgiris, Tamil Nadu, India

^d Chitkara College of Pharmacy, Chitkara University, Punjab, India

^e Department of Research and Scientific Communications, Isthmus Research and Publishing House, New Delhi, 110044, India

^f Department of Pharmacy, Tishk International University, Erbil, Kurdistan Region, Iraq

^g Department of Biotechnology, School of Engineering & Technology (SET), Sharda University, Plot No.32-34 Knowledge Park III Greater Noida, Uttar Pradesh, 201310, India

^h School of Pharmacy, International Medical University, Bukit Jalil, Kuala Lumpur, Malaysia

ⁱ School of Pharmacy, Suresh Gyan Vihar University, Mahal Road, Jagatpura, 302017, Jaipur, India

^j Department of Life Sciences, School of Basic Sciences and Research, Sharda University, Plot No. 32-34, Knowledge Park III, Greater Noida, 201310, India

^k Discipline of Pharmacy, Graduate School of Health, University of Technology Sydney, Australia

^l Faculty of Health, Australian Research Centre in Complementary and Integrative Medicine, University of Technology Sydney, Ultimo, NSW2007, Australia

^m Department of Pharmacology, Saveetha Dental College, Saveetha Institute of Medical and Technical Sciences, Saveetha University, Chennai, India

ARTICLE INFO

Keywords:

Vanillic acid
Antioxidant
Nutraceutical
VA derivatives
Therapeutic agent












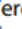
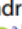

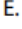

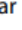
ABSTRACT

Background: Vanillic acid is a phenolic compound, found in various dietary sources and medicinal plants. Apart from its extraction from these biological sources, it is also synthesized chemically. It is used as flavouring agent in various food products. It possesses anticancer, antiobesity, antidiabetic, antibacterial, anti-inflammatory, and antioxidant effects. Despite possessing good therapeutic potential and safety profile, it has not been well explored as nutraceutical or, therapeutic moiety.

Scope and approach: Literature search was conducted to systematically review the various mechanistic pathways through which vanillic acid showed multiple therapeutic effects. Along with these pathways, other applications of vanillic acid and its derivatives are highlighted. Some of the patents that have been filed hitherto, for the production and uses of vanillic acid are also entailed in the manuscript.

Key findings and conclusion: Vanillic acid exerts diverse bioactivity against cancer, diabetes, obesity, neurodegenerative, cardiovascular, and hepatic diseases by inhibition of the associated molecular pathways. Its derivatives also possess the therapeutic potential to treat autoimmune diseases as well as fungal and bacterial infections. Owing to these benefits, vanillic acid has great potential to be used as a nutraceutical and provides scope for therapeutic uses beyond its traditional use as a flavouring agent. However, its oral bioavailability is limited due to its rapid elimination (metabolism) from the plasma. This, in turn, impedes its successful delivery through conventional formulations. Hence, efforts are required to develop nanoformulations of vanillic acid to overcome the associated challenges.

Biomedical Applications of polymeric micelles in the treatment of diabetes mellitus: Current success and future approaches

Jaskiran Kaur ^a, Monica Gulati ^{a,b}, Flavia Zacconi ^{c,d}, Harish Dureja ^e, Raimar Loebenberg ^f, Md Salahuddin Ansari ^g, Othman AlOmeir ^g, Aftab Alam ^h, Dinesh Kumar Chellappan ⁱ, Gaurav Gupta ^{j,k,l}, Niraj Kumar Jha ^m, Terezinha de Jesus Andreoli Pinto ⁿ, Andrew Morris ^o, Yahya E. Choonara ^p, Jon Adams ^b, Kamal Dua ^{b,q} and Sachin Kumar Singh ^{a,b}

^aSchool of Pharmaceutical Sciences, Lovely Professional University, Phagwara, India; ^bFaculty of Health, Australian Research Centre in Complementary and Integrative Medicine, University of Technology Sydney, Ultimo, Australia; ^cde Farmacia, Pontificia Universidad Cat'olica de ChileDepartamento de Química Org'ánica, Facultad de Química y , Santiago, Chile; ^dInstitute for Biological and Medical Engineering, Schools of Engineering, Medicine and Biological Sciences, Pontificia Universidad Cat'olica de Chile, Macul, Chile; ^eDepartment of Pharmaceutical Sciences, Maharshi Dayanand University, Rohtak, India; ^fFaculty of Pharmacy and Pharmaceutical Sciences, University of Alberta, Edmonton, Alberta AB, Canada; ^gDepartment of Pharmacy Practice, College of Pharmacy Aldawadmi, Shaqra University Shaqra, Saudi Arabia; ^hDepartment of Pharmacognosy, College of Pharmacy, Prince Sattam Bin Abdulaziz University, Kharj, KSA; ⁱDepartment of Life Sciences, School of Pharmacy, International Medical University, Bukit Jalil, Malaysia; ^jDepartment of pharmacology, School of Pharmacy, Suresh Gyan Vihar University, Jagatpura, India; ^kDepartment of Pharmacology, Saveetha Dental College, Saveetha Institute of Medical and Technical Sciences, Saveetha University, Chennai, India; ^lUttaranchal Institute of Pharmaceutical Sciences, Uttaranchal University, Dehradun, India; ^mDepartment of Biotechnology, School of Engineering & Technology (SET), Sharda University, Greater Noida, India; ⁿDepartment of Pharmacy, Faculty of Pharmaceutical Sciences, University of São Paulo, São Paulo, Brazil; ^oSwansea University Medical School, Swansea University, Singleton Park, Swansea; ^pWits Advanced Drug Delivery Platform Research Unit, Department of Pharmacy and Pharmacology, School of Therapeutic Sciences, University of Witwatersrand, Johannesburg, South Africa; ^qDiscipline of Pharmacy, Graduate School of Health, University of Technology Sydney, Ultimo, Australia

ABSTRACT

Introduction: Diabetes mellitus (DM) is the most common metabolic disease and multifactorial, harming patients worldwide. Extensive research has been carried out in the search for novel drug delivery systems offering reliable control of glucose levels for diabetics, aiming at efficient management of DM.

Areas covered: Polymeric micelles (PMs) as smart drug delivery nanocarriers are discussed, focusing on oral drug delivery applications for the management of hyperglycemia. The most recent approaches used for the preparation of smart PMs employ molecular features of amphiphilic block copolymers (ABCs), such as stimulus sensitivity, ligand conjugation, and as a more specific example the ability to inhibit islet amyloidosis.

Expert opinion: PMs provide a unique platform for self-regulated or spatiotemporal drug delivery, mimicking the working mode of pancreatic islets to maintain glucose homeostasis for prolonged periods. This unique characteristic is achieved by tailoring the functional chemistry of ABCs considering the physicochemical traits of PMs, including sensing capabilities, hydrophobicity, etc. In addition, the application of ABCs for the inhibition of conformational changes in islet amyloid polypeptide garnered attention as one of the root causes of DM. However, research in this field is limited and further studies at the clinical level are required.

ARTICLE HISTORY

Received 27 January 2022
Accepted 6 June 2022

KEYWORDS

Amphiphilic block copolymers; micelles; diabetes mellitus; drug delivery; insulin



Contents lists available at ScienceDirect

Chemico-Biological Interactions

journal homepage: www.elsevier.com/locate/chembioint

Review Article

Advances in designing of polymeric micelles for biomedical application in brain related diseases



Jaskiran Kaur^a, Monica Gulati^{a,b}, Bhupinder Kapoor^a, Niraj Kumar Jha^{c,s}, Piyush Kumar Gupta^{d,q}, Gaurav Gupta^{e,f,r}, Dinesh Kumar Chellappan^g, Hari Prasad Devkota^h, Parteek Prasherⁱ, Md Salahuddin Ansari^j, Faris F. Aba Alkhalil^{k,l}, Mohammed F. Arshad^m, Andrew Morrisⁿ, Yahya E. Choonara^o, Jon Adams^b, Kamal Dua^{b,p}, Sachin Kumar Singh^{a,b,*}

^a School of Pharmaceutical Sciences, Lovely Professional University, Phagwara, 144411, Punjab, India^b Faculty of Health, Australian Research Centre in Complementary and Integrative Medicine, University of Technology Sydney, Ultimo, NSW, 2007, Australia^c Department of Biotechnology, School of Engineering & Technology (SET), Sharda University, Plot No.32-34 Knowledge Park III, Greater Noida, Uttar Pradesh, 201310, India^d Department of Life Sciences, School of Basic Sciences and Research, Sharda University, Plot no. 32 - 34, Knowledge Park III, Greater Noida, 201310, Uttar Pradesh, India^e School of Pharmacy, Suresh Gyan Vihar University, Mahal Road, Jagatpura, Jaipur, India^f Department of Pharmacology, Saveetha Dental College, Saveetha Institute of Medical and Technical Sciences, Saveetha University, Chennai, India^g Department of Life Sciences, School of Pharmacy, International Medical University, Bukit Jalil 57000, Kuala Lumpur, Malaysia^h Graduate School of Pharmaceutical Sciences, Kumamoto University, 5-1 Oehonmachi, Kumamoto, 862-0973, Japanⁱ Department of Chemistry, University of Petroleum & Energy Studies, Energy Acres, Dehradun, 248007, India^j Department of Pharmacy Practice, College of Pharmacy, Shaqra University, Aldawadmi, Saudi Arabia^k Department of Pharmaceutical Chemistry and Pharmacognosy, College of Dentistry and Pharmacy, Buraydah Colleges, Buraydah, Saudi Arabia^l Department of Medical Laboratories, College of Applied Medical Sciences, Qassim University, Buraydah, Saudi Arabia^m Department of Research and Scientific Communications, Isthmus Research and Publishing House, New Delhi, 110044, Indiaⁿ Swansea University Medical School, Room 262, 1st Floor, Grove Building, Swansea University, Singleton Park, Swansea, Wales, SA2 8PP, UK^o Wits Advanced Drug Delivery Platform Research Unit, Department of Pharmacy and Pharmacology, School of Therapeutic Sciences, University of Witwatersrand, 7 York Road, Parktown, Johannesburg, 2193, South Africa^p Discipline of Pharmacy, Graduate School of Health, University of Technology Sydney, Ultimo, NSW, 2007, Australia^q Department of Biotechnology, Graphic Era Deemed to be University, Dehradun 248002, Uttarakhand, India^r Uttaranchal Institute of Pharmaceutical Sciences, Uttaranchal University, Dehradun, India^s Department of Biotechnology, School of Applied & Life Sciences (SALS), Uttaranchal University, Dehradun 248007, India

ARTICLE INFO

Keywords:

Amphiphilic polymers
Brain targeting
Functionalization
Polymeric micelles

ABSTRACT

In recent years, unique physicochemical properties of amphiphilic block copolymers have been utilized to design the polymeric micelles for brain-specific delivery of drugs, proteins, peptides and genes. Their unique properties such as nano-size, charge-switching ability, stimuli-responsive cargo release, flexible structure, and self-assembly enable them to overcome limitations of conventional dosage forms that include rapid drug release, drug efflux, and poor brain bioavailability, and poor stability. These limitations hinder their therapeutic efficacy in treating brain diseases. Their ease of functionalization and enhanced penetration and retention effect make them suitable nanocarriers for the diagnosis of various brain diseases. In this context, the present manuscript provides an insight into the progress made in the functionalization of micelles such as the incorporation of stimuli-sensitive moieties in copolymers, conjugation of cargo molecules with the core-forming block via responsive smart linkers, and conjugation of active ligands and imaging moieties with the corona forming block for brain targeting and imaging. Further, the review also expounds on the role of polymeric micelles in delivering neurotherapeutic to the brain. Some patents related to polymeric micelles formulated for brain delivery are also enlisted.



Contents lists available at ScienceDirect

International Journal of Pharmaceutics

journal homepage: www.elsevier.com/locate/ijpharm

Polymeric micelles loaded with glyburide and vanillic acid: I. Formulation development, in-vitro characterization and bioavailability studies

Jaskiran Kaur^a, Monica Gulati^{a,b}, Paras Famta^c, Leander Corrie^a, Ankit Awasthi^a, Sumant Saini^a, Gopal L. Khatik^d, Vidya G. Bettada^e, SubbaRao V. Madhunapantula^e, Keshav Raj Paudel^f, Gaurav Gupta^{g,h,m}, Dinesh Kumar Chellappanⁱ, Mohammed F. Arshad^j, Jon Adams^b, Kuppusamy Gowthamarajan^{k,*}, Kamal Dua^{b,l,*,**}, Philip M. Hansbro^f, Sachin Kumar Singh^{a,b,*,**}

^a School of Pharmaceutical Sciences, Lovely Professional University, Jalandhar-Delhi G.T Road, Phagwara, Punjab, India

^b Faculty of Health, Australian Research Centre in Complementary & Integrative Medicine, University of Technology Sydney, Ultimo, NSW 2007, Australia

^c Department of Pharmaceutics, National Institute of Pharmaceutical Education and Research, Hyderabad, India

^d National Institute of Pharmaceutical Education and Research, Bijnor-Sisendi Road, Sarojini Nagar, Lucknow, Uttar Pradesh 226301, India

^e Center of Excellence in Molecular Biology and Regenerative Medicine Laboratory (A DST-FIST Supported Center), Department of Biochemistry (A DST-FIST Supported Department), JSS Medical College, JSS Academy of Higher Education and Research, Bannimantapa, Sri Shivarathreshwara Nagar, Mysore 570 015, Karnataka, India

^f Centre of Inflammation, Centenary Institute and University of Technology Sydney, Faculty of Science, School of Life Sciences, Sydney 2007, Australia

^g School of Pharmacy, Suresh Gyan Vihar University, Mahal Road, Jagatpura, Jaipur, India

^h Department of Pharmacology, Saveetha Dental College and Hospitals, Saveetha Institute of Medical and Technical Sciences, Saveetha University, Chennai, India

ⁱ School of Pharmacy, International Medical University, Bukit Jalil, 57000 Kuala Lumpur, Malaysia

^j Department of Research and Scientific Communications, Isthmus Research and Publishing House, New Delhi 110044, India

^k Department of Pharmaceutics, JSS College of Pharmacy, JSS Academy of Higher Education & Research, Ooty, Nilgiris, Tamil Nadu, India

^l Discipline of Pharmacy, Graduate School of Health, University of Technology Sydney, Ultimo, NSW 2007, Australia

^m Uttaranchal Institute of Pharmaceutical Sciences, Uttaranchal University, Dehradun, India

ARTICLE INFO

Keywords:

Micelles
mPEG-b-PCL
Vanillic acid
Glyburide
Bioavailability
Insulin resistance

ABSTRACT

The co-formulation of glyburide (Gly) and vanillic acid (VA) as such in the form of nanomedicine has never been explored to treat metabolic diseases including type 2 diabetes mellitus. Both the drugs possess dissolution rate-limited oral bioavailability leading to poor therapeutic efficacy. Hence, co-loading these drugs into a nanocarrier could overcome their poor oral bioavailability related challenges. Owing to this objective, both drugs were co-loaded in amphiphilic polymeric micelles (APMs) and evaluated for their biopharmaceutical outcomes. The APMs were prepared using mPEG-b-PCL/CTAB as a copolymer-surfactant system via the liquid antisolvent precipitation (LAP) method. The design of these APMs were optimized using Box Behnken Design by taking various process/formulation based variables to achieve the desired micellar traits. The release of both the drugs from the optimized co-loaded APMs was compared in different media and displayed a remarkable sustained release profile owing to their hydrophobic interactions with the PCL core. The *in vitro* cytotoxicity study of co-loaded APMs on Caco-2 cells revealed 70 % cell viability in a concentration-dependent manner. The preventive effects of Gly and VA co-loaded in APMs on glucose uptake was studied in insulin-responsive human HepG2 cells treated with high glucose. The co-loading of both the drugs in optimized APMs exhibited synergistic glucose-lowering activity ($p < 0.001$) than raw drugs with low cytotoxicity on HepG2 cells within the test concentration. This could be attributed to an increase in the relative oral bioavailability of both the drugs in APMs i.e., 868 % for Gly and 87 % for VA respectively.



Contents lists available at ScienceDirect

Medical Hypotheses

journal homepage: www.elsevier.com/locate/mehy

Combination therapy of vanillic acid and oxaliplatin co-loaded in polysaccharide based functionalized polymeric micelles could offer effective treatment for colon cancer: A hypothesis

Jaskiran Kaur^a, Monica Gulati^a, K. Gowthamarajan^{b,c}, Sukriti Vishwas^a,
Dinesh Kumar Chellappan^d, Gaurav Gupta^e, Kamal Dua^{f,g}, Narendra Kumar Pandey^a,
Bimlesh Kumar^a, Sachin Kumar Singh^{a,*}

^a School of Pharmaceutical Sciences, Lovely Professional University, Phagwara, Punjab 144411, India

^b Department of Pharmaceutics, JSS College of Pharmacy, JSS Academy of Higher Education & Research, Ooty, Nilgiris, Tamil Nadu, India

^c Centre of Excellence in Nanoscience & Technology, JSS College of Pharmacy, JSS Academy of Higher Education & Research, Ooty, Nilgiris, Tamil Nadu, India

^d Department of Life Sciences, School of Pharmacy, International Medical University, Bukit Jalil, 57000, Kuala Lumpur, Malaysia

^e School of Pharmacy, Suresh Gyan Vihar University, Mahal Road, Jagatpura, Jaipur, India

^f Discipline of Pharmacy, Graduate School of Health, University of Technology Sydney, NSW 2007, Australia

^g Faculty of Health, Australian Research Centre in Complementary and Integrative Medicine, University of Technology Sydney, Ultimo, NSW 2007, Australia

ARTICLE INFO

Keywords:

Colon cancer
Colon targeted delivery
Functionalized polymeric micelles
Oxaliplatin
Vanillic acid

ABSTRACT

Colon cancer is characterised by the persistent change in bowel habits due to the formation of polyps (cancerous) in the inner lining of the colon. Clinically, there are several anticancer drugs available to treat colon cancer. Oxaliplatin (third generation platinum drug) is widely prescribed anticancer drug due to its broad range anticancer properties and low toxicities over cisplatin and carboplatin. Currently, use of oxaliplatin as adjuvant chemotherapy represents a standard care for the treatment of advanced colon cancer. Despite this, its rapid degradation in systemic circulations upon administration, lack of tumor specificity, and low bioavailability limits its anticancer potential. On the other hand, vanillic acid (VA) has shown anticancer potential in colon cancer by targeting mTOR/Ras pathway, HIF-1 α inhibition, NF- κ B, and Nrf2 that regulate cell growth, cell survival, proliferation and adaptation to cancer microenvironment. Normal oral delivery of these two drugs offers non-specific drug release in gastrointestinal tract that leads to unwanted toxicity and very less amount of drug become available for colonic site. Therefore, loading of these two drugs in polysaccharide based functionalized polymeric micelles (FPMs) can offer selective targeting at colonic site and could offer better therapeutic efficacy at much lesser doses of drugs. Therefore, a new hypothesis has been proposed that the combination of vanillic acid with oxaliplatin co-loaded in FPMs could provide colon targeting ability with enhanced potency and safety profile by targeting multiple pathways than current adjuvant chemotherapies available in the market for the treatment of colon cancer.



Contents lists available at ScienceDirect

Journal of Controlled Release

journal homepage: www.elsevier.com/locate/jconrel



Review article

Harnessing amphiphilic polymeric micelles for diagnostic and therapeutic applications: Breakthroughs and bottlenecks



Jaskiran Kaur^a, Vijay Mishra^a, Sachin Kumar Singh^{a,*}, Monica Gulati^a, Bhupinder Kapoor^a, Dinesh Kumar Chellappan^b, Gaurav Gupta^c, Harish Dureja^d, Krishnan Anand^e, Kamal Dua^f, Gopal L. Khatik^g, Kuppusamy Gowthamarajan^{h,i}

^a School of Pharmaceutical sciences, Lovely Professional University, Jalandhar-Delhi G.T Road, Phagwara, Punjab, India

^b School of Pharmacy, International Medical University, Bukit Jalil, Kuala Lumpur, Malaysia

^c School of Pharmacy, Suresh Gyan Vihar University, Jagatpura Mahal Road, Jaipur, India

^d Department of Pharmaceutical Sciences, Maharshi Dayanand University, Rohtak, Haryana, India

^e Department of Chemical Pathology, School of Pathology, Faculty of Health Sciences and National Health Laboratory Service, University of the Free State, Bloemfontein, South Africa

^f Discipline of Pharmacy, Graduate School of Health, University of Technology Sydney, Ultimo, NSW 2007, Australia

^g National Institute of Pharmaceutical Education and Research, Bijnor-Sisendi road, Sarojini Nagar, Lucknow, Uttar Pradesh 226301, India

^h Department of Pharmaceutics, JSS College of Pharmacy, JSS Academy of Higher Education & Research, Ooty, Nilgiris, Tamil Nadu, India

ⁱ Centre of Excellence in Nanoscience & Technology, JSS College of Pharmacy, JSS Academy of Higher Education & Research, Ooty, Nilgiris, Tamil Nadu, India.

ARTICLE INFO

Keywords:

Amphiphilic polymeric micelles
Block copolymer
Drug delivery
Theranostics
Cancer

ABSTRACT

Amphiphilic block copolymers are widely utilized in the design of formulations owing to their unique physicochemical properties, flexible structures and functional chemistry. Amphiphilic polymeric micelles (APMs) formed from such copolymers have gained attention of the drug delivery scientists in past few decades for enhancing the bioavailability of lipophilic drugs, molecular targeting, sustained release, stimuli-responsive properties, enhanced therapeutic efficacy and reducing drug associated toxicity. Their properties including ease of surface modification, high surface area, small size, and enhanced permeation as well as retention (EPR) effect are mainly responsible for their utilization in the diagnosis and therapy of various diseases. However, some of the challenges associated with their use are premature drug release, low drug loading capacity, scale-up issues and their poor stability that need to be addressed for their wider clinical utility and commercialization. This review describes comprehensively their physicochemical properties, various methods of preparation, limitations followed by approaches employed for the development of optimized APMs, the impact of each preparation technique on the physicochemical properties of the resulting APMs as well as various biomedical applications of APMs. Based on the current scenario of their use in treatment and diagnosis of diseases, the directions in which future studies need to be carried out to explore their full potential are also discussed.